
**THE NOVEL ROLE OF APOBEC3C IN
MEDIATING NF- κ B ACTIVATION TO ENHANCE
CLEAR CELL RENAL CELL CARCINOMA
PROGRESSION**

Dissertation

zur Erlangung des akademischen Grades

doctor rerum naturalium

(Dr. rer. nat.)

der

Naturwissenschaftlichen Fakultät I – Biowissenschaften
der Martin-Luther-Universität Halle-Wittenberg

vorgelegt

von Nora Hase

1. Gutachter/in: Prof. Dr. Stefan Hüttelmaier
2. Gutachter/in: Prof. Dr. Sonja Keßler
3. Gutachter/in: Prof. Dr. Florian Heyd

Datum der Einreichung: 22.4.2024

Datum der öffentlichen Verteidigung: 28.04.2025

TABLE OF CONTENT

1	INTRODUCTION.....	1
1.1	Renal cell carcinoma (RCC).....	1
1.1.1	Subtypes of RCC.....	2
1.1.2	Characteristics of clear cell RCC.....	3
1.1.3	Treatment of RCC.....	5
1.2	The NF- κ B pathway.....	7
1.2.1	Subunits of the NF- κ B family.....	8
1.2.2	The NF- κ B signaling pathways and their regulators.....	9
1.2.3	The role of NF- κ B in cancer.....	12
1.3	RNA-binding proteins in cancer.....	13
1.4	The AID/APOBEC protein family.....	16
1.4.1	The APOBEC3 (A3) protein family.....	17
1.4.2	Main function of the A3 family.....	19
1.4.3	The role of A3 proteins in cancer.....	21
1.5	Aims of the study.....	24
2	MATERIAL AND METHODS.....	25
2.1	Material.....	25
2.1.1	Chemicals and reagents.....	25
2.1.2	Standard systems and Kits.....	25
2.1.3	Standard buffers.....	26
2.1.4	Primary and secondary antibodies.....	27
2.1.5	Bacteria strain.....	28
2.1.6	Plasmids.....	28
2.1.7	Cell lines.....	30
2.1.8	Animals.....	30
2.1.9	Patient samples.....	30
2.1.10	Oligonucleotides.....	32
2.1.11	Devices.....	37
2.2	Molecular biological methods.....	37
2.2.1	Cloning.....	37
2.2.1.1	DNA amplification by polymerase chain reaction.....	37
2.2.1.1	Oligonucleotide annealing.....	38
2.2.1.2	Plasmid digestion.....	38
2.2.1.3	Agarose gel electrophoresis.....	38
2.2.1.4	DNA gel extraction and ligation.....	38
2.2.1.5	<i>E. coli</i> transformation.....	39
2.2.1.6	DNA preparation from <i>E. coli</i>	39
2.2.2	Isolation of genomic DNA.....	39
2.2.3	Semiquantitative RT-PCR.....	40
2.2.4	RNA isolation.....	40
2.2.5	Reverse transcription and qRT-PCR.....	40
2.2.6	RNA co-Immunoprecipitation.....	41
2.2.7	Northern blot.....	42
2.2.8	Sucrose gradient.....	42
2.2.9	RNA decay.....	42
2.2.10	Nascent RNA.....	42
2.3	Cell biological methods.....	43
2.3.1	Cell culture.....	43
2.3.2	Transfection of siRNAs and plasmids.....	43

TABLE OF CONTENT

2.3.3	Generation of CRISPR/Cas9-mediated knockout clones	44
2.3.4	Establishment of stable shRNA-mediated A3C knockdown clones.....	44
2.3.5	Generation of stable overexpressing cell clones.....	45
2.3.6	Proliferation and 3D spheroid assays.....	45
2.3.7	Anoikis resistance assay and density stress	45
2.3.8	Apoptosis assay	45
2.3.9	Drug treatment.....	46
2.4	Protein-biochemical methods	46
2.4.1	Protein extraction, SDS-PAGE and Western blot	46
2.4.2	Immunofluorescence staining.....	47
2.4.3	Pull-down.....	47
2.4.4	Luciferase reporter assay	47
2.4.5	Subcellular fractionation	48
2.5	Mouse xenograft studies	48
2.6	Studies involving patient samples	48
2.7	Data analyses.....	49
2.7.1	Next Generation Sequencing.....	49
2.7.2	Gene set enrichment analyses	49
2.7.3	Kaplan-Meier analyses	49
2.7.4	CLIP analyses	50
2.8	Statistics.....	50
2.9	BioRender Licenses.....	50
3	RESULTS.....	51
3.1	Characterization of APOBEC3 protein family members	51
3.1.1	A3C and A3G are associated with different RNP complexes.....	51
3.1.2	Subcellular localization of A3C	53
3.1.3	RNA-editing activity of A3C	54
3.2	The A3C 3' UTR harbors regulatory elements	56
3.3	A3C is upregulated in ccRCC and correlates with poor survival in RCC.....	58
3.4	Investigating mechanisms responsible for the upregulation of A3C expression in ccRCC61	
3.4.1	The 3' UTR of A3C contains <i>cis</i> - and <i>trans</i> -acting regulatory elements	61
3.4.2	A3C is not an IFN- α -responsive gene	65
3.4.3	A3C is upregulated at transcriptional level as response to stress.....	66
3.5	Molecular function of A3C in the context of ccRCC.....	67
3.5.1	Depletion of A3C impairs the NF- κ B signaling pathway.....	67
3.5.1.1	NF- κ B activity is affected upon modification of A3C expression	70
3.5.1.2	Expression of NF- κ B target genes is impaired upon A3C depletion	71
3.5.1.3	Suppression of NF- κ B target gene expression upon A3C depletion is a conserved effect in RCC cell lines.....	73
3.5.2	A3C binds transcripts of NF- κ B signaling pathway regulators.....	74
3.5.3	A3C affects transcript levels of NF- κ B signaling pathway regulators.....	77
3.5.4	Depletion of A3C restrains NF- κ B subunits in the cytoplasm.....	80
3.6	A3C is a survival factor for tumor growth <i>in vivo</i>	83
3.7	A3C depletion enhances the susceptibility of ccRCC-derived cells to drug treatment	87
4	DISCUSSION.....	88
4.1	The A3 protein family is distinctive in subcellular localization, interaction partners and molecular functions	89
4.2	A3C gene expression.....	91
4.2.1	NF- κ B-mediated A3C expression as response to stress in ccRCC.....	91
4.2.2	Repressive regulatory elements in the 3' UTR of A3C transcripts act as mechanisms to control A3C gene expression	94
4.3	A3C is involved in ccRCC progression by promoting the NF- κ B pathway.....	96

TABLE OF CONTENT

4.4	Transcripts of NF- κ B pathway regulators are bound and presumably stabilized by A3C affecting translocation of NF- κ B subunits	98
4.4.1	A3C interacts with NF- κ B signaling pathway regulators independently of its cytidine deaminase activity	98
4.4.2	A3C binding partners may be stabilized by protection from miRNA-mediated degradation	100
4.4.3	Regulation of A3C-mediated NF- κ B activity occurs through NF- κ B subunits translocation.....	102
4.5	A3C may be a target for ccRCC therapy.....	104
5	SUMMARY	107
6	REFERENCES	108
7	APPENDIX.....	I
7.1	Supplemental Figures	I
7.2	Supplemental Tables.....	IV
7.3	List of Figures	VIII
7.4	List of Tables	X
7.5	List of Abbreviations	XI
	DANKSAGUNG	XV
	CURRICULUM VITAE	XVI
	LIST OF PUBLICATIONS	XVII
	EIDESSTÄTTLICHE ERKLÄRUNG	XVIII

1 INTRODUCTION

1.1 Renal cell carcinoma (RCC)

The kidney is an essential organ responsible for maintaining the homeostatic balance of fluids and solutes in the body, eliminating waste products from the bloodstream and secreting essential hormones. Structurally, the kidney consists of two main components: the parenchyma and the collecting system. The parenchyma, composed of the outer cortex and inner medulla, primarily comprises nephrons, which are functional units responsible for filtering blood through glomeruli and tubules (Figure 1A, left panel). The other main component is the central region of the kidney, consisting of the renal pelvis surrounded by calyces, which collects the urine.

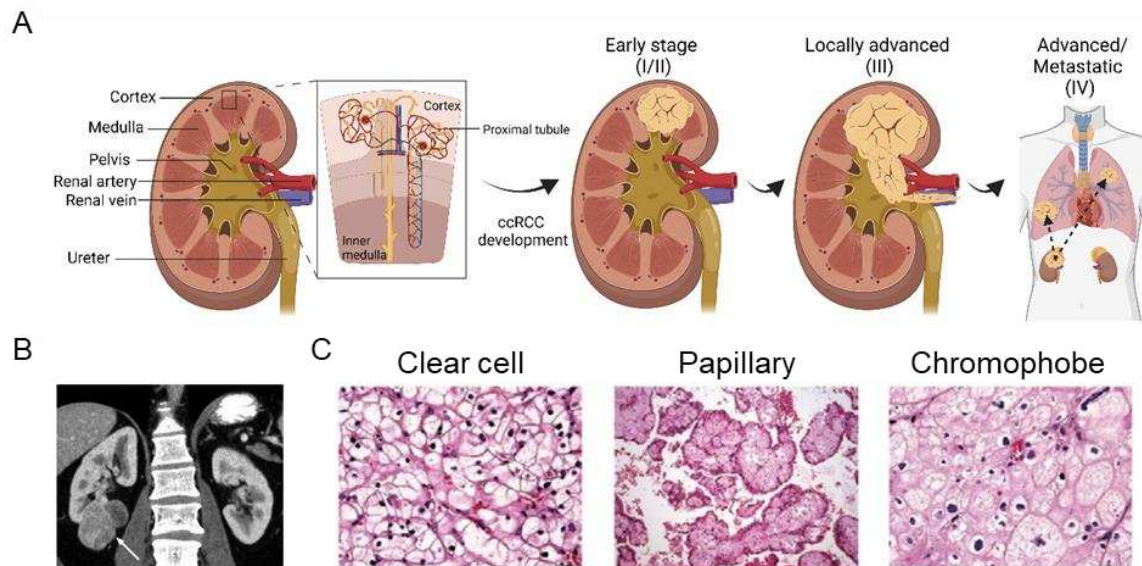


Figure 1: Origin, stages and histotypes of renal cell carcinoma (RCC). (A) Clear cell renal cell carcinoma (ccRCC) originates from the cortical proximal tubule. Staging of ccRCC is based on tumor size, position, lymph node involvement and spreading of cancer cells (schematic adapted from (Braun et al., 2021; Peired et al., 2021; created with BioRender.com)). (B) Computed tomography image shows ccRCC (arrow) in the right kidney of a 45-year-old male (Low et al., 2016). (C) Histological subtypes of RCC are visualized by hematoxylin and eosin (H&E) staining.

Adult kidney cancers that arise in the renal parenchyma are classified as adenocarcinomas, also known as renal cell carcinomas (RCCs). In contrast, kidney cancers originating from the collecting system are mainly transitional cell carcinomas. RCCs account for more than 90% of adult kidney carcinomas (Chow et al., 2010).

RCC has emerged as one of the top 10 most common cancers, with a significant rise in incidence observed in recent years, as approximately 400,000 individuals were diagnosed with RCC worldwide in 2018 (Chowdhury, Drake, 2020). Most RCCs occur sporadically; however, numerous studies (Chow et al., 2000; van Dijk et al., 2006) have identified specific risk factors associated with RCC development, including age (mean age at diagnosis is 65 year [Ljungberg et al., 2011]) obesity, smoking and hypertension.

Furthermore, there is a modest link between chronic kidney disease and polycystic kidney disease, albeit with a weaker association (Hancock, Georgiades, 2016).

Characterized by diverse clinical manifestations and a lack of early warning signs, RCC has long been challenging to diagnose. However, with the widespread use of cross-sectional imaging, most renal tumors (75%) are indeed detected incidentally at stage I (Figure 1B; Hancock, Georgiades, 2016). This early detection comes with a significant advantage, as approximately 70% of these cases have a high probability of being cured at the time of presentation (Hancock, Georgiades, 2016). The prognosis of patients with RCC is mostly influenced by the stage of the disease at the time of diagnosis. The stages of RCC reflect the tumor size, extent of invasion beyond the kidney, involvement of lymph nodes and metastasis (Figure 1A, right panel). For instance, patients diagnosed with stage I tumors, which are smaller than 7 cm, confined to the organ and without vascular invasion, have a 5-year survival rate of approximately 93% (SEER Cancer Statistics Review, 1975–2012, National Cancer Institute. Bethesda, MD, 2015). Stage II tumors are larger or show minimal invasion beyond the kidney, while stage III tumors involve nearby lymph nodes or extend into major blood vessels. In stage IV, the cancer has already spread to distant sites and the 5-year survival rate drops to only 12% (SEER Cancer Statistics Review, 1975–2012, National Cancer Institute. Bethesda, MD, 2015). Patients with advanced or metastatic RCC (mRCC) face universally poor outcomes, mainly due to the lack of effective systemic chemotherapy. Furthermore, mRCC remains one of the most treatment-resistant malignancies, with response rates for treated patients ranging from 15-25% and an overall median survival of less than one year (Linehan, Zbar, 2004; Mickisch, 2002; Motzer et al., 2015).

The need for improved therapies, especially targeting metastasizing RCCs, and early detection methods remains a great challenge to enhance the prognosis and survival of RCC patients.

1.1.1 Subtypes of RCC

RCC is not a single entity but rather a diverse collection of several distinct subtypes, each originating from different parts of the nephron. The subtypes exhibit unique genetic characteristics, histological features and clinical phenotypes resulting in varied prognosis and treatment options.

The most common subtype is the clear cell RCC (ccRCC), accounting for approximately 75% of all cases (Low et al., 2016). Its name is derived from the clear appearance of the cytoplasm, resulting from the dissolution of the high lipid content during histological preparation (Figure 1C). CcRCC is often associated with the deletion of the short arm of chromosome 3 (3p loss), as found in up to 95% of ccRCC cases, and somatic inactivating mutations of the *von Hippel-Lindau (VHL)* gene (Kovacs, Frisch, 1989).

Papillary RCC (papRCC) constitutes around 10-15% of all kidney cancers and is further subclassified into type 1 and a more aggressive type 2 variant based on histopathologic features (Antonelli et al., 2010). PapRCC is characterized by malignant epithelial cells forming papillae and tubules (Figure 1C). Genetic abnormalities associated with the papillary subtype include trisomies of chromosomes 3, 7, 12, 16, 17 and 20, c-MET mutations and loss of the Y chromosome (Hsieh et al., 2017; Padala et al., 2020).

The chromophobe subtype is a rare variant, accounting for 3-5% of kidney cancers. Histopathologically, it is composed of large polygonal cells with cloudy cytoplasm and prominent cell membranes (Figure 1C; Amin et al., 2008). The nuclei can be irregular in shape and surrounded by perinuclear halos (Rini et al., 2009). Binuclear features are frequently observed (Nagashima, 2000). Cytogenetic abnormalities associated with chrRCC include loss of multiple chromosomes such as 1, 2, 6, 10, 13, 17 and 21 (Hsieh et al., 2017). In contrast to ccRCC, the vascular density is low in chrRCC, and *TP53* gene mutations are frequently reported (Nagashima, 2000).

In terms of clinical outcomes, the clear cell subtype generally shows a less favorable prognosis compared to the papillary and chromophobe subtypes. Clear cell tumors are more likely to be symptomatic, present at an advanced stage and have a higher propensity to metastasize (Kammerer-Jacquet et al., 2017). The 5-year survival rate is 44-69% for clear cell tumors, 82-92% for papillary tumors and 78-92% for chromophobe tumors (Lee-Felker et al., 2014). Furthermore, clear cell tumors account for 94% of metastases derived from RCC tumors (Lee-Felker et al., 2014).

1.1.2 Characteristics of clear cell RCC

As mentioned above, ccRCC is genetically frequently initialized by the loss of chromosome 3p. This region harbors the tumor suppressor gene *VHL*. The absence of heterozygosity for *VHL* is a common occurrence in approximately 75-95% of non-inherited (sporadic) ccRCC cases (Kovacs, Frisch, 1989; Sari Khaleel et al., 2022). The malignant transformation of ccRCC is further driven by biallelic inactivation of *VHL*, which can result from point mutations in about 70-80% or through gene silencing via methylation in 5-10% of clear cell tumors (Sari Khaleel et al., 2022).

VHL encodes the von Hippel-Lindau protein (pVHL), a crucial component of an E3 ubiquitin ligase complex. Under normal conditions (normoxia; Figure 2, left panel), this complex targets the hypoxia-inducible factor (HIF), a transcription factor involved in critical oncogenic pathways, for ubiquitination and proteasome-mediated degradation (Zhang, Zhang, 2018). Consequently, the absence of functional pVHL results in the accumulation and activation of HIF (Figure 2, right panel). HIF activation also occurs under hypoxic conditions, which are common in RCCs and other solid tumors (Fouad, Aanei, 2017), enhancing the malignant effect. Activated HIF, composed of the inducible alpha (HIF-1 α)

and the constitutively expressed beta subunit (HIF-1 β), translocates into the nucleus, causing increased expression of various target genes, including VEGF, PDGF and TGFA. These genes promote processes like angiogenesis, proliferation and migration, which contribute to ccRCC tumorigenesis (Linehan et al., 2010; Shen, Kaelin, 2013).

Besides *VHL*, other tumor suppressor genes on chromosome 3, such as *PBRM1*, *BAP1* and *SETD2*, are frequently mutated in ccRCC (Sari Khaleel et al., 2022). These alterations influence chromatin remodeling, DNA accessibility, DNA double-strand break repair and DNA methylation, further contributing to the oncogenic transformation in ccRCC (Hsieh et al., 2018; Sari Khaleel et al., 2022). Other typically tumor-related genes like *TP53*, *mTOR* or *PTEN* are less frequently altered in ccRCC (Turajlic et al., 2015; Wang et al., 2018a).

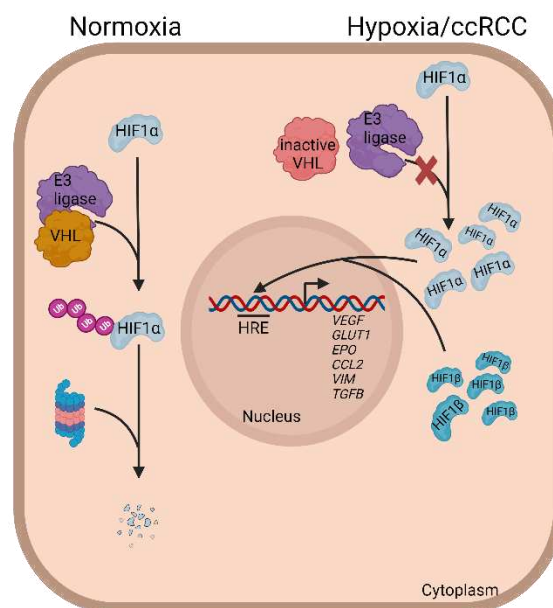


Figure 2: The role of pVHL and HIF-1 α in ccRCC progression. Under normoxia conditions (depicted on the left), the hypoxia-inducible factor alpha (HIF)-1 α is ubiquitinated (Ub) by the ubiquitin ligase von Hippel-Lindau (VHL) E3 ubiquitin ligase complex and subsequently degraded. In the presence of low tissue oxygenation levels or inactivation of *VHL* (depicted on the right), the regulatory process of the transcription factor HIF-1 α is disrupted. In the absence of functional pVHL, HIF-1 α is not degraded, accumulates in the cytoplasm and dimerizes with the constitutively present HIF-1 β . Upon nuclear translocation, the transcription factor binds to hypoxia response elements (HRE) and regulate expression of genes involved in cancer progression. Schematic adapted from (Clark, 2009; created with BioRender.com).

One distinctive hallmark of ccRCC is its unique immune landscape, characterized by a rich tumor immune microenvironment containing diverse immune cell populations, including T-cells, myeloid cells, natural killer cells and B-cells (Chevrier et al., 2017; Şenbabaoğlu et al., 2016). Notably, RCC has been identified as the most T-cell-inflamed cancer across 31 solid tumor types based on the expression of T-cell inflammation genes (Luke et al., 2019). While immune infiltration is generally considered a favorable prognostic factor in various cancer types (Becht et al., 2016; Fridman et al., 2017; Luke et al., 2019), as it indicates the potential for a strong immune response against the tumor as part of multiple immunotherapies, RCC exhibits a distinctive immunological behavior. The high density of

tumor-infiltrating CD8⁺ T-cells in ccRCC has been associated with poor prognosis (Giraldo et al., 2017; Murakami et al., 2021), providing evidence that immune cells and inflammatory pathways can also contribute to tumor growth (Vivar Chevez et al., 2014). This apparent contradiction may be attributed to the complex interplay between the tumor and the immune system. In addition to immune cell infiltration, ccRCC demonstrates the expression of tumor-associated antigens, sensitivity to immunotherapy and spontaneous regression, classifying it as an immunogenic tumor (Kim et al., 2021; Oliver et al., 1989; Vivar Chevez et al., 2014).

Tumors, including ccRCC, have developed mechanisms to evade destruction by the immune system. One such mechanism of immune escape involves the activation of protective pathways, including immune checkpoints like PD-1 (Programmed death 1; Tang, Heng, 2013). Upon T-cell activation, PD-1 is expressed and can bind to its ligands, PD-L1 or PD-L2, resulting in suppressed T-cell function facilitating immune evasion. Approximately 56% of RCC tumors show infiltration of PD-1⁺ T-cells, which, along with the expression of the ligand PD-L1, is associated with poor prognosis in renal tumors (Thompson et al., 2006; Thompson et al., 2007).

Overall, the complex and distinct immunogenic landscape of RCC contributes to its atypical behavior in response to therapies and prognosis compared to other cancer types. Understanding these immunological characteristics is important for developing effective treatments and improving outcomes for patients with RCC.

1.1.3 Treatment of RCC

RCC is frequently diagnosed at stage I, enabling a high rate of cure (approximately 70%; Hancock, Georgiades, 2016) through surgical intervention, which remains the primary and most effective treatment for localized RCC without metastases (Campbell et al., 2017; Ljungberg et al., 2022; Walther et al., 1999). The surgical approaches include partial nephrectomy for tumors up to 7cm or total nephrectomy for more extensive cases. Nevertheless, prognosis becomes poor for the 25-30% of patients who present with regional or distant metastases (Sánchez-Gastaldoa et al., 2017). Furthermore, it is noteworthy that approximately 30% of patients initially diagnosed with localized ccRCC eventually develop metastases, which are associated with high mortality rates (Osawa et al., 2019; Sánchez-Gastaldoa et al., 2017).

In the context of advanced RCC, conventional chemotherapy have demonstrated poor efficacy, with response rates as low as 5-6% in clinical trials involving over 4,000 cases and numerous agents (Motzer, Russo, 2000; Yagoda et al., 1995). Additionally, chemotherapeutic drugs face significant barriers due to their poor selectivity, strong side effects and the development of drug resistance (Makhov et al., 2018). Historically, therapeutic strategies for patients with mRCC relied on immunotherapy, specifically the use of several cytokines, as the pivotal role of immune mechanisms in RCC is well-established

(Raman, Vaena, 2015). Cytokines, such as interferon-alpha (IFN- α) and interleukin-2 (IL-2) are immunomodulatory signaling molecules aimed at activating the anti-tumor immune response. However, these treatments yielded limited efficacies, with response rates in the range of 10-15% and a median overall survival of 10–12 months (Coppin et al., 2005; Sánchez-Gastaldoa et al., 2017).

As a result, targeted therapy has emerged as a more promising option for advanced RCC patients since 2006. The significant advancements in understanding RCC's molecular biology in recent decades have led to the development of several targeted agents. These agents aim to block tumor growth, proliferation and survival by specifically targeting key signaling molecules. The majority of these innovative targeted therapies approved for advanced ccRCC focuses on the unique HIF-related molecular biology of kidney cancer, particularly the increased expression of VEGF and PDGF contributing to the highly vascular nature of ccRCC (Slaton et al., 2001). Targeted therapies include tyrosine kinase inhibitors (TKI), such as sorafenib, sunitinib, pazopanib and cabozantinib, which inhibit the VEGF receptor family (Choueiri et al., 2017; Escudier et al., 2009; Motzer et al., 2009; Sternberg et al., 2010). Additionally, a monoclonal anti-VEGF antibody, bevacizumab, effectively blocks the ligand itself (Escudier et al., 2010). Nowadays, these treatments are widely used and have remarkably improved patient outcomes (Motzer et al., 2009; Shuch et al., 2008), as they have demonstrated disease stabilization or regression, leading to prolonged survival in up to 30% of mRCC patients (Piao et al., 2023).

Numerous ongoing studies are investigating combination therapies that involve anti-VEGF agents along with a new generation of immunotherapy agents known as T-cell immune checkpoint inhibitors (ICI). These ICIs include antibodies against PD-L1, like avelumab (Motzer et al., 2019), and antibodies against PD-1, such as nivolumab (Hammers et al., 2016). Their goal is to restore and enhance the immune activity by blocking the PD-1/PD-L1 axis, which is involved in inhibiting immune responses and promoting self-tolerance through modulating the activity of T-cells. ICI-based doublet combination therapies have demonstrated improved progression-free survival and overall survival compared to sunitinib alone in the treatment of mRCC (Bedke et al., 2021).

Despite the progress, TKIs and ICIs are only partially effective in treating mRCC and resistance to targeted therapy remains a significant challenge (Makhov et al., 2018; Rini et al., 2016). This resistance is presumably caused by the heterogeneous nature of RCC. Among RCC subtypes, the sporadic clear cell subtype, in particular, exhibits relatively high levels of intra-tumor heterogeneity compared to other tumor types (Gerlinger et al., 2012; Tabata et al., 2023). Intra-tumor heterogeneity refers to the genetic diversity and variability within a single tumor mass. Different regions within the tumor may possess distinct genetic alterations, leading to variable responses to therapies or the emergence of resistant subclones (Beksac et al., 2017). For instance, it has been reported that low intra-tumor

heterogeneity in ccRCC is associated with better survival and clinical benefit from anti-PD-1 immunotherapy (Ran et al., 2020).

In conclusion, RCC patients diagnosed at an early-stage benefit from surgical interventions with a high cure rate. However, for those with advanced or metastatic RCC, conventional chemotherapy and radiation have limited efficacy, while targeted therapies show partial effectiveness. Immunotherapeutic approaches hold promise, but further research is needed to enhance response rates and overcome resistance. Continued advancements in understanding the molecular pathways and tumor heterogeneity of RCC are essential in driving the development of novel therapeutic strategies.

1.2 The NF- κ B pathway

As previously mentioned, one of the hallmarks of ccRCC is the biallelic inactivation of *VHL*. Several studies (Djordjević et al., 2008; Matušan-Ilijaš et al., 2011; Meteoglu et al., 2008; Oya et al., 2003b; Sourbier et al., 2007) have provided evidence that pVHL acts as a negative regulator of the transcription factor family NF- κ B (Nuclear Factor kappa-light-chain-enhancer of activated B-cells). In the absence of a functional pVHL, for instance in RCC-derived cell models, NF- κ B expression and activity are significantly enhanced compared to RCC-derived cells with intact pVHL (Qi, Ohh, 2003). Furthermore, a direct correlation between tumor grade, invasion and metastasis of RCC and the expression and activation of NF- κ B was suggested (Oya et al., 2003b).

NF- κ B is a collective term for transcription factors belonging to the reticuloendotheliosis (Rel) family, which recognize a common 10 base pair DNA sequence motif called the κ B-binding site, which can be highly variable (5'-GGGRNWYYCC-3'; R = A or G; N = A, C, G, or T; W = A or T; Y = C or T (Lenardo, Baltimore, 1989). Originally described as a B-cell factor binding to the immunoglobulin κ light chain gene enhancer region (Sen, Baltimore, 1986), NF- κ B is now known to be a ubiquitous transcription factor found in almost all cell types (Morais et al., 2011). It regulates the expression of more than 400 different genes including enzymes (e.g., COX-2 and iNOS), cytokines (e.g., TNF, IL-1, IL-6, IL-8), adhesion molecules (e.g., ICAM1, E-selectin), cell cycle regulators (e.g., cyclin D1, D2, D3 and E, c-myc), angiogenic factors (e.g., VEGF), factors involved in invasion (e.g., matrix metalloproteases) and multidrug resistance factors (e.g., P-glycoprotein; Dolcet et al., 2005; Meteoglu et al., 2008). Thus, NF- κ B plays a crucial role in critical aspects of RCC biology that pose challenges to conventional therapy. Considering the increased activity of NF- κ B in RCC, inhibiting this transcription factor has become a promising treatment strategy and the subject of intense research using chemotherapeutic approaches (Du Shi et al., 2021; Tafani et al., 2013).

1.2.1 Subunits of the NF- κ B family

The NF- κ B family of transcription factors comprises two distinct subfamilies: the ‘Rel’ proteins and the ‘NF- κ B’ proteins. All of these proteins share a highly conserved N-terminal Rel homology domain (RHD), which mediates dimerization, sequence-specific DNA-binding and interaction with specific inhibitors (Gilmore, 1990); Figure 3A, right panel). The RHD contains a nuclear localization sequence (NLS) towards the carboxyl end.

The ‘Rel’ subfamily includes RelA (p65), RelB and c-Rel, all synthesized in their mature forms containing C-terminal transactivation domains (TAD) responsible for the transcriptional activity (Hoffmann et al., 2006). Among the ‘Rel’ proteins, RelB stands out with an additional leucine zipper (LZ) motif in its N-terminus, potentially influencing transcriptional regulation (Hayden, Ghosh, 2008), though its functional specificity and interaction partners require further research.

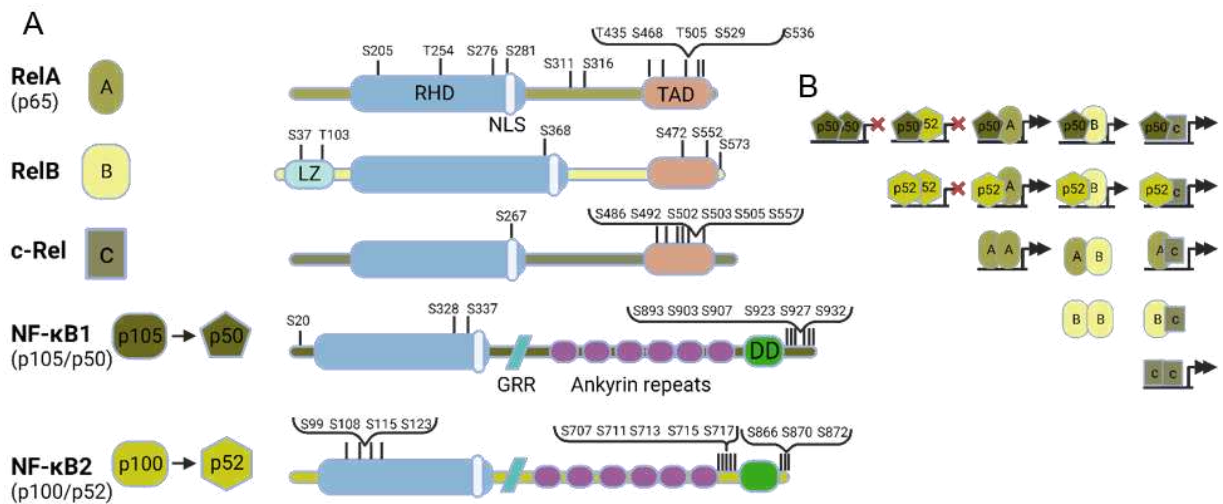


Figure 3: Phosphorylation and dimerization of NF- κ B subunits. (A) The five members of the NF- κ B family are schematically presented in the left panel. Alternative names are mentioned in parentheses. Processing NF- κ B1 and NF- κ B2 into their mature forms p50 and p52, respectively, is indicated by arrows. In the right panel, major domains and phosphorylation sites indicated by a line labeled with a number of the amino acid corresponding to the human protein sequence are highlighted. RHD, REL homology domain; TAD, transactivation domain; NLS, nuclear localization sequence; LZ, leucine zipper domain; GRR, glycine-rich region; DD, death domain; S, serine; T, threonine. (B) Compositions of potential NF- κ B dimers are shown. Indicated are the capacities to bind DNA (horizontal line) and to activate transcription (indicated by arrows). Schematic adapted from (Christian et al., 2016; Mitchell et al., 2016; Zhang, Sun, 2015; created with BioRender.com).

On the other hand, the ‘NF- κ B’ subfamily includes NF- κ B1 and NF- κ B2, which are initially synthesized in a precursor form, p105 and p100, respectively. These precursors contain a long C-terminal domain with ankyrin repeats that interact preferentially with their corresponding N-terminal part acting as inhibitors (Dolcet et al., 2005). It has also been shown that these ankyrin repeats interact and thereby inhibit c-Rel and RelA by retaining Rel/NF- κ B proteins in the cytoplasm (Naumann et al., 1993). Maturation of the precursors occurs through ubiquitin-dependent proteolytic cleavage, removing the C-terminal domain and generating the active forms (p105 to p50 and p100 to p52; Karin, 1999; Morais et al., 2011; Figure 3A, left panel). Both p50 and p52 contain the DNA-binding domain but

generally do not serve as transcriptional activators unless they form dimers with members of the 'Rel' subfamily (Dolcet et al., 2005).

NF- κ B subunits assemble into a dynamic array of homo- and heterodimers (Figure 3B) due to their inherent instability as monomers. This process is tightly regulated and different cell types express distinct NF- κ B monomers, resulting in a plethora of NF- κ B dimers during cell differentiation and development (Mitchell et al., 2016). Evidence suggests that the 15 potential NF- κ B dimers have dramatically different dimerization affinities (Mitchell et al., 2016). For example, RelB prefers to heterodimerize with p100 (Dobrzanski et al., 1995) and its processed form p52 (Senftleben et al., 2001), whereas RelA and c-Rel predominantly heterodimerize with p50 (Karin, Ben-Neriah, 2000). Among the 15 putative dimers, three dimers (RelB:RelB, RelB:RelA and RelB:cRel; Figure 3B) are unable to bind DNA (Huang et al., 2005) due to their low affinity for the κ B element. This leaves 12 NF- κ B dimers capable of binding DNA. Out of these, nine contain at least one of the activator proteins, RelA, cRel, or RelB, with RelA being the most potent and RelB the least potent subunit, and generally function as transcriptional activators (Mitchell et al., 2016).

The diverse NF- κ B dimer combinations regulate distinct, yet overlapping, gene sets for three reasons: (I) unique DNA-binding specificities enable interaction with different gene regulatory regions; (II) diverse protein-protein interactions at target promoters influence transcriptional activity and gene regulation; (III) the gene activation profile of different dimers varies under specific physiological conditions, providing a fine-tuned response to various cellular stimuli (Gilmore, 2006).

The DNA-binding capacity and transcriptional activity of NF- κ B are further modulated by post-translational modifications at different parts of the molecules, including phosphorylations and acetylations (Vallabhapurapu, Karin, 2009). Various phosphorylation events (mapped in Figure 3A) have been reported to regulate not only selective NF- κ B activity but also to influence stability, degradation and interactions with other factors (reviewed in Christian et al., 2016). These phosphorylation events result from signaling via upstream components of the NF- κ B pathway or from factors involved in other signaling pathways, establishing crosstalk nodes within the broader cellular signaling network.

1.2.2 The NF- κ B signaling pathways and their regulators

The NF- κ B activation is mediated by two main signaling pathways: the canonical (classical) and the non-canonical (alternative) pathways. Both pathways are triggered by various extracellular stimuli, leading to a phosphorylation cascade that releases NF- κ B homo- and heterodimers from their inhibitors or process them into their mature forms (reviewed in Bonizzi, Karin, 2004; Mitchell et al., 2016; Vallabhapurapu, Karin, 2009). Consequently, translocation to the nucleus is enabled and transcription of NF- κ B target genes initiated.

The canonical pathway is induced by activation of numerous receptors, including pro-inflammatory cytokine receptors (e.g., TNFR1, IL-1R), B-cell and T-cell antigen receptors (BCR or TCR), Toll-like receptors (TLR; e.g., TLR3, TLR4, TLR7) and growth factor receptors (e.g., EGFR family members; Pires et al., 2018; Sun, Ley, 2008; Figure 4, left panel). These receptors engage different adaptor molecules and signaling complexes, converging on the trimeric I κ B kinase (IKK or IKBK) complex, consisting of the catalytic subunits IKBKA (also called IKK α or CHUK) and IKBKB (also called IKK β) as well as the regulatory/scaffold subunit IKBKG (also called IKK γ or NEMO). The IKK complex activation through phosphorylation leads to subsequent phosphorylation of serine residues (Ser32 and Ser36) on the inhibitor of NF- κ B (I κ B), which retains NF- κ B subunits in the cytoplasm. Phosphorylation triggers I κ B ubiquitination and its proteosomal degradation, thereby exposing the NLS of bound NF- κ B subunits and inducing nuclear translocation (Karin, Ben-Neriah, 2000). Predominantly, the NF- κ B dimers p50:RelA and p50:c-Rel are released via the canonical pathway, which induces rapid but transient transcriptional responses (Schreuder et al., 2017).

In contrast, the non-canonical NF- κ B signaling results in a more delayed and sustained transcriptional response (Schreuder et al., 2017). This pathway is based on processing of the NF- κ B2 precursor protein p100. As p100 preferentially interacts with RelB, its processing generates p52:RelB dimers (Dejardin, 2006). Non-canonical NF- κ B signaling is regulated by the NF- κ B-inducing kinase (NIK). Normally, NIK is degraded in resting cells by an E3 ligase complex consisting of TRAF2/TRAF3 adaptor proteins and the E3 ligases BIRC2/3. Activation of a specific subset of TNFR family members, like CD40, B-cell-activating factor receptor (BAFFR), lymphotoxin β receptor (LT β R) or receptor activator of NF- κ B (RANK; Vallabhapurapu, Karin, 2009; Figure 4, right panel), leads to the stabilization of NIK via inactivation of the TRAF/BIRC complex. Increased NIK protein levels promote phosphorylation of the homodimer IKBKA/IKBKA, which transfers the phosphate group to specific serine residues within the p100 C-terminal ankyrin repeat domain (Liang et al., 2006). This phosphorylation results in the polyubiquitination of p100; however, because of the presence of a specific STOP signal located between the p52 N-terminal part and the p100 C-terminal ankyrin repeat domain, p100 is only partially degraded by the proteasome (Vallabhapurapu, Karin, 2009). The N-terminal p52 fragment bound to RelB is released and ultimately, RelB:p52 dimers are translocated to the nucleus inducing target gene expression (Pires et al., 2018).

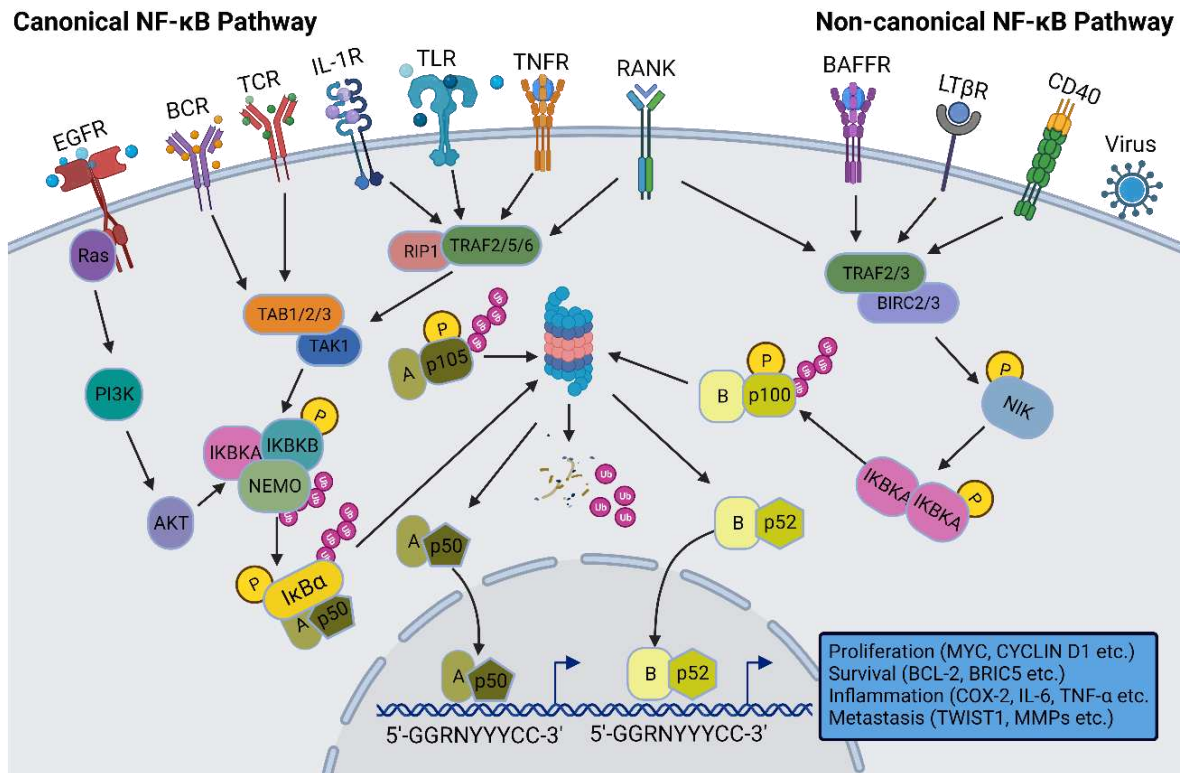


Figure 4: Overview of the canonical and non-canonical NF- κ B pathway. Both pathways are induced by various activators or stimuli. The signal is transduced by distinct adaptor proteins and signaling complexes. The main feature of the canonical pathway is the inhibitor of NF- κ B (I κ B) that restrains NF- κ B subunits in the cytoplasm. Upon phosphorylation by I κ B kinases (IKK/I κ BK), I κ B is ubiquitinated and degraded by the proteasome. Classical NF- κ B dimers like RelA/p50 are released and enter the nucleus to induce gene expression. The non-canonical NF- κ B pathway is primarily regulated by the kinase NIK. Upon activation of specific receptors, NIK is stabilized and phosphorylates IKBKA, which in turn phosphorylates RelB/p100. Limited proteosomal degradation of p100 releases the active form p52 that translocates to the nucleus as a dimer with RelB. EGFR, epidermal growth factor receptor; BCR, B-cell receptor; TCR, T-cell receptor; IL-1R, interleukin-1 receptor; TLR, Toll-like receptor; TNFR, tumor necrosis factor receptor; RANK, receptor activator of NF- κ B; BAFFR, B-cell activating factor receptor; LT β R, lymphotoxin beta receptor; CD40, cluster of differentiation 40; TRAF, TNFR-associated factor; RIP1, receptor interacting protein 1; TAK1, TGF β activating kinase 1; TAB, TAK-binding protein; BIRC, baculoviral IAP repeat containing; NIK, NF- κ B-inducing kinase; NEMO, NF- κ B essential modulator; PI3K, phosphatidylinositol 3-kinase. Schematic adapted from (Morgan et al., 2020; Pires et al., 2018; created with BioRender.com).

The canonical and non-canonical pathways were initially considered distinct, with separate physiological functions, as the classical NF- κ B pathway was associated with inflammatory responses, whereas the alternative pathway was linked to developmental cues (Shih et al., 2011). However, recent studies have revealed extensive interconnections and crosstalk between these pathways (reviewed in Mitchell et al., 2016; Oeckinghaus et al., 2011; Shih et al., 2011; Vallabhapurapu, Karin, 2009). This crosstalk involves the expression control of NF- κ B monomers by other NF- κ B subunits, interdependent proteolytic processing events of precursors and the activity of I κ B δ , which is unprocessed p100 forming higher-molecular-weight complexes by binding to NF- κ B subunits, acting as an inhibitor (Basak et al., 2007). Consequently, NF- κ B2 serves as the primary signaling node at which canonical and non-canonical signals interact. For instance, the classical IKK signaling pathway feeds into the alternative pathway through upregulation of NF- κ B2 expression, as the *NF- κ B2* gene contains κ B-binding sites in its promoter region and its expression

depends on RelA (Liptay et al., 1994; Vallabhapurapu, Karin, 2009). Additionally, I κ B δ can trap NF- κ B dimers, reducing their association with canonical I κ Bs and thereby regulating the nuclear localization of RelA (Basak et al., 2007). The IKK complex itself also acts as a crosstalk node, with key serine residues in the IKK complex being phosphorylated by various kinases (e.g., MAPKs, NIK, NAK, TAK1, MEKK1, MEKK3, PKC- θ , PKC- ζ and PKC- λ ; Oeckinghaus et al., 2011) activated by non-NF- κ B pathways, such as MAPKs, Akt and p38. Moreover, stabilization of NIK can also induce classical NF- κ B signaling by activating I κ BKB (Zarnegar et al., 2008), providing another example of crosstalk.

In summary, NF- κ B transcription factors play critical roles in immunity, stress responses, apoptosis and differentiation, with two main signaling pathways mediating their activation in response to a variety of stimuli. NF- κ B-dependent transcription is subjected to tight control through a network of positive and negative regulatory mechanisms. Moreover, it is intricately interconnected and closely coordinated with various other signaling pathways, enhancing adaptability and allowing for cell type-specific responses in different contexts.

1.2.3 The role of NF- κ B in cancer

The NF- κ B transcription factors, found ubiquitously in cells, play an important role in immune, inflammatory and stress responses. Orchestrating the expression of over 400 target genes, NF- κ B influences cell cycle progression, apoptosis, adhesion, angiogenesis and metastasis (Meteoglu et al., 2008; Serasanambati, Chilakapati, 2016). Dysregulated NF- κ B activity significantly contributes to inflammation-related diseases and various cancer types (review in Ben-Neriah, Karin, 2011; DiDonato et al., 2012; Dolcet et al., 2005; Perkins, 2012), particularly those derived from epithelial cells (Bassères, Baldwin, 2006; Baud, Karin, 2009). Elevated NF- κ B activity is observed in a range of solid tumors, including breast, prostate, ovarian, lung, colon, liver, pancreatic, thyroid, bladder and renal cancers (Bassères, Baldwin, 2006; Baud, Karin, 2009).

Though rare, oncogenic activating mutations in NF- κ B genes were identified in some lymphoid malignancies (DiDonato et al., 2012). However, most mutations activating NF- κ B-mediated transcription occur in upstream signaling components that feed into the NF- κ B pathway. For instance, genomic deletions in TRAF3, which negatively regulates the NF- κ B pathway by mediating NIK degradation (Liao et al., 2004), result in low mRNA and protein levels, ultimately enhancing NF- κ B activity (Annunziata et al., 2007). Furthermore, NF- κ B can be activated by various carcinogens (Guan et al., 2022) or by inflammatory cytokines within the tumor microenvironment (Ben-Neriah, Karin, 2011).

In RCC, heightened NF- κ B activity is observed in both cell lines (Morais et al., 2006; Oya et al., 2001; Sourbier et al., 2007) and ccRCC tumors (Djordjević et al., 2008; Matušan-Ilijaš et al., 2011; Meteoglu et al., 2008; Ng et al., 2018; Peri et al., 2013). This heightened

activity is partly due to deficient pVHL, indirectly driving NF- κ B activation by HIF-1 α -induced expression of genes involved in NF- κ B regulation (An, Rettig, 2005), and the inflammatory tumor microenvironment (DiDonato et al., 2012). Constitutively active NF- κ B, a common feature of ccRCC, is characterized by a disproportionate elevation of NF- κ B regulators and target genes compared to normal renal tissue (Peri et al., 2013), underscoring NF- κ B as a putative target in the treatment of RCC (Morais et al., 2011).

These target genes, including pro-angiogenic factors like VEGF, IL-6 and IL-8 (Morais et al., 2011), anti-apoptotic factors like BCL2 (Reed, 1994) and proliferative factors such as EGFR (Meteoglu et al., 2008), play crucial roles in RCC progression. High VEGF expression results in increased microvascular density, linked to poor prognosis in advanced RCCs (Zhang et al., 2002). The intracellular membrane protein BCL2, known for its anti-apoptotic role in several cancer types, likely contributes to increased resistance to chemotherapy in advanced RCCs (Huang et al., 1999). Additionally, EGFR overexpression in RCC has been associated with tumor development and progression, frequently linked to high-grade tumors (An, Rettig, 2007).

A distinctive feature of advanced RCC is the resistance to conventional anti-cancer therapies. Generally, tumors with constitutive NF- κ B activation tend to be resistant to chemotherapy and radiotherapy (Wang et al., 1999), as these therapies primarily induce apoptosis in proliferating cells (Guan et al., 2022). Consequently, inhibiting NF- κ B activation has emerged as a promising option to enhance RCC treatment efficacy (Baud, Karin, 2009; Morais et al., 2011). Encouragingly, initial studies demonstrate that blocking NF- κ B with small-molecule inhibitors, like the proteasome inhibitor bortezomib, sensitizes drug-resistant ccRCC-derived cells to EGFR inhibitors (An, Rettig, 2007) and to TRAIL (tumor necrosis factor-related apoptosis-inducing ligand)-mediated apoptosis (Brooks et al., 2010). Thus, small-molecule inhibitors targeting the NF- κ B pathway hold potential as components of combination therapies for advanced ccRCC (Peri et al., 2013).

In conclusion, the NF- κ B pathway plays a critical role in cancer initiation and progression by orchestrating gene expression affecting cell proliferation, survival, metastasis, angiogenesis and resistance to anti-cancer therapies. In ccRCC, NF- κ B is associated with key prognostic indicators and specific target genes, highlighting its promising therapeutic potential, particularly in chemotherapy-resistant cases. This approach offers the possibility of selectively inhibiting NF- κ B's pro-tumorigenic functions without the broader side effects of upstream NF- κ B blockade.

1.3 RNA-binding proteins in cancer

After transcription initiation by transcription factors, the synthesized RNA is subjected to various processing events, predominantly mediated by RNA-binding proteins (RBPs;

Keene, 2007), as part of post-transcriptional gene regulation. The RBPs orchestrate processes like splicing, cleavage, polyadenylation, subcellular localization, degradation and translation of RNA (Kang et al., 2020). RBPs interact with diverse RNA classes such as ribosomal RNAs, mRNAs, small nuclear RNAs (snRNA), small nucleolar RNAs (snoRNA), tRNAs and other non-coding RNAs. Interactions with mRNAs occur particularly in the 3' and 5' untranslated regions (UTR) due to the presence of RNA-binding domains in these segments (Kang et al., 2020; Mignone et al., 2002; Zhang, Chen, 2008). With more than 1 500 RBPs identified to date (Gerstberger et al., 2014; Wang et al., 2018b), the generated ribonucleoprotein (RNP) complexes are intricate and dynamic based on the specific RNA processing events that modulate the fate of target RNAs.

Besides well-studied transcription factors, RBPs have emerged as fundamental players in tumorigenesis. As master regulators of mRNA processing, dysregulation in cancer results in aberrant maturation of target RNAs encoding oncogenes and tumor suppressor genes involved in cancer hallmarks such as proliferation, angiogenesis, apoptosis, invasion and metastasis (reviewed in (Kang et al., 2020; Mohibi et al., 2019; Wurth, 2012). Numerous investigations have demonstrated that RBPs are predominantly upregulated across various cancers (Kechavarzi, Janga, 2014; Zhang et al., 2020). Dysregulation of RBP expression in cancer may derive from a variety of events. Although somatic copy number alterations are frequently reported in cancer genomes (Beroukhi et al., 2010; Zack et al., 2013), they appear to play a minor role in aberrant RBP expression in cancer (Wang et al., 2018b). Instead, epigenetic events and microRNA (miRNA)-dependent control of gene expression seem to be the primary drivers of dysregulated RBP expression (Wurth, 2012). Additionally, perturbed signaling pathways in malignancies can induce the upregulation of RBP expression through specific transcription factors and modulate post-translational modifications of RBPs, such as acetylation, phosphorylation, methylation, ubiquitination and N⁶-methyladenosine modification (m⁶A; Kim et al., 2008; Qin et al., 2020; Wurth, 2012; Xu et al., 2019). These processes can alter the subcellular localization, abundance and activity of RBPs.

Dysregulated RBP expression affects every step of tumorigenesis and cancer progression. For instance, IGF2BP1 is considered an oncogene due to its high expression in a wide array of tumors, including breast, ovarian, colon, lung and liver cancer (Gu et al., 2009; Gutschner et al., 2014; Hamilton et al., 2015; Ioannidis et al., 2003; Köbel et al., 2007; Vainer et al., 2008). This elevated expression leads to the dysregulation of key oncogenic factors like MYC and KRAS (Müller et al., 2018; Weidensdorfer et al., 2009). IGF2BP1 exerts its function by binding to specific recognition elements on target mRNAs. This binding stabilizes transcripts like PTEN, CD44 and CTNBN1, effectively preventing endonuclease cleavage and miRNA-mediated degradation (Gu et al., 2008; Stöhr et al., 2012; Vikesaa et al., 2006). The resulting mRNA stabilization eventually contributes to enhanced cell

migration and invasion. Furthermore, IGF2BP1 controls the subcellular localization of mRNAs encoding proteins involved in cell motility and focal adhesions, such as β -actin, E-cadherin and α -actinin (Gu et al., 2012). Thus, this multifaceted impact on gene expression ultimately promotes proliferation, differentiation and cell migration, thereby enhancing metastasis and worsening prognosis (Bell et al., 2013). It is worth noting that studies suggest IGF2BP1 associates with up to 1 000 target mRNAs (Jønson et al., 2007; Patel et al., 2012), explaining the severe impact IGF2BP1 has on cell fate and carcinogenesis.

Moreover, RBPs play crucial roles in mRNA translation. One such RBP is eIF4E, a component of the translation initiation complex, which binds to the 5'-terminal m⁷G cap of mRNAs, initiating mRNA translation (Kang et al., 2020). In cancer, eIF4E is often overexpressed and exerts oncogenic potential by regulating the translation of mRNAs associated with key processes such as proliferation (c-MYC, CDK2 and Cyclin D1), metastasis (MMP9), inhibition of apoptosis (BCL2 and BIRC5) and angiogenesis (VEGF; Hsieh, Ruggero, 2010). Other RBPs involved in translation regulation belong to the Pumilio (PUM) family. PUM1 and PUM2 are critical players in translation control, mRNA repression and degradation. These RBPs induce de-adenylation, often followed by degradation, or they promote miRNA-induced repression (Smialek et al., 2021). For instance, by binding to the 3' UTR of CDKNB1 mRNA, PUM1/2 induce local conformational changes, making the miRNA complementary site accessible for miRNA hybridization, enabling the repression of CDKN1B translation (Kedde et al., 2010). Furthermore, PUM1 has been demonstrated to regulate cell proliferation, migration and invasion in ovarian cancer by modulating levels of STAT3, BCL2, MMP2 and VEGFA (Guan et al., 2018).

Collectively, these examples demonstrate that a single RBP often interacts with a variety of different RNAs (Bell et al., 2013; Kim et al., 2009; Porter et al., 2021; Smialek et al., 2021). In collaboration with cofactors, RBPs maintain the stability of thousands of potential target mRNAs, impede miRNA-induced RNA decay and enhance the expression of oncogenes, collectively contributing to a carcinogenic effect.

However, the biological significance of RBPs in ccRCC has only recently begun to receive attention. Two studies revealed differential expression of 115 (Hua et al., 2021) and 200 RBPs (Zhu et al., 2020) with predominantly upregulated expression in ccRCC tumor tissues compared to normal tissues. Enrichment analyses linked these RBPs to critical processes such as transcriptional regulation, metabolism and RNA transport (Zhu et al., 2020). Furthermore, these altered RBPs correlate with the malignancy of ccRCC, as they have been linked to oncogenic pathways like epithelial-mesenchymal transition, G2M checkpoint regulation, KRAS signaling and IL6 JAK STAT3 signaling pathway (Hua et al., 2021). Another study, conducted by (Wu et al., 2020), identified 40 differentially expressed RBPs in ccRCC, comprising 10 downregulated and 30 upregulated RBPs. This study not only highlights the molecular relevance of these RBPs but also underscores their clinical

significance. Certain RBPs, including eIF4A1, IGF2BP3, APOBEC3D and APOBEC3G, were identified as potential biomarkers due to their correlation with overall survival and disease-free survival in ccRCC patients (Wu et al., 2020; Zhu et al., 2021).

Despite the progress in understanding RBPs in ccRCC, one intriguing group of RBPs, the APOBEC family, remains largely unexplored. The APOBEC family has been recognized as RBPs since the close of the last century, following the identification of the first member, APOBEC1 (Chen et al., 1990; Navaratnam et al., 1993; Powell et al., 1987). Additionally, various studies have suggested their involvement in different cancers (Chen et al., 2019; Navaratnam, Sarwar, 2006; Roberts et al., 2013; Saraconi et al., 2014; Swanton et al., 2015). However, their specific role in ccRCC remains to be elusive. Further research is essential to elucidate the function of the APOBEC family in the context of ccRCC.

1.4 The AID/APOBEC protein family

Activation-induced deaminase (AID) and apolipoprotein B mRNA-editing catalytic polypeptide-like (APOBEC) proteins form a family of zinc-dependent deaminases. These enzymes share the ability to catalyze cytidine to uridine (C-to-U; Figure 5C) deamination in single-stranded DNA (ssDNA) or RNA (Conticello, 2008; Harris et al., 2002; Knisbacher et al., 2016; Silvas, Schiffer, 2019; Smith et al., 2012). Despite their high pairwise sequence identity, ranging from 30% to more than 80% within the APOBEC3 family, and conserved regions (Shandilya et al., 2014), each member within this RBP family displays unique target sequence specificities, molecular functions, interaction networks and subcellular localizations (Salter et al., 2016).

The AID/APOBEC family is found across vertebrates including bony fish, birds, amphibians and mammals (Conticello et al., 2005). Due to the rapid expansion of the *APOBEC3* gene locus in primates through a complex history of gene duplications and fusions, 11 members have emerged: AID, APOBEC1 (A1), APOBEC2 (A2), APOBEC3 (A3) with seven subfamily members (A3A, A3B, A3C, A3D, A3F, A3G and A3H; Figure 5A) and APOBEC4 (A4; Conticello et al., 2005; Jarmuz et al., 2002). As previously mentioned, A1 was first identified and characterized for its role in editing C⁶⁶⁶ in an AU-rich regions of the apolipoprotein B (ApoB) pre-mRNA (Navaratnam et al., 1993).

In general, AID/APOBEC proteins play essential roles in cellular innate and adaptive immune responses. AID contributes to antigen-driven antibody diversification processes, while A3 proteins participate in the innate defense against viruses and retroelements. The functions of A2 and A4 proteins in humans remain elusive. Given their ability to mutate DNA, a role for the AID/APOBEC family in tumorigenesis has been proposed.

1.4.1 The APOBEC3 (A3) protein family

All members of the A3 family share a conserved zinc-coordinating cytidine deaminase (CD) domain characterized by the amino acid sequence motif H-X-E-X₂₃₋₂₈-P-C-X₂₋₄-C (X represents any amino acid; Wedekind et al., 2003). Within the A3 family, A3A, A3C and A3H feature a single CD domain, whereas A3B, A3D, A3F and A3G comprise two zinc-coordinating domains in tandem (Kitamura et al., 2011). However, only the C-terminal deaminase domain is catalytically active (Navarro et al., 2005; Prohaska et al., 2014). The core structure of all AID/APOBEC cytidine deaminases domains consists of five β -strands and six α -helices (Holden et al., 2008; Figure 5B). The β -strands form a hydrophobic β -sheet, while the α -helices stabilize the histidine and the cysteine residues that coordinate the zinc ion and thus generate the catalytic pocket (Conticello, 2008). The cytidine molecule bound within this pocket is deaminated through a nucleophilic attack by an activated water molecule (coordinated by the zinc ion) and a neighboring glutamic acid, serving as a proton donor.

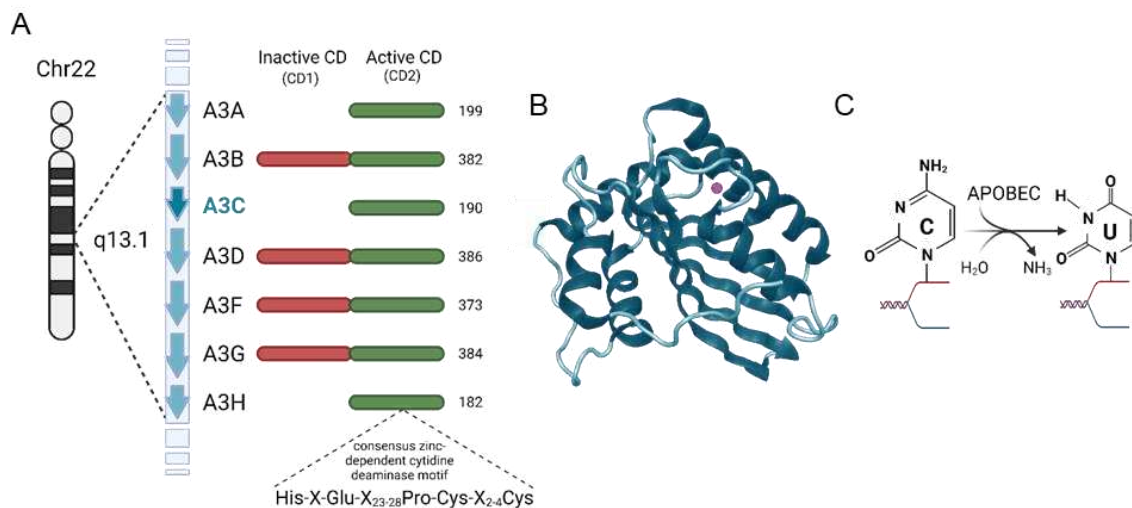


Figure 5: Structure and catalytic activity of APOBEC3 (A3) cytidine deaminase family. (A) The seven members of the human A3 family (A3A-A3D and A3F-A3H) encoded on chromosome 22 are schematically depicted. The proteins consist of one or two zinc-coordinating cytidine deaminase (CD) domains, whereby only one domain is catalytically active (depicted in green). All domains contain the consensus motif H-X-E-X₂₃₋₂₈-P-C-X₂₋₄-C. Numbers on the right correspond to amino acid sequence length for each A3. (B) Crystal structure of A3C with the coordinated zinc ion (purple bubble) is shown (PDB: 3VOW). (C) A schematic of the deamination reaction converting cytidine (C) to uridine (U) catalyzed by APOBEC family members on single-stranded nucleic acids. Schematic modified from (Delviks-Frankenberry et al., 2020; Harris, Dudley, 2015; Kitamura et al., 2011; created with BioRender.com).

A3 proteins possess the ability to assemble into oligomers through both direct protein–protein interactions and indirect nucleic acid-dependent interactions (Li et al., 2014; Salter et al., 2016). The oligomeric state of A3 proteins affects the catalytic function, nucleic acid binding and cellular distribution, mainly by influencing the orientation of loop regions. Studies demonstrated that the A3 protein members A3A and A3C, bearing a single deaminase domain, exist as monomers. In contrast, members with dual deaminase domains are predominantly multimeric (Li et al., 2014). Furthermore, dual deaminase

domain A3 proteins mainly bind RNA via their non-catalytic N-terminal CD domain, resulting in impaired catalytic activity on ssDNA (Friew et al., 2009; Xiao et al., 2017). In the case of A3G, the C-terminal segment is required for ssDNA-binding and deaminase activity, while the N-terminal domain is involved in RNA-binding, RNA-dependent A3G multimerization (Prohaska et al., 2014) and putatively also in RNA-editing (Sharma et al., 2016). Thus, A3G is present in two distinct cytoplasmic forms: low molecular mass (LMM) and high molecular mass (HMM) complexes, where the latter is RNA-dependent (Chiu et al., 2006; Chiu, Greene, 2008; Smith, 2011).

While APOBEC proteins share structural similarities, their nucleic acid binding partners are diverse, encompassing ssDNA and viral or cellular RNA, revealing both specific and non-specific modes of binding. Unlike other enzymes, members of the AID/APOBEC family lack a universal RNA or DNA substrate for cytidine/deoxycytidine deamination (Salter et al., 2016). Instead, A3 proteins have been found to promiscuously interact with diverse RNA classes, such as 7SL RNA, *Alu* RNA, human Y RNAs or mRNA, and with ssDNA from various sources, including genomic DNA, retroelements and viruses (Apolonia et al., 2015; Bach et al., 2008; Salter, Smith, 2018; Smith, 2016). Their substrate preferences vary based on specific sequence motifs and the secondary structures within the nucleic acid sequence (Conticello, 2008; McDaniel et al., 2020; Prohaska et al., 2014). *In vitro* studies revealed that all A3 enzymes show detectable deamination activity on ssDNA (Ito et al., 2017), primarily within di-nucleotide motifs of 5'-CC-3' or 5'-TC-3' (McDaniel et al., 2020; Salter et al., 2016; Silvas, Schiffer, 2019), as well as in tri-nucleotide motifs of 5'-TCA-3' or 5'-TCT-3' (Ebrahimi et al., 2014; Ito et al., 2017). However, it is important to note that not all putative editing sites are equally deaminated, underscoring the significance of both the sequence context and secondary structure in substrate recognition (McDaniel et al., 2020). Notably, the ability to target specific RNAs for C-to-U editing has only been reported for A3A in monocytes (Sharma et al., 2015) and for A3G upon transient expression in HEK293T cells (Sharma et al., 2016), in addition to the well-known mRNA-editing activity of A1. This highlights the multifaceted nature of RNA-binding by A3 proteins, raising questions about additional functions in RNA-related processes. Indeed, it has been proposed that A3 binding to both coding and non-coding RNA may serve deamination-independent roles, potentially involving the redistribution or sequestration of RNAs in cellular compartments like processing bodies (P-bodies) and stress granules, facilitating further processing in response to environmental changes (Hakata, Miyazawa, 2020; Smith, 2016). Further research is required to unravel the full extent of these intriguing functions.

Because of the similar overall fold of A3 active domains, differences in sequence preference cannot be attributed to major structural features. Instead, variations in the length, composition and spatial location of loop regions play a pivotal role in substrate recognition, binding affinity and overall function among A3 family members (Salter et al., 2016; Silvas,

Schiffer, 2019). Moreover, considering that A3 proteins bind non-selectively to cellular and viral RNAs, interactions with cofactors are crucial for sequence specificity. For example, A1 associates with A1CF, enabling site-specific editing of ApoB mRNA, compensating for its genuinely low RNA-binding sequence specificity (Lellek et al., 2000; Salter et al., 2016; Smith et al., 2012). Unlike RNA-editing, ssDNA-editing does not require interaction with cofactors (Smith et al., 2012).

In summary, A3 proteins feature conserved cytidine deaminase domains responsible for catalyzing the conversion of cytidines within nucleic acids. Interestingly, research indicates that not all predicted cytidine deaminase domains are catalytically active nor are all putative editing sites subjected to deamination, suggesting the existence of functions independent of the deamination activity. A3 proteins bind promiscuously to both ssDNA and RNA. Intriguingly, each member of the A3 family demonstrates unique preferences for target sequences and distinct subcellular localization patterns. These features, together with their ability to form multimers and to interact with cofactors, underscore the diverse and essential role of A3 proteins in human health and disease.

1.4.2 Main function of the A3 family

Proteins of the APOBEC/AID family are key players in the complex landscape of the human immune system (Figure 6). As part of the adaptive immune system, the cytidine activity of AID, highly expressed in activated B-cells, induces point mutations and double-strand breaks within the genomic immunoglobulin (Ig) loci (Moris et al., 2014; Muramatsu et al., 2000). This process facilitates antibody diversification through class switch recombination and somatic hypermutation, ultimately resulting in B-cell maturation (Hwang et al., 2015).

Complementary to the basal function of AID in adaptive immunity, A3 proteins play a critical role in innate immunity by restricting both exogenous viruses and endogenous retroelements (Figure 6). A3G, most extensively studied within the protein family in this regard, was the first cytidine deaminase shown to restrict HIV-1 infection (Harris et al., 2003; Sheehy et al., 2002). Briefly, A3G is incorporated into budding virions, followed by the deamination of cytidines within viral cDNA during reverse transcription upon infection of susceptible cells. The generated uracils then act as templates for adenine incorporation, leading to distinctive G-to-A hypermutations in the proviral DNA plus strand, which severely impairs viral viability (Harris et al., 2003; Mangeat et al., 2003; Zhang et al., 2003).

Notably, all seven human A3 proteins exhibit, to varying degrees, viral restriction potential (Knisbacher et al., 2016; Sheehy, Erthal, 2012), differing in their target specificity and restriction efficacy (Bishop et al., 2006; Hultquist et al., 2011). A3C, for instance, while detectable in HIV-1 virions, exhibits only a weak activity against this virus and induces less cytidine deaminations in HIV-1 DNA compared to A3G (Langlois et al., 2005; Yu et al., 2004). Furthermore, the antiviral activity of A3 proteins extends beyond retroviruses, effectively targeting a wide range of viruses, including herpes simplex virus-1 (Suspène et al., 2011), hepatitis viruses (Peng et al., 2011; Turelli et al., 2004), parvoviruses (Narvaiza et al., 2009) and papillomaviruses (Vartanian et al., 2008; reviewed in Harris, Dudley, 2015; Koito, Ikeda, 2012; Moris et al., 2014).

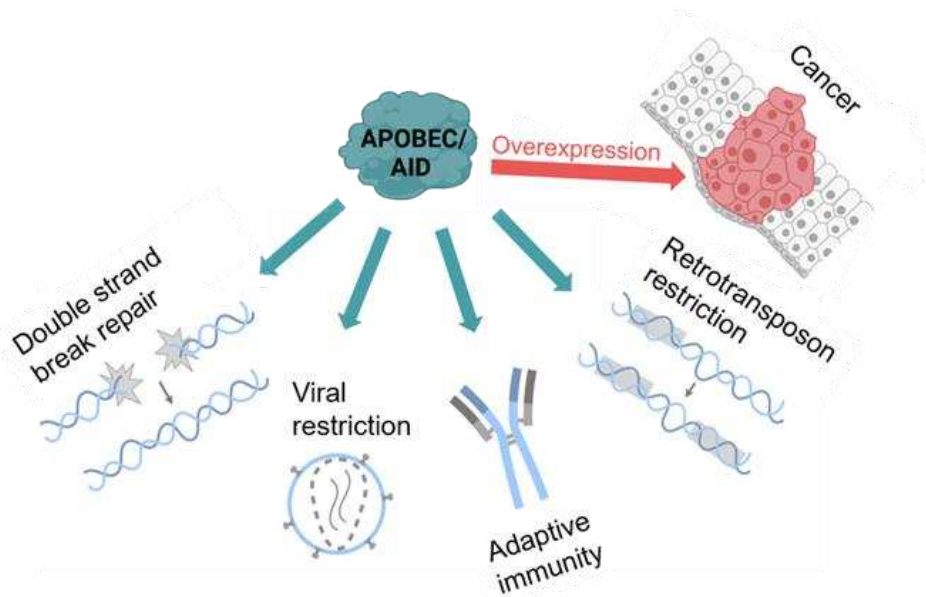


Figure 6: Functions of cytidine deamination by the APOBEC family. The schematic displays the effects that result from the deamination reaction. Turquoise arrows represent functions in the cell that are promoted or inhibited by the APOBEC/AID family. Red arrow represents the consequence of overexpressed family members. Schematic modified from (Silvas, Schiffer, 2019).

In addition to the deaminase-dependent mechanism of viral restriction, catalytic activity-independent restriction strategies were proposed (Harris, Dudley, 2015). These mechanisms encompass genomic RNA-binding, interference with reverse transcription initiation or direct interaction with reverse transcriptase (Hakata, Miyazawa, 2020; Holmes et al., 2007a; Holmes et al., 2007b; Newman et al., 2005). The predominant model suggests that genomic RNA-binding induces a steric impediment to reverse transcription.

The original A3 targets may have been endogenous genetic transposable elements (Arias et al., 2012; Schumann, 2007), as invasion of transposable elements coincided with the emergence of the A3 genes, which occurred approximately 33 million years ago (Uriu et al., 2021). These elements, known as retrotransposons, replicate via RNA intermediates followed by reverse transcription, dsDNA synthesis and integration at new genomic locations (Feng et al., 2017). Retrotransposons comprise two groups based on the

presence or absence of long terminal repeats (LTR). Non-LTR retrotransposons include LINE (long interspersed nuclear element) such as LINE-1 and SINE (short interspersed nuclear element) such as *Alu* elements. Across eukaryotic genomes, retrotransposons constitute a substantial portion, contributing to approximately 45% of the human genome (Arias et al., 2012; Koito, Ikeda, 2012). Insertions of retrotransposons into random locations within the genome lead to genomic instability, causing genetic diseases such as hemophilia A (Arias et al., 2012; Kazazian et al., 1988). To counteract these deleterious effects, mammals have developed intrinsic immunity mechanisms, involving A3 proteins, that provide resistance against retrotransposition (Modenini et al., 2022). Experimental assays have demonstrated that all human A3 proteins are able to inhibit various classes of retroelements, including LINE-1 and *Alu* elements, albeit at varying rates (Arias et al., 2012; Kinomoto et al., 2007).

In parallel to virus restriction, several mechanisms have been proposed to inhibit retrotransposition. A deamination-dependent mechanism to restrict LINE-1 retrotransposition has been reported for A3A, as transiently exposed single-stranded LINE-1 cDNA is subjected to A3A-mediated C-to-U deamination (Richardson et al., 2014). Uracils in DNA trigger cDNA degradation through the host base excision repair pathway, generating abasic sites and nicks, or result in transition mutations using uracil as a template, leaving functionally inactive LINE-1 (Feng et al., 2017). Deamination-independent mechanisms include blocking reverse transcriptase DNA polymerization or the transport of LINE-1 RNA into the nucleus and sequestering retrotransposon RNPs in high molecular weight cytoplasmic complexes such as stress granules and P-bodies for potential degradation by RNA interference (Chiu et al., 2006; Feng et al., 2017; Gallois-Montbrun et al., 2007; Lu et al., 2011). For instance, A3C has been shown to restrict LINE-1 retrotransposons in a deamination-independent manner by forming RNA-dependent RNPs, resulting in co-localization with stress granules and interference with reverse transcriptase (Horn et al., 2014). This suggests that A3C may prevent the entry of LINE-1 RNPs into the nucleus by sequestering them through A3C-mediated interactions.

In conclusion, A3 proteins, with their mutation-inducing potential, can be seen as double-edged swords in cellular biology. On the one edge, they serve as an intrinsic immune defense system against viruses and maintain genomic integrity. However, on the other edge, their potent enzymatic activity can catalyze 'off-target' cytidine deaminations in genomic ssDNA intermediates when not tightly regulated, potentially resulting in carcinogenesis (Figure 6; Henderson, Fenton, 2015; Rebhandl et al., 2015).

1.4.3 The role of A3 proteins in cancer

Cancer is characterized by uncontrolled cell growth, driven by somatic mutations in oncogenes and tumor suppressor genes. Mutations can be random events induced by DNA

replication errors or by DNA damaging agents (Granadillo Rodríguez et al., 2020). Approximately a decade ago, distinct mutation signatures were identified in multiple human cancers by genome sequencing (Alexandrov et al., 2013; Burns et al., 2013b; Nik-Zainal et al., 2012; Roberts et al., 2013). These unique signatures have been attributed to the AID/APOBEC family of deaminases, specifically due to the enrichment of C-to-T substitutions within the 5'-TCW-3' substrate motif. The deamination activity of AID/APOBEC proteins in ssDNA leads to C>T transitions and C>G or C>A transversion (Rebhandl et al., 2015). These induced point mutations contribute to genomic variations, ultimately affecting critical cellular processes such as sustained proliferative signaling, evasion of growth suppressors and genome instability (Granadillo Rodríguez et al., 2020; Guo et al., 2022; Shilova et al., 2022; Swanton et al., 2015).

The initial evidence of APOBEC-induced mutation clusters was observed in somatic mutations at TpC dinucleotides within regions of chromosomal rearrangements in breast cancer (Nik-Zainal et al., 2012). Subsequent studies have reinforced the prevalence of the APOBEC mutation signature, ranking it second after age-related signatures characterized by C-to-T substitutions at NpCpG trinucleotides (Alexandrov et al., 2013). Moreover, pan-cancer screens have identified the APOBEC mutation signature in over 50% of human cancer types with breast, head/neck, lung, bladder and cervical cancers exhibiting the highest APOBEC-induced mutation burdens (Burns et al., 2013b; Roberts et al., 2013). Interestingly, these studies also revealed that some cancer types, including ccRCC, lack this specific APOBEC mutation signature.

While all members of the A3 family possess ssDNA deamination activity, A3A and A3B have emerged as key contributors to the APOBEC mutation signature (Burns et al., 2013a; Chen et al., 2019; Guo et al., 2022). Consequently, these members have gained significant attention in cancer research. Their involvement in somatic mutagenesis relies on their ability to localize to the nucleus, for instance by harboring a NLS as present in A3B (Salamango et al., 2018). In the nucleus, they catalyze the deamination of transiently accessible ssDNA occurring during processes like transcription, replication or double-strand break repair, driving somatic mutations within preferred A3 motifs (Hoopes et al., 2016; Lackey et al., 2013; Rebhandl et al., 2015).

Furthermore, increasing evidence supports the notion that A3 genes, especially A3B, are often deregulated in various cancer types. This deregulation can occur through mechanisms such as increased transcription, alternative splicing of mRNAs, localization changes, post-translational modifications, turnover modulation, copy number alterations and interactions with other proteins or RNAs (Henderson, Fenton, 2015; Rebhandl et al., 2015; Salter et al., 2016). Consequently, overexpression of A3B has been observed in several malignancies and is closely associated with the initiation and progression of cancer (Guo et al., 2022; Luo et al., 2021). In breast cancer, A3B mRNA is upregulated in 90% of

cell lines and 65% of primary tissue samples (Burns et al., 2013a), correlating with higher mutation rates, including *TP53* mutations (Olson et al., 2018). Moreover, A3A is elevated in various cancers, including ovarian, breast and pancreatic cancer, leading to distinct mutation signatures and cancer progression (Cortez et al., 2019; Wörmann et al., 2021; Xu et al., 2021). A3A, in particular, seems to be the more potent mutator due to its proficiency in generating DNA breaks, which can induce the formation of single-stranded hypermutation substrates (Chan et al., 2015; Cortez et al., 2019; Jalili et al., 2020).

In addition to A3A and A3B, other A3 proteins have also been implicated in cancer (Guo et al., 2022; Nowarski, Kotler, 2013). A3G, highly expressed in lymphoma cells, acts as a pro-survival factor (Nowarski et al., 2012; Nowarski, Kotler, 2013). In colorectal tumors, A3G has been shown to promote metastasis by a mechanism that involves inhibition of miR-29-mediated suppression of MMP2, a well-known metastasis activator (Ding et al., 2011). It has been suggested that A3G counteracts the miRNA-mediated inhibition of protein synthesis by releasing target mRNA from bound miRNA in P-bodies, thereby enhancing the expression level of miRNA-targeted mRNA (Huang et al., 2007; Zhang, 2010).

Furthermore, A3G expression has been linked to unfavorable prognosis and increased immune infiltration in ccRCC (Peng et al., 2022). This study further revealed significantly higher mRNA levels of A3C/D/G/H in ccRCC tumor tissue compared to normal tissue, and high expression levels of A3B/C/D/G/H were predictive of poor prognosis (Peng et al., 2022). However, the specific molecular mechanisms resulting in tumor progression remain to be elucidated.

Recent research has highlighted the crucial role of the A3 family in driving genomic instability, intra-tumor heterogeneity and branched evolution in cancer cells, contributing to subclonal mutations (Bruin et al., 2014; Guo et al., 2022; Rosenthal et al., 2016; Venkatesan et al., 2022). A strong correlation exists between A3 mutation signatures and the overall number of subclonal mutations (Jamal-Hanjani et al., 2017). Genomic intra-tumor heterogeneity is clinically relevant as it is associated with immune evasion, anti-cancer treatment resistance and disease progression (Venkatesan et al., 2022). Understanding the underlying mechanisms that fuel cancer diversity is an essential step in developing strategies to attenuate tumor evolution and adaptation. Targeting A3 family members may be a promising approach to impair tumor diversity and subclonal evolution.

However, despite the observed increased expression or altered localization of A3 family members, including A3C, in various cancer tissues, including ccRCC, their precise roles in oncogenesis remain uncertain. Notably, ccRCC lacks an APOBEC-mediated mutation signature, raising questions about the specific functions of A3 proteins like A3C in this cancer type. Thus, further research is desperately needed to unravel the great significance that A3 proteins may play in tumor development and progression across diverse cancers, ultimately leading to improved patient outcomes.

1.5 Aims of the study

Clear cell renal cell carcinoma (ccRCC), the predominant RCC subtype, presents unique challenges, as it is resistant to traditional chemotherapy and radiation therapy. While novel immunotherapies have become the standard treatment for ccRCC, the existence of non-responsive and progressing patients emphasize the need for innovative therapeutic strategies targeting advanced ccRCC.

The AID/APOBEC protein family, a family of cytidine deaminases, has been reported to be overexpressed in various cancer types, including ccRCC, correlating with poor outcomes, treatment resistance and metastasis. While A3A and A3B have been extensively studied in the context of cancer-related APOBEC-mediated mutagenesis, other family members like A3G and A3F have primarily been investigated for their antiviral immune activity. Despite extensive research on the AID/APOBEC protein family, the specific molecular functions of other family members, especially A3C, remain largely unclear.

A3C stands out as the most abundantly expressed family member across various tissues and cancer cell lines (Jarmuz et al., 2002). However, in ccRCC, where the characteristic APOBEC-induced mutation signature is absent, the functions of A3 proteins, particularly A3C, remain elusive. Further research is needed considering that some studies have suggested the existence of deamination-independent roles for these proteins. This study aims to address these gaps in knowledge.

Specifically, this study has four objectives:

- (I) To explore the molecular mechanisms responsible for the upregulation of A3C in ccRCC. This will entail analyzing the A3C gene structure, including the deletion of the 3' UTR region containing regulatory elements.
- (II) To investigate the oncogenic role of A3C in ccRCC, including its impact on cell survival, cancer progression and stress response. This will be achieved through transcriptome analyses in ccRCC-derived cell lines upon modulation of A3C expression. Additionally, cell-based phenotypic assays and xenograft studies will be conducted to confirm the oncogenic potential of A3C *in vivo*.
- (III) To identify novel mRNAs directly associating with A3C. This will involve RNA co-Immunoprecipitation studies, also with a focus on investigating the C-to-T editing activity of A3C. Reporter analyses, RNA decay and signaling pathway investigations via Western blotting will be used to characterize A3C-dependent control of RNA fate.
- (IV) To assess the therapeutic target potential of A3C in ccRCC treatment. Initial testing will involve the use of small-molecule inhibitors in ccRCC-derived cell models to evaluate their efficacy in dependence on A3C levels.

2 MATERIAL AND METHODS

2.1 Material

2.1.1 Chemicals and reagents

All chemicals used in this study were obtained from Thermo Fisher Scientific, Carl Roth, Sigma Aldrich, Promega and Jena Bioscience. Cell culture dishes were received from Techno Plastic Products and Corning. Cell culture medium, Opti-MEM and Trypsin were supplied by Thermo Fisher Scientific. Fetal bovine serum (FBS) provided by Pan Biotech was used. Transfection reagents were obtained from Thermo Fisher Scientific or Horizon. Restriction enzymes, corresponding reaction buffers, DNA markers, protein ladders, cloning kits and ligase enzyme were purchased from New England Biolabs and Promega. Master mix for qRT-PCR was received from High Qu GmbH.

2.1.2 Standard systems and Kits

Unless otherwise stated, all standard systems and kits were used according to the manufacturers' instructions.

Table 1: Commercial kits

Kit	company	Cat. No.
Agarose Gel Extraction Kit	Jena Bioscience	PP-202
Caspase-Glo® 3/7 Assay System	Promega	G8090
CellTiter-Glo® Luminescent Cell Viability Assay	Promega	G7570
Click-iT® Nascent RNA Capture Kit	Thermo Fisher Scientific	C10365
DC Protein Assay	Bio-Rad	5000111
Dual-Glo® Luciferase Assay System	Promega	E2920
ORA™ qPCR Green ROX L Mix	HighQu	QPD0101
Phusion® High-Fidelity PCR Kit	New England Biolabs	E0553
Plasmid Mini-Prep Kit	Jena Bioscience	PP-204
PureLink™ HiPure Plasmid Midiprep Kit	Thermo Fisher Scientific	K210004
PureLink™ Genomic DNA Mini Kit	Thermo Fisher Scientific	K182001
SuperScript® VILO™ cDNA synthesis kit	Thermo Fisher Scientific	11754-050
Zero Blunt® PCR Cloning Kit	Thermo Fisher Scientific	K27002

2.1.3 Standard buffers

Table 2: Composition of standard buffers

Name	Recipe
2x FASB	93.65% (v/v) Formamide 0.025% (w/v) SDS 18 mM EDTA 0.25% (w/v) Bromphenol blue
Fractionation buffer	10 mM Hepes-KOH (pH 7.2) 150 mM KCl 5 mM MgCl ₂ Digitonin (concentration depends on cell line)
Gradient lysis buffer	10 mM HEPES-KOH (pH 7.2) 150 mM KCl 5 mM MgCl ₂ 0.5% (v/v) NP-40
MES buffer	50 mM MES 50 mM Tris 1 mM EDTA 0.1% (w/v) SDS
NuPAGE blotting buffer	50 mM Tris 40 mM glycerin 0.04% (w/v) SDS 10% (v/v) methanol
PBS (phosphate buffered saline; 0.01 M)	137 mM NaCl 2.7 mM KCl 10 mM Na ₂ HPO ₄ 2 mM KH ₂ PO ₄
PBS-T (phosphate buffered saline-Tween)	0.01 M PBS 1% (v/v) Tween-20
Ponceau-S	0.1% (w/v) Ponceau S 5% (v/v) acetic acid
RIP buffer	10 mM Hepes-KOH (pH 7.2) 300 M KCl 5 mM MgCl ₂ 0.5% (v/v) NP-40
TAE (Tris/Acetate/EDTA)	40 mM Tris 20 mM acetic acid 1 mM EDTA
TBE (Tris/Borate/EDTA)	45 mM Tris 45 Mm borate 1 mM EDTA
Total lysis buffer	50 mM Tris (pH 7.4) 50 mM NaCl 1% (w/v) SDS 2 mM MgCl ₂ 0.2% (v/v) Turbo Nuclease

Name	Recipe
TRIzol	0.8 M guanidinium thiocyanate 0.4 M ammonium thiocyanate 0.1 M sodium acetate (pH 0.5) 5% (v/v) Glycerin 48% (v/v) Roti@Aqua Phenol
Trypsin-EDTA	0.05% (v/v) Trypsin 0.4 mM EDTA sterile PBS

2.1.4 Primary and secondary antibodies

Table 3: Primary antibodies

Primary antibodies	Species	Company	Cat. No.
A3C	rabbit	Genetex	GTX102164
AGO2	mouse	Abcam	ab57113
BCL2	rabbit	Cell signaling	#2872
BIRC3	rabbit	Abcam	ab32059
BIRC5	rabbit	Novus	nb500-201
C3	rabbit	Genetex	GTX101316
CDK6	mouse	Cell signaling	#3136
DCP1A	rabbit	Bethyl	A303-592A
EEF2	mouse	Santa Cruz	sc-166409
ERK1/2	rabbit	Cell signaling	#4695
FLAG	mouse	Sigma Aldrich	F3165
GFP (for IP)	mouse	Roche	11814460001
GFP (for WB)	rabbit	Cell signaling	#2956S
HUR	mouse	Santa Cruz	sc-5261
IGF2BP1	mouse	BSBS AB facility	Stohr et al., 2012
IKBKA	mouse	Cell signaling	#11930
IKBKB	rabbit	Cell signaling	#8943
I κ B α	mouse	Cell signaling	#4814
NF- κ B1	rabbit	Cell signaling	#3035
NF- κ B2	rabbit	Cell signaling	#4882
p38	rabbit	Cell signaling	#9212
PABP	mouse	Santa Cruz	sc-32318
p-p38 (Thr180/Tyr182)	mouse	Cell signaling	#9216
p-ERK1/2 (Thr202/Tyr204)	mouse	Cell signaling	#9106
p-I κ B α (Ser32/Ser36)	rabbit	Cell signaling	#2859
p-RelA (Ser536)	rabbit	Cell signaling	#3033

Primary antibodies	Species	Company	Cat. No.
PTB	mouse	Antibody Facility, Braunschweig, Germany	
RelA	rabbit	Cell signaling	#8242
RelB	rabbit	Cell signaling	#4922
Ro60	mouse	Santa Cruz	sc-100844
RPL5	rabbit	Bethyl	A303-933A
RPL7	rabbit	Bethyl	A300-741A
STAT1	mouse	Cell signaling	#9176
VCL	mouse	Sigma Aldrich	V9131
YB1	rabbit	Abcam	ab12148

Table 4: Secondary antibodies

Secondary antibodies for Western blotting	Company	Cat. No.
IRDye 680RD Donkey anti-Mouse IgG	Li-COR	926-68072
IRDye 680RD Donkey anti-Rabbit IgG	Li-COR	926-68073
IRDye 800CW Donkey anti-Mouse IgG	Li-COR	926-32212
IRDye 800CW Donkey anti-Rabbit IgG	Li-COR	926-32213
Secondary antibodies for immunofluorescence imaging	Antigen	Company
anti-mouse Cy5	mouse IgG	Dianova
anti-rabbit Cy3	rabbit IgG	Dianova

2.1.5 Bacteria strain

Transformation of plasmids was performed in the bacteria strain *Escherichia coli* TOP10 (genotype: F-mcrA $\Delta(mrr-hsdRMS-mcrBC)$ $\Phi 80lacZ\Delta M15 \Delta lacX74 recA1 deoR araD139 \Delta(ara-leu)7697 galU galK rpsL$ (StrR) *endA1 nupG*). Bacteria were cultivated in lysogeny broth (LB) culture medium (1% (w/v) Trypton; 0.5% (w/v) yeast extract; 1% (w/v) NaCl). To selectively propagate recombinant bacterial populations, the LB culture medium was supplemented with antibiotics (30 $\mu\text{g}/\text{mL}$ Kanamycin or 150 $\mu\text{g}/\text{mL}$ Ampicillin). Additionally, 1.5% (w/v) Agar was added to the liquid medium to culture bacteria on LB dishes.

2.1.6 Plasmids

In this study, various plasmids (as listed in Table 5) served as cloning vectors for modifying protein expression or as reporter vectors.

Table 5: Commercial and generated plasmids

Plasmids	Company	Cat. No.
pCR®-blunt	Thermo Fisher Scientific	K270020
pcDNA3.1	Addgene	128047
pcDNA3.1-Cas9-T2A-GFP	Prof. Hüttelmaier	
pEGFP-C2	Clontech	632481
pEGFP-C2-A3C	this study	
pLVX	Clontech	632164
pLVX-SBP-FLAG-RFP-A3C	this study	
pLVX-SBP-FLAG-RFP-A3C	this study	
pLVX-Puro-shRNA3	Prof. Hüttelmaier	
pLVX-Puro-shRNA3-shA3C	this study	
pmirGLO Dual luciferase	Promega	E1330
pmirGLO-long (A3C) 3' UTR	this study	
pmirGLO-flipped <i>Alu</i>	this study	
pmirGLO- Δ <i>Alu</i>	this study	
pmirGLO- Δ <i>Alu</i> F1 + F2	this study	
pmirGLO- Δ <i>Alu</i> F1 + F3	this study	
pmirGLO- Δ <i>Alu</i> F2 + F3	this study	
pmirGLO-mir17 as	Prof. Hüttelmaier	
pmirGLO-CDK6 3' UTR_2	this study	
pmirGLO-CDK6 3' UTR 3	this study	
pmirGLO-IKBKA 3' UTR_1	this study	
pmirGLO- IKBKA 3' UTR_2	this study	
pmirGLO- IKBKA 3' UTR_3	this study	
pmirGLO-MAP3K7 3' UTR	this study	
pmirGLO-MTPN 3' UTR	this study	
pmirGLO-TAB3 3' UTR	this study	
pmirGLO-1st kb of CDK6 3' UTR	this study	
pmirGLO-2 BS in CDK6 3' UTR	this study	
pmirGLO-500 bp of IKBKA 3' UTR	this study	
pmirGLO-Promo+Stopp*HindIII-EV	Prof. Hüttelmaier	
pmirGLO-Promo+Stopp*HindIII-NF- κ B	this study	
pSG-leer-RFP + BbsI-GFP -EV-	Prof. Hüttelmaier	
pSG-sgRNA3-A3C#1-RFP	this study	
pSG-sgRNA3-A3C#3-RFP	this study	
pSG-sgRNA3-3'UTR_A3C_start-RFP	this study	
pSG-sgRNA3-3'UTR_A3C_end-RFP	this study	

2.1.7 Cell lines

Unless stated otherwise, cell lines were purchased from ATCC.

Table 6: Parental cell lines

Cell line	Origin	Cat. No.	Publication
769-P	Kidney, adenocarcinoma	CRL-1933	(Dobashi et al., 2009)
786-O	Kidney, adenocarcinoma	CRL-1932	(Dobashi et al., 2009); (Blankenship et al., 1999)
A-704	Kidney, adenocarcinoma	HTB-45	(Bernard et al., 2001)
ACHN	Kidney, adenocarcinoma	CRL-1611	(Rohde et al., 1998)
HCT116	Large intestine, colon	kindly provided by Prof. Gutschner	
HEK293T	Human embryonic kidney	CRL-11268	(DuBridg e et al., 1987; Graham et al., 1977)
RPTEC/ERT1	Kidney, proximal tubule	CRL-4031	(Jennings et al., 2012)

Table 7: Cell clones generated by the CRISPR/Cas9 system

Cell clone	Parental cell line	Reference
786-O A3C knockout	786-O	this study
786-O A3C 3' UTR deletion	786-O	this study
769-P A3C knockout	769-P	this study
HCT116 DICER knockout	HCT116	Prof. Gutschner

2.1.8 Animals

In this study, the immunodeficient athymic nude mouse strain Crl:NU(NCr)-Foxn1nu was used. Mouse strain was purchased from Charles River Laboratories (Wilmington, MA, US).

2.1.9 Patient samples

The RCC cohort is composed of 38 patient tissue samples (Table 8). The normal tissue samples originated from tumor adjacent tissue in five cases from ccRCC patients, in one

case from a collecting duct carcinoma patient, in one case from a chromophobe renal cell carcinoma patient and in one case from an oncocytoma patient.

Table 8: Patient tissue samples

Sequenced samples	E/CCC number	Tissue type
NH2	2016-89.02	ccRCC
NH3	2016-89.03	normal tissue
NH4	2016-89.04	ccRCC
NH6	2016-89.06	Bellini duct carcinoma
NH7	2016-89.07	papRCC Type 2
NH9	2016-89.09	papRCC Type 1
NH11	2016-89.11	papRCC Type 2
NH12	2016-89.12	normal tissue
NH13	2016-89.13	papRCC Type 2
NH14	2016-89.14	normal tissue
NH15	2016-89.15	ccRCC
NH16	2016-89.16	chrRCC
NH17	2016-89.17	normal tissue
NH18	2016-89.18	chrRCC
NH19	2016-89.19	papRCC Type 1
NH20	2016-89.20	papRCC Type 1
NH21	2016-89.21	chrRCC
NH22	2016-89.22	oncocytoma
NH23	2016-89.23	normal tissue
NH26	2016-89.26	oncocytoma
NH27	2016-89.27	normal tissue
NH28	2016-89.28	Bellini duct carcinoma
NH29	2016-89.29	normal tissue
NH30	2016-89.30	ccRCC
NH31	2016-89.31	ccRCC
NH32	2016-89.32	normal tissue
NH33	2016-89.33	normal tissue
NH34	2016-89.34	ccRCC
NH35	2016-89.35	normal tissue
NH36	2016-89.36	ccRCC
NH37	2016-89.37	normal tissue
NH38	2016-89.38	ccRCC

2.1.10 Oligonucleotides

All oligonucleotides, siRNAs and sgRNAs were purchased from Eurofins Genomics GmbH. Oligonucleotides for cloning were used to generate diverse plasmids (listed in Table 9) either for gene expression manipulation or for reporter vectors.

Table 9: Oligonucleotides for molecular cloning

Name	Sequence sense (5' – 3')	Restriction site
A3C fwd	GGGAATTCATGAATCCACAGATCAGAAACCCGATGAAG	EcoRI
A3C rev	GGCTCGAGTCACTGGAGACTCTCCCGTAGCCTTCTTTT	XhoI
A3G fwd	GGGAATTCATGAAGCCTCACTTCAGAAACACAGTGGAG	EcoRI
A3G rev	GGCTCGAGTCACTTTTTCTGATTCTGGAGAATGGCCCG	XhoI
A3C 3' UTR fwd	GGGCTAGCGGGTCTCCCTGGGCCTCATGGTCTGTC	NheI
A3C 3' UTR rev	GGCTCGAGTCTTGTTAAGGGTGACAGCCTGCAAGGT	XhoI
revAlu1 for	GGCCTAGGTTATTTTCAGGCAGGGTCTCTATCTGTTGC	AvrII
revAlu1 rev	CCATCGATTGGGCATGGTGACTCACGCCTGTAATCCC	Clal
A3C Δ Alu F1 rev	CCCTCGAGTTACCGCGGTTAGAATTCTAGGATGAGTTTA GTAAGATTTGGT	EcoRI
A3C Δ Alu F2 fwd	GGGAATTCGATAAATAAACTCAACCTAACAGG	EcoRI
A3C Δ Alu F2 rev	GGCCGCGGGATGATATTTGGAGGCAGAGAGATC	SacII
A3C Δ Alu F3 fwd	GGCCGCGGGGATCATATGTTCCACACATGTTT	SacII
NF- κ B fwd	TGAATTCGGGAATTTCCGGGGACTTTC	EcoRI
NF- κ B rev	TGGATCCGGTGGCTTTACCAACAGTAC	BamHI
CDK6 3' UTR_2 fwd	CTAGCTAAAACAAATCCCAGCAGTAATACATTTCTTAAA CCTCACAGTGCATGATATATCTTTTG	NheI
CDK6 3' UTR_2 rev	TCGACAAAAGATATATCATGCACTGTGAGGTTTAAGAAA TGTATTACTGCTGGGATTTGTTTTAG	XhoI
CDK6 3' UTR_3 fwd	CTAGCATAAAAAGGGATTTTAAACAACCAACAATTCCCAAC ACCTCAAAAAGCTTGTTGCATTTTTTGG	NheI
CDK6 3' UTR_3 rev	TCGACCAAAAATGCAACAAGCTTTTGAGGTGTTGGGA ATTGTTGGTTGTTAAAATCCCTTTTATG	XhoI
IKBKA 3' UTR_1 fwd	CTAGCTAAGACCAAATGTAGTTTTGTATACAGAGAAGAA AACCTCAAGTAATAGGCATTTTAAGTAG	NheI
IKBKA 3' UTR_1 rev	TCGACTACTTAAAATGCCTATTACTTGAGGTTTTCTTCTC TGATACAAAACACTACATTTGGTCTTAG	XhoI
IKBKA 3' UTR_2 fwd	CTAGCCAAGTTCTATTTCTTGAAGAATAAATTCTACCTCC TTGTGTTGCACTGAACAGGG	NheI
IKBKA 3' UTR_2 rev	TCGACCCTGTTTCAGTGCAACACAAGGAGGTAGAATTTAT TCTTCAAGAAATAGAACTTGG	XhoI
IKBKA 3' UTR_3 fwd	CTAGCTCAGGAGAAGTTCGGTTTAGTAGCCATTTACCTC AACCAATAGCCTTTGTAGTTG	NheI
IKBKA 3' UTR_3 rev	TCGACAACACTACAAAGGCTATTTGGTTGAGGTAAATGGCT ACTAAACCGAACTTCTCCTGAG	XhoI
MAP3K7 3' UTR fwd	CTAGCTCCATTTTTTTCATATTAGAGGTGGAACCTCAAGA ATGACTTTATTCTTGTAG	NheI
MAP3K7 3' UTR rev	TCGACTACAAGAATAAAGTCATTCTTGAGGTTCCACCTC TAATATGAAAAAATGGAG	XhoI
MTPN 3' UTR fwd	CTAGCTGCTAAAAATATTAAGACCAAGTCATGCAATAAT TGAATGTACCTCAAATTTTTAGGGGAGGGTGGGG	NheI
MTPN 3' UTR rev	TCGACCCACCCCTCCCCTAAAAATTTGAGGTACATTCAA TTATTGCATGACTTGGTCTTAATTTTTTAGCAG	XhoI
TAB3 3' UTR fwd	CTAGCGAACGAACAGAACAGAAGTGCAGCTACTCCTCC	NheI

Name	Sequence sense (5' – 3')	Restriction site
	TTCACAACCACCTCAACAGCCATCTTCCATGCAAAG	
TAB3 3' UTR rev	TCGACTTTGCATGGAAGATGGCTGTTGAGGTGGTTGTG AAGGAGGAGTAGCTGCACTTCTGTTCTGTTTCGTTTCG	XhoI
1st kb of CDK6 3' UTR fwd	GGTCTAGAGGCCTCAGCAGCCGCCTTAAGC	XbaI
1st kb of CDK6 3' UTR rev	GGCTCGAGGTTAGAGAGAACTACTCTCCAAACCAAAC	XhoI
2 BS in CDK6 3' UTR fwd	GGGCTAGCAATATTTCTGTGATCACCAAC	NheI
2 BS in CDK6 3' UTR rev	GGCTCGAGCTGCTCTTCTATACCAAACACTTG	XhoI
500 bp of IKBKA 3' UTR fwd	GGGCTAGCAGCCTCTAAACAGACAGGAATTTAG	NheI
500 bp of IKBKA 3' UTR rev	GGCTCGAGACAGGCATCTTCTCTTTGATATTATTAATG	XhoI

Table 10: Oligonucleotides for qRT-PCR

Gene	Sequence sense (5' – 3')	Sequence antisense (5' – 3')
A3C	GGGAAGCCAACGATCGGAA	CAGTATGTCGTCGCAGAACCA
ACTB	AGAAAATCTGGCACCACACC	AGAGGCGTACAGGGATAGCA
BCL2	ACTGAGTACCTGAACCGGCA	AGAAAATCAAACAGAGGCCGCA
BCL3	CCGGAGGCGCTTTACTACC	TGGGGTATAGGGGTGTAGGC
BIRC2	AGAAGAAAATGCTGACCCACCA	AGCCCATTTCCAAGGCAGATT
BIRC3	GCTTGCAAGTGCGGGTTTT	AACTGGCTTGAACCTGACGGA
BIRC4	TCACTTGAGTTCTGGTTGCAG	CGCCTTAGCTGCTCTTCAGT
BIRC5	CGGTTGCGCTTTCCTTTCTG	CGCACTTCTCCGCAGTTTC
C3	TGGCGAACAGAGGATTTCCC	CTGGTAGGGAGAGGTCACGA
CDK6	TGTGCACAGTGTACGAACA	AGATCGCGATGCACTACTCG
CSF1	CCCTCCCACGACATGGCT	CCACTCCCAATCATGTGGCT
CSF2	TCATCTCAGAAATGTTTGACCTCCA	TAATCTGGGTTGCACAGGAAGTTT
EDA2R	CAGGACCAAGAGTGCATCCC	CAACAAGTGTGGCCTCCTGA
EEF2	GGAGTCGGGAGAGCATATCA	GGGTCAGATTTCTTGATGGG
GNG5	GCCGGACTCAACCGCGTA	GGAACAGACTTTCTGGGGTCTGA
ICAM1	ACCCCGTTGCCTAAAAGGAG	CCAGTTCCACCCGTTCTGGA
IDS	TGGATGGACATCAGGCAACG	TGTTGGCCAGCTGAAGATCG
IKBKA	CGGTCCCTTGTAGGATCCAGT	GCTTAAATGGCCAAGGCAGTTC
IKBKE	AAGAGCCGGGATCAGGTACA	ACCTGCAGGAGTCTTTTGGC
IRF1	CGCATGAGACCCTGGCTAGA	CATGGCACAGCGAAAGTTGG
MAP3K7	TGGTGCTGAACCATTGCCATA	CCCCTGCAACCAGCAGTAAG
MAP3K8	CGCTCAGCCTATCCCTCCTA	GGGTTCAAGGCCTCATGTTT
MTPN	GCAGATTGTGGGCAGCTTGA	TCAAAGGCGGTCAGTCCATC
MYC	AGCGACTCTGAGGAGGAA	CGTAGTTGTGCTGATGTGTG
NF-κB2	CACCTTTGCGGGAACACAC	CGCTATCAGAGGTAGGGGGT
PDGFB	CTACCTGCGTCTGGTCAGC	CAGCAGGCGTTGGAGATCAT
RelB	GCTCTACTTGCTCTGCGACA	CGGCGTCTTGAACACAATGG
RIPK2	GGCCATTGAGATTTCCGATCC	TCGTGACTGTGAGAGGGACA
TAB2	GCACCTCACGGACCCTACAT	GTTCCATTCTGGCCTTCTGGT
TAB3	GAGGAAACTTTGATCCAAAAGCCAT	TCTCAATTGTGCAGGGGTCTG
TNFAIP3	TCAGTACATGTGGGGCGTTC	TGAAGTCCACTTCGGGCCAT

Gene	Sequence sense (5' – 3')	Sequence antisense (5'– 3')
TNFRSF9	AGGACACTCTCCGCAGATCAT	GCAGCTACAGCCATCTTCCTCT
TRAF3	CACGTGGAGAAGGCGTGTA	TTCGAAGCATTTCCTTTTGTCTCTC
TRAF6	GACCAGAACTGTCCTTTGGCA	TTCTCTTGTAGGTGGCGTGC
TRAM1	CGGACATCGTCTCCTGTGTG	GTTGCTGGGAGGGTGACATT
TRAM2	GCCAGGAGTTCGTCATCCAC	GTGCACGGTCTCACTGTCTG
TRIM62	ATCGAGCAGAAAGTCCAGCG	ACTTGGAGGTCCGGAAGTCT
VEGFA	TCTTCAAGCCATCCTGTGTGC	CTTGCTCTATCTTTCTTTGGTCTGC
VIM	AGAGGAAGCCGAAAACACCC	AGGTCAGGCTTGAAACATCC
ZFP36	GGATCTGACTGCCATCTACGAG	GGAGTCGGAGGGGCTCA

Table 11: Oligonucleotides for editing targets

Gene	Sequence sense (5' – 3')	Sequence antisense (5'– 3')
AGPAT3_editing	ACTGGTTGATCTCTTGGTGGTTT	GAGACGTCCAGGAGGTAGGG
AMIGO2_editing	TGCGTGGCCAGTATCGTTTT	TTCTGCCCTGCTGCAGTATC
ANKLE2_editing	CCCCCGCCTCAGGTGAAA	AATCCTTTGTGGGTCTGGC
ANKLE2_genomic	TGGATGCTCTGTTGGCTCG	CTCCTTAGACGCAGTCGCTC
B4GALNT1_editing	CTATCTCATGCCCTTCGGCAA	TGCCGATAAGTGGTGGCAA
B4GALNT1_genomic	ACCTCTGTGGGGATCTGCATT	CTGTGGCCTTAGCCTGTTCAAG
DDIT3_editing	TCCTGCAGATGTGCTTTTCCA	AGCCAGAGAAGCAGGGTCAA
EVA1B_editing	CCCCTCAACGTCAACGTCTT	AAGGTGTGGGGTAGCTCTGA
FAM129A_editing	CATAGGACCTGGCATGCGTC	CTGCCCTTGGACTTTGGAC
GCN1_editing	TGTGCTTGAAGCTCTGGTTTGA	CAAACCTATACCCCTCCCAGA
GLTP_editing	TCTCCTTGGAAATTTACGACAGC	CCCAGCCATCATGTGCTTATTTTT
HSPG2_editing	CCTCCTGATGGCACTGGC	CCGAGGTAGAGCCCACTCC
HSPG2_genomic	CCTCCTGATGGCACTGGC	GCAGGACAGACCGATGTAGCC
MOV10_editing	CTTCCCTGCCAAACTGGACC	TTCTCCACTCTGGCTCCAC
PANX2_editing	GGACGTGGGGGACCTCATC	CCAGGCCACACGACACAG
PLAU_editing	AGAAGAGACTGGGAAGATAGGCT	TTGAGTCAGGACCACCCT
PPIL2_editing	CAAGGAGTTCAAAGGGGACGAG	CAAACCTGGTAGCGCAGCACA
PPP6R2_editing	CATGAGACGTGGGAACATGGG	CTCACTTGAGGAGTGAAGGTGG
PXN_editing	CTGTGGCATCCTGAGTGCTT	TGAGCTGCTTGAAGCAGAAG
PXN_genomic	CATGGGAAACGCCTAGCAAGT	GCACCTAGCAGAAGAGCTTGA
RER1_editing	CATGGTTTGC GCGGGTCTTT	AACCTGCGCCAGAGAGTTCA
RNF220_editing	AAATGGGACAACCTCCTCGCC	CAGGAGAGAGAGAGGCAGGT
SBF1_editing	GCACCTGGAAAACCCACAGG	GCTTGTCTTTCCACCACGGTT
TNS1_editing	CCAGAGTATGGCAAAGTGGAGT	GTTGTCGTAGGAGTCCCAGC
TRRAP_editing	TCCACTTCGGATTCAGTGGGT	GGAACAGAAAGACTAAAGCTAGC GA
TSPAN9_editing	TCGGACTTCTCAGTGGGTGG	GGGGACAAAGTGTCAAGTGTGA
TWF1_editing	TGCTGTCACAATCTTCCCCTG	TCTCGAGAAATGGGAAATGCTAC TC
TWF1_genomic	ACAAAATGCTAGCAGGACCGT	ACTACCAAAAAGAGCAGCCACT
UBE4B_editing	GCAGATTCAGGCGTGGATGA	TGGGGTTGGTTTGCACATT
WDR4_editing	CCCAGCTCCGCGTGTATTTA	AGTGAGATCCTCCAGATGGC

Table 12: Oligonucleotides for PCR/Sanger sequencing/semiquantitative RT-PCR

PCR/Sanger sequencing	Sequence sense (5' – 3')	Sequence antisense (5'– 3')
A3C KO	GCGGGGGTCTCTGCATTGGGG	GCACACAGGAGAGCCCACG
A3C 3' UTR deletion	GGGGTCTCCCTGGGCCTCATG GTCTGT	TCTTGTTAAGGGTGACAGCCT GCAAGGT
Semiquantitative RT-PCR	Sequence sense (5' – 3')	Sequence antisense (5'– 3')
A3C CDS	GGGAAGCCAACGATCGGAA	CAGTATGTCGTCGCAGAACCA
A3C 3' UTR	TTGCCATCTCTTTGCTCTCTCAA	GGCCACAGCATGAAAGGGTC
ACTB	AGAAAATCTGGCACCACACC	AGAGGCGTACAGGGATAGCA

Table 13: sgRNAs for establishing CRISPR/Cas9-mediated cell clones

sgRNA	Sequence sense (5' – 3')	Sequence sense (5' – 3')
sgA3C #1	CACCGCCAACGATCGGAACGAACT	AAACAGTTTCGTTCCGATCGTTGGC
sgA3C#3	CACCGGCGGCGCTTTATACCTTCCA	AACTGGAAGGTATAAAGCGCCGCC
sg3'UTR_ A3C_start	CACCGCACGGGCTCCCTCCACCC	AAACGGGTGGAGGGGAGGCCCGTGC
sg3'UTR_ A3C_end	CACCGAACACCAGAGACAGACATTT	AAACAAATGTCTGTCTCTGGTGTTC

Table 14: shRNAs for shRNA-mediated inhibition of gene expression

shRNA	Sequence sense (5' – 3')	Sequence antisense (5'– 3')
shC	GATCCCCTTGTACTACACATAAGT ACTGTTCAAGAGACAGTACTTATG TGTAGTACAATTTTTG	TCGACAAAAATTGTACTACACATAA GTACTGTCTCTTGAACAGTACTTAT GTGTAGTACAAGG
shA3C	GATCCCCGCACATTCTACTTCCAA TTTACAAGATAAATTGGAAGTAGA ATGTGCTTTTTG	AATTCAAAAAGCACATTCTACTTCC AATTTATCTTGTAATTGGAAGTAG AATGTGCGGG

Table 15: siRNAs for siRNA-mediated gene knockdown

siRNA	Sequence (5' – 3')
control siRNA (siC)	UUGUACUACACAAAAGUACUG
A3C siRNA pool	GCCAACGAUCGGAACGAAA CGGAACGAAACUUGGCUGU
BIRC3 siRNA pool	AGUCAUUGAUCUUGUGUUA CCUAGCAACUGGAGAGAAU
CDK6 siRNA pool	GAAGACUGGCCUAGAGAUG UCAAGACUUGACCACUAC AAGACCUACUUCUGAAGUG
eIF4G2 siRNA pool	GGACAAAGCCCTAGAAGAG GCTCCTTGATGTTAAGTAA

siRNA	Sequence (5' – 3')
FAM120A siRNA pool	TGCCATAGCTAAAGATGTT GGATATTATTCAGCGACTA
IGF2BP1 siRNA pool	CCGGGAGCAGACCAGGCAA UGAAUGGCCACCAGUUGGA CCAGGCAAGCCAUCAUGAAGCUGAA GGCUGCUCCCUAUAGCUCCUUUAUG GGGAAGAGCUGGAGGCCUA CCAUCCGCAACAUCACAAA AAGCTGAATGGCCACCAGTTG AACACCTGACTCCAAAGTTCTG GTATGGTACAGTAGAGAAC CCUGAAGAAGGUAGAGCAA GUUCGUAUGGUUAUCAUCA GUGAACACCGAGAGUGAGA
NF-κB2 siRNA pool	GGACGAGAACGGAGACACA AGACGAGUGUGGUGAGCUU
PCBP2 siRNA pool	GATTGAAGGTGGATTAAT GAGAATCAGTTAAGAAGAT
PUM1 siRNA pool	GGAGAUUGCUGGACAUAUA CAGCAAAGAUGGACCAAAA
PUM2 siRNA pool	GCACTAATCTGCAATCTAA ACTAATAGCTCCCAGAGTA
RelB siRNA pool	GAGCAAACGGCGGAAGAAA CUGCGGAUUUGCCGAAUUA
STAU1 siRNA pool	GAAAATGGGACTAGTAATA CCTCTGAGCAACTGGACTA
UPF1 siRNA pool	AAGAUGCAGUUCGCUCCA CTGCGAACGTGGAGAAGAT

All hybridization probes were ordered from Eurofins Genomics GmbH and are labelled with fluorescence dyes (IRDye®).

Table 16: Hybridization probes for Northern blot

Probe	Sequence (5' – 3')	Label
Y3	CTGTAACCTGGTTGTGATCAATTAGT	682
Y1	ATAACTCACTACCTTCGGACCAGCC	682
Y5	AGCTAGTCAAGCGCGGTTGTGGGGG	682
Y4	GTTAATAAGTTCTGATAACCCACTA	782
5S	AAGTACTAACCAGGCCCGAC	782
7SL	GGCATAGCGCACTACAGCCCAGAACTCCTG	682

2.1.11 Devices

Table 17: Devices used in this study

Application	Device (Company)
Microscopy	SP5X (Leica) Sartorius Incucyte S3® (Essen Bioscience) TS-100 (Nikon)
FACS	FACS Melody (BD)
Luminescence	GloMax® Discover 96 well Microplate Reader (Promega)
Spectroscopy	Infinite® 200 PRO, 96 well Microplate und Nanodrop (Tecan)
SDS-PAGE	NuPAGE® MOPS Electrophoresis System (Life Technologies)
Western blot	XCell II™ Mini-Cell Blot Module (Thermo Fisher Scientific)
Infrared scanner	Odyssey Infrared Scanner (Li-COR)
qRT-PCR	LightCycler® 480 II (Roche)
Thermocycler	Mastercycler Nexus II (Eppendorf)
Agarose gel electrophoresis	Mini-Sub® Cell GT Cell (Bio-Rad)
UV Cross-linker	Biostep® Cross-linker 254nm
Centrifuges	Biofuge Stratos (Heraeus) Biofuge fresco (Heraeus) miniSpin (Eppendorf)
Cell counter	T-20 (Bio-Rad)

2.2 Molecular biological methods

2.2.1 Cloning

To generate plasmids two standardized cloning strategies were executed. For cloning vectors for A3C depletion (pLVX-Puro-shRNA or pSG-sgRNA3) and luciferase plasmids (pmirGLO) containing fragments of 3' UTRs of diverse targets or NF-κB-binding sites, annealed oligonucleotides were directly inserted into linearized target vectors. For overexpression, A3C recovery or insertion of longer sequences into the pmirGLO vector, the respective sequence was amplified from cDNA of 786-O cells and inserted into a cloning vector. Subsequently, the sequence was subcloned into the respective target vector. All information about plasmids, cloning oligonucleotids, restriction sites and oligonucleotides for annealing are summarized in Tables 5, 9, 13 and 14. All cloned constructs were validated by Sanger sequencing performed by Eurofins Genomics GmbH.

2.2.1.1 DNA amplification by polymerase chain reaction

The target sequence was amplified by polymerase chain reaction (PCR) using 0.5 µg genomic DNA or cDNA as template, 10 µM oligonucleotides and the Phusion® High-Fidelity

DNA Polymerase (NEB, #M0530) or the Q5® Hot Start High-Fidelity DNA Polymerase (NEB, #M0493), according to the manufacturer's instructions. For amplification, the following protocol was used:

Table 18: Procedure of a PCR

Step	Temperature	Time	
Initial denaturation	98 °C	5 min	
Denaturation	98 °C	15 sec	} 35 cycles
Primer annealing	57-65 °C	15 sec	
Elongation	72 °C	20-60 sec	
Final elongation	72 °C	3 min	

Amplified products were size separated by agarose gel electrophoresis (2.2.1.3) and purified (2.2.1.4). Purified PCR products were inserted into the pCR®-blunt vector using the Zero Blunt® PCR Cloning Kit (Thermo Fisher Scientific) following the manufacturer's protocol. The verified cloning vector was digested using the indicated restriction sites to cut out the inserted fragment, which was subcloned into the target vector.

2.2.1.1 Oligonucleotide annealing

For annealing of oligonucleotides, 5 µl sense, 5 µl antisense oligonucleotides (100 µM each; Table 9, 13 and 14) and 10 µl nuclease-free water was mixed. The mixture was incubated at 95 °C for 4 minutes, followed by 37 °C waterbath for 15 minutes for hybridization. Annealed oligonucleotides were ligated into linearized vectors.

2.2.1.2 Plasmid digestion

For restriction cloning, 2 µg vector DNA (Table 5) was digested with 1 µl of the restriction enzyme (NEB), as listed in Table 9, and the respective buffer (NEB) for 30 minutes at 37 °C. Cut vectors were separated by agarose gel electrophoresis.

2.2.1.3 Agarose gel electrophoresis

For separation of nucleic acids, gel electrophoresis was performed on a 1% TAE agarose gel (peqGOLD Universal Agarose, peqlab) containing ethidium bromide. The DNA samples were mixed with 6x DNA loading dye (NEB). The Quick-Load® 2-Log DNA Ladder (NEB) was used as size marker. Separated DNA fragments were detected with an UV light imager.

2.2.1.4 DNA gel extraction and ligation

Gel piece containing the cut vector or amplified target sequence was removed from the agarose gel. DNA isolation from agarose gel was performed with the Agarose Gel Extraction Kit (Jena Bioscience), according to the manufacturer's instructions.

Subsequently, linearized DNA fragments and vectors were ligated using the following reaction mix:

10x T4 DNA Ligase Reaction Buffer (NEB, #B0202S)	3 μ l
T4 Ligase (NEB)	1 μ l
Insert / Vector	4 / 1 mol. ratio
Nuclease-free water	ad. to 30 μ l

The reaction mix was incubated at room temperature for 15 minutes.

2.2.1.5 *E. coli* transformation

For the transformation of ligated plasmids, chemo-competent *E. coli* TOP10 bacteria were thawed on ice for 10 minutes. Subsequently, the ligation reaction mix was added to the reaction tube and incubated for 30 minutes on ice. Afterward, the bacteria were heat shocked at 42 °C for 60 sec and incubated on ice for three minutes. 500 μ l LB medium was added and bacteria were incubated at 37 °C for 60 minutes. Subsequently, the bacteria were plated on LB-agar plates containing the respective antibiotic (100 mg/ml Ampicillin or 50 mg/ml Kanamycin) and grown overnight at 37 °C for the selection of positive colonies.

2.2.1.6 DNA preparation from *E. coli*

Positive clones were verified by PCR using the oligonucleotides provided in the kit and OneTaq® 2X Master Mix (NEB, #M0483). Positive clones were cultivated in liquid LB medium containing the respective antibiotic (30 μ g/ml Kanamycin or 150 μ g/ml Ampicillin) overnight at 37 °C under constant shaking in an incubator. Extraction of DNA was performed by using either the Plasmid Mini-Prep Kit (Jena Bioscience) or the PureLink™ HiPure Plasmid Midiprep Kit (Thermo Fisher Scientific), according to manufacturers' instructions. For confirmation of correct insertion, generated plasmids were sequenced by Eurofins Genomics GmbH.

2.2.2 Isolation of genomic DNA

Genomic DNA (gDNA) was extracted from cell pellets using the PureLink™ Genomic DNA Mini Kit (Thermo Fisher Scientific) according to the manufacturer's instructions. Concentration was measured by nanodrop system with the Infinite® 200 PRO spectrometer (Tecan). Isolated gDNA was analyzed by semiquantitative RT-PCR (2.2.3) followed by agarose gel electrophoresis (2.2.1.4) or by Sanger sequencing. The gDNA was stored at -20°C.

For analyzing putative editing events, gDNA and cDNA derived from 786-O cells with modulated A3C expression levels were used to amplify the region harboring the editing site (see Table 11 for oligonucleotides), followed by agarose gel electrophoresis (2.2.1.3), DNA gel extraction (2.2.1.4) and Sanger sequencing. DNA sequences were analyzed using

Mutation Surveyor software (V5.1.2).

2.2.3 Semiquantitative RT-PCR

To estimate the relative amount of RNA populations, a semiquantitative reverse transcriptase PCR (semiquantitative RT-PCR) was performed using 5 μ l of cDNA and the OneTaq® 2X Master Mix (NEB, M0482) containing OneTaq® DNA Polymerase. The PCR reaction was executed as described in 2.2.1.1, however, only 30 cycles were completed. Expression levels were normalized to the housekeeping gene ACTB. Oligonucleotides are listed in Table 12.

2.2.4 RNA isolation

Total RNA was extracted either from cells or primary tissue that was mechanically disrupted in TRIzol (Table 2) prior to RNA isolation. In detail, cells were lysed in 1 ml TRIzol and transferred to an RNase-free 1.5 ml reaction tube. 200 μ l chloroform was added and samples were mixed well. The phases were separated by centrifugation for 15 minutes at 13,000x g and 4 °C. The RNA-containing aqueous phase was transferred to a new 1.5 ml reaction tube. 700 μ l isopropanol was added and samples were mixed well for RNA precipitation. Subsequently, the RNA was pelletized by centrifugation at 13,000x g and 4 °C for 30 minutes. RNA pellet was washed twice in 80% ethanol, dried and resuspended in 30 μ l nuclease-free water. RNA quality and concentration were determined by Infinite® 200 PRO spectrometer (Tecan). Isolated RNA served for reverse transcription combined with qRT-PCR (2.2.5) or Northern blot (2.2.7).

2.2.5 Reverse transcription and qRT-PCR

For the synthesis of complementary DNA (cDNA) a reverse transcription reaction, as listed below, was performed using equal amounts of total RNA as templates.

2 μ g RNA	13.25 μ l
5x RT buffer (Promega)	4 μ l
10 mM dNTPs	1 μ l
M-MLV Reverse Transcriptase (Promega, # M1701)	0.5 μ l
RNasin® Ribonuclease Inhibitor (Promega, #N2511)	0.25 μ l
5 μ M random-hexamer (R6) oligonucleotides	1 μ l

In case of analyzing FFL mRNA, the FFL DNA introduced by transfecting cells with pmirGlo plasmids, as described in 2.3.2, was degraded by using DNaseI (Thermo Scientific™, #EN0521). Additionally, a control reverse transcription reaction, which did not contain reverse transcriptase, was performed.

The reverse transcription reaction was performed at 42 °C for two hours, followed by

transcriptase inactivation at 75 °C for 15 minutes using a Thermocycler (Eppendorf).

Changes in RNA abundance of several targets were determined by quantitative real-time polymerase chain reaction (qRT-PCR) with SYBRgreen technology on a LightCycler® 480 II (Roche) using a 384-well plate. Equal amounts of ORA™ qPCR Green ROX L Mix (HighQu) with 0.2 µM of each oligonucleotide were mixed with 1:10 diluted cDNA in a total volume of 5 µl. Oligonucleotides (Table 10) were designed with Primer-BLAST from NCBI (National Center for Biotechnology Information) to amplify the gene of interest spanning exon-exon borders. The following PCR reaction was used:

Table 19: Procedure of a qRT-PCR

Step	Temperature	Time	
DNA polymerase activation	95 °C	5 min	
Denaturation	95 °C	10 sec	} 40 cycles
Primer annealing	60 °C	10 sec	
Elongation	72 °C	20 sec	
Melting curve	55 °C-95 °C	1 µl	

Cycle threshold (CT)-values were used for the calculation of RNA abundance. Differential expression was calculated based on the $\Delta\Delta CT$ method (Livak, Schmittgen, 2001) and relative to the expression of house-keeping genes (ACTB, EEF2, VCL, PPIA, RL) and control populations or input or no treatment, as indicated at the corresponding graph.

2.2.6 RNA co-Immunoprecipitation

With RNA co-immunoprecipitations (RIP) analyses, associations between a target protein and the bound RNAs can be investigated. 5×10^6 786-O A3C Rec cells per condition were lysed using RIP buffer (Table 2). The supernatants were incubated with 5 µg anti-GFP antibody (Roche; Table 3) or anti-FLAG antibody (Sigma Aldrich; Table 3) as an IgG control and pre-washed magnetic Dynabeads™ Protein G (Thermo Fisher Scientific, #10004D) for 60 minutes at room temperature on a spinning-wheel. The respective cell lysate served as input control for normalization. After three washing steps with RIP buffer, protein–RNA complexes were eluted by incubation in RIP buffer supplemented with 1% SDS at 65 °C for 10 minutes. Protein enrichment was analyzed by Western blotting (WB; 2.4.1). Co-purified RNAs were extracted using TRIzol (2.2.4) and analyzed by qRT-PCR (2.2.5) and Next Generation Sequencing (NGS, 2.7.1).

2.2.7 Northern blot

For Northern blotting (NB), 2.5 µg of total RNA was diluted in 2x FASB (Table 2) and size separated on a 15% denaturing Urea-TBE-gel. RNA was subsequently blotted onto nylon membranes (Roche) using TBE and the Mini Gel Tank Blotting system (Thermo Fisher Scientific). The membranes were UV-cross-linked (Stratalinker 2400) at 120 J and pre-hybridized with PerfectHyb™ Plus (Sigma Aldrich, #H7033). Northern probes (Table 16) were diluted to 100 ng/µl in PerfectHyb™ Plus and hybridized for one hour at room temperature. Prior to detection with Odyssey Infrared Scanner (Li-COR), membranes were washed twice with 2x SSC, 0.1% SDS.

2.2.8 Sucrose gradient

To investigate the association of A3C and A3G with complexes of different size, the sucrose gradient approach was performed. 1.2×10^6 HEK293T cells stably overexpressing A3C or A3G were harvested in Gradient Lysis Buffer (GLB; Table 2) containing 0.5% NP-40 and pelletized. Pellets were dissolved in 1 ml GLB, from which 100 µl was saved as input and 900 µl were loaded onto linear 15-45% (w/v) sucrose gradients prepared with Gradient buffer lacking NP-40. Samples were centrifuged in a Beckman SW 40 Ti swinging-bucket rotor at 40,000 rpm for two hours. Gradients were fractionated into 11 fractions and total protein was isolated by TCA precipitation. Distributions of target proteins in each fraction were analyzed by SDS-PAGE and subsequently by WB analyses, as described in 2.4.1.

2.2.9 RNA decay

In order to investigate RNA stability, transcription is blocked by actinomycin D (ActD; Sigma Aldrich, #A4262), which intercalates into DNA, or by α -amanitin (Sigma Aldrich, #A2263), which blocks the enzymatic activity of RNA polymerase II by binding to it. 24 h prior to the ActD or α -amanitin treatment, 2×10^5 786-O cells were seeded in 6-wells plates. 5 µM ActD or 10 µM α -amanitin were added, the same volume DMSO was added to the control cells. Cells were harvested at indicated time points and RNA was immediately isolated as described in 2.2.4. RNA abundance was analyzed by qRT-PCR (2.2.5). In case of analyzing FFL mRNA, the FFL DNA was degraded by using DNaseI.

2.2.10 Nascent RNA

To investigate changes in the transcriptome upon depletion of A3C, the Click-iT® Nascent RNA Capture Kit (Thermo Fisher Scientific, #C10365) was used. This approach facilitates the division of newly synthesized RNA transcripts from the already existing RNA.

Thus, 4×10^5 786-O C and A3C KO cells were seeded in 6-well plates 24 h prior to the experiment, which was performed according to the manufacturer's protocol. In short, cells

were incubated with 0.5 mM of an analog of uridine, 5-ethynyl uridine (EU) for one hour at 37 °C. RNA was isolated as described in 2.2.4. 5 µg of isolated RNA was used for a copper catalyzed click reaction with 0.5 mM azide-modified biotin, followed by RNA precipitation. Subsequently, 1 µg of biotinylated total RNA was captured using 50 µl of Dynabeads® MyOne™ Streptavidin T1 magnetic beads (Thermo Fisher Scientific, #65604D). RNA captured on the beads was immediately used as a template for cDNA synthesis with the SuperScript® VILO™ cDNA synthesis kit (Thermo Fisher Scientific, #11754-050) in accordance with the manufacturer's protocol. Finally, cDNA was used for qRT-PCR as described in 2.2.5.

2.3 Cell biological methods

2.3.1 Cell culture

Human renal cell carcinoma cells (786-O, 769-P, A-704, ACHN) and immortalized normal kidney cells (HEK293T, RPTEC/TERT1) were obtained from the American Type Culture Collection (ATCC; Table 6). These cell lines were regularly checked for mycoplasma contamination by PCR. 786-O and 769-P cells were maintained in RPMI 1640 medium (Thermo Fisher Scientific) supplemented with 10% FBS (Pan Biotech, #P303031). A-704, ACHN, HEK293T and HCT116 cells were maintained in high-glucose (4.5 g/L) DMEM (Thermo Fisher Scientific) supplemented with 1% GlutaMAX (L-Alanyl-L-glutamin) supplement (Thermo Fisher Scientific) and 10% FBS. RPTEC/TERT1 cells were cultured in DMEM supplemented with hTERT Immortalized RPTEC Growth Kit (ATCC). All cells were incubated in a humidified atmosphere at 37 °C and 5% CO₂. For cell cultivation, cell assays or transfections, cells were washed with PBS, removed from the culture dishes using Trypsin-EDTA (Table 2) and resuspended in the corresponding medium.

2.3.2 Transfection of siRNAs and plasmids

One day prior to transfection, 1.5×10^5 cells for 786-O, 2×10^5 cells for 769-P, 3×10^5 cells for A-704 and ACHN or 5×10^5 cells for HEK293T were seeded in a 6-well plates (TPP, #92006). For siRNA-mediated gene silencing, cells were transfected with 50 pmol of the indicated siRNA pool (Table 15) using Lipofectamine RNAiMAX (Thermo Fisher Scientific) according to the manufacturer's protocol. Plasmid transfection was performed with 2 µg and 4 µg plasmid DNA (Table 5) using Lipofectamine 3000 (Thermo Fisher Scientific) or DharmaFECT kb DNA transfection reagent (Horizon Discovery), respectively, in accordance with the instructions provided by the manufacturers. In case of reporter plasmid transfections with pmirGLO, cells were seeded into 12-well plates (TPP, #92012) and 1 µg vector DNA was transfected using DharmaFECT kb DNA transfection reagent. One day after transfection, the medium was changed or harvested to determine reporter activity (see

2.4.4). If a double transfection was performed, 48 h post siRNA transfection reporter plasmids were transfected as described above. Unless stated otherwise, cells were harvested for further analyses 72 h post transfection.

2.3.3 Generation of CRISPR/Cas9-mediated knockout clones

For CRISPR (clustered regularly interspaced short palindromic repeats)/Cas9-mediated genomic deletion in the A3C locus either of the coding sequence (CDS) or the 3' UTR, initially, sgRNAs were designed, including a PAM motif (NGG) and 20 nucleotides complementary to a genomic region downstream and upstream of the target sequence. After annealing, sgRNAs were cloned into the pSG-leer-RFP + BbsI-GFP vector via BbsI. 786-O and 769-P cells were co-transfected with two CRISPR sgRNA-encoding plasmids (pSG-sgRNA3-A3C#1-RFP and pSG-sgRNA3-A3C#3-RFP or pSG-sgRNA3-3'UTR_A3C_start-RFP and pSG-sgRNA3-3'UTR_A3C_end-RFP) and a Cas9 nuclease-encoding plasmid (pcDNA3.1-Cas9-GFP; Table 5) as described above in 2.3.2. Transfection efficiency was determined by fluorescence microscopy. 24 h post-transfection, cell populations were diluted until single-cell level in 24-well plates (TPP, #92024) or GFP- and RFP-double positive cells were sorted with the flow cytometer BD FACS Melody at either single-cell level (786-O) or cell population level (769-P). Since 769-P cells do not grow at single-cell level, a cell population harboring CRISPR/Cas9-mediated knockout (KO) of A3C was generated. To avoid cell contamination of cell clones, RPMI growth medium was supplemented with 1% penicillin-streptomycin (Thermo Fisher Scientific, #15140-122). Cells were cultured to verify A3C KO by WB analyses and Sanger sequencing. Deletion of A3C 3' UTR was determined by PCR of genomic DNA from single-cells with the Q5[®] High-Fidelity 2X Master Mix (NEB). In order to generate a stable A3C recovery clone, 786-O A3C KO cells were transfected with pEGFP-(C2)-A3C (Table 5), sorted for GFP-positive cells using the flow cytometer BD FACS Melody, selected with 500 µg/ml geneticin (Sigma Aldrich, #G8168) one day after sorting, and cultured under constant geneticin selection pressure (50 µg/ml).

2.3.4 Establishment of stable shRNA-mediated A3C knockdown clones

For stable A3C knockdown (KD) clones, 786-O and 769-P cells were transfected with pLVX-shRNA3-shA3C and pLVX-shRNA3-shC (Table 5) as described above (2.3.2). For selection, transfected cells were treated with 4 µg/ml puromycin (Sigma Aldrich, #P9620) one day after transfection. Cells were cultured under constant selection pressure by applying 2 µg/ml puromycin to the medium.

2.3.5 Generation of stable overexpressing cell clones

To generate stable A3C and A3G overexpressing (OE) cells, HEK293T cells were transfected with pLVX-SBP-FLAG-RFP, pLVX-SBP-FLAG-RFP-A3C and pLVX-SBP-FLAG-RFP-A3G (Table 5) as described in 2.3.2. Cells were selected for four weeks by applying 400 µg/ml Zeocin (Thermo Fisher Scientific, #R25001) to the medium. Protein overexpression (OE) was determined by WB analyses and subsequent incubation with an anti-FLAG antibody.

2.3.6 Proliferation and 3D spheroid assays

Proliferation of stable cell clones was monitored under 2D and 3D growth conditions. For 2D cell growth, 5×10^3 cells were seeded into 12-well plates. For 3D spheroid growth, 1×10^3 cells were seeded in 100 µl growth medium into round bottom ultra-low attachment 96-well plates (Corning; #7007), centrifuged for three minutes at 300x g and cultured overnight to induce spheroid formation. Proliferation was continually monitored for five days using an Incucyte S3 device. Cell number of 2D growth conditions and object area of the spheroids were analyzed by the *Incucyte* software. Images of the first time point served as normalization control.

2.3.7 Anoikis resistance assay and density stress

In order to assess cell viability under diverse stress conditions, 1×10^3 cells were seeded either into flat bottom ultra-low attachment 96-well plates (Corning; #3474) or into high attachment 96-well plates (TPP, #Z707902) in RPMI medium either supplemented with 1% FBS or 10% FBS. When indicated, siRNA-mediated KD (see 2.3.2) was transfected 24 h prior to seeding, otherwise stable cell lines were used. Initial cell viability used as input control as well as cell viability after five days of culturing were determined by CellTiter-Glo according to manufacturer's protocol.

In order to analyze A3C expression upon density stress, 2×10^5 786-O and 769-P WT cells, referring to low density (LD), and 5×10^5 786-O and 769-P WT cells, referring to high density (HD), were seeded onto a 6 cm cell culture dish (TPP; #93060). Cells were harvested to determine A3C expression at RNA and protein level by qRT-PCR (2.2.5) or WB (2.4.1), respectively, 24 h after seeding.

2.3.8 Apoptosis assay

To measure apoptosis, the relative Caspase3/7 activity was determined by using the Caspase-Glo3/7 assay (Promega) according to the manufacturer's instructions. Prior to the apoptosis assay, protein expression was either transiently modulated in 786-O and 769-P cells as described in 2.3.2 or 1×10^5 786-O and 769-P A3C KO cells were seeded into 12-

well plates. Cells were harvested in medium from the well 48 h post-transfection or upon starvation (1% FBS) for 48 h. Caspase3/7 activity was measured with a Luminometer (Promega). Luminescent signal was normalized to cell number determined by CellTiter-Glo (Promega).

2.3.9 Drug treatment

In order to assess cell viability in response to APOBEC inhibitor and drugs used in the treatment of RCC, 786-O C, A3C KO and A3C Rec cells were incubated with different compounds. Prior to cell treatment, compounds were added to 786-O WT cells at diverse concentrations to determine EC₅₀-value. EC₅₀-values were calculated using *GraphPad Prism* software (V9.0). For inhibitor studies, 5x10⁴ 786-O C, A3C KO and A3C Rec cells were seeded into 6-well plates and incubated with 100 µM Aurothioglucose (AuTG; Sigma Aldrich, #A0606) for five days. For drug treatment, 1x10⁵ 786-O C and A3C KO cells were seeded into 6-well plates and incubated with 3.5 µM Sorafenib (Sigma Aldrich, #SML2653), 15 µM Pazopanib (Sigma Aldrich #SML3076) or 6 µM Sunitinib (Sigma Aldrich, #PZ0012) for 48 h. Cells were harvested and cell viability was determined using CellTiter-Glo according to the manufacturer's protocol.

2.4 Protein-biochemical methods

2.4.1 Protein extraction, SDS-PAGE and Western blot

For total protein extraction, cell pellets or pestled primary tissue samples were incubated in total lysis buffer (Table 2) for five minutes and pelletized by centrifugation at 12,000 rpm for two minutes with the miniSpin (Eppendorf). For phosphorylation analyses, a protease/phosphatase inhibitor (Cell Signaling, #5872) was added to the lysis buffer. Protein concentration was determined with the colorimetric DC Protein Assay (BioRad) according to manufacturer's protocol. Absorbance at 650 nm was measured with the GloMax® Discover 96 well Microplate Reader (Promega). Equal amounts of total protein (40 µg) were diluted with 4x NuPAGE® LDS sample buffer (Thermo Fisher Scientific) containing 0.1 M DTT and denatured at 95 °C for five minutes. Proteins were size separated by NuPAGE® Novex 4-12% Bis-Tris Protein Gels (Thermo Fisher Scientific) and the corresponding NuPAGE® MOPS SDS running buffer (Thermo Fisher Scientific). After SDS-PAGE, proteins were transferred onto a nitrocellulose membrane (Amersham, GE Healthcare) by using the Mini Gel Tank Blotting system (Thermo Fisher Scientific) and NuPAGE® blotting buffer (Table 2) with 10% methanol. After blocking with 5% BSA (w/v) in PBS for one hour at room temperature, protein abundance was detected using respective primary antibodies and fluorescence-labelled secondary antibodies (Table 3, Table 4). Fluorescence intensities were visualized at 680 nm or 800 nm with the Odyssey Infrared

Scanner (Li-COR) and quantified via the *Image Studio*[™] software (Li-COR V3.1.4) with respect to the loading control and control sample.

2.4.2 Immunofluorescence staining

Localization of different proteins was investigated by immunofluorescence staining of fixated cells and visualization by microscopy. Therefore, 786-O A3C Rec cells were cultured for 48 h on coverslips, which were previously incubated in 40% (v/v) ethanol and 60% (v/v) hydrochloric acid. Cells were fixed with 4% (v/v) formaldehyde in PBS for 20 minutes and permeabilized with 0.5% (v/v) Triton X-100 in PBS for three minutes. Unspecific binding was blocked with 2% (w/v) BSA in PBS for 30 min. Cells were incubated with primary antibodies (Table 3) 1:500 in blocking solution. After washing with PBS, Cy3- or Cy5-fluorescently labeled secondary antibodies (1:500 in blocking solution; Table 4) were added. Nuclei were stained by incubating cells in DAPI (Sigma Aldrich; 1:1,000 in PBS) for three minutes. Stained cells were washed several times with PBS, two times with distilled water and subsequently dehydrated by adding >99% ethanol. Afterward, coverslips were mounted with ProLong[™] Diamond Antifade Mountant (Thermo Fisher Scientific, # P36970). Imaging was performed with the Leica SP5X confocal microscope.

2.4.3 Pull-down

To investigate RNAs and proteins associated with A3C and A3G, HEK293T cells stably expressing either SBP-FLAG-RFP-A3C or SBP-FLAG-RFP-A3G (see 2.3.5) were used for a pull-down (PD) with Dynabeads[™] MyOne[™] Streptavidin (Thermo Fisher Scientific, #65604D). Therefore, 3×10^6 cells per condition were harvested, washed with PBS, pelletized and resuspended in 300 μ l GLB (Table 2). After incubation at room temperature for five minutes, cells were centrifuged at 12,000 rpm for five minutes. Input samples were transferred to new tubes. Upon washing of Dynabeads[™] Streptavidin with GLB, 25 μ l of Dynabeads[™] Streptavidin were added to each sample lysate, mixed well and incubated at room temperature for 30 minutes under constant rotation. Samples were washed with GLB using a DynaMag[™]-2 Magnet (Thermo Fisher Scientific, #12321D). Elution of captured complexes containing proteins was realized by incubating beads in 1x NuPAGE[®] LDS sample buffer at 95 °C for five minutes, followed by SDS-PAGE and WB as described in 2.4.1. To analyze RNAs associated with the target protein, beads were incubated in GLB containing 1% SDS at 65 °C for five minutes, followed by RNA isolation described in 2.2.4 and Northern blot described in 2.2.7.

2.4.4 Luciferase reporter assay

In order to investigate regulatory elements in the 3' UTR of A3C or of modulators of the NF- κ B signaling pathway, and additionally the transcriptional activity of NF- κ B subunits in

promoter regions of target genes, the Dual-Glo® Luciferase Assay System (Promega) was used. Diverse pmirGLO reporter plasmids (Table 5) containing putative regulatory elements in the 3' UTR or the 5' UTR, respectively, of the Firefly luciferase were generated, as described in 2.2. Renilla luciferase on the same plasmid served as the normalization control. Cells were transfected with the respective plasmids as described in 2.3.2. The activities of Firefly and Renilla luciferases were determined 48 h post transfection by Dual-Glo® (Promega) in accordance with the manufacturer's protocol and the GloMax® 96-well microplate (Promega) device.

2.4.5 Subcellular fractionation

For fractionation, 1.5×10^6 cells per condition were harvested in fractionation buffer (Table 2) supplemented with 130 µg/ml digitonin (Sigma Aldrich) for 786-O and 200 µg/ml for 769-P. Subcellular fractions were separated by centrifugation at 1000x g for two minutes. Supernatant containing the cytoplasmic fraction was transferred to a new tube. The remaining pellet was washed with fractionation buffer supplemented with digitonin and centrifuged at 1000x g for two minutes. Pellets containing the nuclear fraction were lysed in total lysis buffer. Further analyses were performed by WB as described above (2.4.1). Subcellular fractionation was confirmed by detecting EEF2 in the cytoplasmic and PTB in the nuclear fraction.

2.5 Mouse xenograft studies

Nude mice (FOXN1^{nu/nu}) were used for xenograft studies. All animals were handled in accordance with European Directive (2010/63/EU) and local guidelines of the Martin Luther University Halle/Wittenberg.

For subcutaneous xenograft assays, 6×10^5 786-O C, A3C KO and A3C Rec cells were harvested in media supplemented with 50% (v/v) matrigel (Sigma Aldrich) and injected into both flanks of six-week old female mice (16 mice in total). Subcutaneous tumor growth was measured in two diameters with calipers to allow calculation of tumor volume. The volume was calculated using the formula $V = [\pi/6 \times (l + w + h)]$. Mice were sacrificed after eight weeks, as C and A3C Rec derived tumors reached termination criteria.

2.6 Studies involving patient samples

All procedures concerning the patient tissue samples were performed in accordance with the ethical standards established in the 1964 Declaration of Helsinki and its later amendments. All patients gave informed consent. The study was based on the approval of the Ethics Commissions of the University Hospital Erlangen, Germany (No. 4607).

The snap-frozen tissue samples were obtained from the Comprehensive Cancer Center (CCC) tissue biobank of the University Hospital Erlangen, Germany. The tumor histology was reviewed by experienced uropathologists, as previously described in (Wach et al., 2019).

2.7 Data analyses

2.7.1 Next Generation Sequencing

For total RNA-sequencing (RNA-seq) 300 ng RNA of primary tissue samples, of stable 786-O CRISPR/Cas9-mediated A3C KO and A3C Rec clones and of 786-O A3C Rec RIP-samples were used. Novogene (Hong Kong) performed the library preparation and sequencing on an Illumina HiSeq platform. First, low quality read ends as well as remaining parts of sequencing adapters were clipped using *Cutadapt* (V 1.4; 2.8). Subsequently, reads were aligned to the human genome (UCSC GRCh38/hg38) using *HiSat2* (V2.1.0; Kim et al., 2015). *FeatureCounts* (v 1.5.3; 2.0; Liao et al., 2014) was used for summarizing gene-mapped reads. *Ensembl* (GRCh38.89; GRCh38.102; Yates et al., 2020) was used for annotations. Differential gene expression (DE) was determined by the R package *edgeR* (v3.28.0; 3.34; Robinson et al., 2010) using TMM normalization on raw count data. RNA expression values were obtained as FPKM (fragments per kilobase million mapped reads) values.

2.7.2 Gene set enrichment analyses

For Gene set enrichment analyses (GSEA), either RNA-seq data of 786-O C, A3C KO, A3C Rec cells or the publicly available dataset of the TCGA-KIRC RNA-seq obtained from the GDC portal (<https://portal.gdc.cancer.gov/>) were used. GSEA were performed on pre-ranked lists using the GSEA software (V3.0; Subramanian et al., 2005) selecting HALLMARK gene sets from MSigDB (v 6.1; Liberzon et al., 2015). All protein-coding genes were ranked according to the fold changes (FC) in 786-O C to A3C KO, A3C KO to A3C Rec or normal tissue (NT) to ccRCC. A permutation number of 1000 was applied, and classical enrichment statistics were elected.

2.7.3 Kaplan-Meier analyses

For patient survival analyses, overall survival data of RCC patients was obtained from TCGA (Weinstein et al., 2013) datasets for ccRCC (KIRC), papRCC (KIRP) and chrRCC (KICH) patients with median group cutoff. For overall survival based on the expression status of A3C, the *GraphPad Prism* software (V9.0) was used to calculate Kaplan-Meier plot and Hazard ratio (HR) by using the log-rank (Mantel-Cox) test. For survival analyses

based on the expression status of other indicated genes, Kaplan-Meier plots and HR were determined using *GEPIA 2* (<http://gepia2.cancer-pku.cn/#survival>).

2.7.4 CLIP analyses

Publicly available data of enriched CLIP hits for the protein A3C were obtained from ENCODE (<http://www.encodeproject.org/>; identifiers: ENCFF921RKR, ENCFF571IFM). eCLIP-seq was performed in K562 cells by Gene Yeo, UCSD, 2018. Additionally, CLIP hits in the 3' UTR of A3C were analyzed by Dr. Danny Misiak with publicly available data in K652 and HepG2 cells (van Nostrand et al., 2020b).

2.8 Statistics

All experiments were performed in at least three independent, biological replicates, unless stated otherwise. Statistical analyses were executed by using *GraphPad Prism* software (V9.0). Statistical significance (* $p < 0.05$; ** $p < 0.01$; *** $p < 0.001$; **** $p < 0.0001$) was tested by unpaired, two-tailed Student's t-test on equally distributed data, by two-way ANOVA if the mean of several groups was compared, by one-way ANOVA with Tukey's multiple comparisons test or Šídák's multiple comparisons test, as indicated in the figures' legends. WB quantifications are shown as mean \pm standard deviation (SD). The box and whiskers plots depict the 5-95 percentiles. Bar plots depict mean \pm standard error of the mean (SEM). All outliers are shown.

2.9 BioRender Licenses

Licenses to use the BioRender content have been granted for all graphics in this thesis.

Table 20: Licenses for graphics created with BioRender

Graphics	License number
Figure 1	UE267G9RTN
Figure 2	WK267GBNIR
Figure 3	JJ267GCE3Y
Figure 4	CT267GA4JI
Figure 5	TV267GCLTN
Figure 25	UA267GHTG8
Figure 26	FW267GF43C
Figure 28	IS267GGYW8
Figure 30	IE267GGQF3
Figure 31	IK267GIPBO

3 RESULTS

3.1 Characterization of APOBEC3 protein family members

Prior to exploring the molecular function of A3C in the context of ccRCC, detailed information on selected properties of the A3 family members, especially A3C, are provided. Due to previous studies identifying A3G as a promising prognostic factor for ccRCC (Ji et al., 2022; Mei et al., 2017; Wu et al., 2020), this member of the A3 family was included in comparative analyses. As mentioned above, although all A3 genes originated from A1 through gene duplication (Jarmuz et al., 2002), their distinct expression profiles (Koning et al., 2009; Middlebrooks et al., 2016; Ng et al., 2019), cellular localization (Kinomoto et al., 2007; Lackey et al., 2013) and varying antiviral activity (Haché et al., 2006; Liddament et al., 2004; Marin et al., 2008; Zhang et al., 2010) indicate diversified functions within this family of RBPs.

3.1.1 A3C and A3G are associated with different RNP complexes

A3C differs from A3G not only in the number of cytidine deaminase domains but also in its association with different molecular complexes, as demonstrated by a sucrose density gradient assay (Figure 7A). A3C was found in less dense fractions (fractions one to three) of a 15-45% sucrose gradient, while A3G showed a more widespread distribution throughout the gradient, excluding fraction one. The upper fractions of the sucrose gradient are known to contain soluble proteins, cytoplasmic proteins and nucleic acids (McConkey, 1967). Together with A3C, Ro60 and the mRNA-decapping enzyme 1A (DCP1A) were detected in the top fractions of the gradient (Figure 7A, Supplemental Figure 1). Ro60 binds medium-sized Y RNAs (Slobbe et al., 1992) and associates with small nuclear RNA-protein complexes (Wahren et al., 1996). DCP1A forms the mRNA decapping complex along with other proteins to initiate mRNA degradation (Tritschler et al., 2009). This suggests a potential molecular role of A3C in connection with Y RNAs and P-bodies, considering that DCP1A is a P-body marker (Sheth, Parker, 2003). In contrast, A3G demonstrated enrichment in the intermediate and bottom fractions, indicating its association with high molecular weight complexes, as previously reported (Chiu et al., 2006).

As a side note, it is worth mentioning that these analyses were conducted prior to the application of a functional A3C antibody. Thus, recombinant FLAG-tagged A3C/A3G protein expression was utilized for WB detection with an anti-FLAG antibody, with awareness that this approach may entail artifacts. The results regarding A3C accumulation in the top fractions of a sucrose gradient were subsequently validated by using an A3C antibody and ccRCC-derived cell lines expressing endogenous A3C (Supplemental Figure 1).

To expand the understanding of A3C's interactions and diversified functions within the A3 family, a streptavidin pull-down assay was conducted using HEK293T cells expressing SBP-FLAG-tagged A3C and A3G. This approach facilitates capturing and analyzing co-precipitated proteins and RNAs (Figure 7, B and C). As interaction studies for A3C are currently unavailable, the BioGRID database (<https://thebiogrid.org/>) was used as a reference for putative interactions partners. The database search revealed potential interactions of A3C with well-known RBPs, such as ELAVL1 and HNRNPK, as well as with subunits of the ribosome, such as RPL7, RPL28 and RPS13. The pull-down experiment showed that both A3 proteins, A3C and A3G, interacted with AGO2 and Ro60 to varying extent (Figure 7B). Additionally, A3C exclusively associated with RPL5 and DCP1A. Furthermore, both proteins demonstrated efficient interactions with Y1, Y3 and 7SL RNAs, while a robust association of A3C with Y4 and Y5 could not be detected (Figure 7C).

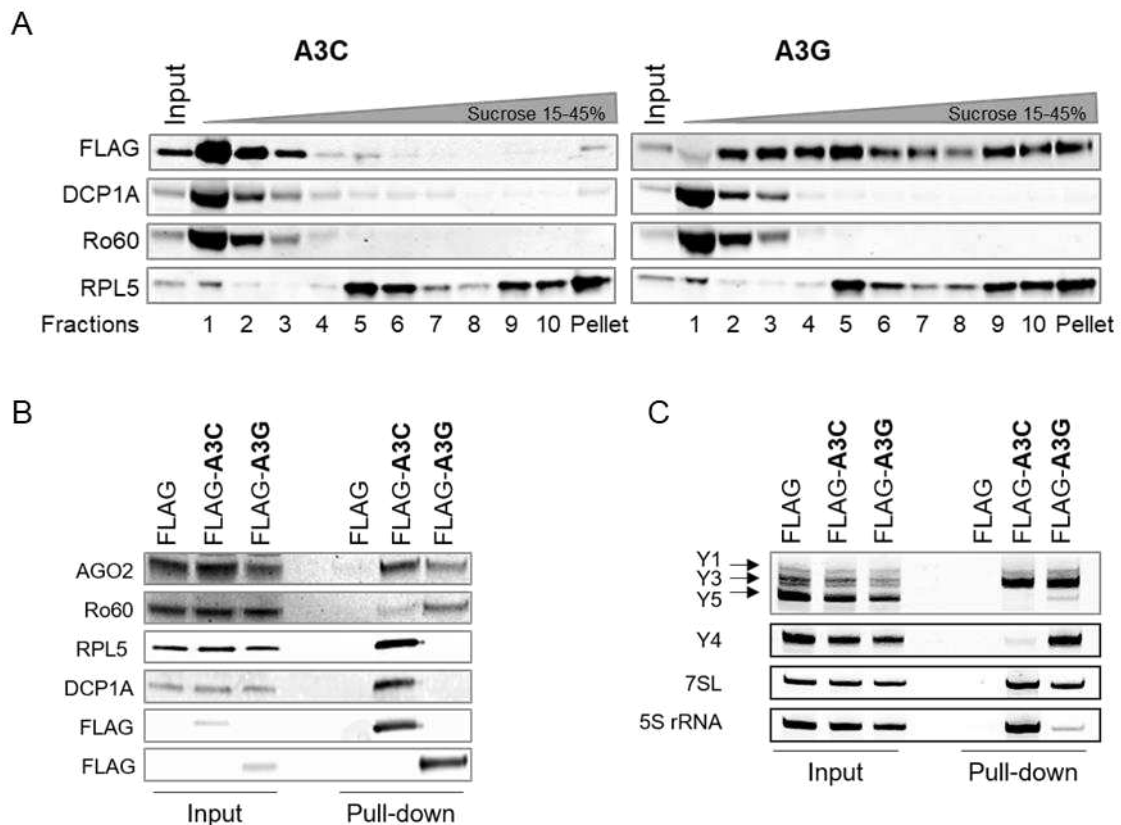


Figure 7: Differences in sucrose density gradient profiles and binding partners between A3C and A3G indicate distinct functions within the A3 protein family. (A) Total cell lysates from HEK293T cells stably overexpressing A3C (FLAG-A3C) or A3G (FLAG-A3G) were separated by ultracentrifugation on a sucrose gradient (15-45%). Western blot (WB) analyses show the distribution of A3C and A3G in fractions of the sucrose gradient. **(B and C)** Pull-down analyses using streptavidin-coated magnetic beads and HEK293T cells stably expressing SBP-FLAG-tagged A3C or A3G demonstrate different association behaviors. Upon elution of the target proteins, co-purified proteins **(B)** and RNAs **(C)** were determined using WB and Northern blot (NB) analyses, respectively. Note that the experiments were performed once **(A-C)**.

These findings suggest that A3 proteins may play a role in post-transcriptional gene silencing, translation regulation and stress response, as their interaction partners have been reported to fulfill these biological functions (Bocitto, Wolin, 2019; Kohn et al., 2013; Liu et

al., 2005). Furthermore, the comparative analyses of the RNA and protein association profiles of A3C and A3G highlight functional differences within this group of RBPs. While the binding of 7SL and Y RNAs by A3G has been previously reported (Bach et al., 2008; Gallois-Montbrun et al., 2008), information regarding the binding capacity of A3C is limited, underscoring the need for further research.

3.1.2 Subcellular localization of A3C

To confirm the previously reported cellular localization of A3C (Bogerd et al., 2006; Kinomoto et al., 2007), subcellular fractionation analyses were conducted and immunofluorescence microscopy was performed using the ccRCC-derived cell line 786-O with modulated A3C expression levels (Figure 8). Based on the size of A3C (~23 kDa), which is below the exclusion size of approximately 40 kDa for passive diffusion through the nuclear pore complex (Görlich, Kutay, 1999), it is reasonable to suggest that A3C localizes to both the nucleus and the cytoplasm. However, in the cell system employed in this study, A3C predominantly localized to the cytoplasm, as demonstrated in the WB of subcellular fractionation (Figure 8A).

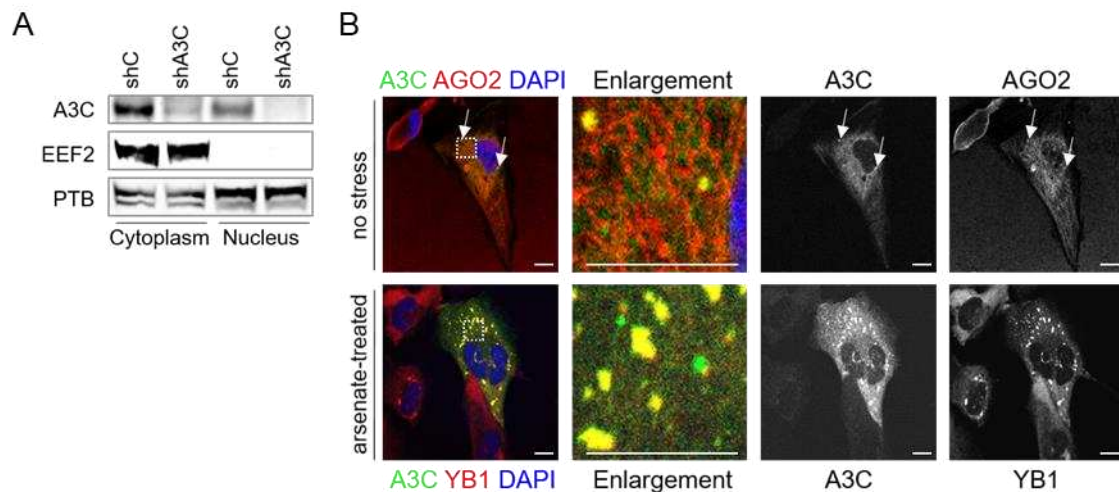


Figure 8: Subcellular localization of A3C. (A) Subcellular fractionation was performed using 786-O cells with a stable knockdown (KD) of A3C by shRNAs (shA3C). 786-O control cells (shC) were included. Subcellular distribution of A3C protein was analyzed by WB. To verify the subcellular fractionation process, EEF2 was used as positive control for the cytoplasmic fraction and PTB as positive control for the nuclear fraction. To demonstrate A3C antibody specificity, A3C expression was impaired by shA3C. (B) Immunofluorescence imaging of AGO2 and YB1 in 786-O cells stably overexpressing GFP-A3C. A3C (green) co-localized with the P-body marker AGO2 (red; upper panel; arrows indicate P-bodies). Upon arsenate treatment (lower panel), A3C co-localized with YB1 (red), which is a marker for stress granules. DAPI visualizes nuclei. Dashed boxes depict enlarged regions. Merged images and single stainings are shown. Scale bars correspond to 10 μ m.

Furthermore, A3C was enriched in P-bodies, as it co-localized with the P-body marker AGO2 (Sen, Blau, 2005; Figure 8B). The co-purification of the P-body markers AGO2 and DCP1A in the pull-down analysis with A3C (Figure 7B) previously suggested the potential involvement of A3C in post-transcriptional gene regulation. This includes functions like mRNA degradation or translational suppression, which are reported activities associated

with P-bodies (Eulalio et al., 2007). Additionally, A3C co-localized with the stress granule marker YB1 under arsenate stress conditions (Figure 8B), suggesting the involvement of A3C in stress response mechanisms. Stress granules are dynamic cytoplasmic messenger RNP (mRNP) granules that aggregate when translation initiation is inhibited during stressful conditions (Kedersha et al., 1999).

In summary, these findings confirm that A3C is primarily localized in the cytoplasm, suggesting a potential involvement in post-transcriptional gene regulation under stress conditions, as evidenced by its accumulation in P-bodies and stress granules.

3.1.3 RNA-editing activity of A3C

Belonging to the family of cytidine deaminases, A3C has the potential to edit the sequence of bound transcripts. However, its mainly cytoplasmic localization (Figure 8) raises doubts about its enzymatic activity. Before the RNA-editing function of A3C is discussed, the binding preference for repeated RNA sequences was investigated. Notably, endogenous A3C from 786-O cells exhibited a strong affinity for U-rich sequences (Figure 9A). This finding aligns with previous studies on A1, which is known for binding AU-rich elements (Anant et al., 1995; Blanc, Davidson, 2010). These AU-rich elements, typically located in the 3' UTR of many mRNAs exhibiting rapid turnover, act as destabilizing elements (Chen, Shyu, 1995). A1 has been reported to bind the 3' UTR of c-myc, TNF- α and IL-2, enhancing mRNA stability, suggesting a function independent of its cytidine deaminase activity (Anant, Davidson, 2000).

To assess the RNA-editing activity of A3C, RNA-sequencing (RNA-seq) data from 786-O control cells (C), CRISPR/Cas9-mediated A3C knockout cells (A3C KO) and A3C KO cells with re-inserted GFP-A3C (A3C Rec) were analyzed. For these analyses, conducted by Dr. Danny Misiak in the group of Prof. Hüttelmaier, specific criteria were employed to identify putative editing sites:

- C-to-U nucleotide change on the plus strand; G-to-A on the minus strand
- Sufficient read coverage at the nucleotide of interest (≥ 20 reads in the mean of 786-O C)
- Minimum change rate ($\geq 20\%$ change rate in one sample; $\geq 5\%$ change rate in the mean of 786-O C)

Initially, hundreds of C-to-U editing events were identified. However, after applying more stringent criteria, such as focusing on mRNA or considering change rates in 786-O A3C KO vs. C, the list of potential editing candidates was narrowed down to 71 (Supplemental Table 1). In-depth analyses revealed that most putative editing sites were either not recoverable in 786-O A3C Rec cells (Figure 9C) or were located in the wobble position of a codon, resulting in no amino acid alteration in the final protein. Furthermore, putative editing sites were often found in the 3' UTR of transcripts, potentially influencing mRNA degradation rates. However, as indicated in Figure 9B, these putative editing events

resulted in altered gene expression levels in only a few cases (e.g., TNS1, RHOF, HSPG2 and GAS6).

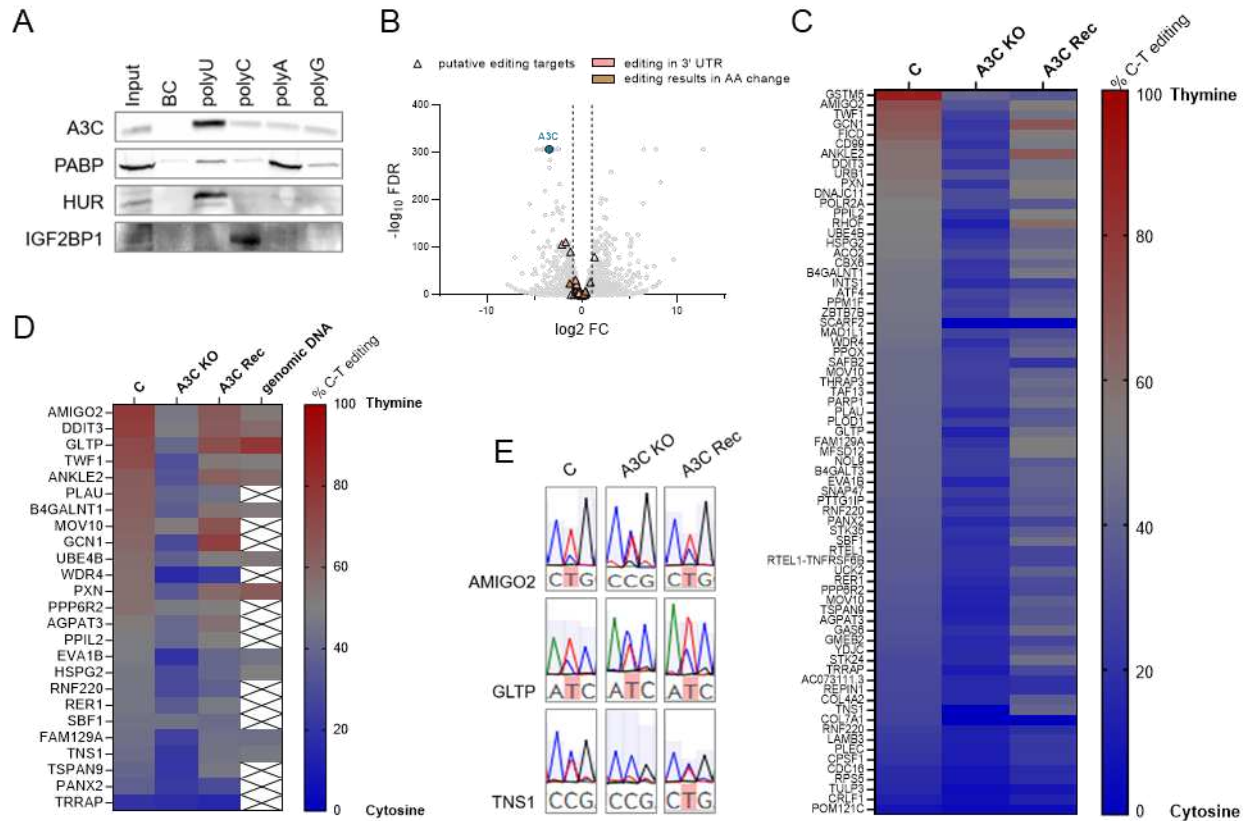


Figure 9: C-to-T editing is probably not the main function of A3C. (A) 786-O wild type (WT) cell lysates were incubated with biotinylated poly(U/C/A/G) RNAs. WB analyses indicate associated proteins that were recovered by a pull-down assay using streptavidin magnetic beads. PABP, HUR and IGF2BP1 served as positive controls for binding polyA, polyU or polyC RNAs, respectively. Beads only (BC) were used as specificity control. (B) In the volcano plot, \log_2 mRNA fold change (FC) was plotted against the $-\log$ false discovery rate (FDR) for 786-O control (C) and CRISPR/Cas9-mediated A3C knockout (A3C KO) cells. Dashed lines indicate thresholds of differentially expressed genes (DEG; upregulated, $\log_2 \text{FC} \geq 1$; downregulated, $\log_2 \text{FC} \leq -1$). In RNA-seq identified C-to-U editing events are depicted by triangles. (C) Heat map shows the C-to-T editing rate of putative editing events identified in the RNA-seq of 786-O C, A3C KO and A3C KO cells with re-inserted GFP-A3C (A3C Rec). (D) Putative editing by A3C was confirmed for some selected targets in 786-O C, A3C KO and A3C Rec cells by amplifying the regions harboring the editing sites on cDNA and genomic DNA followed by Sanger sequencing. DNA sequences were analyzed using *Mutation Surveyor* software. Heat map shows mutant peak percentage of C-to-T editing. (E) Chromatograms indicate edited sites in cDNA of putative targets in 786-O C, A3C KO and A3C Rec cells. The corresponding reference sequence is displayed in the lower panel; T highlighted in red refers to editing event.

To confirm editing for selected targets, the respective regions harboring potential editing sites were amplified from cDNA derived from 786-O C, A3C KO and A3C Rec cells, followed by Sanger sequencing. The majority of putative editing sites indeed exhibited C-to-T modifications at the respective site to a lesser extent in A3C KO cells compared to control cells (Figure 9, D and E). However, contrary to the expected editing activity of A3C, not all editing events were recovered in A3C Rec cells (Figure 9D). Furthermore, to discriminate RNA-editing sites from genome-encoded single-nucleotide polymorphisms (SNPs), it is critical to compare sequence differences with matched genomic DNA from the

same sample. Missing DNA sequencing data from the same sample may lead to read-mapping errors or artifacts being mistakenly interpreted as RNA-editing sites.

Genomic datasets from the Cancer Cell Line Encyclopedia (CCLE; <http://portals.broadinstitute.org/ccle>) were used to analyze somatic mutation frequencies for the putative A3C editing targets. This analysis revealed that the queried genes were altered in 79% of all studied cell lines, with the primary mutation event being the C-to-T alteration (Supplemental Figure 2). Monitoring the somatic mutation status for some genes encoding the putative A3C editing targets by sequencing genomic DNA of 786-O C cells revealed that many of these targets showed nucleotide exchanges at the genomic level (Figure 9D). This suggests that the mutation event may occur independently of A3C, especially considering its predominant cytoplasmic localization and reported exclusion from DNA damage sites (Constantin et al., 2022).

In conclusion, these findings suggest that A3C may facilitate RNA-editing; however, they also raise questions regarding its functional significance. Despite belonging to the cytidine deaminase family and showing affinity for U-rich sequences, the predominantly cytoplasmic localization of A3C challenges its enzymatic activity. The analysis of RNA-seq data from 786-O C, A3C KO and A3C Rec cells identified potential editing sites. However, many putative editing sites were either unrecoverable in A3C Rec cells, resulted in no amino acid alterations or did not alter the expression levels of potentially edited transcripts. These findings suggest that A3C may have functions independent of its cytidine deaminase activity in ccRCC-derived cells. Further research is needed to fully elucidate the role of A3C in RNA-editing and its broader implications in cellular processes.

3.2 The A3C 3' UTR harbors regulatory elements

As part of the investigation of the less-understood member of the A3 family, the gene structure of A3C was examined. Based on the human genome assembly GRCh37.p13, the annotated 3' UTR of A3C spanned approximately 430 bp (indicated by a blue arrow in Figure 10A, lower panel). However, upon analyzing the gene structure of A3C using RNA-seq data from 786-O cells and the *Integrative Genomics Viewer* (IGV) software, reads extending beyond the annotated 3' end were detected (Figure 10A, middle panel). The read coverage substantially decreased upstream of an endogenous poly(A)-stretch, explaining the annotated 3' end in GRCh37.p13 human genome assembly.

Interestingly, RNA-seq reads spanned a region of approximately 2 kb downstream of the end of the A3C coding sequence (CDS) until a poly(A)-signal, suggesting that the 3' UTR of A3C is approximately five times longer than annotated. To validate the expression of the longer A3C 3' UTR, semiquantitative RT-PCR using oligonucleotides that bind downstream of the reported 3' end was performed, and the results confirmed expression

levels comparable to the A3C CDS (Figure 10C). As a side note, the GRCh38.p14 human genome assembly includes the A3C gene structure with the longer 3' UTR.

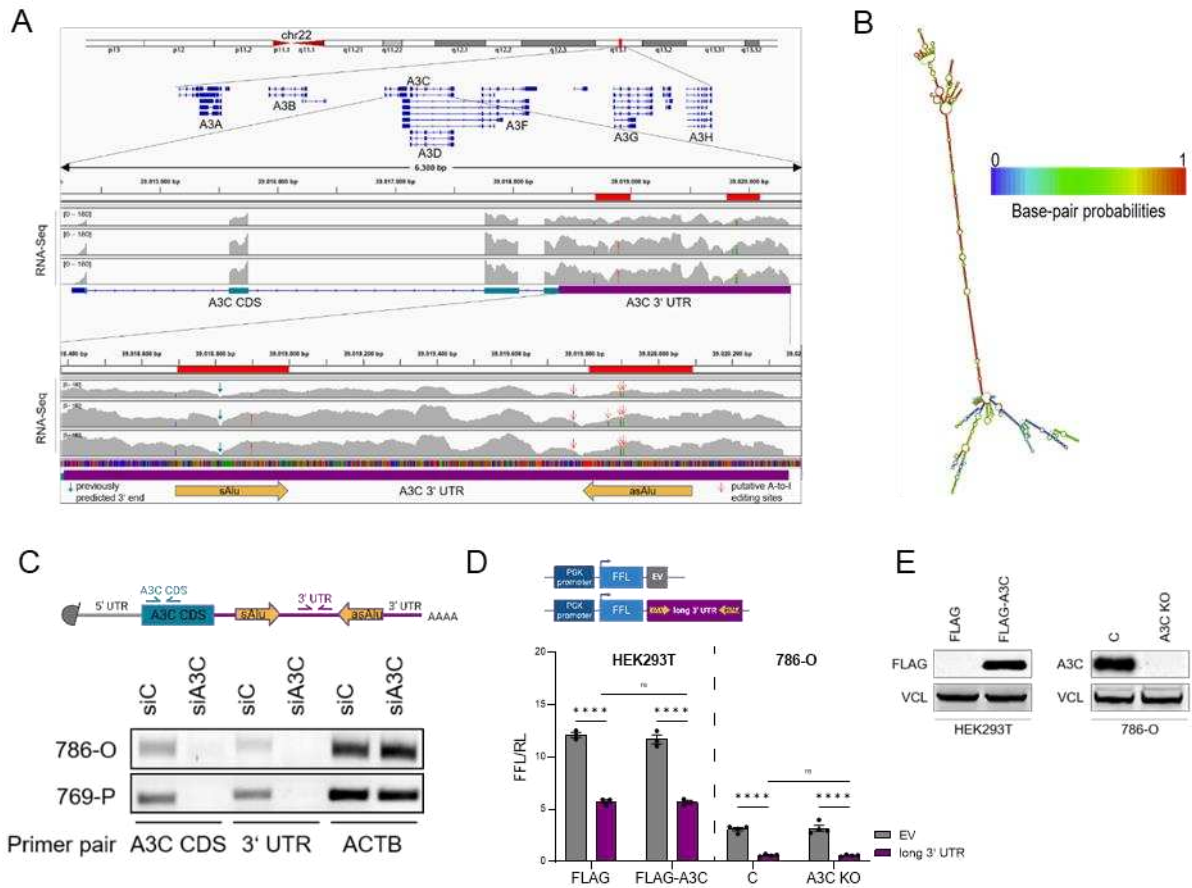


Figure 10: The 3' untranslated region (UTR) of A3C contains regulatory elements. (A) Schematic illustrates the *APOBEC3* gene cluster on chromosomes 22 (upper panel). The middle panel shows the annotated A3C gene structure with exons (blue) and the 3' UTR (purple) as well as read coverages of three RNA-seqs of 786-O C cell populations. The lower panel highlights the A3C 3' UTR with predicted *Alu* elements (yellow), putative editing sites (red arrow) and the previously reported A3C 3' end (blue arrow). *Integrative Genomics Viewer* (IGV) software was used to visualize RNA-seq read coverages. The y-axis indicates total count of reads. (B) The secondary structure of the A3C 3' UTR is predicted. Folding prediction was generated with the *RNAfold WebServer* using the minimum free energy folding algorithm. (C) Semiquantitative RT-PCR was used to analyze expression levels of the coding sequence (CDS) and the 3' UTR of A3C in 786-O and 769-P cells. The schematic above the agarose gel picture illustrates location of the used primer pairs. To confirm the primer specificity, a siRNA-mediated KD of A3C was performed. A control siRNA (siC) was used. (D) The bar plot indicates the activity ratios of the luciferase reporters containing either the 3' UTR of A3C (long 3' UTR) or a vector-encoded 3' UTR (EV) downstream of the Firefly luciferase (FFL). Renilla luciferase (RL) served as internal control. Luciferase activity was determined in HEK2993T cells expressing FLAG or FLAG-A3C and in 786-O C or A3C KO cells. (E) WB analyses demonstrate the overexpression (FLAG-A3C) and deletion of A3C (A3C KO) protein levels in HEK2993T and 786-O cells, respectively. **** $p < 0.0001$ by two-way ANOVA (D; mean \pm SEM).

In-depth analyses of the gene structure of A3C revealed a pair of inverted *Alu* elements within its 3' UTR (sense *Alu* and antisense *Alu*, depicted by yellow arrows in Figure 10A). *Alu* elements are conserved, approximately 300 nucleotide-long repetitive sequences belonging to the SINE family of retrotransposons. They are highly abundant in the human genome, comprising approximately 10% of the whole genome mass (Lander et al., 2001). *Alu* elements tend to be concentrated in gene-rich regions, particularly within non-coding portions of genes including introns and untranslated regions (Versteeg et al., 2003).

Although the functional significance of *Alu* elements is not fully understood, they are involved in human genome evolution by affecting gene structure through insertions, gene conversion and recombination (Häsler, Strub, 2006). Pairs of inverted *Alu* repeats in RNA transcribed from *Alu* elements can form intramolecular long RNA duplex structures (Chen et al., 2008). Accordingly, folding prediction analysis using the A3C 3' UTR sequence revealed the formation of robust secondary structures (Figure 10B). Additionally, A-to-I RNA-editing sites were identified (indicated by A-to-G substitutions in RNA-seq data; depicted by red arrows in Figure 10A, lower panel), which are known to occur within *Alu* sequences (Athanasiadis et al., 2004; Kim et al., 2004; Levanon et al., 2004). While the precise role of A-to-I RNA-editing is not yet fully defined, it is speculated that it may affect gene expression at various steps, such as RNA stability, splicing or premature translational termination (Häsler, Strub, 2006).

To assess potential effects of the inverted *Alu* sequences within A3C 3' UTR on gene expression, a reporter gene construct was generated using the 2 kb A3C 3' UTR as the 3' UTR of a Firefly luciferase (FFL) reporter gene (depicted in Figure 10D). Luciferase signals were examined in HEK293T and 786-O cells, demonstrating a significant reduction in Firefly luciferase activity by 50% (HEK293T) or 80% (786-O) when harboring the A3C 3' UTR (Figure 10D), indicating that the 3' UTR contains repressive elements. Furthermore, transfecting the same reporter gene construct into cells with modulated A3C expression levels, either A3C overexpression (OE) in HEK293T or A3C KO in 786-O cells (indicated in Figure 10E), led to comparable reduction in the Firefly luciferase signal as observed in cells with endogenous A3C levels (Figure 10D). This suggests that the repressive regulation of gene expression potentially mediated by inverted *Alu* elements within the 3' UTR of A3C is independent of A3C itself.

In conclusion, these findings indicate that the 3' UTR of A3C is longer than previously annotated and contains inverted *Alu* elements that may be involved in gene regulation, as demonstrated by reduced luciferase activity in reporter gene assays. However, these regulatory elements are likely not subject to autoregulatory mechanisms.

3.3 A3C is upregulated in ccRCC and correlates with poor survival in RCC

By initially analyzing the expression of A3 family members in the kidney renal clear cell carcinoma (KIRC cohort) dataset obtained from the TCGA PanCancer Atlas (<https://www.cancer.gov/tcga>), a significant upregulation of A3C ($p < 0.0001$), A3D ($p < 0.05$), and A3G ($p < 0.0001$) was discovered. Notably, A3C exhibited the highest upregulation among this group of proteins in primary ccRCC, as shown in Figure 11A. Furthermore, the levels of A3C expression in other subtypes of RCC were investigated

(Figure 11B). The papillary subtype demonstrated elevated A3C levels similar to ccRCC, while the chromophobe subtype did not show increased A3C levels compared to normal tissue (NT).

Moreover, the expression levels of A3C in different stages of renal cancer were explored using data from the TCGA database. The results demonstrated a significant increase in mean A3C expression in stage III ($p=0.0014$) and stage IV ($p=0.0004$) ccRCC samples compared to stage I (Figure 11C), indicating a correlation between high A3C expression and renal cancer progression.

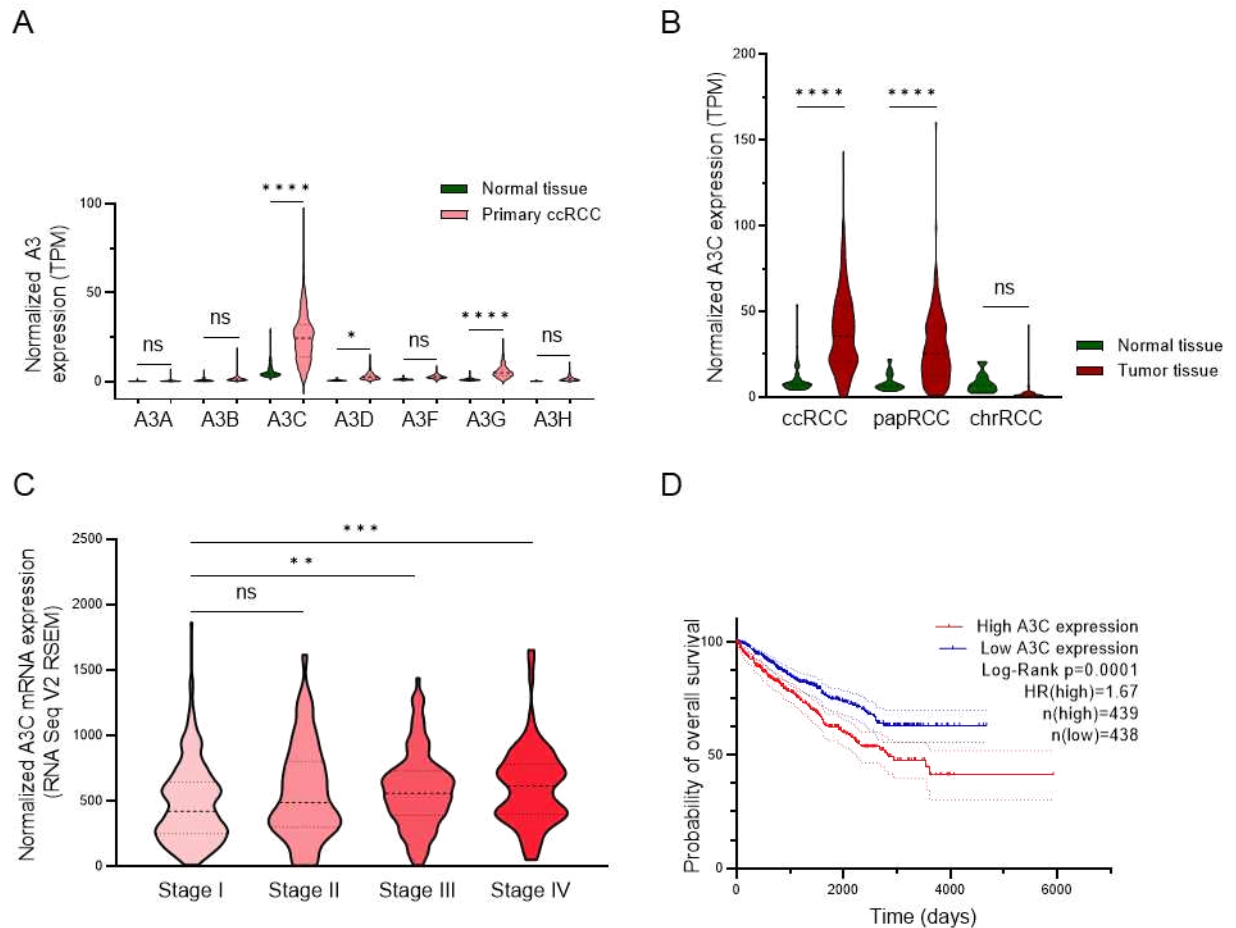


Figure 11: Clinical association of A3C levels in ccRCC. (A) Expression levels of A3 family members in primary ccRCC samples were compared to normal tissue samples (NT). Data was obtained from TCGA ($n(\text{NT})=72$; $n(\text{primary ccRCC})=538$). (B) A3C expression in diverse RCC subtypes compared to NT. Data were obtained from TCGA (ccRCC, $n=507$, $n(\text{NT})=72$; papRCC, $n=161$, $n(\text{NT})=30$; chrRCC, $n=66$, $n(\text{NT})=25$). (C) Violin plot presents relative A3C expression in stage I ($n=268$), stage II ($n=57$), stage III ($n=123$) and stage IV ($n=83$) ccRCC patients (TCGA data). (D) Kaplan-Meier analysis shows the overall survival of 877 RCC patients based on different A3C expression status. Data were gained from TCGA (Weinstein et al., 2013). The overall survival probabilities, hazard ratio (HR) and p-values were determined using *GraphPad Prism*. * $p < 0.05$; ** $p < 0.01$; *** $p < 0.001$ and **** $p < 0.0001$ by Tukey's multiple comparisons test (A and B) or unpaired, two-tailed Student's t-test (C). Kaplan-Meier survival curve was calculated using the log-rank (Mantel-Cox) test (D).

Additionally, to assess the putative prognostic value of A3C expression, the overall survival data from the TCGA was used. The samples were divided into two equal groups based on A3C expression levels, revealing that RCC patients with higher A3C levels exhibited poorer overall survival ($p=0.0001$) and a higher likelihood of succumbing to the

disease (HR=1.67; Figure 11D). Collectively, these results indicate that A3C serves as a valuable prognostic marker in RCC.

To confirm the observed elevated expression levels of A3C in ccRCC samples from publicly available datasets, a separate, smaller RCC cohort (Table 8) was examined. Except for A3A, all A3 family members displayed significantly increased expression in ccRCC samples (Figure 12A). Among these family members, A3C exhibited the highest upregulation compared to NT. Consistent with the publicly available datasets, the separate RCC cohort revealed elevated A3C mRNA levels in papRCC (type 1 or 2), while A3C levels remained unchanged in chrRCC (Figure 12B). Furthermore, a significant increase in A3C at protein level was confirmed in ccRCC patient samples compared to NT samples using WB analyses (Figure 12C).

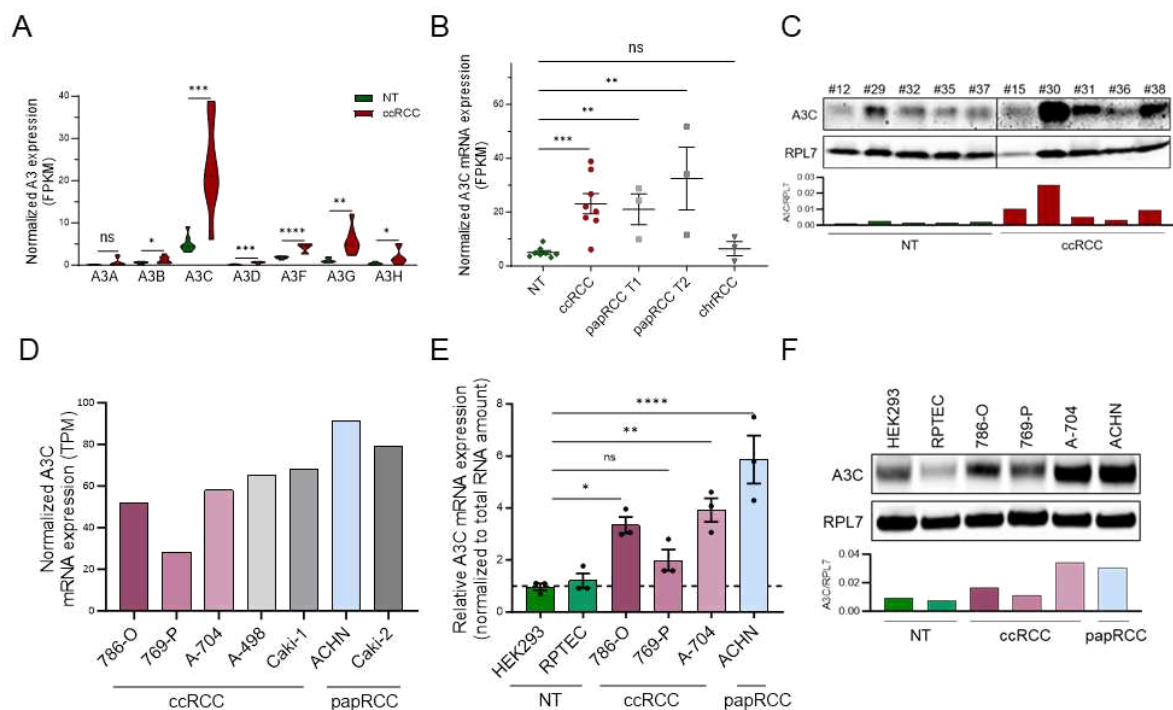


Figure 12: Confirmation of elevated A3C levels in a separate RCC cohort and RCC-derived cell lines. (A) The violin plot presents relative mRNA levels of A3 family members in ccRCC (n=8) samples and corresponding NT (n=8). (B) A3C expression was analyzed in ccRCC, papRCC type 1 (T1), papRCC T2 and chrRCC samples at mRNA level. (C) A3C protein levels in ccRCC primary tissue samples compared to NT were investigated by WB analyses. The ribosomal protein L7 (RPL7) was used as a reference for quantification. Relative A3C levels are depicted in the bar plot below the WB. (D) A3C mRNA levels were analyzed in ccRCC-derived cell lines (786-O, 769-P, A-704, A-498 and Caki-1) and papRCC-derived cell lines (ACHN and Caki-2) using expression data provided by the CCLE. (E and F) A3C levels were determined in RCC cell lines and normal kidney cell lines (HEK293 and RPTEC/TERT1) available in the laboratory at mRNA level by qRT-PCR (E) and at protein level by WB analyses (F). The bar plot below the WB shows relative A3C protein levels normalized to RPL7 (F). * $p < 0.05$; ** $p < 0.01$; *** $p < 0.001$; **** $p < 0.0001$ by unpaired, two-tailed Student's t-test (A and B) or ordinary one-way ANOVA with Tukey's multiple comparisons test (E). Data are representative of three independent experiments (mean \pm SEM in E).

For reasons of reproducibility, availability and culture consistency, cell models were employed for further analyses. These models include cell lines derived from ccRCC, such as 786-O, 769-P and A-704, as well as the papRCC-derived cell line ACHN (Sinha et al., 2017). Additionally, control cell models originating from normal renal epithelium (HEK293

and RPTEC/TERT1) were utilized. To validate the similarity between RCC cell lines and primary tumor tissues regarding A3C abundance, initially, the expression levels of A3C were assessed using publicly available datasets provided by the CCLE (Figure 12D), followed by analyses of cell lines utilized in the laboratory (Figure 12E). Overall, ccRCC-derived cells exhibited elevated A3C expression levels compared to NT-derived cells, while papRCC-derived cells displayed even greater upregulation. Consistent with mRNA levels, A3C also showed higher expression at the protein level in RCC-derived cells compared to control cells (Figure 12F).

In conclusion, these findings suggest that the A3 protein family is significantly upregulated in RCC. A3C emerged as the most significantly upregulated member and its increased expression was associated with advanced cancer progression and poorer overall survival.

3.4 Investigating mechanisms responsible for the upregulation of A3C expression in ccRCC

Subsequently, the cause of A3C upregulation in RCC was investigated by exploring different methods to understand the underlying cellular mechanism.

3.4.1 The 3' UTR of A3C contains *cis*- and *trans*-acting regulatory elements

To investigate the regulatory function of the pair of inverted *Alu* elements identified in the 3' UTR of A3C (see 3.2), a series of luciferase reporter constructs containing different sections of the 3' UTR of A3C (depicted in Figure 13A) were generated and transfected into 786-O WT cells. Initially, the Firefly luciferase signal was repeatedly significantly reduced with the reporter construct comprising the endogenous A3C 3' UTR (long 3' UTR; Figure 13B). Interestingly, a comparable reduction in Firefly activity was observed with the reporter construct containing a flipped sense *Alu* element (flipped *Alu*; Figure 13B), implying that the RNA duplex structure formed by inverted *Alu* repeats is not necessary for restricting gene expression. Furthermore, the deletion of the entire *Alu* elements still resulted in a 60% reduction in Firefly luciferase activity (Δ *Alu*; Figure 13B), suggesting the presence of regulatory elements outside the *Alu* sequences in the A3C 3' UTR. Subsequently, the Δ *Alu* sequence of the 3' UTR was divided into three fragments (F1, F2 and F3; depicted in Figure 13E, lower panel) to confine the localization of regulatory elements. The luciferase assay indicates that the inhibitory regulatory elements may be primarily located upstream and downstream of the antisense *Alu* element, as the reporter construct Δ *Alu* F2 + F3 exhibited the most reduced Firefly luciferase activity.

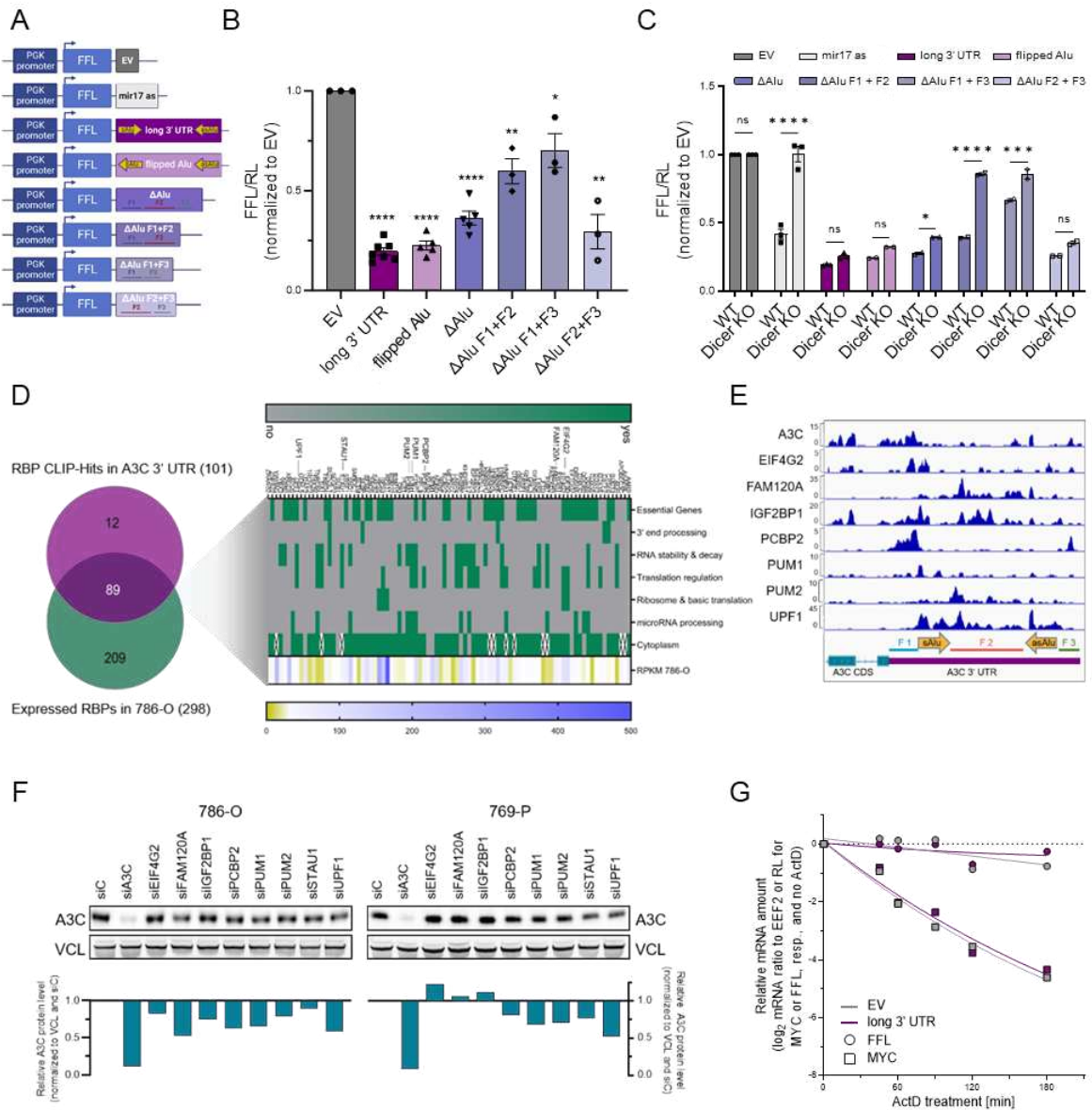


Figure 13: Putative regulation of A3C expression by miRNA or RNA-binding proteins (RBPs). (A) Diverse luciferase reporter constructs containing different elements of the 3' UTR of A3C or a binding site for the microRNA miR-17 (mir17 as) were cloned. A vector comprising a vector-encoded 3' UTR (EV) served as normalization control. (B and C) FFL activity was determined in 786-O cells (B) or HCT116 WT and CRISPR/Cas9-mediated Dicer KO cells (C). The activity of the FFL signal was normalized to RL and EV. (D) The Venn diagram (left panel) shows the number of RBPs that bind the 3' UTR of A3C identified in publicly available CLIP-seqs in K562 and HepG2 cells (encodeproject.org; van Nostrand et al., 2020b) and are concurrently expressed in 786-O cells (mean FPKM in 786-O control cells > 2). The right panel depicts selected functions of intersecting RBPs regarding regulation of the 3' UTR as well as cytoplasmic localization (according to van Nostrand et al., 2020a; upper panel) and expression (FPKM) according to the total RNA-seq in 786-O C cells (lower panel). (E) IGV screenshot illustrates the A3C 3' UTR and RNA peaks of CLIP-seqs from RBPs specified on the left of each track in K562 or HepG2 cells obtained from (van Nostrand et al., 2020b). The track below the coverage tracks shows the gene map of A3C (exon, blue; 3' UTR, purple). (F) Protein expression levels of A3C in 786-O and 769-P cells upon siRNA-mediated KD of selected RBPs identified in (D) were analyzed by WB. Signals were normalized to VCL and siC, ratios are indicated below the WBs. (G) The relative amount of MYC and FFL mRNA was analyzed by qRT-PCR in 786-O WT cells upon actinomycin D (ActD) treatment at indicated time points. Transcript abundance of MYC was normalized to EIF2 and DMSO-treated cells; FFL to RL and DMSO-treated cells. **p* < 0.05; ***p* < 0.01; ****p* < 0.001 and *****p* < 0.0001 by unpaired, two-tailed Student's *t*-test (B) or Šidák's multiple comparisons tests (C). Data are representative of at least three, in case of datasets with empty symbols (in C; flipped *Alu*, Δ *Alu*, Δ *Alu* F1+F2, Δ *Alu* F1+F3, Δ *Alu* F2+F3) two independent experiments (mean \pm SEM in B and C). Experiments presented in (F and G) were performed once.

Next, the role of miRNA in gene regulation mediated by the 3' UTR of A3C was investigated. Analyses of the luciferase reporters were conducted in HCT116 cells with CRISPR/Cas9-mediated KO of DICER, a key enzyme involved in miRNA maturation. Upon transfection of reporter constructs containing the native A3C 3' UTR (long 3' UTR; Figure 13C), the Firefly luciferase activity in Dicer KO cells, which have depleted levels of miRNAs, was reduced to levels similar to those observed in HCT116 WT cells. This result suggests that gene silencing facilitated by the A3C 3' UTR appears to be independent of miRNA regulation. Notably, the presence of a specific sequence, F1, within the 3' UTR of the luciferase construct led to a significant increase in Firefly luciferase activity in DICER KO cell, similar to the positive control (mir17 as), indicating that F1 may contain regulatory elements that respond to miRNA-mediated gene silencing. However, the depletion of miRNAs did not significantly affect the endogenous A3C 3' UTR, suggesting that A3C gene expression may be independent of miRNA regulation overall.

Subsequently, to assess if RBPs are involved in regulating A3C expression via its 3' UTR, publicly available CLIP studies in HepG2 and K562 cells (van Nostrand et al., 2016) were utilized to identify RBPs associated with the 3' UTR of A3C (analyses performed by Dr. Danny Misiak). Out of 101 RBPs identified in the 3' UTR, 89 RBPs were determined as putative candidates for regulating A3C gene expression based on their expression levels in 786-O cells (mean FPKM in 786-O C >2; Figure 13D, left panel). Functional characterization of these RBPs using a systematic study (van Nostrand et al., 2020a) revealed that most of the RBPs are essential and cytoplasmic proteins (Figure 13D, right panel). Several RBPs were selected for further analyses based on their molecular functions related to RNA stability and translation regulation (PCBP2, PUM2, STAU1; Figure 13D, right panel) as well as their correlation with favorable prognosis in renal cancer combined with downregulated expression in RCC (eIF4G2, FAM120A, PUM1, UPF1; data not shown).

CLIP peak profiles of these selected RBPs showed distinct binding patterns in the A3C 3' UTR, such as F2 for FAM120A or F1 and F3 for PCBP2 (Figure 13E). Interestingly, the selected RBPs shared common CLIP peaks at the start of the sense and antisense *Alu* elements, although of this group of RBPs, only STAU1 contains double-stranded RNA-binding domains. Unfortunately, the CLIP profile of STAU1 was not available. Next, selected RBPs were transiently knocked down in 786-O and 769-P cells, followed by investigating A3C expression at protein level (Figure 13F). Overall, the KD of RBPs resulted in a 10% to 40% reduction in A3C expression in 786-O, while the effects in 769-P cells were contrary. The KD of UPF1 resulted in substantial downregulation of A3C in both cell lines, whereas the KD of eIF4G2 and FAM120A showed opposing effects (Figure 13F).

In summary, given that several of these candidate RBPs have been identified as favorable prognostic markers for RCC, the downregulation of these RBPs would likely have a positive impact on RCC progression, meaning that A3C expression should be

upregulated. Thus, the selected RBPs are likely not the explanation for dysregulated A3C levels in RCC.

Furthermore, mRNA decay analyses of luciferase reporters containing either a minimal vector-encoded 3' UTR (EV) or the endogenous A3C 3' UTR demonstrated comparably robust FFL mRNA abundances over a three-hour period (Figure 13G). This suggests that the A3C 3' UTR does not contain very strong destabilizing elements. Supporting the hypothesis of slow A3C mRNA turnover, RNA decay analyses of A3C transcripts across diverse cell lines revealed relatively stable mRNA over a time span of at least two hours (Supplemental Figure 3). The stability of A3C mRNA may result from secondary structures mediated by *Alu* elements with the 3' UTR, which have been reported to extend mRNA half-life (Mauger et al., 2019). However, the regulation of A3C gene expression remains elusive.

To investigate the role of the 3' UTR regarding A3C gene expression under native conditions, 786-O cells harboring a CRISPR/Cas9-mediated deletion of the A3C 3' UTR were generated (Figure 14A). Analyses of A3C protein levels in 3' UTR KO cells showed a 40% reduction in A3C expression compared to 786-O WT cells (Figure 14B), with sufficient A3C levels still remaining. These findings suggest that the 3' UTR of A3C may contain regulatory elements influencing translation, yet it appears that the 3' UTR is not a critical determinant of A3C expression. Importantly, 786-O cells lacking the A3C 3' UTR exhibited similar viability to 786-O WT cells (Figure 14C).

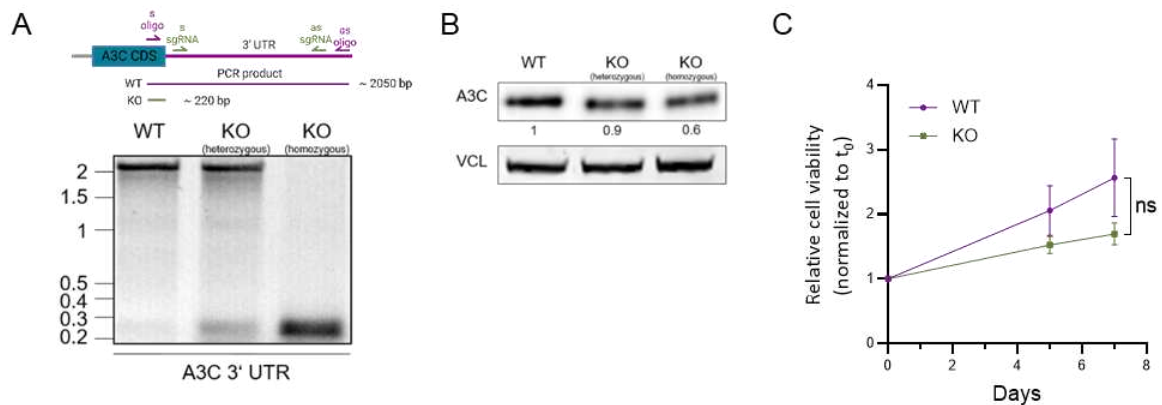


Figure 14: The effect on expression of A3C upon deletion of its 3' UTR. (A) 786-O cells with CRISPR/Cas9-mediated deletion of the 3' UTR of A3C were generated. Schematic on top illustrates localization of sgRNAs used for 3' UTR deletion and the primer pair used to verify deletion via PCR. Agarose gel shows PCR products of the long A3C 3' UTR (WT) and deleted 3' UTR (KO). Sizes of DNA ladder are listed on the left in kb. (B) WB analyses demonstrate A3C protein levels in dependence on the presence (WT) or deletion (KO) of the 3' UTR of A3C. Levels were normalized to VCL and WT, ratio is indicated below the WB. (C) Cell viability of 786-O WT or A3C 3' UTR KO cells was determined using CellTiter-Glo. Signals were normalized to values on the day of seeding (t_0). ns by multiple unpaired t-tests.

In conclusion, the analyses of the role of the 3' UTR in A3C expression revealed that although the 3' UTR features *cis*-acting (such as *Alu* sequences) and *trans*-acting regulatory elements (such as miRNA or RBPs), their contribution to the overall regulation of A3C expression appears to be minor. This is supported by the mRNA decay analyses (Figure 13G, Supplemental Figure 3) and the fact that CRISPR/Cas9-mediated deletion of

the A3C 3' UTR did not significantly affect A3C expression (Figure 14B), hinting at a regulation of A3C expression predominantly at the transcriptional level.

3.4.2 A3C is not an IFN- α -responsive gene

To investigate the transcriptional regulation of A3C in 786-O cells, initially, mRNA levels of luciferase reporters containing the endogenous 3' UTR of A3C were assessed using qRT-PCR. Comparative analyses presented in Figure 15A demonstrate a significant repression of FFL mRNA levels, consistent with the decreased FFL activity observed in the reporter construct containing the endogenous A3C 3' UTR (Figure 15A, left panel). As mentioned earlier, A3C transcripts appear to be relatively stable, suggesting transcriptional regulation of A3C expression.

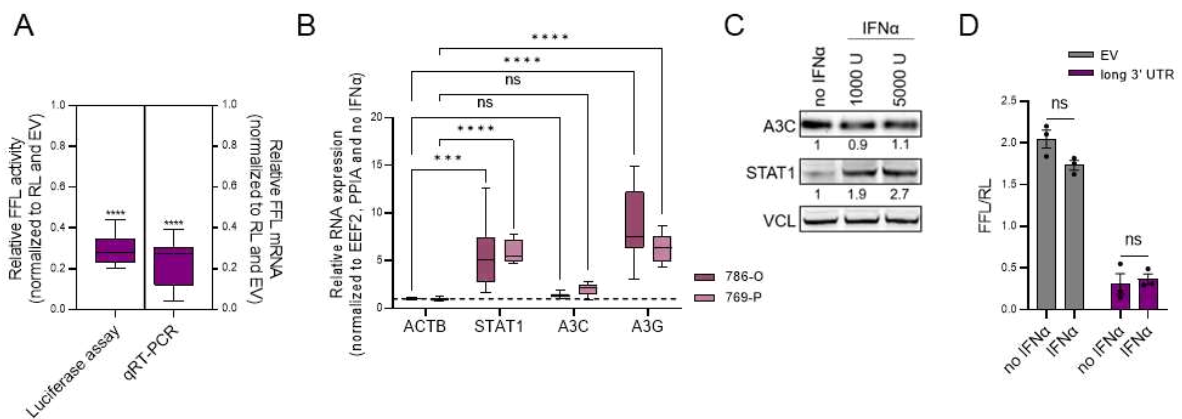


Figure 15: IFN- α does not induce expression of A3C. (A) The box plots show a comparison of the FFL activity (left) and FFL mRNA levels (right) of reporters containing the 3' UTR of A3C in 786-O WT cells normalized to EV and RL. (B-D) 786-O or 769-P WT cells were treated with 1000 U IFN- α (B and D) or indicated IFN- α amount (C) for 12 h before analyses. (B) Expression levels of A3C and A3G mRNA upon IFN- α treatment were determined. As previously reported, STAT1 is IFN- α -inducible (Ramana et al., 2000) and served as positive control for the IFN- α treatment. (C) WB analyses show A3C protein levels upon IFN- α treatment in 786-O WT cells. Signals were normalized to VCL and no IFN- α treatment. Ratios are indicated below the WB. (D) Luciferase ratios of reporters containing either the 3' UTR of A3C (long 3' UTR) or a vector-encoded 3' UTR (EV) were investigated in 786-O WT cells upon IFN- α treatment. *** p < 0.001 and **** p < 0.0001 by unpaired, two-tailed Student's t-test (A and D) or two-way ANOVA with Tukey's multiple comparisons tests (B). Data are representative of at least six (A and B) or three (D) independent experiments (5-95 percentile in A and B; mean \pm SEM in D).

Previous studies have reported that members of the A3 protein family, such as A3A, A3B, A3F and A3G, are transcriptionally induced upon IFN- α stimulation (Chen et al., 2010; Peng et al., 2006). IFN- α is an important component of the immune response against viral infections and activates the expression of genes associated with antiviral defense, immune activation and inflammation via the JAK-STAT signaling pathway (Liu et al., 2012b). Since A3 proteins are involved in the innate antiviral defense, their IFN- α -inducible expression is expected. However, this study reveals that A3C behaves differently from the A3 protein family in terms of IFN- α inducibility. Despite successful IFN- α treatment, as evidenced by the upregulation of STAT1 and A3G at mRNA level (Figure 15B) and protein level

(Figure 15C), no significant induction of A3C expression was observed. This result suggests that transcription of A3C is not stimulated by IFN- α .

Furthermore, the role of the 3' UTR of A3C in IFN- α responsiveness was examined. Luciferase reporter assays with the endogenous A3C 3' UTR showed no substantial increase in luciferase activity upon IFN- α treatment, indicating that the 3' UTR of A3C is not responsive to IFN- α stimulation (Figure 15D).

These findings emphasize on the one hand that A3C expression is regulated at the transcriptional level and on the other hand that gene expression of A3 family members is differentially regulated. While several members are known to be inducible by IFN- α , this study shows that A3C and its 3' UTR are not responsive to IFN- α signaling.

3.4.3 A3C is upregulated at transcriptional level as response to stress

A growing tumor encounters a range of stress factors as it develops and expands, such as nutrient deprivation, hypoxia, high cellular density or cell detachment as cancer cells invade nearby tissues (Hockel, 2001; Kimmelman, White, 2017; Weiss, Ward, 1983). In response to these stressors, adaptive mechanisms aimed at enhancing survival and tumor progression are activated, such as angiogenesis or metabolic reprogramming (Wek, Staschke, 2010). These adaptations are mediated by signaling pathways that induce the activation of transcription factors, leading subsequently to differential gene expression (Izuishi et al., 2000; Keith, Simon, 2007; Reuter et al., 2010).

To investigate if A3C is part of the stress-induced transcriptional response, A3C expression was assessed under conditions that mimic cellular stress in a growing tumor. 786-O and 769-P WT cells were cultured under diverse stress conditions, including high density (HD), low attachment (LA) or serum deprivation (1% FBS). Analyses of A3C expression on both the mRNA (Figure 16, A and B) and protein levels (Figure 16, C and D) revealed upregulation of A3C in response to high cellular density, cell detachment and serum deprivation compared to control conditions.

These findings suggest that A3C expression is probably transcriptionally induced in response to various stress factors encountered by growing tumors. The activation of stress-induced pathways involving A3C may contribute to the adaptive survival mechanisms of RCC cancer cells under adverse conditions.

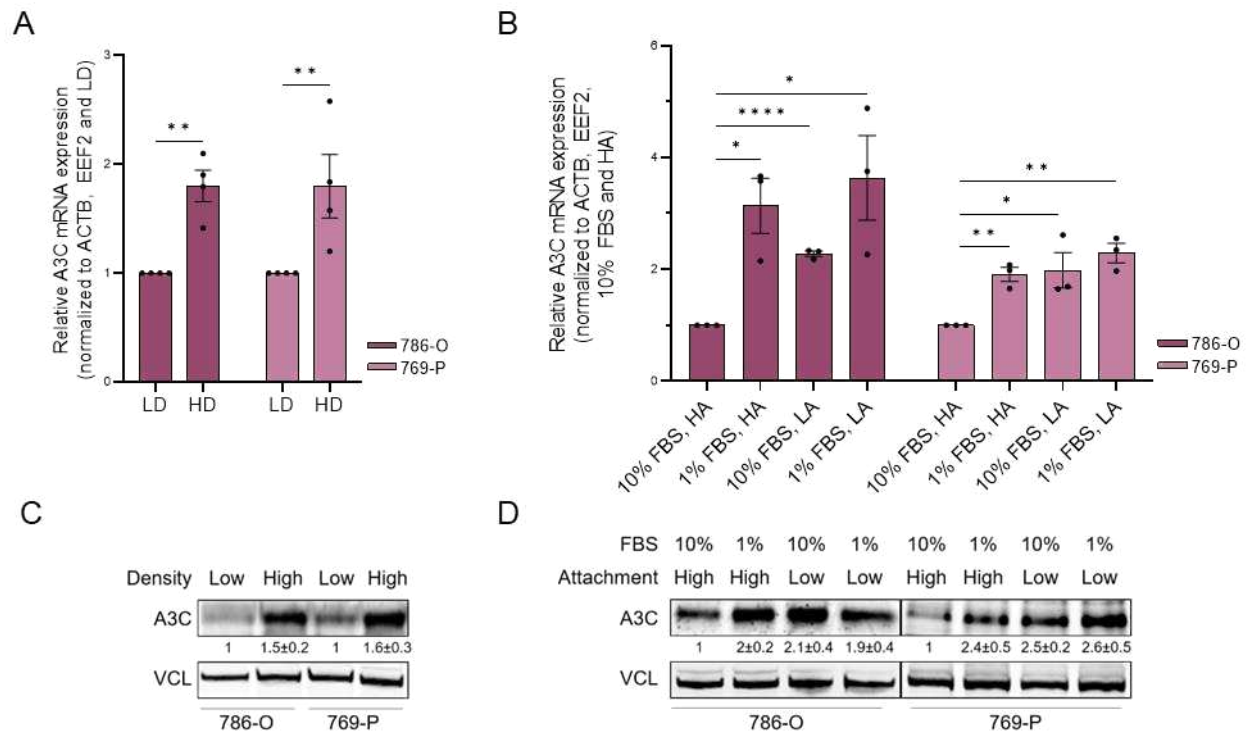


Figure 16: A3C expression is elevated upon exposure to diverse stress factors. Expression levels of A3C were investigated in 786-O and 769-P WT cells under diverse growth conditions. **(A and B)** Bar plots indicate mRNA levels of A3C under low (LD) or high (HD) density growth conditions **(A)** and fetal calf serum (FBS) depleted conditions (1% FBS) combined with low (LA) or high (HA) attachment **(B)**. **(C and D)** WB analyses demonstrate A3C protein levels under LD compared to HD conditions **(C)** and FBS depleted conditions combined with LA or HA **(D)**. * $p < 0.05$; ** $p < 0.01$ and **** $p < 0.0001$ by unpaired, two-tailed Student's t-test **(A and B)**. Data are representative of four **(A)** or three **(B)** independent experiments (mean \pm SEM in **A and B**). Protein levels were normalized to VCL and control growth conditions (LD for **C**; 10% FBS and HA for **D**) in at least three biological replicates; mean \pm SD is indicated below the representative WBs **(C and D)**.

3.5 Molecular function of A3C in the context of ccRCC

After investigating the structural characterization of the A3C transcript and analyzing the regulation of A3C gene expression, the focus shifts to exploring the molecular function of A3C in the context of ccRCC, which was the primary objective of this study.

3.5.1 Depletion of A3C impairs the NF- κ B signaling pathway

To elucidate the potential oncogenic role of A3C, the spectrum of target genes regulated by A3C was explored using global gene expression profiles of 786-O C, A3C KO and A3C Rec cell populations. By comparing transcript levels between 786-O C and A3C KO cells, 644 significantly downregulated and 656 significantly upregulated transcripts were identified (up: \log_2 FC ≥ 1 ; down: \log_2 FC ≤ -1 ; FDR ≤ 0.01 considered significant; Figure 17B). Additionally, RNA-seq analysis revealed that the expression of 340 genes was significantly downregulated in A3C KO cells and simultaneously upregulated in A3C Rec cells (FDR ≥ 0.01), identifying high-confidence targets regulated by A3C. To validate the recovery analyses, transcript levels of A3C KO cells were compared with A3C Rec cells (no FC restriction; FDR < 0.001 ; Figure 17C). It was observed that over 60% of the down- or

upregulated transcripts in A3C KO cells were significantly recovered, confirming the validity of the recovery model.

Interestingly, a substantial downregulation of A3C mRNA itself in A3C KO cell populations was identified. This phenomenon is frequently observed for CRISPR/Cas9-mediated KO cells, indicating a degradation of A3C mRNA by nonsense-mediated decay (NMD; Popp, Maquat, 2016).

To gain insight into the functional significance of the differentially expressed genes between 786-O C and A3C KO cells, gene set enrichment analyses (GSEA) using HALLMARK pathways were performed (Figure 17D, left panel). The HALLMARK pathway 'TNFA SIGNALING VIA NFkB' was the most significantly altered pathway upon A3C deletion (Figure 17E, upper panel). Furthermore, other immunological cancer signatures associated with the NF- κ B signaling pathway, such as 'INFLAMMATORY RESPONSE', 'KRAS SIGNALING' (Pak, Miyamoto, 2013), 'INTERFERON GAMMA RESPONSE', 'IL6 JAK STAT3 SIGNALING' (Brasier, 2010) and 'COMPLEMENT' (Sugihara et al., 2010), were significantly altered. Notably, GSEA using differentially expressed genes between A3C KO and A3C Rec cells revealed the same HALLMARK pathways as significantly positively enriched upon A3C re-expression (Figure 17D, right panel), with 'TNFA SIGNALING VIA NFkB' being the most significantly altered pathway (Figure 17E, lower panel). Additionally, the transcript levels of a variety of chemokines and cytokines were altered upon A3C modulation (Supplemental Figure 4). This includes well-known activators of the NF- κ B pathway like TGF- β , IL18, CCL2, CCL20, CXCL5 (Jia et al., 2021; Kaplanski, 2018; Ma et al., 2021; Tang, Tsai, 2012; Zeng et al., 2014).

The NF- κ B signaling pathway has previously been described as a crucial factor in RCC progression, regulating important aspects of RCC biology, such as resistance to apoptosis, angiogenesis and multidrug resistance (Du et al., 2014; Morais et al., 2011; Oya et al., 2003a; Pei et al., 2015). By investigating the separate, smaller RCC cohort, upregulation of NF- κ B subunits (NF- κ B2, RelA and RelB) in ccRCC samples compared to NT was observed (Figure 17F). Likewise, high levels of these NF- κ B subunits are associated with reduced overall survival rates of RCC patients (Figure 17H), suggesting a prognostic potential of the NF- κ B signaling pathway for RCC patients. Additionally, a positive correlation between A3C expression and the expression of NF- κ B2, RelA and RelB was identified (Figure 17I). Furthermore, GSEA using differentially expressed genes from the RCC cohort revealed a significant positive enrichment of a plethora of HALLMARK pathways associated with the NF- κ B signaling pathway in ccRCC samples compared to NT (Figure 17G).

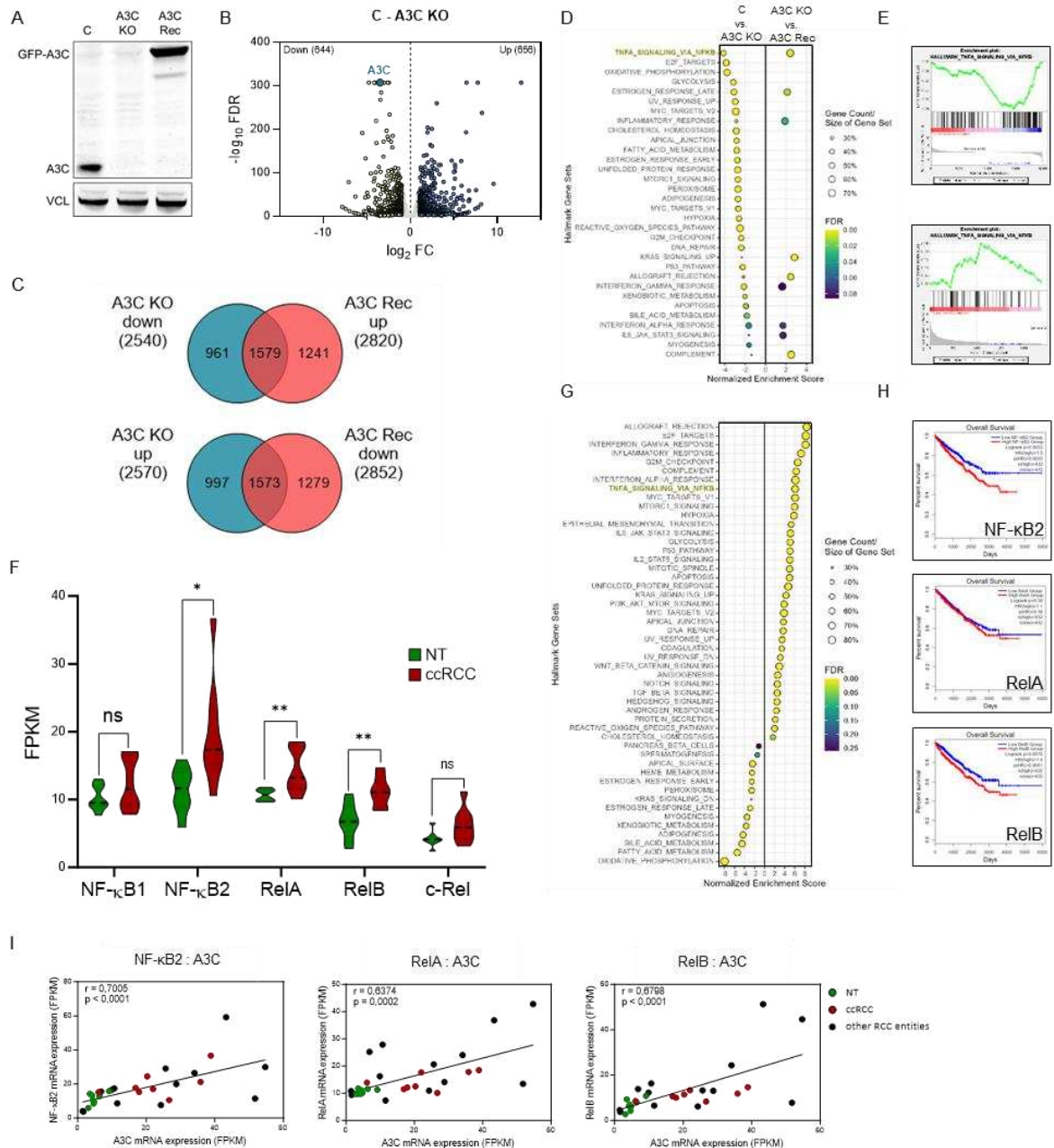


Figure 17: The NF-κB signaling pathway is impaired upon A3C KO. (A) WB indicates the A3C protein levels in 786-O C, A3C KO and A3C Rec cells. VCL was used as the loading control. (B) Volcano plot of log₂ mRNA FC plotted against -log₁₀ FDR shows DEG in 786-O C and A3C KO cells. Downregulated genes (FC ≤ -2; FDR ≤ 0.01) are highlighted in yellow, upregulated genes (FC ≥ 2; FDR ≤ 0.01) in blue. (C) The upper Venn diagram shows the overlap of downregulated genes in A3C KO compared to C and upregulated genes in A3C Rec compared to A3C KO (FPKM in C > 0.1; FDR < 0.001). The lower Venn diagram shows the overlap of upregulated genes in A3C KO compared to C and downregulated genes in A3C Rec compared to A3C KO (FPKM in C > 0.1; FDR < 0.001). (D) Gene set enrichment analyses (GSEA) were performed using differentially expressed mRNAs in 786-O C vs. A3C KO (left panel; n=5 864 genes) or A3C KO vs. A3C Rec (right panel; n=2 379 genes) and the HALLMARK gene sets (n=50). (E) Enrichment plots of the HALLMARK gene set ‘TNFA SIGNALING VIA NFκB’ are presented. The upper panel shows the GSEA using DEG in 786-O C vs. A3C KO; the lower panel shows the GSEA using DEG in 786-O A3C KO vs. A3C Rec. (F) Relative mRNA expression of the NF-κB family members was analyzed in ccRCC (n=8) and corresponding NT (n=8). (G) GSEA of genes dysregulated in ccRCC vs. RCC determined in the separate RCC cohort were performed using the HALLMARK gene sets. (H) Overall survival of RCC patients based on different NF-κB2 (upper panel), RelA (middle panel) and RelB (lower panel) expression status was investigated by Kaplan-Meier analyses. Kaplan-Meier plots were generated using <http://gepia2.cancer-pku.cn/> with data obtained from TCGA. (I) NF-κB2 (left panel), RelA (middle panel) and RelB (left panel) mRNA abundances were plotted over A3C mRNA levels (FPKM) as determined in RNA-seq of the separate RCC cohort. Association of expression was analyzed by Spearman correlation studies. Correlation coefficient (r), significance (p) and the linear regression line are shown. *p < 0.05 and **p < 0.01 by unpaired, two-tailed Student’s t-test (F).

In summary, these findings strongly suggest that A3C appears to regulate the NF- κ B signaling pathway, establishing a novel connection between A3C and the NF- κ B signaling pathway. Furthermore, the NF- κ B signaling pathway plays a crucial role in RCC development.

3.5.1.1 NF- κ B activity is affected upon modification of A3C expression

To investigate the impact of A3C modification on NF- κ B activity, a luciferase reporter construct containing NF- κ B binding motifs in the minimal promoter region of a Firefly luciferase gene was generated (Figure 18A).

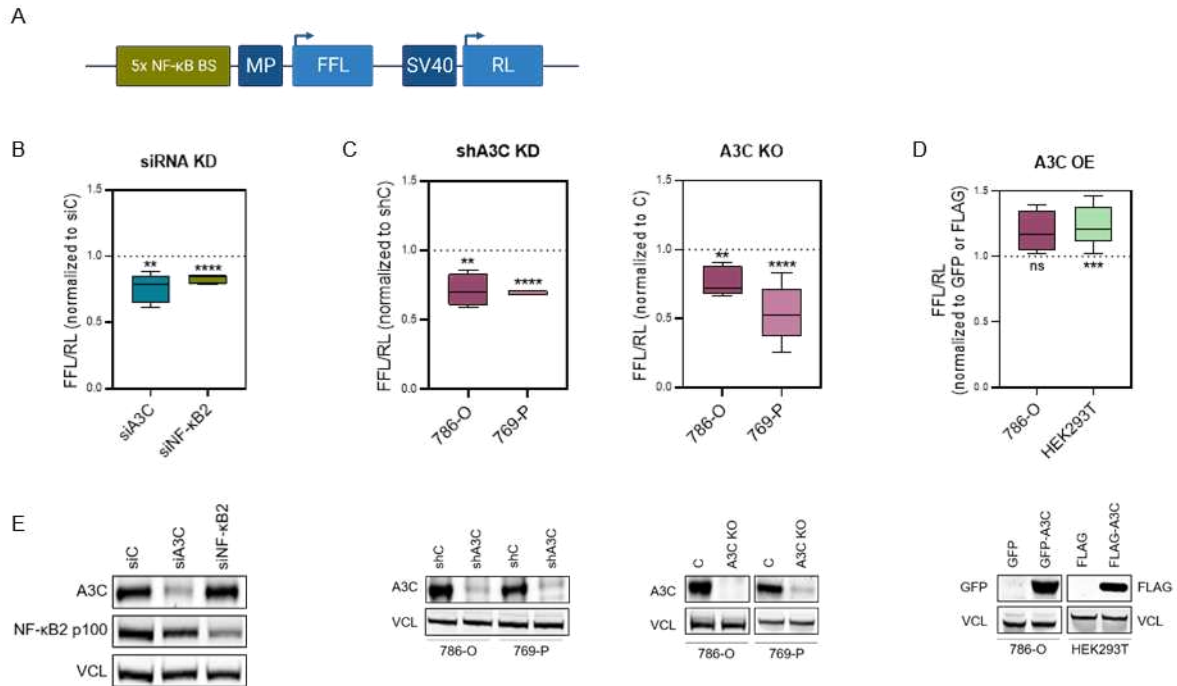


Figure 18: Altered A3C expression levels correlate with altered NF- κ B activity. (A) The schematic depicts the luciferase reporter that contains besides a minimal promoter (MP) five NF- κ B-binding sites in the promoter region of FFL. SV40 guided RL served as internal normalization control. (B) Luciferase activity was determined in 786-O cells upon transient A3C or NF- κ B2 depletion by siRNA pools. (C) Activity ratios of the luciferase reporter were analyzed in cell lines upon stable A3C KD by shRNAs (left panel) or CRISPR/Cas9-mediated A3C KO (right panel). (D) Luciferase activity was determined in 786-O or HEK293T cells upon stable overexpression (OE) of A3C. (E) WB analyses indicate modified levels of A3C and NF- κ B2 in cells used for the luciferase reporter assay described in (B-D). VCL served as loading control. ** $p < 0.01$; *** $p < 0.001$ and **** $p < 0.0001$ by unpaired, two-tailed Student's t-test (B-D). Data are representative of at least four independent experiments (5-95 percentile in B-D).

Initially, the luciferase reporter was transfected into 786-O cells with transiently depleted NF- κ B2 to assess the responsiveness of the reporter to modified NF- κ B subunit levels. As indicated in Figure 18B, there was a mild effect on Firefly activity under these conditions. Notably, transient KD of A3C resulted in a greater reduction of NF- κ B activity (Figure 18B), suggesting a potentially global impact of A3C on NF- κ B signaling. It is important to note that the consensus sequence recognized by NF- κ B can exhibit significant variability, particularly in the central portion (Mulero et al., 2019). Thus, the used reporter construct may not encompass all putative κ B-binding sites. Given the limited variation of

κ B-binding sites in the reporter vector and the KD of a single NF- κ B subunit, a modest effect on NF- κ B activity was expected.

To further support the involvement of A3C in regulating NF- κ B activity, the luciferase reporter was transfected into 786-O and 769-P cells with stably depleted A3C levels (either stable shA3C KD or A3C KO). The Firefly luciferase activity was significantly reduced (Figure 18C), indicating an impaired NF- κ B pathway, possibly due to less active NF- κ B subunits. This finding strengthens the hypothesis that A3C plays a role in NF- κ B pathway regulation. Consistently, restored luciferase activity was observed in HEK293T and 786-O cells with stable A3C OE (Figure 18D).

Collectively, these results indicate that A3C depletion negatively affects the NF- κ B signaling pathway in different cell lines, and overexpression of A3C compensates for this effect, suggesting a regulatory function of A3C in NF- κ B activity.

3.5.1.2 Expression of NF- κ B target genes is impaired upon A3C depletion

The diminished activity of the NF- κ B transcription factor is anticipated to impair the transcription of target genes containing κ B-binding sites in their promoter or enhancer regions. Initially, a list of genes containing validated κ B-binding sites in their promoter regions was compiled using resources such as <https://bioinfo.lifl.fr/NF-KB/> and www.bu.edu/nf-kb/gene-resources/target-genes/. After excluding genes with negligible expression in 786-O cells (FPKM < 0.1; p < 0.01), in-depth analyses of the RNA-seq data revealed that a substantial fraction of NF- κ B-inducible genes (~25%) exhibited reduced expression in 786-O A3C KO cells compared to C, and this expression was concurrently restored upon A3C re-expression (Figure 19A).

To validate these findings, WB analyses of four randomly selected NF- κ B target genes (C3, BIRC3, BIRC5 and BCL2) were performed, confirming aberrant expression in 786-O A3C KO cells and recovery upon A3C re-expression (Figure 19B). Similarly, stable KD of A3C in 786-O and 769-P cell populations resulted in reduced protein levels of C3, BIRC3, BIRC5 and BCL2 (Figure 19C). Furthermore, using qRT-PCR on additional NF- κ B-inducible genes in stable A3C KD cells confirmed their decreased expression levels, including genes such as CSF2, TNFRSF9, TNFAIP3, VEGFA and BIRC4 (Figure 19D).

Supporting these observations, RNA-seq analyses of the separate ccRCC cohort revealed elevated expression levels of the NF- κ B target genes C3, BIRC3 and BIRC5 (Figure 19E) as a consequence of elevated NF- κ B activity in RCC. Additionally, these NF- κ B target genes were associated with decreased overall survival rates of RCC patients (Figure 19F).

RESULTS

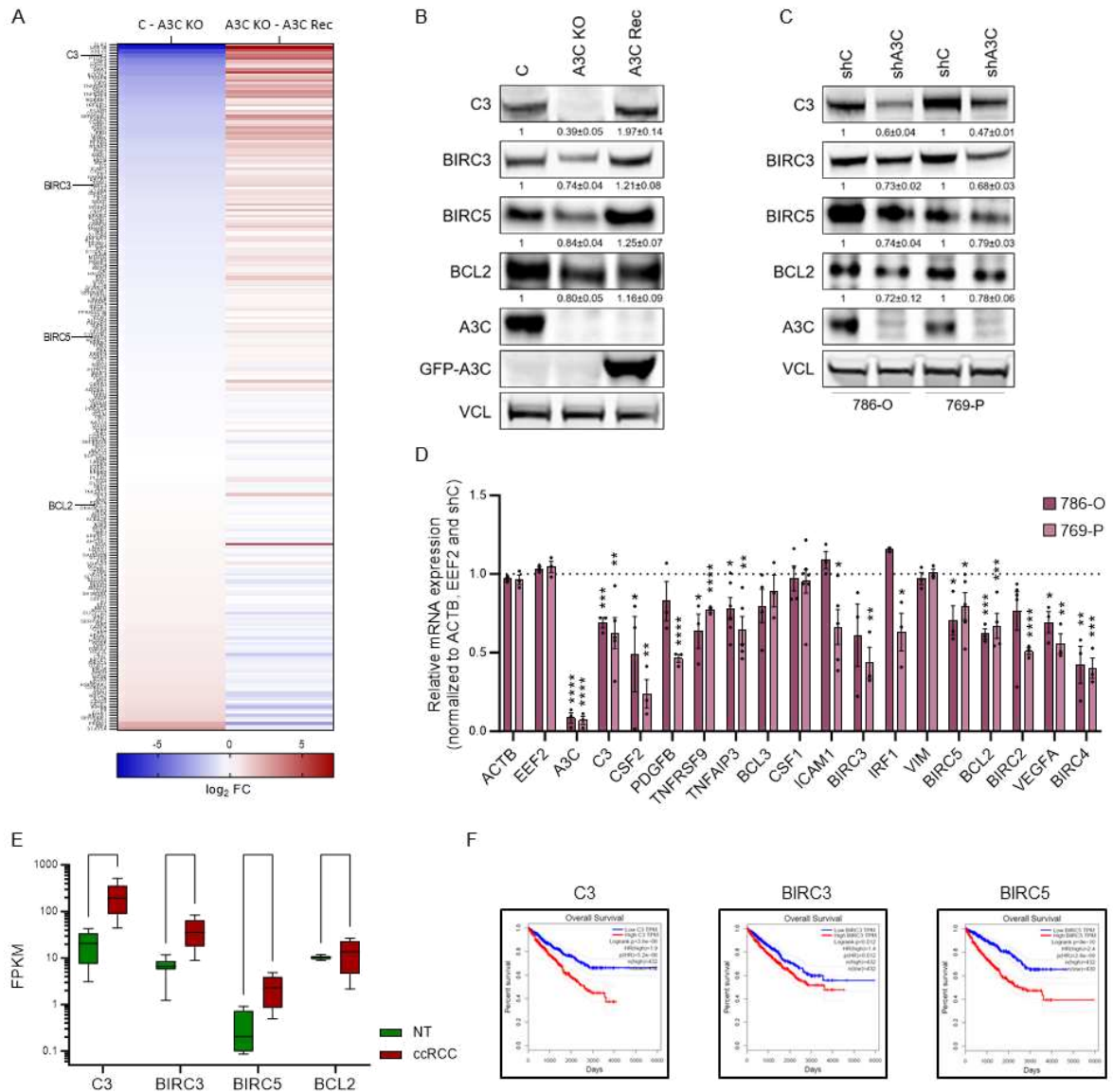


Figure 19: Expression of clinically relevant NF- κ B target genes is reduced upon A3C depletion. (A) Heat map presents the \log_2 FC for NF- κ B target genes according to <https://bioinfo.lifl.fr/NF-KB/> and www.bu.edu/nf-kb/gene-resources/target-genes/ upon KO of A3C and rescue of A3C in 786-O cells. (B and C) Protein levels of four NF- κ B target genes (C3, BIRC3, BIRC5 and BCL2) in 786-O C, A3C KO and A3C Rec cells (B) as well as upon stable A3C KD (shA3C) in 786-O and 769-P cells (C) are depicted in representative WBs. (D) NF- κ B target genes were investigated at mRNA level in 786-O and 769-P shA3C cells. Note that the majority of the randomly selected NF- κ B target genes shows lower expression upon stable KD of A3C. (E) The box plot indicates relative mRNA expression of selected NF- κ B target genes in ccRCC patients (n=8) and corresponding NT (n=8). (F) Overall survival of RCC patients based on different C3 (left panel), BIRC3 (middle panel) and BIRC5 (right panel) expression status was investigated by Kaplan-Meier analyses. * $p < 0.05$; ** $p < 0.01$; *** $p < 0.001$ and **** $p < 0.0001$ by unpaired, two-tailed Student's t-test (D and E). Protein levels were quantified by normalization to VCL and C (B) or shC (C) in at least three biological replicates; mean \pm SD is indicated below the representative WBs. Data are representative of at least three independent experiments (D; mean \pm SEM in D; 5-95 percentile in E). Kaplan-Meier plots were generated using <http://gepia2.cancer-pku.cn/> with data obtained from TCGA (F).

In conclusion, these findings provide compelling evidence that A3C has a significant impact on NF- κ B activity in ccRCC-derived cells, resulting in the suppression of NF- κ B-inducible gene expression.

3.5.1.3 Suppression of NF- κ B target gene expression upon A3C depletion is a conserved effect in RCC cell lines

Following the discovery of the impact of A3C depletion on the expression of NF- κ B target genes, this effect was explored in various RCC-derived cell lines. A3C levels were transiently reduced using siRNAs. Subsequently, the expression of two high-confidence NF- κ B target genes, C3 and BIRC3, was assessed by qRT-PCR and WB analyses. Figure 20A and B demonstrate that A3C depletion affected the expression of C3 and BIRC3 in A-704 and ACHN cells, highlighting that the suppression of NF- κ B target gene expression upon A3C depletion is a conserved phenomenon in RCC cell lines.

Furthermore, intriguing differences in the responsiveness of NF- κ B target genes to the transient depletion of NF- κ B2 and RelB were discovered, as demonstrated in Figure 20C. These observations suggest the presence of distinct κ B-binding sites in the promoter regions of NF- κ B-inducible genes. Specifically, C3 expression was strongly downregulated upon NF- κ B2 KD, whereas the transient KD of RelB only mildly affected its expression. In contrast, both NF- κ B2 and RelB KD equally impaired the expression of BIRC3. These results indicate that NF- κ B target genes respond to different combinations of NF- κ B homo- and heterodimer formation and harbor unique κ B-binding sites. Furthermore, it was discovered that A3C showed a mild reduction in expression upon NF- κ B2 and RelB KD (Figure 20C), suggesting that A3C may be a target of NF- κ B transcription factors.

To further support the hypothesis that A3C indirectly regulates NF- κ B target gene expression due to impaired NF- κ B activity, RNA decay and a nascent RNA capturing assay were conducted, with C3 serving as a representative NF- κ B target gene. Figure 20D indicates that C3 mRNA remained stable upon A3C depletion compared to endogenous A3C expression, suggesting that reduced transcript levels shown in Figure 20A are not a result of mRNA destabilization due to the absence of A3C. Additionally, a nascent RNA capture kit, which facilitates the separation of newly synthesized RNA transcripts from existing RNA, was utilized to measure the transcription rate of C3. This assay revealed reduced transcription of C3 upon A3C KO (Figure 20E), indicating that NF- κ B target genes are indirectly regulated by A3C at transcriptional level.

In conclusion, these findings highlight that the reduced expression levels of NF- κ B target genes observed in various RCC-derived cell lines result from impaired transcription induction indirectly mediated by A3C via NF- κ B activity, rather than mRNA degradation.

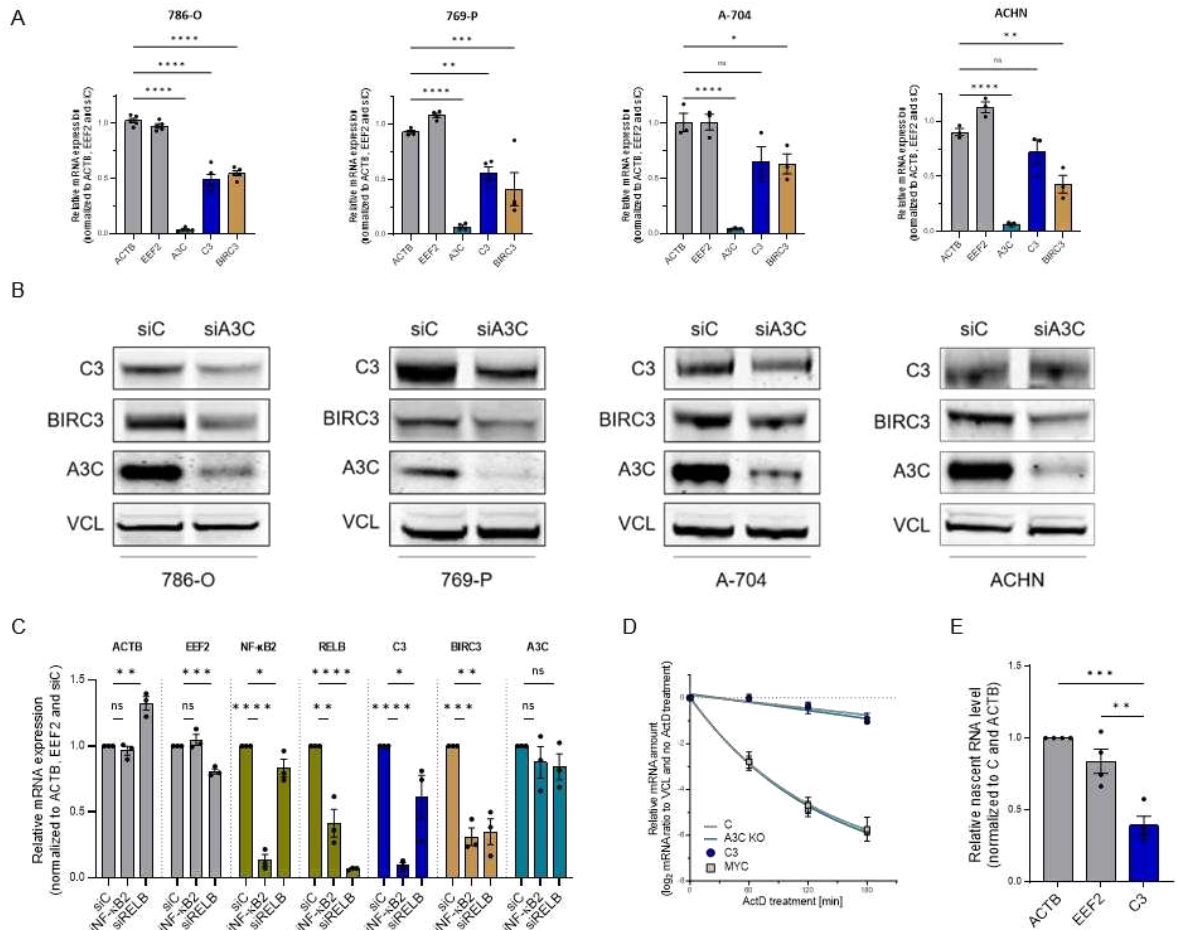


Figure 20: Reduced expression of NF-κB target genes upon A3C depletion is a global effect in RCC cell lines. (A) C3 and BIRC3 mRNA expression levels were investigated upon transient KD of A3C in diverse cell lines. (B) WBs show the protein levels of C3 and BIRC3 upon siRNA-mediated KD of A3C in indicated cell lines. VCL served as a loading control. (C) Expression of A3C, C3 and BIRC3 were determined at mRNA level upon siRNA-mediated KD of NF-κB2 and RelB. Expression was normalized to ACTB, EEF2 and siC. (D) The relative amount of MYC and C3 mRNA was analyzed by qRT-PCR in 786-O C and A3C KO cells upon ActD treatment at indicated time points. Transcript abundance was normalized to VCL and DMSO-treated cells. (E) Nascent C3 mRNA amount was investigated in 786-O C and A3C KO cells. ACTB and EEF2 served as normalization control. *p < 0.05; **p < 0.01; ***p < 0.001 and ****p < 0.0001 by ordinary one-way ANOVA (A and E) and multiple unpaired t-tests (C). Data are representative of at least three independent experiments (A, C-E; mean ± SEM in A, C-E). WB analyses presented in (B) were performed once.

3.5.2 A3C binds transcripts of NF-κB signaling pathway regulators

As an interim conclusion, it can be noted that A3C plays a role in regulating the NF-κB signaling pathway, as evidenced by the observed reduction of NF-κB activity and target gene expression. Notably, this regulatory function of A3C has not been previously reported, thus the underlying molecular mechanism remains elusive. The complexity of the NF-κB signaling network presents a challenge in unraveling this process.

The NF-κB signaling network is highly intricate and interconnected, involving multiple pathways, regulatory factors and feedback loops. This complexity is evident from the extensive annotations related to the ‘positive regulation of NF-kappaB transcription factor activity’ gene ontology term, which lists a total of 230 annotations for *Homo sapiens* (<https://amigo.geneontology.org/amigo/term/GO:0051092>). Additionally, the interaction

database IntAct identified 306 binary interactions along with the NF- κ B member RelA (Hoesel, Schmid, 2013). To provide a partial illustration of this complex network, the STRING database (<http://string-db.org/>) was utilized to visualize the physical and functional interactions between NF- κ B subunits and other proteins (Figure 21).

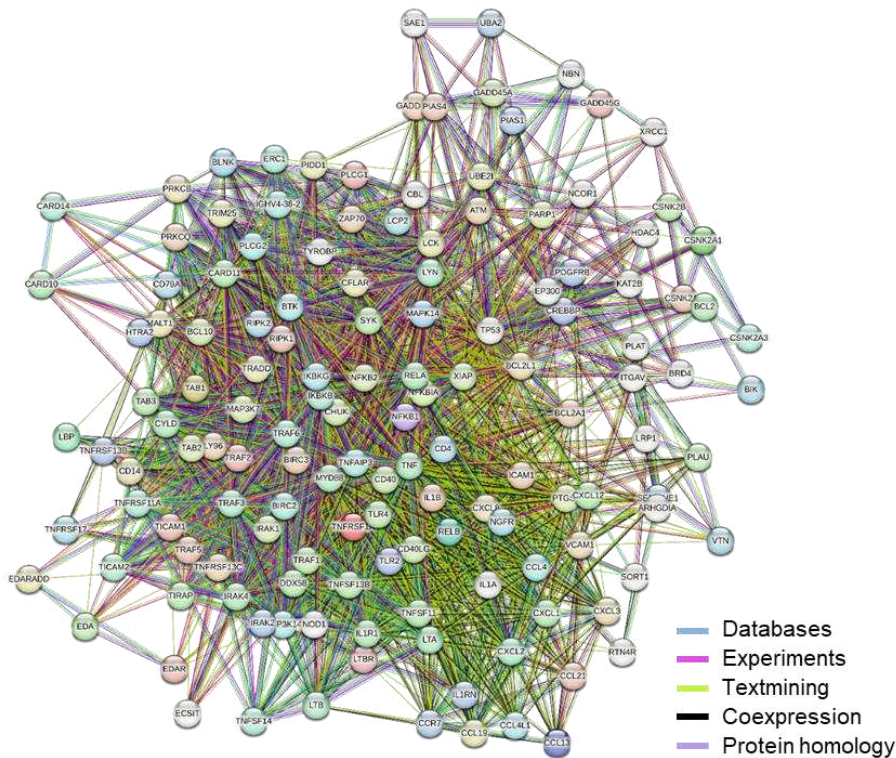


Figure 21: The network of NF- κ B interactors. The schematic illustrates functional and physical interactors of the NF- κ B components (generated with <http://string-db.org/>).

To gain further insight into the regulatory function of A3C within this network, RNA co-immunoprecipitations (RIP) analyses were conducted to identify RNAs directly bound by A3C. For immunoprecipitation of RNP complexes, 786-O A3C Rec cells were used, and GFP-A3C was efficiently purified with anti-GFP-coated magnetic beads confirmed by WB analysis (Figure 22A). As previously reported in this study, A3C interacts with subunits of the ribosome (Figure 7B) and with Y RNAs (Figure 7C). Therefore, RPL7 served as a positive control in WB analyses (Figure 22A), indicating association of A3C with components of RNPs, thus validating the RIP analyses. RNAs purified from A3C-IP samples were sequenced (RIP-seq), followed by analyzing the four human Y RNA loci, confirming robust association of A3C with Y1 and Y3 RNAs (Figure 22B).

RIP-seq analyses identified more than 5 300 protein-coding and non-coding transcripts enriched in the A3C-IP (FC compared to input ≥ 2 ; mean FPKM in input > 0.1). To gain insight into the functional annotation of the putative protein-coding binding partners of A3C ($n=2\,770$), the RIP-seq data was interpreted using DAVID, with a focus on the REACTOME_PATHWAY category.

RESULTS

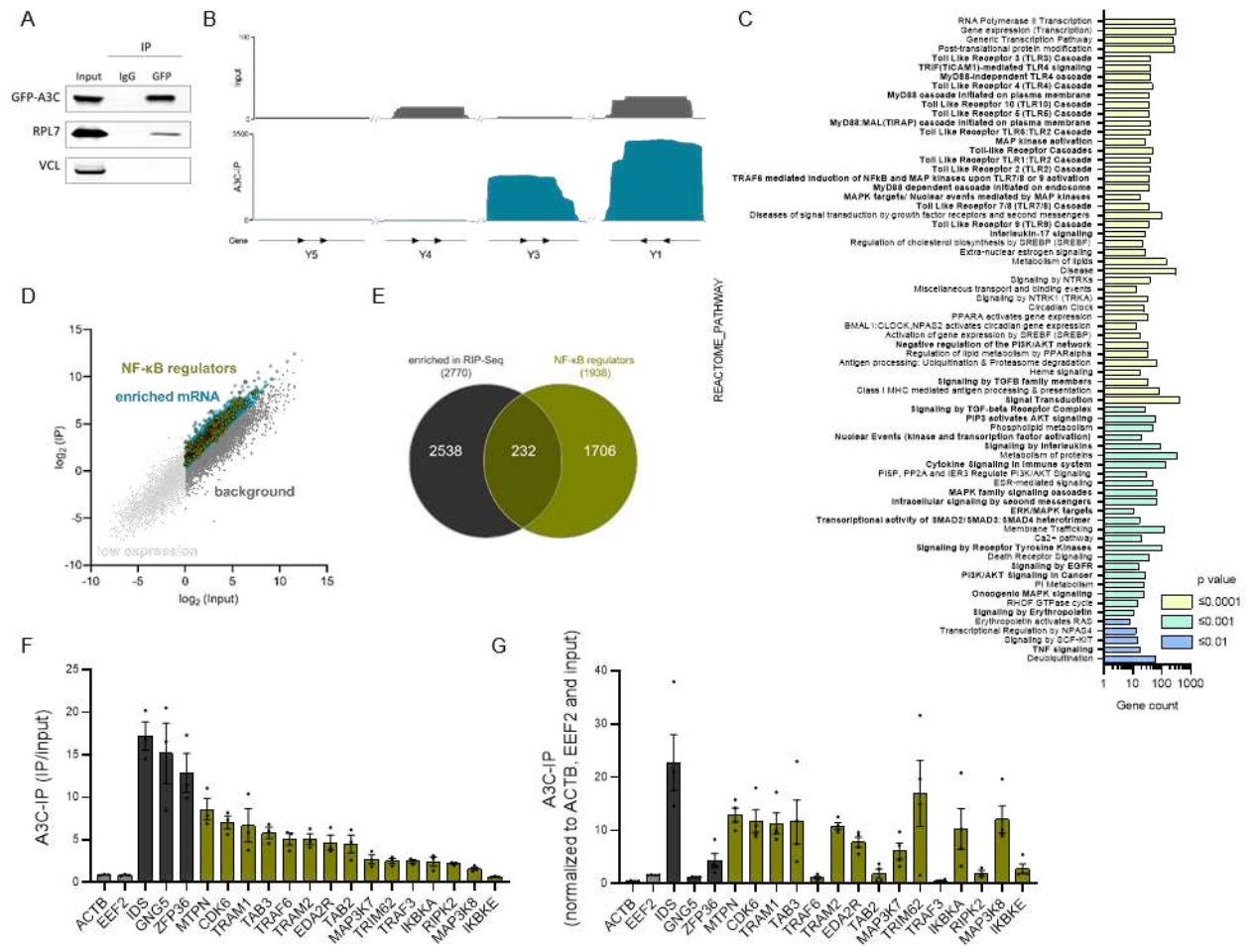


Figure 22: A3C associates with transcripts of NF- κ B signaling pathway regulators. (A) 786-O A3C Rec cells were used for immunoprecipitation (IP) with an anti-GFP antibody. RPL7 and VCL served as positive and negative controls, respectively. IP with an anti-FLAG antibody (IgG) was used as specificity control. (B) Inputs and normalized reads of the sequencing results of RNAs co-purified with A3C-IPs (RIP-seq) were investigated at four Y RNA loci to analyze the reported association of A3C with Y RNAs. (C) Gene list of transcripts enriched in RIP-seq ($n=2\ 770$) was used for REACTOME PATHWAY enrichment analysis with DAVID. Gene count indicates the number of genes from the input list found in each pathway; sorted by p value. (D) Scatter plot shows results of the RIP-seq in 786-O A3C Rec cells. High-confidence binding partners of A3C are marked in blue (A3C-IP/input > 1). Within this group, NF- κ B signaling pathway regulators are colored in yellow. Transcripts with a ratio of A3C-IP/input ≤ 1 are considered background (gray). Transcripts with low expression (mean FPKM in input < 0.1) are depicted in light gray. (E) The Venn diagram shows the overlap of RIP-seq enriched transcripts (A3C-IP/input ≥ 2 ; $p < 0.05$; FPKM in input > 0.1) with reported NF- κ B signaling regulators (obtained from www.gsea-msigdb.org/gsea/msigdb/; Supplemental Table 2). (F) Bar plot presents examples of enriched transcripts identified in RIP-seq of the A3C-IPs (IDS, GNG5 and ZFP36 within top 30). Reported NF- κ B signaling pathway regulators are depicted in yellow. (G) Bar plot shows the same transcripts as in (F) obtained in separate A3C-IPs analyzed with qRT-PCR. Note that the majority of enriched NF- κ B signaling regulators identified in the RIP-seq are also enriched in A3C-IPs analyzed by qRT-PCR (A3C-IP/input > 1). Data are representative of three independent experiments (mean \pm SEM in F and G).

Notably, many of the identified pathways were associated with the NF- κ B signaling pathway (Figure 22C; bold letters), including TLR or MAPK cascades, which trigger signaling pathways activating NF- κ B transcription factors downstream. Furthermore, comparison of the significantly enriched protein-coding genes from the A3C-IP ($FC \geq 2$; $p < 0.05$; mean FPKM in input > 0.1) with reported NF- κ B signaling pathway regulators (gene sets obtained from www.gsea-msigdb.org/gsea/msigdb/; Supplemental Table 2) identified 232 putative mRNA-binding partners of A3C involved in regulating the NF- κ B

signaling pathway (Figure 22, D and E; Supplemental Table 3). However, it was also observed that a variety of potential A3C target RNAs belong to pathways not significantly affected by A3C modulation, which implies a broad A3C target spectrum (Supplemental Figure 5).

To validate the results of the RIP-seq analyses, separate A3C-IPs from 786-O A3C Rec cell populations were performed, and transcript levels were quantified by qRT-PCR. The RIP-seq suggested enrichment of mRNAs encoding IDS, GNG5, ZFP36 and NF- κ B signaling pathway regulators, and these targets were largely recapitulated by qRT-PCR (Figure 22, F and G). Importantly, this validation process revealed several high-confidence binding partners of A3C, including MTPN, CDK6, TRAM1, TAB3, TRAM2, EDA2R, MAP3K7, TRIM62, IKBKA and MAP3K8. Intriguingly, all these factors positively regulate the NF- κ B signaling pathway, indicating that modulation of A3C levels may affect their regulatory function, consequently influencing NF- κ B activity.

As previously discussed in this study (see 3.1.3), despite belonging to a family of cytidine deaminases, A3C may perform a function independent of its enzymatic activity. Indeed, by comparing the identified putative editing candidates of A3C (Supplemental Table 1) with putative A3C binding targets, seven target transcripts were identified that appeared in both datasets, including GLTP, PANX2, PXN, SBF1, TWF1, UBE4B and WDR4. Interestingly, none of these editing candidates are considered NF- κ B regulators.

Overall, these findings strongly suggest that A3C could efficiently affect the NF- κ B signaling pathway by modulating its regulators by a mechanism independent of its cytidine deaminase function.

3.5.3 A3C affects transcript levels of NF- κ B signaling pathway regulators

RBPs play a crucial role in regulating the stability and degradation of RNA molecules by selectively binding to RNA sequences. To investigate the impact of A3C on the stability of transcripts involved in the NF- κ B signaling pathway, initially, the expression levels of the identified potential binding targets were determined in 786-O and 769-P shA3C cells. Notably, a reduction in the expression of transcripts involved in NF- κ B regulation was observed upon A3C depletion (Figure 23, A and B). In contrast, the expression of non-NF- κ B-regulating factors, such as IDS and GNG5 mRNAs, remained largely unaffected. Furthermore, the decrease in expression upon A3C KD was validated at the protein level for CDK6 and IKBKA (Figure 23, C and D).

To understand how A3C modulates the stability of bound transcripts, the hypothesis of A3C protecting these transcripts from miRNA-mediated degradation by blocking RISC (RNA-induced silencing complex) association was explored. The let-7a miRNA was identified as the most abundant miRNA in 786-O cells, according to CCLE data. Consequently, transcripts bound by A3C were examined for potential let-7a binding sites

(BS), revealing validated let-7a BS in MTPN, CDK6, TAB3, TRAM2, TAB2, MAP3K7 and IKBKA, primarily located in their 3' UTRs (analyses performed by Dr. Markus Glaß; Figure 24A).

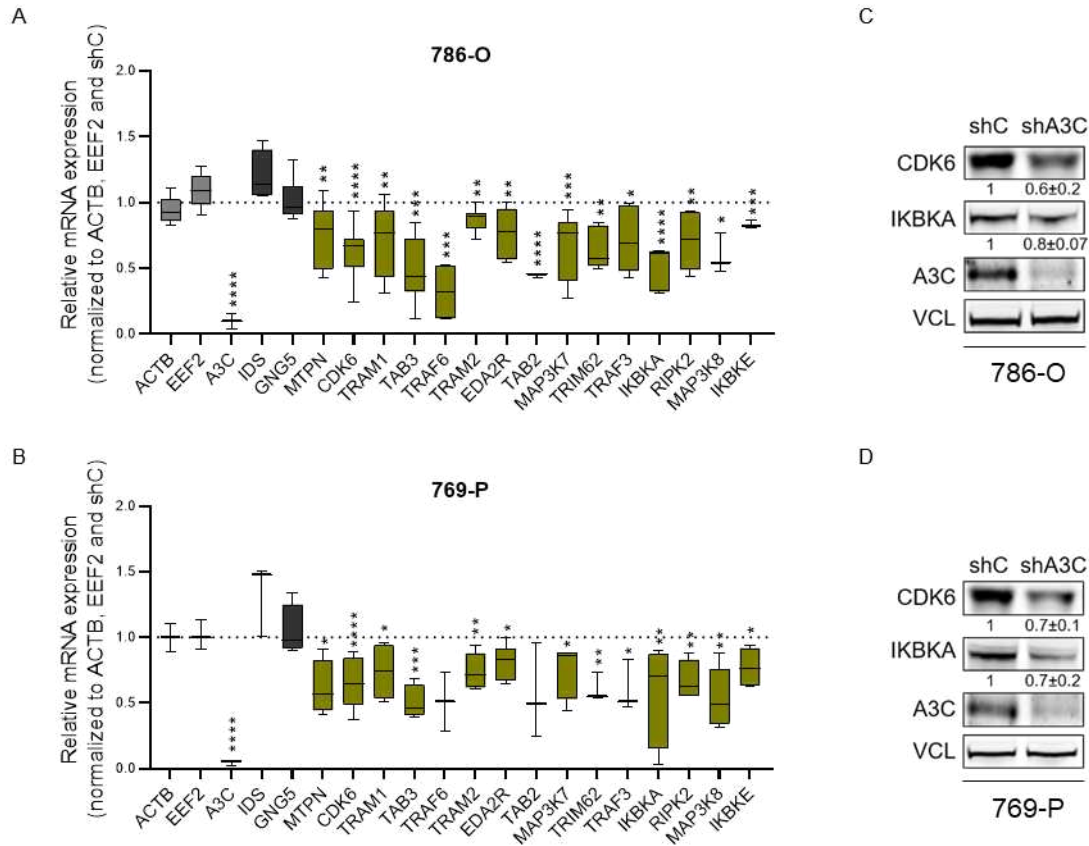


Figure 23: A3C depletion results in reduced expression of NF- κ B signaling pathway regulators. (A and B) mRNA expression levels of NF- κ B signaling pathway regulators (marked in yellow) were analyzed in 786-O shA3C (A) and 769-P shA3C (B) cells by qRT-PCR. ACTB and EEF2 (light gray) served as negative controls. IDS and GNG5 (dark gray) are putative binding partners of A3C, but not considered NF- κ B signaling pathway regulators. (C and D) WB analyses show decreased expression of CDK6 and IKBKA in 786-O shA3C (C) and 769-P shA3C (D) cells. * $p < 0.05$; ** $p < 0.01$; *** $p < 0.001$ and **** $p < 0.0001$ by unpaired, two-tailed Student's t-test compared to 786-O shC (A) or 769-P shC (B). Data are representative of at least three independent experiments (5-95 percentile in A and B). Protein levels were normalized to VCL and shC in at least three biological replicates; mean \pm SD is indicated below the representative WBs (C and D).

Furthermore, publicly available A3C-CLIP studies conducted in K562 cells (van Nostrand et al., 2020a) indicated the presence of A3C-CLIP peaks in various transcripts, particularly in 3' UTRs (e.g., MTPN and CDK6). However, it is worth noting that not all identified let-7a BS overlapped with A3C-CLIP peaks, as exemplified by BS#2 for IKBKA (Figure 24A).

To assess the functional impact of let-7a BS on target transcripts, luciferase reporter constructs harboring the let-7a responsive element of MTPN, CDK6, TAB3, MAP3K7 and IKBKA in the 3' UTR of the Firefly luciferase gene were generated. The Firefly luciferase activity was determined in stable 786-O and 769-P shA3C cells. As shown in Figure 24B, the luciferase activity was unaffected (TAB3) or mildly decreased, with a maximum reduction of 20% observed for MTPN, CDK6 let-7a BS#2, IKBKA BS#1 and IKBKA BS#2.

RESULTS

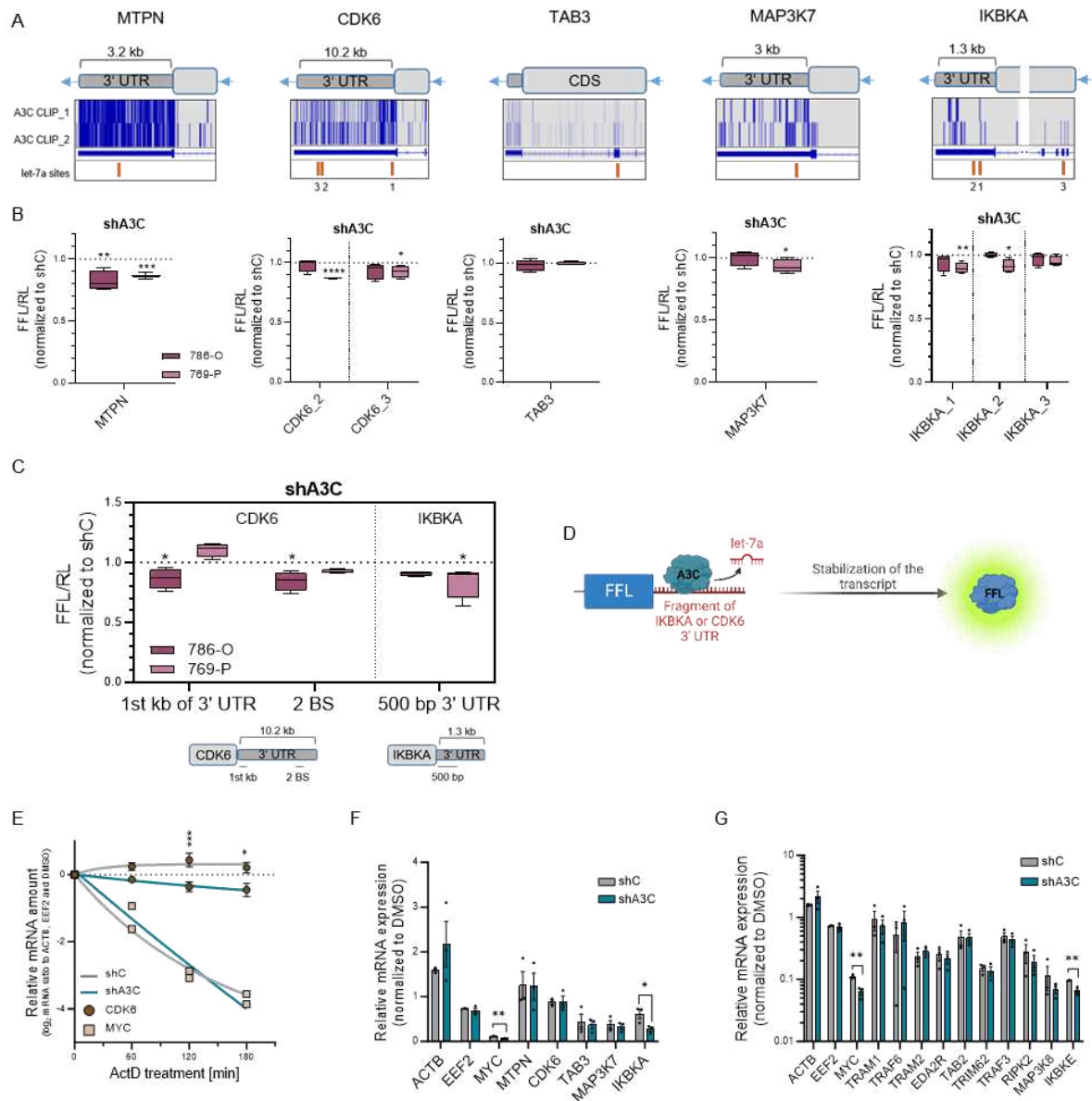


Figure 24: A3C could potentially stabilize transcripts of NF- κ B signaling pathway regulators. (A) IGV screenshots show A3C-CLIP peaks in the 3' UTR and partly the CDS of the indicated genes. Data obtained from two experiments performed in K562 cells by Gene Yeo, UCSD, 2018. The upper panel depicts the 3' UTR (dark gray) and part of the CDS (light gray); blue arrows specify the orientation of the genes. Orange bars illustrate let-7a binding sites (BS) identified with *multiMiR*. (B) Luciferase reporters containing the let-7a BS as depicted in (A) within the 3' UTR of FFL were generated. Numbers in the label refer to the numbers of the let-7a BS in (A; 1st BS of let-7a in the 3' UTR of CDK6 was not successfully cloned in a reporter vector). Reporter vectors were transfected into 786-O and 769-P shC and shA3C cells. FFL signal was normalized to RL and shC cells. (C) Luciferase reporters containing longer fragments of the 3' UTRs of CDK6 and IKBKA were generated. The schematics below the box plot illustrates the cloned regions of the 3' UTRs indicated by a black line. FFL signal was normalized to RL and shC cells. (D) Schematic demonstrates the putative stabilizing mechanism of FFL mRNA harboring sequences of 3' UTRs of NF- κ B regulators by A3C. (E) MYC and CDK6 mRNA amount was analyzed in 786-O shC and shA3C cells upon ActD treatment at indicated time points. Transcript abundance was normalized to ACTB, EEF2 and DMSO-treated cells. (F and G) 786-O shC and shA3C cells were treated with 10 μ M α -amanitin for 24 h. (F) Bar plot presents the relative mRNA amount of NF- κ B regulators investigated in (A and B). (G) More putative binding targets of A3C identified in the RIP-seq were analyzed. Transcript abundance was normalized DMSO-treated cells. * $p < 0.05$; ** $p < 0.01$ and *** $p < 0.001$ by unpaired, two-tailed Student's t-test compared to shC (B, E-G) or by Tukey's multiple comparisons test (C). Data are representative of at least three independent experiments (5-95 percentile in B and C; mean \pm SEM in E-G).

Considering that the cloned sequences may not contain the complete A3C binding site, longer fragments of the CDK6 and IKBKA 3' UTRs were incorporated into luciferase reporters to better capture the potential influence of A3C (schematically depicted in Figure 24D). Notably, the luciferase activity of reporters containing CDK6 3' UTR fragments was significantly reduced upon A3C KD in 786-O cells, while the IKBKA 3' UTR fragment affected luciferase activity in 769-P cells (Figure 24C). These findings suggest that although A3C's overall effect on reducing NF- κ B activity is consistent among ccRCC-derived cell lines, the specific response of luciferase reporters to A3C KD varies depending on cellular context. Furthermore, these findings indicate that A3C may contribute to maintain the stability and expression of transcripts for factors involved in the NF- κ B pathway, thereby influencing the activity of NF- κ B.

To further investigate whether A3C stabilizes bound transcripts, RNA decay assays were performed to assess the degradation of transcripts upon A3C depletion. Two different approaches of RNA decay assays were employed using ActD or α -amanitin to block transcription in 786-O shC and shA3C cells. As indicated in Figure 24E, RNA decay analyses with ActD revealed that CDK6 transcripts remained relatively stable over a period of 180 minutes and were significantly more stable in the presence of A3C. However, the second approach used for RNA decay analyses revealed no significant difference in CDK6 transcript levels after 24 hours of blocked transcription (Figure 24F). Nevertheless, as shown in Figure 24F, among the transcripts investigated in the luciferase reporter studies, IKBKA showed significantly reduced transcript levels upon A3C depletion. Additionally, other putative A3C binding partners were explored in RNA decay analyses (Figure 24G), and the transcript of IKBKE, another subunit of I κ B kinases, was significantly affected, suggesting a potential stabilization effect by A3C.

In conclusion, these findings indicate that although the individual effects observed in luciferase reporter studies and RNA decay analyses may be mild for single regulatory factors, the cumulative impact of multiple subtle effects could explain the overall greater effect on NF- κ B activity. Thus, A3C may play a stabilizing role for many transcripts of NF- κ B regulators, which in turn has a significant impact on overall NF- κ B activity.

3.5.4 Depletion of A3C restrains NF- κ B subunits in the cytoplasm

While previous studies have reported dysregulated NF- κ B activity in ccRCC (Oya et al., 2003b; Peri et al., 2013), the impact of A3C on NF- κ B regulation presents a novel and unexplored factor in the context of RCC. Particularly, NF- κ B dysregulation in RCC has been associated with dominant RelA-containing complexes that exhibit enhanced nuclear localization compared to normal tissue (Ng et al., 2018; Peri et al., 2013). Consequently, understanding the role of A3C in NF- κ B subunit translocation is crucial in shedding light on this complex molecular mechanism.

To investigate this, initially, the total protein levels of NF- κ B1, NF- κ B2, RelA and RelB were assessed upon A3C depletion. In 786-O cells, protein levels of these subunits remained unchanged, while in 769-P cells, a slight increase in RelA and a decrease in RelB and processed NF- κ B2 p52 were observed (Figure 25A). However, the most striking impact of A3C depletion was observed on the active forms of NF- κ B subunits. Notably, a significant 60% reduction in the phosphorylation of RelA at Ser536 was determined in 786-O shA3C cells compared to shC. Phosphorylation of Ser536 is known to facilitate the nuclear translocation of RelA and subsequent target gene expression (Mattioli et al., 2004; Sasaki et al., 2005). Additionally, processing of NF- κ B2 to the active form p52 was impaired upon A3C depletion, as p52 levels diminished in shA3C cells compared to shC (Figure 25B).

To gain insight into the cellular distribution of the NF- κ B subunits RelA and NF- κ B2, subcellular fractionation analyses were performed in 786-O and 769-P shC and shA3C cells (Figure 25, D-H). In 786-O cells, the cytoplasmic levels of unprocessed NF- κ B2 p100 and RelA increased by 30% and 40%, respectively, compared to shC (Figure 25, D and E), indicating impaired processing and translocation to the nucleus. Similarly, in 769-P cells, A3C depletion resulted in a 40% and 50% accumulation of NF- κ B2 p100 and RelA, respectively, in the cytoplasm (Figure 25, F-H), further supporting the disrupted translocation of NF- κ B subunits upon loss of A3C.

Consistent with previous reports (Buss et al., 2012; Handschick et al., 2014), CDK6 is likely involved in RelA phosphorylation, as demonstrated by the substantial reduction in Ser536 phosphorylation upon transient CDK6 KD in 786-O cells (Figure 25C). Moreover, transient A3C depletion in 786-O cells resulted in reduced RelA phosphorylation. However, in 769-P cells, A3C KD led to increased RelA phosphorylation, emphasizing the cell line-dependent role of A3C in NF- κ B regulation.

The complexity of the NF- κ B regulatory network becomes apparent when considering the diverse kinases involved in the phosphorylation of NF- κ B regulators and subunits. Figure 26A provides an overview of these kinases, although it is not exhaustive. For instance, the I κ B kinases, such as I κ BKA/B/E, have been implicated in the phosphorylation of I κ B α , NF- κ B2 and RelA (Christian et al., 2016; Sakurai et al., 1999; Zandi et al., 1997). On the other hand, kinases such as ERK1/2 and p38 exhibit specific phosphorylation of I κ B α , indirectly influencing NF- κ B components (Korus et al., 2002; Schulze-Osthoff et al., 1997; Ulivi et al., 2008; Vanden Berghe et al., 1998). Direct phosphorylation of NF- κ B subunits is attributed to cyclin-dependent kinases (CDKs; Buss et al., 2012; Henry et al., 2018; Nowak et al., 2008; Perkins et al., 1997; Figure 25C) and Glycogen synthase kinases (GSK3 β ; Arabi et al., 2012; Buss et al., 2004a). RelA, in particular, attracts several kinases that phosphorylate various residues, including protein kinases (Zhong et al., 1998), RSK1 (Bohuslav et al., 2004) and TBK1 (Buss et al., 2004b), exemplifying the complexity of the NF- κ B regulatory network.

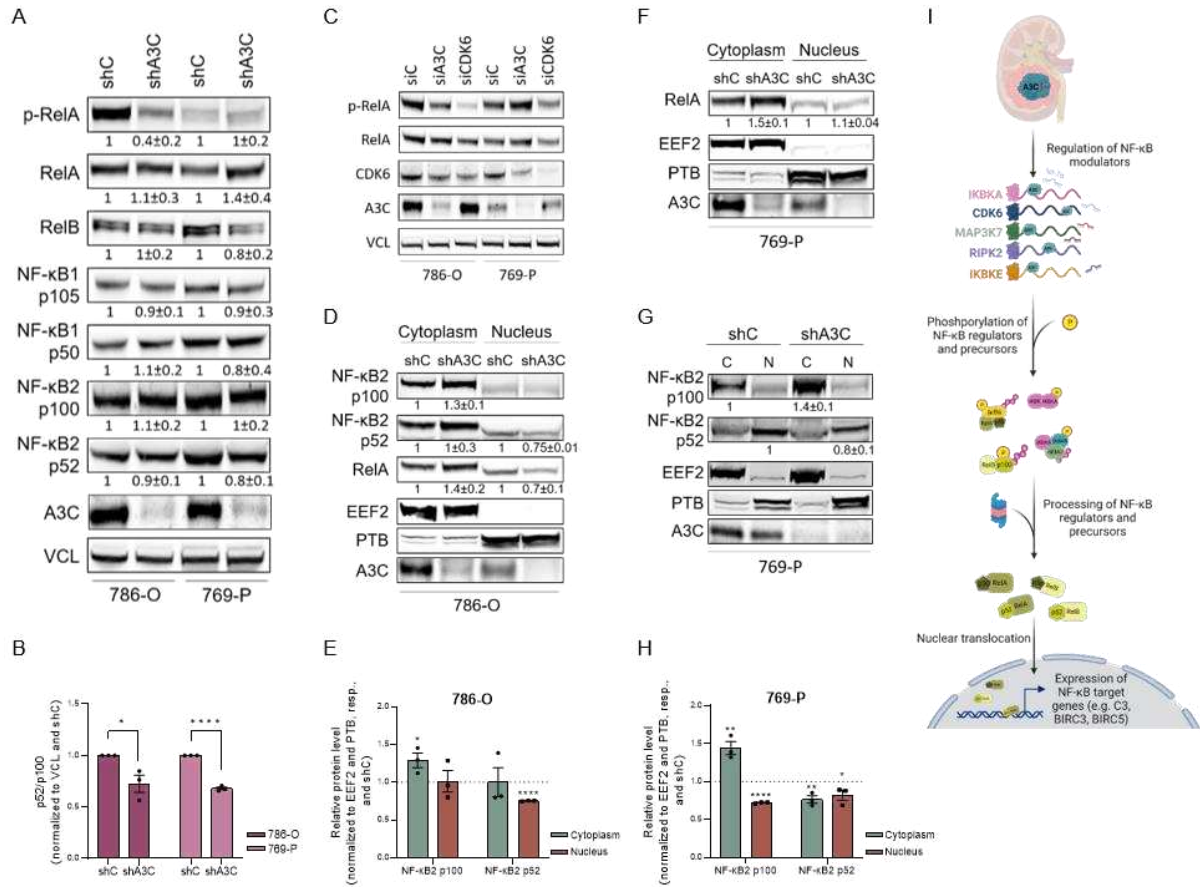


Figure 25: Upon A3C depletion, the nuclear translocation of NF-κB subunits is impaired. (A) WBs show protein levels of the NF-κB subunits RelA, RelB, NF-κB1 (unprocessed, p105; processed, p50) and NF-κB2 (unprocessed, p100; processed, p52) in 786-O and 769-P shA3C cells. Additionally, phosphorylation status at Ser536 of RelA was analyzed. VCL was used for quantification. The phosphorylation signal was normalized to total RelA protein level. (B) The ratio of the active form (p52) of NF-κB2 to unprocessed NF-κB2 (p100) was determined in 786-O and 769-P shA3C cells. (C) Total protein abundance of RelA and its phosphorylation at Ser536 was investigated in 786-O and 769-P cells upon transient siRNA-mediated KD of A3C and CDK6. VCL was used as loading control. (D) Subcellular fractionation was performed using 786-O shC and shA3C cells. The distribution of the NF-κB subunits NF-κB2 and RelA among the cytoplasmic and nuclear fraction is depicted in the WBs. To verify the subcellular fractionation process, EEF2 and PTB were used as positive controls for the cytoplasmic and the nuclear fractions, respectively. Note that due to the usage of different buffers in the cytoplasmic and nuclear fractions, slight differences in the running behavior of the proteins were observed. (E) Bar plot indicates the distribution of the active and inactive form of NF-κB2 in the cytoplasm and nucleus of 786-O shA3C cells. Signals of proteins localized in the cytoplasm were normalized to EEF2, proteins in the nucleus to PTB. (F and G) Subcellular fractionation was performed as described in (D) but with 769-P cells (C, cytoplasm; N, nucleus). (H) Bar plot shows the distribution of the active and inactive form of NF-κB2 in the cytoplasm and nucleus of 769-P shA3C cells, as described in (E). (I) The schematic illustrates a putative regulatory mechanism of the NF-κB signaling pathway by A3C (created with BioRender.com). **p* < 0.05; ***p* < 0.01; *****p* < 0.0001 by unpaired, two-tailed Student's *t*-test compared to shC (B, E and H). Data are representative of three independent experiments (mean ± SEM in B, E and H). Protein levels were normalized to VCL (A) or EEF2 and PTB (D, F and G) and shC in at least three biological replicates; mean ± SD is indicated below the representative WBs (A, D, F and G). Note that the experiment presented in (C) was performed once.

Despite this complexity, the expression levels of selected kinases were investigated upon A3C depletion. In 769-P cells with stable A3C KD, the IκB kinase subunits (IKKBA/B) showed decreased levels, resulting in a mild decrease in the phosphorylation of IκB and subsequent mild accumulation as IκB is degraded upon phosphorylation (Figure 26B). Conversely, A3C depletion in 786-O cells did not affect IκB kinases but significantly reduced

p38 phosphorylation without altering its total protein levels (Figure 26C), suggesting an A3C-mediated p38/CDK6 axis for NF- κ B activation independent of I κ B.

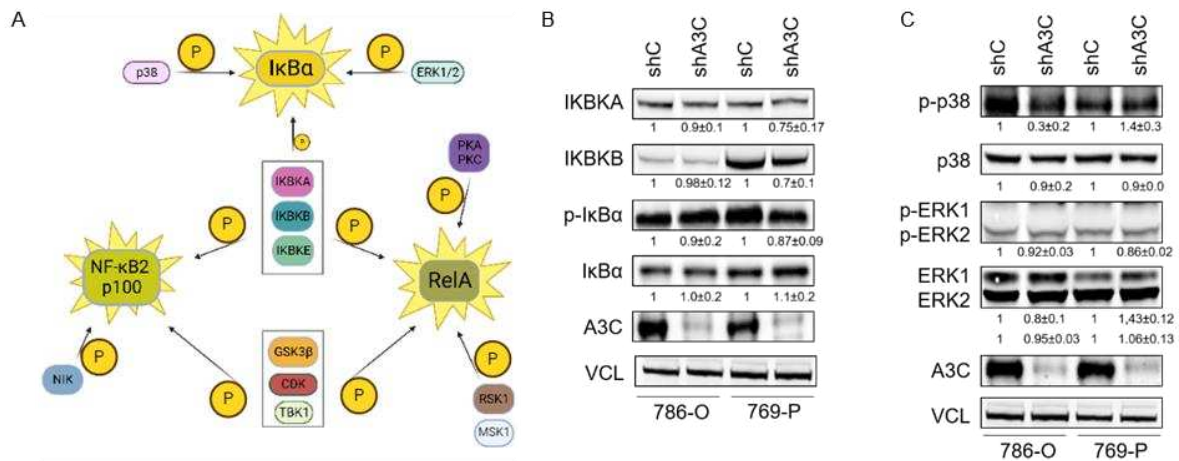


Figure 26: The phosphorylation cascade resulting in NF- κ B activation is affected at different stages in 786-O and 769-P upon A3C depletion. (A) The schematic shows reported kinases that phosphorylate I κ B α and the NF- κ B subunits NF- κ B2 and RelA (CDK, Cyclin dependent kinase; ERK, Extracellular signal-regulated kinases; GSK, Glycogen synthase kinase; MSK1, Mitogen- and stress-activated protein kinase 1; PKA/C, Protein kinase A/C; RSK1, Ribosomal Subunit S6 Kinase 1; TBK1, TANK-binding kinase 1). Note that the list is not exhaustive (created with BioRender.com). **(B)** Protein abundance of I κ B α kinases (IKBKA/IKBKB) as well as I κ B α and its phosphorylation at Ser32/Ser36 (p-I κ B α) were analyzed by WB in 786-O and 769-P shA3C cells. VCL was used for quantification. The phosphorylation signal was normalized to total I κ B α protein level. **(C)** WBs show total protein levels of p38 and ERK1/2 as well as their phosphorylations at Thr180/Tyr182 and Thr202/Tyr204, respectively (phosphorylated ERK1 was not detected), in 786-O and 769-P shA3C cells. VCL was used for quantification. Phosphorylation signals were normalized to total p38 or ERK2 protein levels. WBs are representative of at least three independent experiments; mean \pm SD is indicated below the representative WBs (C, quantification below WB of p-ERK1/2 refers to p-ERK1; quantification below WB of total ERK1/2, upper row refers to ERK1, second row to ERK2).

Collectively, these findings highlight the multifaceted impact of A3C on NF- κ B regulation in ccRCC-derived cell lines. A3C may stabilize various transcripts of NF- κ B regulators, including kinases. The protective mechanism facilitated by A3C may involve shielding transcripts from miRNA-mediated degradation. The kinases subsequently phosphorylate NF- κ B subunits or other regulators of NF- κ B, enhancing the translocation of NF- κ B complexes, which results in increased NF- κ B activity and target gene expression (schematically illustrated in Figure 25I). Further research is required to unravel the full complexity and determine the precise mechanisms involved in the interplay between A3C and NF- κ B regulation.

3.6 A3C is a survival factor for tumor growth *in vivo*

In addition to its molecular function in ccRCC, this study aimed to explore the phenotypic consequences of elevated A3C levels. As previously demonstrated in Figure 16, A3C is upregulated in response to various stress factors occurring in growing tumors, such as high density, serum deprivation and detachment, suggesting its involvement in stress responses activated in cancer cells. Interestingly, the NF- κ B pathway is known to be

activated by various stresses, including anoikis (Paoli et al., 2013), hypoxia stress (Schreck et al., 1992) and anti-cancer drug treatments (Morais et al., 2011), reinforcing the novel connection between A3C and the NF- κ B pathway. Activation of the NF- κ B pathway leads to the upregulation of anti-apoptotic, pro-angiogenic and multidrug resistance pathways, making NF- κ B a pro-survival factor in oncogenesis (Morais et al., 2011).

To examine the cellular consequences of altered A3C levels in response to stress, 786-O and 769-P cells with depleted levels of A3C (KO and KD) as well as 786-O cells with A3C re-expression were subjected to adhesion and starvation stress. The results demonstrated that A3C-depleted cells exhibited impaired cell viability under stress conditions compared to control cells (Figure 27, A and B), indicating that A3C plays a beneficial role in cell proliferation under stress and enhances resistance to anoikis. Notably, A3C re-expression significantly rescued cell viability, further supporting the role of A3C in promoting survival under stress conditions. Importantly, these effects regarding cell viability were specific to stress conditions, as no significant differences were observed when A3C levels were modulated under non-stress conditions (high attachment, 10% FBS).

To determine if the observed stress response is NF- κ B-dependent, NF- κ B subunits were transiently depleted, followed by stress application. KD of NF- κ B2 and RelB resulted in a significant decrease in cell viability upon exposure to stress (Figure 27, C and D), suggesting that A3C's survival function may be mediated by the NF- κ B signaling pathway. Notably, the KD of NF- κ B2 showed the strongest effect on cell survival. Additionally, reducing only NF- κ B2 or RelB was sufficient to drastically decrease cell viability even under non-stress growth conditions, confirming the essential role of NF- κ B in cell survival.

Furthermore, consistent with previous reports (Aggarwal, 2000; Baldwin, 2001), NF- κ B activation inhibits apoptosis by transcriptionally upregulating various anti-apoptotic genes, including BIRC3 (Figure 20C; Silke, Vucic, 2014; Simon et al., 2007). BIRC3, a member of the inhibitor of apoptosis (IAP) protein family, functions as an E3 ubiquitin ligase, binding and inhibiting active caspases (Silke, Vucic, 2014), particularly Caspase3 and Caspase7. By blocking caspase activity, BIRC3 prevents the cleavage of various cellular substrates, such as focal adhesion kinases or polymerases for DNA repair, thus inhibiting apoptosis and promoting cell survival (Luo et al., 2022; Wang et al., 2012; Wang et al., 2019).

Caspase activity assays were conducted to assess the impact of A3C on the inhibition of apoptosis. Depletion of A3C in 769-P cells resulted in a significant upregulation of caspase activity (Figure 27E), suggesting that inhibited apoptosis occurring in RCC is mediated by A3C, possibly due to increased NF- κ B activity resulting in elevated BIRC3 levels. Interestingly, the effects on caspase activity differed in 786-O and 769-P cells, highlighting the heterogeneity of the ccRCC-derived cell lines. Additionally, the role of BIRC3 in inhibiting apoptosis and promoting cell survival was confirmed, as caspase activity increased upon BIRC3 depletion and decreased with BIRC3 overexpression (Figure 27F).

RESULTS

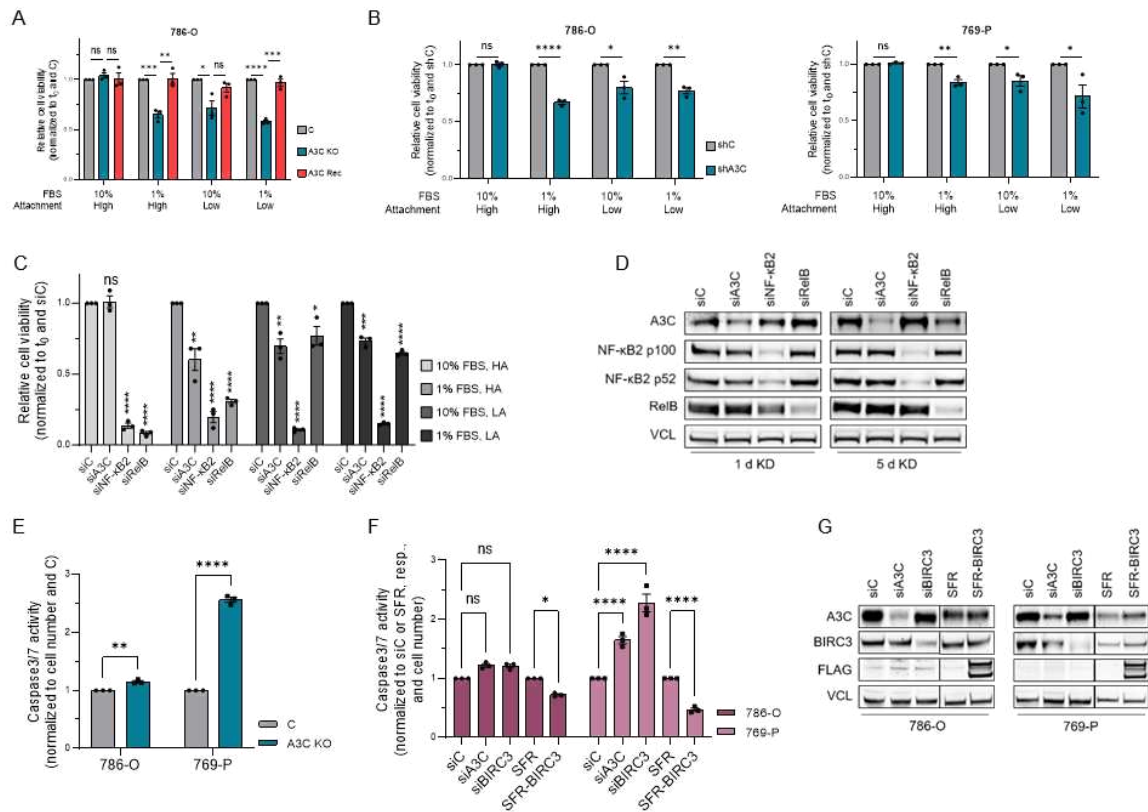


Figure 27: Cell viability under stress conditions depends on A3C expression levels. (A) Cell survival under FBS depletion (1% FBS) combined with LA or HA conditions was investigated in 786-O C, A3C KO and A3C Rec cells. Cell viability was determined after five days using CellTiter-Glo. (B) Growth conditions as described in (A) were applied to 786-O (left panel) and 769-P (right panel) shC and shA3C cell for five days and cell viability was determined. (C) Cell viability of 769-P cells upon transfection of indicated siRNAs was analyzed under various FBS and attachment conditions after five days. (D) KD of proteins mentioned in (C) were detected by WB analyses one day and five days after siRNA transfection. VCL served as loading control. (E) Caspase3/7 activity was investigated in 786-O and 769-P A3C KO cells upon starvation (1% FBS) for 48 h. Viable cells were assessed by CellTiter-Glo. (F) Caspase3/7 activity was analyzed in 786-O and 769-P cells upon transient A3C KD and modulation of the reported apoptosis inhibitor BIRC3, either KD (siBIRC3) or OE (SFR-BIRC3). Luminescent signal was normalized to siC or SBP-FLAG-RFP (SFR) and viable cells determined by CellTiter-Glo. (D) Protein levels of factors indicated in (F) were detected by WB analyses. VCL served as loading control. * $p < 0.05$; ** $p < 0.01$; *** $p < 0.001$ and **** $p < 0.0001$ by unpaired, two-tailed Student's t-test (A – C and E) or two-way ANOVA (F). Data are representative of three independent experiments (mean \pm SEM in A-C, E and F).

In addition to 2D cell culture models, 3D spheroid cell cultures were employed to mimic the microenvironment of growing tumors *in vitro*, including gradients of oxygen and nutrients as well as phenotypic heterogeneity. Monitoring the spheroid area demonstrated that A3C KO significantly reduced spheroid growth (Figure 28B), highlighting the importance of A3C as a survival factor under stress conditions encountered in a growing tumor. In contrast, A3C KO had no significant effect on cell number under 2D culture conditions (Figure 28A). These results of significantly reduced spheroid sizes were reproducible using 786-O and 769-P cells with stable A3C KD (Figure 28, C and D).

To investigate the role of A3C *in vivo*, ccRCC-derived cells with modulated A3C levels were analyzed in xenograft mouse models. Tumor development and vascularization were robust in 786-O C and A3C Rec cells, while barely any tumor formation was observed with

A3C KO cells (Figure 28, E and F). These findings indicate that A3C is required for tumor growth of ccRCC-derived cells *in vivo*.

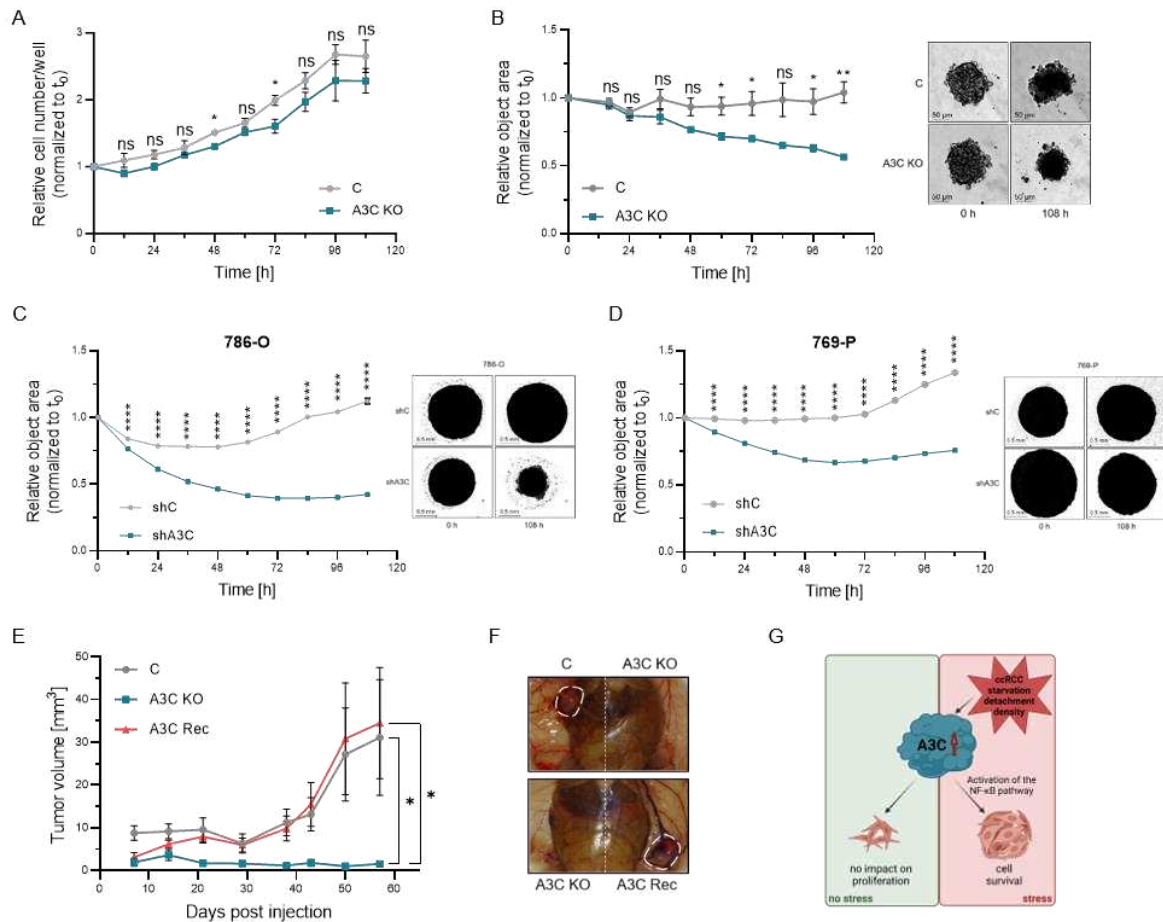


Figure 28: Elevated A3C expression is associated with cell survival *in cellulo* and *in vivo*. (A and B) Proliferation of 786-O C and A3C KO cells was monitored under 2D (A) and 3D (B) growth conditions for five days using an Incucyte S3 device. Cell number (A) or object area of the spheroids (B) were normalized to the input. Representative images of cell spheroids at day zero and day five are shown (B). (C and D) 3D spheroids of shC and shA3C in 786-O (C) and 769-P cells (D) were cultured for five days. The object area was quantified and normalized to the input. Representative images of the initial and terminal spheroids of 786-O (C) and 769-P (D) shC and shA3C cells are presented. (E and F) *Foxn1^{nu/nu}* mice were subcutaneously injected with 786-O C, A3C KO and A3C Rec cells. Tumor growth was monitored for several weeks (E; n=8 mice per group). Representative images of final tumors in nude mice are shown (F). (G) The schematic provides an overview of the effects of stress on A3C expression and function (created with BioRender.com). * $p < 0.05$; ** $p < 0.01$ and **** $p < 0.0001$ by unpaired, two-tailed Student's t-test (A-E). Data are representative of three (A and B) or six (C and D) independent experiments (mean \pm SEM in A-E).

In conclusion, A3C serves as an important survival factor in ccRCC by promoting cell viability and resistance to stress potentially through the regulation of the oncogenic NF- κ B pathway (schematic in Figure 28G). This activation leads to the upregulation of anti-apoptotic and pro-survival factors such as BIRC3. Consequently, A3C enhances the survival of ccRCC-derived cells. Overall, this study highlights the multifaceted role of A3C in regulating cellular responses to stress and its implications in tumor progression and survival.

3.7 A3C depletion enhances the susceptibility of ccRCC-derived cells to drug treatment

Given the constitutive activation of the NF- κ B pathway in ccRCC and its association with cell survival, pro-inflammatory responses and poor patient prognosis, targeting this pathway is considered a promising approach for treating advanced ccRCC (Morais et al., 2011; Peri et al., 2013). The NF- κ B pathway involves a network of phosphorylation cascades mediated by kinases. Therefore, drugs that block these kinases and, thus, inhibit the activation of oncogenic factors have been developed for RCC treatment.

In this study, three FDA-approved small-molecule inhibitors, namely Sorafenib, Pazopanib and Sunitinib were investigated. These inhibitors target multiple tyrosine protein kinases and receptor tyrosine kinases, including platelet-derived growth factor receptors (PDGFRs) and vascular endothelial growth factor receptors (VEGFRs), which play critical roles in RCC tumor cell proliferation and angiogenesis. By simultaneously inhibiting target kinases, these compounds reduce tumor vascularization, trigger cancer cell apoptosis and promote tumor shrinkage (Atkins et al., 2006; Kane et al., 2006; Keisner, Shah, 2011; Motzer et al., 2006; Pick, Nystrom, 2012; White, Cohen, 2015).

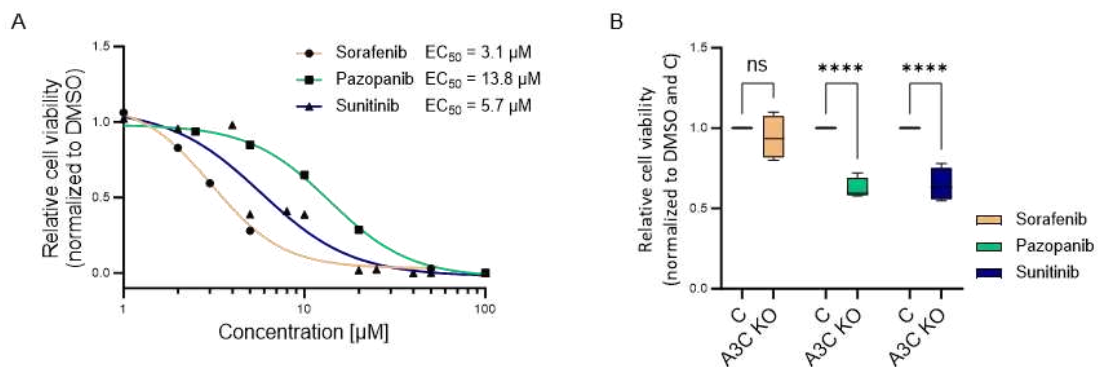


Figure 29: Upon A3C depletion, ccRCC-derived cells are more susceptible to drug treatment. (A) Cell viability of 786-O WT cells treated with Sorafenib, Pazopanib or Sunitinib was determined at indicated concentrations after 48 h. The EC₅₀ value of each drug was calculated using *GraphPad Prism*. **(B)** 786-O C and A3C KO cells were treated with Sorafenib (3.5 μM), Pazopanib (15 μM) or Sunitinib (6 μM) for 48 h. Cell viability was analyzed using CellTiter-Glo and normalized to DMSO-treated cells and 786-O C cells. ****p < 0.0001 by Šidák's multiple comparisons test **(B)**. Data are representative of four **(B)** independent experiments (5-95 percentile in **B**).

To assess the impact of A3C on the efficacy of these drugs, EC₅₀ values were determined for each molecule in 786-O cells (Figure 29A). Subsequently, cell viability was evaluated upon A3C depletion and drug treatment. As demonstrated in Figure 29B, cells with depleted levels of A3C exhibited significantly reduced cell viability when treated with Pazopanib or Sunitinib, suggesting that ccRCC-derived cells become more susceptible to drug treatment with tyrosine kinase inhibitors upon depletion of A3C. These results indicate that targeting A3C in combination with these compounds may present a potential therapeutic strategy for treating ccRCC effectively. Further research in this area is reasonable to explore the potential benefits of this combination therapy.

4 DISCUSSION

The AID/APOBEC protein family has been extensively studied due to its crucial role in innate and adaptive immune responses. However, while the functions of A3A and A3B, which induce genomic mutations enhancing tumorigenesis, as well as the antiviral activity of A3G and A3F are well understood, other members of this protein family have received little attention. Information about A3C, for instance, remains limited, despite its ubiquitous expression in various tissues and overexpression in different solid tumors, including ccRCC (Guo et al., 2022; Jarmuz et al., 2002). Furthermore, previously unanticipated functions of A3 proteins beyond cytidine deamination have been proposed (Holmes et al., 2007b), such as their involvement in inhibiting miRNA-mediated gene silencing (Huang et al., 2007; Liu et al., 2012a; Rhoads, 2010).

CcRCC, the most aggressive subtype of RCC, is especially challenging as it is resistant to conventional chemotherapy and radiation (Makhov et al., 2018). Thus, novel therapeutic approaches are urgently needed, particularly for advanced ccRCC exhibiting a 5-year survival rate of only 12% (SEER Cancer Statistics Review, 1975–2012, National Cancer Institute. Bethesda, MD, 2015). Furthermore, ccRCC lacks the distinct genomic mutation signature associated with A3 activity despite increased expression (Alexandrov et al., 2013), suggesting that members of the A3 protein family, such as A3C, may have alternative functions independent of cytidine deamination contributing to cancer progression.

This study unveils a novel molecular role for A3C in promoting ccRCC tumor development. Using RNA-seq analyses and cell-based assays in ccRCC-derived cells, A3C was found to be associated with increased NF- κ B activity, playing a crucial role in cell survival under stress conditions and tumor growth *in vivo*. A3C interacts with and putatively stabilizes previously unrecognized mRNA targets that encode factors regulating the NF- κ B signaling pathway. Consequently, A3C enhances NF- κ B activity, resulting in elevated expression of NF- κ B target genes, ultimately driving tumor growth. Depletion of A3C leads to the retention of NF- κ B subunits in the cytoplasm, impairing NF- κ B activity.

These findings suggest that A3C promotes ccRCC tumor development via positive regulation of the NF- κ B signaling pathway. This discovery provides a strong rationale for considering A3C inhibitors as part of combination therapy for advanced ccRCC patients, underscoring the importance of further investigating the molecular role of A3C in tumorigenesis.

4.1 The A3 protein family is distinctive in subcellular localization, interaction partners and molecular functions

Despite sharing structural similarities arising from a common evolutionary origin, A3 proteins exhibit significant diversity. Approximately 33 million years ago, the A3 protein family diverged, coinciding with the peak of LINE-1 retrotransposon and *Alu* element invasions (Sawyer et al., 2004; Uriu et al., 2021). Over time, the A3 protein family has diversified its functions due to co-evolutionary processes and adaptations. The emergence of different A3 genes enabled interactions with diverse target molecules, including viral genomes and cellular RNAs, as well as various cofactors and regulatory proteins. Consequently, these proteins expanded their functions, subcellular localizations and biological activities playing essential roles in antiviral defense, endogenous retroelement regulation and potentially other cellular processes.

A3G, for instances, is effectively sequestered within the cytoplasm due to a cytoplasmic retention signal and remains excluded from chromosomes during mitosis (Smith et al., 2012). In contrast, A3B harbors a NLS (Bogerd et al., 2006), which expands the range of potential functions. Regarding A3C, as demonstrated in Figure 8, it primarily localizes to the cytoplasm. Due to the relatively small size (approximately 23 kDa), A3C has the potential for a cell-wide distribution, including nuclear entry through passive diffusion. Indeed, studies have reported that A3C localizes to the nucleus and accumulates in nucleoli (Constantin et al., 2022; Niewiadomska et al., 2007). However, it is essential to highlight that A3C has been shown to be excluded from DNA breaks (Constantin et al., 2022) and, additionally, from DNA during early mitosis (Lackey et al., 2013). This indicates that A3C does not interact with DNA, distinguishing it from A3B, which exhibits genomic deamination activity during interphase and mitosis (Lackey et al., 2013). This raises questions about the specific functions of A3C and underscores that functions ascribed to A3B, particularly those related to genomic mutations inducing carcinogenesis, might not apply to A3C.

Further evidence of the diverse characteristics within the A3 protein family can be observed in sucrose gradient profiles and pull-down analyses. As previously described (Chiu et al., 2006), A3G is widely distributed across the sucrose gradient, whereas A3C primarily localized to the upper fractions (Figure 7A). The uniform distribution of A3G confirms its presence in two distinct cytoplasmic forms, LMM and HMM complexes. These two RNP complexes are considered to regulate A3G's function. Formation of LMM complexes, consisting of homomultimers, is required for efficient deaminase activity on ssDNA substrates (McDougall et al., 2011). Following RNA binding, A3G forms HMM complexes, inhibiting the ssDNA deaminase activity allosterically or competitively (Chiu et al., 2005; Smith et al., 2012). HMM complexes comprise various types of cellular RNP complexes, including Staufen-containing RNA-transporting granules, Ro RNPs and components of prespliceosomes, along with RNAs such as *Alu* retroelements and Y RNAs

(Chiu et al., 2006; Figure 7, B and C). Previous studies suggest that A3G sequesters *Alu* RNAs in cytoplasmic HMM complexes, effectively isolating them from the nuclear LINE-1 enzymatic machinery and thereby inhibiting the retrotransposition of *Alu* elements efficiently, independently of cytidine deamination (Chiu et al., 2006). In contrast, A3C restricts *Alu* retrotransposition by only 50-70% (Horn et al., 2014), leaving its specific roles in cellular processes unclear.

HMM formation is not a common feature among all A3 proteins (Niewiadomska et al., 2007). A3A, for instance, does not require treatment with RNase to activate its deaminase activity, suggesting that it is not inhibited by RNA in HMM complexes (Niewiadomska et al., 2007; Thielen et al., 2010). As demonstrated in Figure 7, A3C was found in low molecular weight fractions of the sucrose gradient and associated with AGO2, DCP1A and Y RNAs. Furthermore, A3C concentrated in foci determined to be P-bodies and stress granules (Figure 8B), albeit, as reported, to a lesser extent compared to A3D and A3G (Niewiadomska et al., 2007). This difference may be explained by the fact that A3D and A3G comprise two cytidine deamination domains, thus, interacting more strongly with cellular RNAs, potentially directing them to P-bodies (Niewiadomska et al., 2007).

P-bodies are cytoplasmic aggregates consisting of various cellular RNAs and their associated proteins, serving as centers for RNA and ribonucleoprotein degradation and recycling (Smith et al., 2012). A3G has been suggested to promote the dissociation of miRNA-targeted mRNA from P-bodies, thereby facilitating the translation of these mRNAs (Huang et al., 2007). Given that A3C localizes in P-bodies and associates with AGO2, it is possible that it functions in a similar mode like A3G as an RNA-induced gene silencing regulator.

Moreover, considerable variation exists in the antiviral activity among the seven human A3 proteins. A3G strongly inhibits Vif-deficient HIV-1, whereas A3D, A3F and A3H exhibit lower inhibitory potential (Chaipan et al., 2013; Hultquist et al., 2011). In contrast, A3A and A3B do not potently block HIV infection of T-cells, the primary target of HIV (Hultquist et al., 2011). When referring to A3C, there are contradictory findings regarding its viral packaging and cytidine deamination activity (Bourara et al., 2007, 2007; Chaipan et al., 2013; Jaguva Vasudevan et al., 2020; Langlois et al., 2005; Marin et al., 2008). However, the restrictive activity of A3C on both retroviruses and endogenous retroelements appears to be weak (Hultquist et al., 2011; Kinomoto et al., 2007; Wittkopp et al., 2016), making A3C a unique member of the A3 protein family. Interestingly, a SNP in A3C, widely distributed in African populations, enhances its antiviral activity against HIV-1 by increasing its enzymatic activity (Wittkopp et al., 2016).

In summary, the A3 protein family is a diverse group of proteins, with A3C standing out for its unique properties, making A3C an intriguing focus for further research in understanding its specific roles in cellular processes and potential applications.

4.2 A3C gene expression

4.2.1 NF- κ B-mediated A3C expression as response to stress in ccRCC

Various studies have highlighted unique expression patterns for A3 proteins, with A3C typically showing high expression in healthy tissues and heterogeneous expression alterations in various cancer types (Guo et al., 2022; Luo et al., 2021; Ng et al., 2019; Zhang et al., 2023). Although the expression profiles of the A3 protein family are closely associated with tumor occurrence and progression, the reasons behind the upregulation of A3 gene expression and the molecular consequences of elevated A3 levels in tumors with low mutational burdens, as observed in kidney cancer (Jarvis et al., 2018; Zhang et al., 2023), have been widely neglected.

Initially, light is shed on the regulation of A3C expression before the molecular function is discussed below. Once again, A3B stands out as the most extensively studied A3 family member regarding its expression. A3B has been implicated in linking viral infections to cancer, such as HPV-induced cervical cancer, due to elements in the promoter responding to the viral oncoprotein E6, stimulating A3B expression (Mori et al., 2015). Additionally, NF- κ B-binding sites within the A3B promoter region have been identified, facilitating A3B gene expression via the NF- κ B signaling pathway in multiple cancer cell lines and tumors (Fanourakis et al., 2023; Leonard et al., 2015; Periyasamy et al., 2021; Yamazaki et al., 2016).

In contrast, ccRCC has not been linked to virus-related malignancies (Bersanelli et al., 2022), leaving the mechanism behind A3 upregulation in non-viral malignancies elusive. However, *in silico* analysis of the A3C promoter region identified three putative NF- κ B-binding sites (5'-GGRRNNYYCC-3') approximately 1 kb upstream of the A3C transcriptional start site, suggesting a potential role of the NF- κ B transcription factor in A3C expression. Notably, elevated NF- κ B activity, as evidenced by upregulated expression of NF- κ B regulators and target genes, has been observed in ccRCC (Peri et al., 2013), hinting at potential NF- κ B-mediated upregulation of A3C in this malignancy.

However, siRNA-mediated KD of NF- κ B2 and RelB resulted in only a mild reduction in A3C mRNA levels (Figure 20C), questioning A3C as a direct NF- κ B target gene. This modest impact may be attributed to the potential preference of distinct NF- κ B dimers for specific variations of κ B-binding sites (Wan, Lenardo, 2009). The κ B-binding sites within the A3C promoter region may be preferentially recognized by NF- κ B dimers other than NF- κ B2 or RelB. Supportively, analyzing well-established NF- κ B target genes like C3 and BIRC3, which have two and three putative κ B-binding sites in their promoter regions, respectively (Hong et al., 2000; Lian et al., 2015), revealed that the κ B-binding sites exhibit unique responsiveness to the NF- κ B transcription factors. While BIRC3 mRNA levels were similarly reduced upon NF- κ B2 and RelB KD, the silencing of NF- κ B2 resulted in a more pronounced

decrease in C3 expression compared to RelB KD (Figure 20C). Thus, the mild reduction in A3C mRNA levels upon silencing individual NF- κ B subunits suggests the involvement of other NF- κ B dimers in regulating A3C expression.

Additionally, NF- κ B subunits demonstrate tumor type-specific upregulation (Kaltschmidt et al., 2018), emphasizing a particular transcriptional activity in different cancer types. In ccRCC, the expression pattern of NF- κ B subunits appears to be heterogeneous, with NF- κ B1 and c-Rel not showing significant upregulation at the mRNA level (Figure 17F). This leaves RelA, along with NF- κ B2 and RelB, potentially facilitating A3C expression. This may account as well for the modest impact on A3C gene expression observed when silencing individual NF- κ B subunits in a ccRCC-derived cell line. Therefore, the possibility remains that A3C is a direct target gene of NF- κ B. To potentially achieve a stronger reduction of A3C transcript levels, a combined KD of all NF- κ B subunits should be considered.

Another factor contributing to the mild effect may be the lack of induction of the NF- κ B signaling pathway by cytokines or cellular stress conditions in this particular setting. The nature of the NF- κ B system is rather dynamic than static, characterized by various activation states, including a constitutively active state in specific cell types such as B-cells, a 'high-ON' state induced by pro-inflammatory triggers and a 'low-ON' state mediated by malfunctioning autoregulatory negative feedback loops (Meier-Soelch et al., 2021). The later state often occurs in the tumor microenvironment, resulting in low but continuous NF- κ B activation (Ben-Neriah, Karin, 2011; O'Dea et al., 2007). Moreover, the expression of NF- κ B target genes can vary significantly based on the stimulus or the physiological context (Meier-Soelch et al., 2021), influenced additionally by other pathways like p38, JNK and JAK kinase pathways, which cooperate with the NF- κ B system at multiple levels (Gaestel et al., 2009).

Therefore, considering that the experiments were performed in ccRCC-derived cells, A3C might only be transcribed at basic levels under the control of low-grade NF- κ B activation, additionally influenced by other stress pathways, resulting in a mild effect when individual NF- κ B subunits were silenced. Stimulation of the NF- κ B signaling pathway could potentially enhance NF- κ B-dependent gene expression of A3C, providing evidence of A3C being a direct NF- κ B target gene. Accordingly, BIRC3 and C3 are inducible by TNF- α or IL-1, conferred by the consensus NF- κ B-binding sites in their promoter regions (Hong et al., 2000; Lian et al., 2015). Similarly, A3A, A3F and A3G respond to IFN- α , IFN- γ , IL-2, IL-15 and TNF- α with increased expression in different cell types (Bonvin et al., 2006; Koning et al., 2009; Peng et al., 2006; Refsland et al., 2010). However, it is worth noting that A3C expression does not respond to IFN- α treatment (Figure 15). Nevertheless, the effect of other pro-inflammatory cytokines such as TNF- α and IL-1 or other factors activating the NF-

κ B pathway and potentially the effect on A3C expression should be investigated in the future.

The NF- κ B pathway mediates responses to a variety of cellular stressors (Hayden, Ghosh, 2008), including nutrient deprivation and glucose starvation. Key regulators of the NF- κ B pathway, such as kinases (e.g., the IKK multiprotein complex) and phosphatases, are activated by a great variety of stimuli and different mechanisms, including phosphorylation, thereby detecting low nutrient levels, ER stress or reactive oxygen species (Reid, Kong, 2013; Tam et al., 2012). The manifold activation mechanisms ensure that diverse stress conditions induce the catalytic activity of IKK complexes, resulting in adjustments of NF- κ B transcription factor levels, which ultimately leads to the reprogramming of cellular functions and the promotion of survival by altering the gene expression profile (Criollo et al., 2012; Hoesel, Schmid, 2013). Consequently, A3C, as a putative NF- κ B target gene, may be transcriptionally upregulated in response to various stress conditions. Indeed, A3C showed upregulation both at protein and transcript levels when ccRCC-derived cells were exposed to serum deprivation, detachment or cell density-induced stress (Figure 16). This suggests that A3C may function in a NF- κ B-dependent manner, serving as a stress-responsive factor beneficial for ccRCC-derived cells to endure challenging conditions (Figure 30).

Nevertheless, the status of A3C as a direct NF- κ B target gene remains to be confirmed. Several arguments support this hypothesis, including the increase in A3C at transcript level in primary RCC tissues and RCC cell lines exhibiting enhanced NF- κ B activity (Figure 12, A, B, D and E), the positive correlation between A3C expression and expression of NF- κ B subunits in ccRCC (Figure 17I), the identification of putative NF- κ B-binding sites in the A3C promoter region, and the observed elevated A3C transcript levels in response to various stress conditions (Figure 16, A and B). Despite these indicators, additional evidence is required to support NF- κ B-mediated transcription. Chromatin immunoprecipitation (ChIP) using antibodies for NF- κ B subunits can be employed to investigate if the κ B-binding sites in the A3C promoter region are accessible to NF- κ B transcription factors. As previously reported, NF- κ B signaling is also regulated by nuclear activation processes involving the κ B-surrounding chromatin environment, such as cofactors, chromatin accessibility and histone modifications, determining the gene-specific occupancy of DNA by NF- κ B (Meier-Soelch et al., 2021; Natoli et al., 2005). ChIP-Seq in ccRCC-derived cells upon NF- κ B pathway induction would provide valuable insight. Furthermore, the application of NF- κ B inhibitors, such as BAY 11-7082, known for its broad inhibition of several factors involved in the NF- κ B pathway (Lee et al., 2012), or MG132, a proteasome inhibitor that prevents degradation of I κ B and processing of p100 (Nakajima et al., 2011), could be considered to reduce A3C expression. This would provide additional evidence supporting the hypothesis that A3C is a direct NF- κ B target gene.

4.2.2 Repressive regulatory elements in the 3' UTR of A3C transcripts act as mechanisms to control A3C gene expression

In addition to the transcriptional regulation of A3C in response to stress-induced signaling pathways, various alternative mechanisms contribute to regulate gene expression, including epigenetic modifications, autoregulation, feedback loops, RNA processing, RNA stability and translation. Primarily, the untranslated regions of a transcript are involved in these mechanisms.

This study demonstrated that the 3' UTR of the A3C transcripts harbors robust secondary structures and regulatory elements (Figure 10). Secondary structures in the 3' UTR can influence mRNA turnover; for instance, hairpins in transcripts can result in increased stability (Georgakopoulos-Soares et al., 2022; Mignone et al., 2002). Analysis of A3C transcripts across diverse cell lines revealed relatively stable mRNA over a time span of at least two hours (Supplemental Figure 3). Additionally, destabilizing processes mediated by miRNA via the 3' UTR were not observed (Figure 13C). However, using reporter constructs containing the native 3' UTR of A3C resulted in a significant reduction in the activity of the reporter gene (Figure 13B), indicating that the A3C 3' UTR exerts a repressive effect. The reduction in reporter gene activity remained consistent regardless of A3C protein levels, as reporter gene activity decreased similarly with both A3C OE as well as A3C KO (Figure 10D). This finding suggests that autoregulatory feedback loops may not play a significant role in A3C gene expression.

Secondary structures have the potential to modulate rates and amounts of translation, as they affect the accessibility for RBPs, which are critical *trans*-acting factors controlling translation (Jacobs et al., 2012; Mazumder et al., 2003; Szostak, Gebauer, 2013). Furthermore, the identified inverted *Alu* elements in the A3C 3' UTR have been found to act as translation inhibitors (Chen, Yang, 2017; Häsler, Strub, 2006; Stuart et al., 2000), potentially explaining the restrictive effects of the A3C 3' UTR. This regulatory strategy may serve to control A3C protein levels, particularly considering the damaging potential of the putative mutagenic activity on genomic DNA when localized in the nucleus.

In conclusion, the regulation of A3C expression involves a complex interplay of factors affecting transcription, post-transcriptional processes and translation regulation and has further to be categorized into two conditions: basic A3C expression and stress-induced expression, as seen in ccRCC (Figure 30). Under steady-state conditions, A3C mRNA levels appear to remain relatively high, primarily attributed to a low mRNA degradation rate, explaining the generally high transcript levels of A3C in healthy tissue. Repressive elements and secondary structures within the 3' UTR of A3C, likely regulating translation, may counteract these high transcript levels. Furthermore, since previous reports have shown that pVHL as a ubiquitin ligase induces the degradation of all members of the A3 protein

family (Scholtes et al., 2021), pVHL is involved in controlling A3C protein levels in healthy tissue.

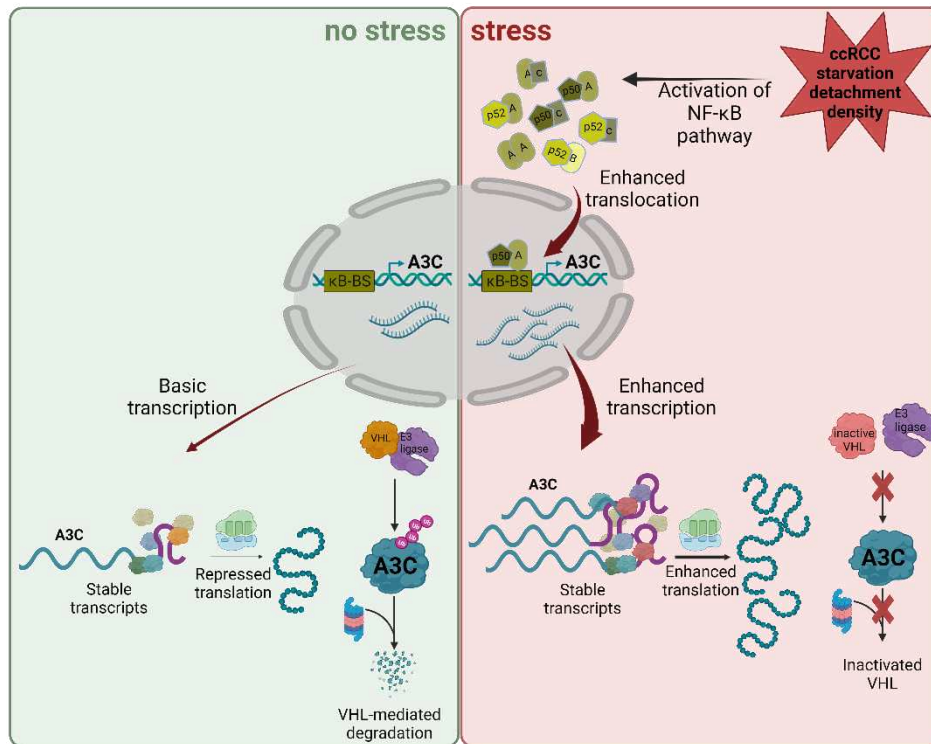


Figure 30: The regulation of A3C gene expression is multifaceted. Schematic created with BioRender.com.

However, under stress conditions, transcription is induced by altered activity of transcription factors, such as NF- κ B transcription factors, as part of stress-responsive signaling pathways. Coupled with a low mRNA degradation rate and robust protein levels due to inactivated *VHL*, which is a common feature of ccRCC, elevated A3C protein levels arise in ccRCC.

The role of the 3' UTR of A3C under stress conditions was not addressed in this study. Investigating the behavior of the reporter construct containing the native A3C 3' UTR under specific stress conditions, such as starvation or cell detachment, could reveal regulatory mechanisms. To gain a comprehensive understanding of A3C gene expression regulation, further experiments should be considered. Using nascent RNA capture to analyze newly synthesized A3C transcripts under stress conditions would offer insights into the transcription rate. Moreover, performing ribosome profiling to investigate the translation rate under distinct conditions could also provide valuable information.

4.3 A3C is involved in ccRCC progression by promoting the NF- κ B pathway

In the following, this study delves into the intricate interplay between A3C, an identified unfavorable prognostic marker in ccRCC, and NF- κ B, a promising therapeutic target in cancer, shedding light on their interconnected roles in ccRCC progression. Previous studies, with a particular focus on kidney cancer (Guo et al., 2022; Wu et al., 2020; Zhu et al., 2021), have highlighted the significant roles of A3 family members in ccRCC, suggesting their potential as biomarkers. The analysis of a small, separate RCC cohort in this study aligns with the observed pattern of increased expression of A3 family members, especially A3C (Figure 12). Combined with worse prognosis of patients with elevated A3C levels (Figure 11D), the prognostic value of A3C in RCC was confirmed.

Furthermore, previous reports have indicated elevated expression of NF- κ B subunits in RCC (Morais et al., 2011; Oya et al., 2003b; Sourbier et al., 2007) and a constitutively activated NF- κ B pathway in a high percentage of patient-derived ccRCC samples, resulting in an 'NF- κ B signature' in ccRCC (Peri et al., 2013). Moreover, investigations highlight the NF- κ B signaling pathway as prominently overexpressed in metastatic ccRCC tumor tissue (Ghatalia et al., 2016). Additionally, studies have revealed a correlation between NF- κ B expression and tumor grade, suggesting an independent prognostic value for specific NF- κ B subunits in RCC (Djordjević et al., 2008; Meteoglu et al., 2008; Ng et al., 2018; Oya et al., 2003b).

For the first time, this study provides a connection between A3C and NF- κ B in ccRCC. It not only suggests that A3C is a direct target gene of NF- κ B, explaining elevated A3C expression levels in ccRCC, but also proposes that A3C promotes ccRCC progression by enhancing the NF- κ B pathway.

Upon depletion of A3C, either by CRISPR/Cas9-mediated KO in 786-O cells or by shRNA-induced gene silencing in 786-O and 769-P cells, a substantial fraction of NF- κ B target genes showed decreased expression (Figure 19, A-D). Furthermore, re-expression of NF- κ B target genes in 786-O A3C Rec cells supports the hypothesis of an A3C-dependent 'NF- κ B signature' in ccRCC-derived cells. This is further validated by GSEA performed with differentially expressed genes between 786-O C and A3C KO cells and the HALLMARK gene sets (Figure 17, D and E). GSEA, a tool for interpreting gene expression data, integrates expression information from the transcriptome with whole sets of functionally related groups of genes (Subramanian et al., 2005). Notably, not only is the pathway 'TNFA SIGNALING VIA NF κ B' the most significantly altered pathway upon A3C modulation, but also pathways associated with the NF- κ B signaling pathway, including 'INFLAMMATORY RESPONSE', 'INTERFERON GAMMA RESPONSE', 'IL6 JAK STAT3 SIGNALING' and 'COMPLEMENT', are significantly altered and, additionally, positively enriched upon A3C re-expression. Moreover, the effect of decreased NF- κ B target gene

expression upon depleted A3C expression was observed across RCC cell lines (Figure 20, A and B). Using C3 as an exemplary NF- κ B target gene, decreased transcript levels upon A3C depletion are indeed a consequence of deficient transcription and not of destabilizing effects, as indicated in Figure 20D and E, showing stable C3 transcript levels in RNA decay analyses and reduced nascent C3 mRNA levels, respectively. This suggests that A3C sufficiently affects NF- κ B transcriptional activity.

Furthermore, the NF- κ B activity was investigated using reporter gene constructs controlled by NF- κ B responsive elements. The minimal promoter of the Firefly luciferase reporter gene was extended to encompass five κ B-binding sites (5'-GGGAATTTCC GGGGACTTTCC GGGGAATTTCC GGGGACTTTCC GGGGAATTTCC-3') that align with the 10 bp defined consensus sequence recognized by NF- κ B (5'-GGGNNNNNCC-3'; N = A, C, G or T; Chen, Ghosh, 1999). However, limitations exist regarding the experimental application of this NF- κ B activity reporter. κ B-binding sites can exhibit significant variability, particularly in the central portion (Mulero et al., 2019), resulting in approximately 1.4×10^4 potential κ B-binding sites in the human genome (Wan, Lenardo, 2009). Therefore, the used reporter construct is not capable of including all putative κ B-binding sites. Moreover, different NF- κ B homo- and heterodimers have differential preferences and affinities for variations of the DNA-binding site, inducing differential target gene expression (Chen, Ghosh, 1999; Hoesel, Schmid, 2013). Therefore, the reporter construct may not capture all NF- κ B binding interactions, potentially leading to an incomplete understanding of the overall NF- κ B activity in this context.

Given the limited variation of κ B-binding sites in the reporter vector and the KD of an individual NF- κ B subunit to validate responsiveness of the reporter construct used in this study, a modest effect on NF- κ B activity can be expected. As depicted in Figure 18B, a transient KD of NF- κ B2 indeed resulted in a modest 20% reduction of NF- κ B activity. Notably, a transient KD of A3C showed a greater reduction of NF- κ B activity (Figure 18B), indicating a potentially global impact of A3C on NF- κ B signaling. Additionally, stable depletion of A3C enhances the effect of reduced NF- κ B activity, particularly in the ccRCC-derived cell line 769-P (Figure 18C), suggesting that the A3C effect depends on long-term adaptations and the cell-specific context. In conditions of elevated A3C levels, representing the tumor microenvironment of ccRCC, NF- κ B activity is increased (Figure 18D). To enhance the sensitivity of the NF- κ B activity reporter and achieve more robust results, it is recommended to incorporate a wider range of κ B-binding sites into the reporter vector. Additionally, the induction of the NF- κ B signaling pathway by diverse stimuli could rapidly activate the NF- κ B system, potentially yielding stronger outcomes using this reporter vector.

Nevertheless, this study convincingly demonstrates that elevated A3C expression is associated with increased NF- κ B activity in ccRCC-derived cells. Although previous reports indicated that members of the A3 family, such as A3D and A3G, can serve as unfavorable

prognostic markers in ccRCC (Wu et al., 2020; Zhu et al., 2021), a potential cellular function has not yet been described. This study provides novel insights into a putative regulatory mechanism of A3C affecting NF- κ B activity and ccRCC disease progression.

4.4 Transcripts of NF- κ B pathway regulators are bound and presumably stabilized by A3C affecting translocation of NF- κ B subunits

One major focus of this study was to elucidate the molecular function of A3C and examine the biological consequences of its upregulation in malignancies. While it has been observed that A3C modulates the NF- κ B pathway, the precise mechanism by which A3C regulates NF- κ B activity remains elusive.

As previously described, the NF- κ B pathway is a highly complex network that integrates various stimuli, signaling pathways, post-translational modifications, feedback circuits and protein-protein interactions, generating an intricate regulatory network (Hoesel, Schmid, 2013; Tieri et al., 2012). Unlike traditional representations of signaling pathways as linear cascades, screens suggest the participation of hundreds of components in the NF- κ B pathway, indicating a network with intricate interdependencies and feedback loops (Fraser, Germain, 2009). Important crosstalk nodes are the NF- κ B subunits containing sites for phosphorylations and other post-translational modifications as well as kinases, such as the I κ B kinase, integrating other signaling pathways into the NF- κ B network (Ghosh, Dass, 2016; Oeckinghaus et al., 2011). Additionally, several kinases, including GSK3- β , a serine/threonine kinase, and various members of the MAP kinase family (e.g., p38, ERK1/2 and JNK), have well-documented interactions and cooperative roles with the NF- κ B pathway, fine-tuning biological functions and cellular responses (Ghosh, Dass, 2016; Schulze-Osthoff et al., 1997). This intricate crosstalk is essential for shaping the activation of such a pleiotropic transcription factor family. However, it is important to note that the effect of a signaling molecule on NF- κ B is cell type- and context-specific, as evidenced by variations in NF- κ B subunit levels (Figure 25A and Supplemental Figure 6) and differing levels of (activated) kinases (Figure 26, B and C) among different cell lines. Consequently, identifying the primary factor affected by A3C in this complex NF- κ B network remains challenging.

4.4.1 A3C interacts with NF- κ B signaling pathway regulators independently of its cytidine deaminase activity

Given that global A3C interaction studies are currently not available, RIP-seq analyses were conducted to identify transcripts associated with A3C. Considering the previously reported promiscuous binding of A3 proteins to various classes of RNAs, such as mRNAs,

Y RNAs or 7SL RNAs (Apolonia et al., 2015; Kozak et al., 2006; Smith, 2016), it was expected that A3C would associate with a high number of RNAs. Indeed, the RIP analyses revealed the co-purification of over 5 300 protein-coding and non-coding transcripts with A3C (FC compared to input ≥ 2 ; mean FPKM in input > 0.1). Using DAVID for systematic analysis of the putative protein-coding binding partners of A3C ($n=2\ 770$), multiple pathways were identified that are associated with the NF- κ B signaling pathway, including TLR cascades, IL-17 signaling and TRAF6-mediated induction of NF- κ B (Figure 22C). Furthermore, comparison of significantly enriched protein-coding genes from the A3C-IP (FC ≥ 2 ; $p < 0.05$; mean FPKM in input > 0.1) with reported NF- κ B signaling pathway regulators identified 232 putative mRNA binding partners of A3C described to be linked to the NF- κ B signaling pathway (Figure 22E; Supplemental Table 3). Among these transcripts are kinases like CDK6, MAP3K7, IKBKA or RIPK2, transmembrane proteins like EDA2R and associated adaptors like TAB3 or TRAF6 (Figure 22, F and G). This highlights the potential for A3C to significantly influence the NF- κ B signaling pathway by modulating its regulators.

However, it is important to note that a hypergeometric test was conducted to assess if the number of transcripts pulled by A3C classified as 'NF- κ B regulator' was significantly higher than expected, revealing that NF- κ B regulators were not significantly overrepresented in the RIP-seq results. As shown in Supplemental Figure 5, transcripts of factors belonging to pathways that were not considered enriched in the GSEA of A3C C vs. A3C KO, such as HEME_METABOLISM, MITOTIC_SPINDLE or SPERMATOGENESIS, showed an overlapping distribution in the A3C RIP-seq with transcripts of factors belonging to the HALLMARK pathway TNFA_SIGNALING_VIA_NFKB. Considering the non-selective association of A3 proteins with RNAs, this result was expected, especially since the hypergeometric test neglects biological dependencies such as RNA abundance and availability in the cell. This suggests that although an association of RNAs with A3C may not be statistically significant for distinct pathways, it may be biologically relevant for the cellular functions especially in the context of malignancies.

The cellular function of A3 proteins is frequently linked to their cytidine deaminase activity on RNA and ssDNA, albeit with varying deamination activities and specificities (Hultquist et al., 2011; Ito et al., 2017; McDougall et al., 2011; Silvas, Schiffer, 2019; Stenglein et al., 2010). *In vitro* studies have demonstrated detectable deaminase activity on cytidine of ssDNA for all A3 proteins, exhibiting varying selectivity despite their evolutionary conserved core structure (Ito et al., 2017). However, these studies often overlook potential post-translational modifications, co-factor binding and subcellular localization occurring *in vivo*. Notably, C-to-U editing on specific RNAs has only been reported for A3A in monocytes (Sharma et al., 2015) and for A3G upon transient expression in HEK293T cells (Sharma et al., 2016), in addition to the well-known mRNA-editing activity of A1.

In this study, putative editing candidates of A3C (Supplemental Table 1) were identified by analyzing RNA-seq data from 786-O control, A3C KO and A3C Rec cell populations. Subsequently, these candidates were compared with putative A3C binding targets, revealing seven targets, including GLTP, PANX2, PXN, SBF1, TWF1, UBE4B and WDR4. Interestingly, none of these editing candidates are considered NF- κ B regulators or prognostic markers in ccRCC. Moreover, C-to-T alterations identified in the RNA-seq data occurred simultaneously in many putative editing targets on the genomic level (Supplemental Figure 2), with ccRCC exhibiting a particularly high number of SNPs identified in whole-genome datasets compared to other cancer types (Roberts et al., 2013). As A3C mainly localizes to the cytoplasm (Figure 8), mutation events likely occur independently of A3C. RNA-editing contributes to transcriptome diversification and the regulation of gene expression by several complementary mechanisms, including the insertion of premature stop codons, nuclear retention of hyper-edited transcripts, modulation miRNA sequences or alteration of dsRNA structure and stability (Levanon et al., 2004; Tang et al., 2012). However, RNA expression data in 786-O cells did not show overall alterations in the expression levels of potentially edited transcripts (Figure 9B).

In conclusion, these findings suggest that A3C binds to a vast array of transcripts, revealing a promiscuous binding behavior. Among the associated RNAs are transcripts encoding regulators of the NF- κ B signaling pathway, highlighting the potential of A3C to modulate NF- κ B activity. Overall, these findings strongly suggest that A3C could efficiently affect the NF- κ B signaling pathway by modulating its regulators by a mechanism independent of its cytidine deaminase function.

4.4.2 A3C binding partners may be stabilized by protection from miRNA-mediated degradation

Current studies offer only preliminary insights into the broader molecular roles of proteins within the APOBEC family. For instance, A1 has been identified to exhibit functions beyond its established role as an ApoB RNA-specific cytidine deaminase, suggesting a spectrum of deamination-independent activities. Mouse Apobec1 has been observed to bind AU-rich sequence elements embedded in the 3' UTR of RNAs with rapid turnover, thereby identifying novel RNA targets in animal models, including c-myc, TNF- α and IL-2, (Anant, Davidson, 2000). These consensus motifs act as destabilizing elements, suggesting that Apobec1 has the capacity to modulate RNA stability (Blanc, Davidson, 2010; Anant et al., 2004). Notably, dysregulation of Apobec1 expression has been implicated in carcinogenesis, as evidenced by liver-specific overexpression in transgenic animals resulting in hepatocellular carcinoma (Blanc, Davidson, 2010; Yamanaka et al., 1995).

Similarly, human A3 proteins have been found to fulfill functions beyond cytidine deamination, including their involvement in inhibiting miRNA-mediated gene silencing

(Holmes et al., 2007b; Huang et al., 2007; Liu et al., 2012a; Rhoads, 2010). Members of the A3 protein family can counteract the inhibitory effects of several miRNAs, such as miR-10b, miR-16, miR-25, miR-29 and let-7a, on protein synthesis (Ding et al., 2011; Huang et al., 2007; Zhang, 2010). For instance, in colorectal tumors, A3G is involved in inhibiting miR-29-mediated suppression of MMP2, promoting metastasis (Ding et al., 2011). Although the precise mechanism remains elusive, it has been proposed that A3G prevents the decay of miRNA-targeted mRNA in P-bodies and instead promotes the association of mRNA with polysomes (Huang et al., 2007; Liu et al., 2012a). Interestingly, A3G is located in both P-bodies and stress granules (Gallois-Montbrun et al., 2007; Wichroski et al., 2006). Since A3C is located in P-bodies and associated with AGO2 (Figure 8B), it is possible that it functions in a similar mode like A3G as a regulator of RNA-induced gene silencing.

In ccRCC, an inverse correlation between immune-associated genes and the expression of multiple miRNAs was identified, such as miR-149 and miR-508, suggesting miRNAs to be key regulators of dysregulated expression of immune-related genes (Saad et al., 2022). Furthermore, signatures of dysregulated miRNA are associated with ccRCC stage, grade and progression, potentially targeting pathways crucial in carcinogenesis and cancer progression, including signaling pathways (Gowrishankar et al., 2014). The let-7 miRNA family, known as tumor suppressors, is consistently downregulated in various cancers compared to normal tissue, including ccRCC (Gowrishankar et al., 2014; Kalantzakos et al., 2022; Liu et al., 2012c; Peng et al., 2015; Su et al., 2014). Moreover, expression levels of members of the let-7 family are decreased in highly aggressive primary metastatic tumors compared to non-metastatic ccRCC (Heinzelmann et al., 2011). Interestingly, several positive regulators of the NF- κ B signaling pathway, identified as binding partners of A3C, such as MTPN, CDK6, TAB3, TRAM2, TAB2, MAP3K7 and IKBKA, harbor putative let-7 binding sites in their coding sequences or 3' UTRs (Figure 24A). This may hint towards a protective function of A3C of NF- κ B regulator transcripts against let-7-mediated degradation, facilitating mRNA stability and subsequently NF- κ B activity. Indeed, depletion of A3C results in reduced expression levels of these putative binding partners (Figure 23).

To evaluate the functional implications of the predicted let-7 target sites and to investigate whether A3C mediates a potential protective role via binding to let-7 complementary sites on target mRNAs, luciferase reporters harboring the let-7 target sequence in the 3' UTR were generated (Figure 24). The impact of post-transcriptional regulation mediated by A3C appears to be modest, albeit significant in certain instances, such as for MTPN, CDK6 and IKBKA (Figure 24B). The cloned fragments of the 3' UTRs, spanning approximately 50 nucleotides, may not cover the entire A3C binding site or lack essential adjacent structural elements. This could impede effective A3C recognition and reduce its protective function. Another possibility for the modest effect is that in A3C-

depleted cell populations, additional factors, such as other members of the APOBEC family, may bind NF- κ B regulator transcripts, compensating for the absent stabilizing factor.

Accordingly, cloning a longer sequence of 3' UTRs of putative A3C binding partners into the luciferase reporter gene led to a mild, though cell-type specific, impact of A3C on reporter gene expression (Figure 24C). It should be noted that these fragments might contain multiple target sites for other miRNAs or other regulatory factors, thereby affecting the reporter mRNA stability and luciferase expression at various levels. Furthermore, given that A3C is a stress-responsive factor, its effects on target gene expression may only manifest upon induction of stress-responsive pathways. Investigating additional miRNAs that are relevant in ccRCC, such as miRNA-21, miRNA-9, miRNA-149 and miRNA-30b (Braga et al., 2019; Xie et al., 2018), and a potential protective function of A3C on these miRNA target transcripts, should be assessed.

Interpreting these results is challenging and further analyses should be considered. Antagomirs, synthetic antagonists of miRNAs that silence the endogenous miRNAs (Krützfeldt et al., 2005), could be used to ascertain whether let-7 is a biologically significant miRNA destabilizing putative A3C binding partners. Additionally, CLIP-seq could be employed to precisely identify the RNA sequence bound by A3C at nucleotide resolution. In this study, RNA stability assays were performed using either actinomycin D or α -amanitin to assess the stability of putative A3C binding partners upon A3C depletion (Figure 24, E - G). Again, the effects of A3C on RNA stability appear to be modest for the investigated targets and time span. However, it is noteworthy that transcripts of kinases, including CDK6, IKBKA, IKBKE or RIPK2, show increased degradation upon A3C depletion. This suggests that A3C facilitates mRNA stability of NF- κ B pathway regulators, potentially leading to alterations in the phosphorylation status of downstream targets, ultimately affecting NF- κ B activity. Despite the seemingly minor impact of A3C on the stability of individual NF- κ B pathway regulators, its cumulative effect on NF- κ B activity may be substantial, achieved by adjusting the expression levels of numerous positive regulators across different levels of the complex regulatory network.

4.4.3 Regulation of A3C-mediated NF- κ B activity occurs through NF- κ B subunits translocation

While the majority of tumors, lymphoid or solid, exhibit augmented NF- κ B activity (DiDonato et al., 2012; Karin et al., 2002), previous studies have indicated that activating oncogenic mutations in NF- κ B subunits are rare, mainly occurring in lymphoid malignancies (Gilmore, 2003; Staudt, 2010). Instead, it is hypothesized that upstream components within the signaling system are activated, mediating post-translational modifications such as phosphorylation and acetylation. These modifications, in turn, regulate NF- κ B activation by

either controlling NF- κ B DNA binding activity or modulating the association of NF- κ B complexes with either I κ Bs or κ B-binding sites (Wan, Lenardo, 2009).

A novel factor potentially influencing multiple positive regulators within the complex regulatory NF- κ B network synergistically is A3C. It could influence various positive regulators by affecting the stability of their transcripts. These regulators include kinases (like CDK6, IKBKA, IKBKE, RIPK2 and MAP3K7), adaptor proteins (such as TAB2 and TAB3) facilitating the formation of kinase complexes, receptor-associated factors (like TRAF6) mediating signal transduction of pro-inflammatory cytokines and transmembrane proteins (such as EDA2R). A3C may control the accumulation levels and post-translational modifications of downstream targets regulated by these factors.

Focusing on kinases influenced by A3C, the complexity of the NF- κ B regulatory network becomes apparent. Several kinases are involved in phosphorylating NF- κ B subunits or key regulatory complexes like I κ B α (exemplary illustrated in Figure 26A; Christian et al., 2016; Oeckinghaus, Ghosh, 2009). For instance, I κ B kinases (IKBKA/B/E) as well as CDKs (e.g., CDK6) are implicated in phosphorylating I κ B α , NF- κ B2 and RelA (Buss et al., 2012; Christian et al., 2016; Handschick et al., 2014; Oeckinghaus, Ghosh, 2009; Sakurai et al., 1999). The upregulation of kinase genes such as IKBKE or MAP3K8 in metastatic ccRCC underscores their potential as disease drivers (Ghatalia et al., 2016). Upon depletion of A3C, levels of CDK6, IKBKA and IKBKB are reduced (Figure 23, C and D; Figure 25C; Figure 26B), suggesting a subsequent impairment in the phosphorylation of downstream targets like RelA (Figure 25A). Additionally, while total levels of NF- κ B subunits remain unaffected, there is a shift in the ratio of processed to unprocessed NF- κ B2 towards less active subunits (Figure 25B).

Moreover, the p38 MAP kinase has been reported to be associated with the activation of the NF- κ B pathway, regulating NF- κ B-dependent gene expression (Campbell et al., 2004; Carter et al., 1999; Koul et al., 2013; Sakai et al., 2002; Schulze-Osthoff et al., 1997). Depletion of A3C significantly reduces p38 phosphorylation without affecting its total protein levels (Figure 26C), indicating multifaceted control of various kinases.

Consequently, dimers containing activated RelA and NF- κ B2 p52 are translocated to the nucleus in a cell type-specific and A3C-dependent manner, while unprocessed subunits accumulate in the cytoplasm (Figure 25, D, F and G). Binding to specific chromatin loci across the genome, transcription of NF- κ B target genes crucial for cell survival, proliferation and invasion is induced, thereby promoting tumor progression (schematically depicted in Figure 25I; DiDonato et al., 2012). In ccRCC, these target genes such as IAP proteins (e.g., BIRC3 and BIRC5) were previously reported to correlate with advanced stages and more aggressive ccRCCs, thus serving as unfavorable prognostic markers (Figure 19F; Li et al., 2021; Tsujimoto, 2002; Xiong et al., 2016).

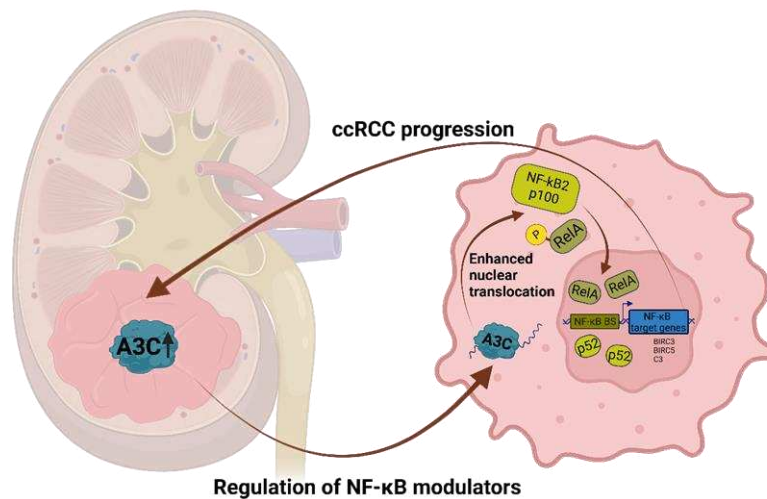


Figure 31: Putative function of A3C in ccRCC. Schematic created with BioRender.com.

In summary (Figure 31), in ccRCC, upregulated A3C affects transcript levels of NF-κB pathway regulators, subsequent signal transduction and subunit translocation to the nucleus. Induced expression of NF-κB target genes, including A3C, enhances ccRCC progression in a positive feedback loop, resulting in persistent NF-κB activation with oncogenic potential.

4.5 A3C may be a target for ccRCC therapy

CcRCC presents a challenging clinical scenario characterized by resistance to traditional chemotherapy and radiation therapies, leading to poor patient outcomes (Makhov et al., 2018; Motzer, Russo, 2000). Particularly, the demand for innovative therapeutic strategies targeting advanced ccRCC is high, given its low 5-year survival rate of only 12% (SEER Cancer Statistics Review, 1975–2012, National Cancer Institute. Bethesda, MD, 2015). One potential avenue for improving outcomes in ccRCC therapy involves targeting the NF-κB pathway (Morais et al., 2011; Ng et al., 2018; Peri et al., 2013; Sourbier et al., 2007), a crucial player in cancer initiation and progression, due to its orchestration of gene expression affecting cell proliferation, survival, metastasis, angiogenesis and resistance to anti-cancer therapies (Dolcet et al., 2005; Meteoglu et al., 2008).

Despite the promising potential of small-molecule inhibitors and synthetic compounds to inhibit NF-κB activation (An, Rettig, 2007; Castro Barbosa et al., 2017; Sourbier et al., 2007; Thapa et al., 2013), targeting NF-κB therapeutically is challenging due to its complex biological functions, intrinsic pathway complexity, crosstalk with other pathways, lack of biomarkers, poor drug specificity and drug resistance (Baud, Karin, 2009; DiDonato et al., 2012; Erstad, Cusack, 2013; Morais et al., 2011). Moreover, the variable expression and activity levels of different NF-κB subunits, along with poorly understood regulation, add to

the challenges of this therapeutic approach, highlighting the need for novel approaches in targeting NF- κ B for ccRCC therapy.

A promising new avenue in ccRCC therapy involves A3C as this RBP regulates NF- κ B activity synergistically. In this study, three different multiple tyrosine kinase inhibitors (TKI; Sorafenib, Pazopanib and Sunitinib) were tested. These small-molecule inhibitors have been approved for the treatment of patients with metastatic ccRCC due to their reported abilities to reduce tumor vascularization, trigger cancer cell apoptosis and, thus, promote tumor shrinkage (Kane et al., 2006; Keisner, Shah, 2011; Motzer et al., 2006; Rini et al., 2016). As these compounds target multiple receptor tyrosine protein kinases such as VEGFR and PDGFR that transduce signals via the Ras/MAPK and the PI3K/AKT pathway, promoting cell proliferation, survival, migration and angiogenesis, NF- κ B activation is indirectly affected (Lai et al., 2018, 2018; Welsh, Fife, 2015).

Initial investigations to assess the impact of A3C on the efficacy of these TKIs were performed. Viability was significantly reduced in A3C-depleted cells when treated with Pazopanib or Sunitinib (Figure 29B), suggesting that targeting A3C in combination with small-molecule TKIs may offer a promising strategy to effectively treat ccRCC.

Additionally, in this study it was determined that high A3C levels are essential for the viability of ccRCC-derived cells under stress conditions (Figure 27, A-C) as well as for the survival of 3D spheroids (Figure 28, A-D). Under non-stress conditions, cell survival was not affected upon modulation of A3C levels. Accordingly, the single *Apobec3* gene encoded in the mouse genome is non-essential for mouse development, survival or fertility (Mikl et al., 2005). Furthermore, ccRCC-derived cells with high A3C levels showed robust tumor development in xenograft analyses, in contrast to negligible tumor formation observed with A3C KO cells (Figure 28, E and F). This highlights the essential role of A3C in facilitating 786-O tumor growth *in vivo*. Consequently, inhibition of A3C could be a novel strategy for developing treatment options in ccRCC. Indeed, ongoing studies focus on the use of nucleic acid-based inhibitors (Barzak et al., 2019; Kvach et al., 2019), substrate-mimics (Serrano et al., 2022) or small molecule inhibitors (Olson et al., 2015) to counteract A3 activity.

In this study, Aurothioglucose (AuTG) was employed to assess the inhibitory potential against A3C. AuTG, a gold derivative of glucose (Karabulut, Leszczynski, 2015; Figure 32A), is used as effective anti-inflammatory drug to treat rheumatoid arthritis (van Riel et al., 1984). Studies have indicated that AuTG inhibits A3G catalytic activity by affecting A3G-ssDNA complex formation (Li et al., 2012). Initial investigations using AuTG in ccRCC-derived cells showed reduced cell viability (Figure 32B). However, depletion of A3C did not alter cell viability compared to 786-O C cells (Figure 32D).

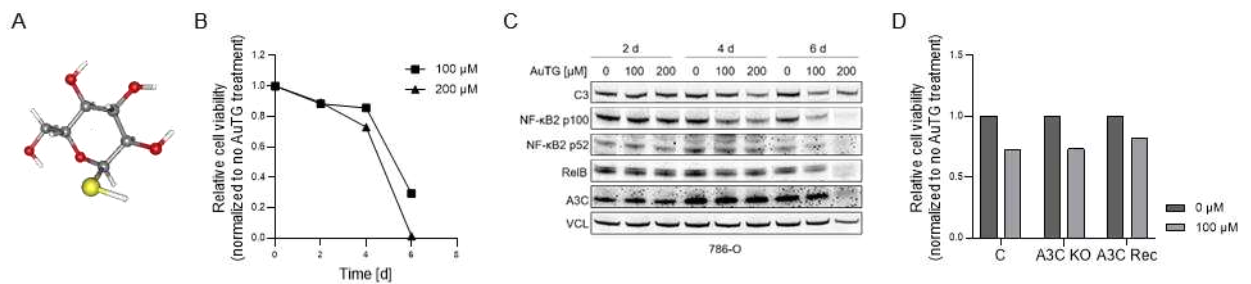


Figure 32: Impaired cell viability upon Aurothioglucose treatment may not be mediated by A3C. (A) The model depicts the chemical structure of Aurothioglucose (AuTG). (B) 786-O WT cells were treated with 100 μ M and 200 μ M AuTG for six days. Cell viability was determined at indicated time points using CellTiter-Glo. (C) Protein levels of A3C, NF- κ B subunits and the NF- κ B target gene C3 were analyzed upon applying 100 μ M or 200 μ M AuTG to 786-O WT cells for two, four and six days. VCL served as loading control. (D) Cell viability of 786-O C, A3C KO and A3C Rec cells was investigated upon treatment with 100 μ M AuTG for five days. Note that experiments in (B-D) were performed once.

Interestingly, AuTG has been reported to impair NF- κ B-dependent gene expression as gold ions inhibit NF- κ B DNA-binding via a redox mechanism *in vitro* (Traber et al., 1999; Yang et al., 1995; Yoshida et al., 1999). Furthermore, AuTG has demonstrated the ability to suppress IKK activity *in vitro* (Jeon et al., 2000) and PKC, thus blocking growth and metastasis of pancreatic and non-small-cell lung cancer both *in vitro* and in mice (Mucke, 2016). As shown in Figure 32C, expression of NF- κ B subunits and the NF- κ B target gene C3 are impaired upon AuTG treatment, suggesting its potential use in the treatment of ccRCC. However, the effect appears to be independent of A3C.

In conclusion, this study highlights the importance of exploring novel therapeutic avenues targeting ccRCC. While challenges such as drug resistance and complex pathway interactions persist, targeting the NF- κ B pathway through strategies like A3C's impact on NF- κ B regulation may provide a promising strategy. This targeted approach offers the potential to inhibit NF- κ B's pro-tumorigenic functions without the broad side effects of upstream NF- κ B blockade, thus presenting a more precise and effective treatment option for patients with advanced ccRCC. The potential of targeting A3C opens avenues for further investigation into combination therapies that could significantly enhance patient prognosis and survival outcomes in advanced ccRCC cases.

5 SUMMARY

Clear cell renal cell carcinoma (ccRCC), the most prevalent type of kidney cancer, presents significant challenges in clinical management, particularly the need for efficient therapies targeting metastatic ccRCC. Understanding the molecular mechanisms driving ccRCC progression is crucial for developing effective therapeutic strategies. This study investigates the role of the RNA-binding protein APOBEC3C (A3C) in ccRCC, revealing its substantial upregulation in ccRCC tissue and ccRCC-derived cell lines, particularly in advanced stages, correlating with diminished overall survival.

Functional analyses employing RNA-sequencing and cell-based assays in ccRCC-derived cell lines with modulated A3C levels elucidate the impact of A3C on gene expression, specifically its involvement in the NF- κ B signaling pathway. Upon A3C depletion, subunits of the NF- κ B family are abnormally restrained in the cytoplasm leading to deregulation of NF- κ B target gene expression. A3C binds and potentially stabilizes a plethora of transcripts encoding positive regulators of the NF- κ B pathway, thereby promoting NF- κ B activity and facilitating ccRCC tumor growth. Notably, A3C's influence on NF- κ B activity appears to be independent of its cytidine deamination function, indicating a novel regulatory mechanism. Moreover, A3C's stress-responsive nature and its role in ccRCC cell viability under adverse conditions underscore its pivotal role in tumor survival mechanisms.

The study suggests A3C as a potential therapeutic target in ccRCC, shedding light on its regulatory role in NF- κ B signaling and tumor growth. Further investigations aim to unravel the precise mechanisms underlying A3C-mediated modulation of NF- κ B activity, providing a basis for understanding its role in ccRCC pathogenesis, potentially leading to the development of targeted therapeutic interventions.

In conclusion, this study advances the understanding of the molecular mechanisms underlying ccRCC progression and identifies A3C as a pivotal player in promoting ccRCC tumor growth through the positive regulation of the NF- κ B pathway. The findings highlight the potential of targeting A3C as a novel therapeutic approach for ccRCC, offering promising prospects for improving patient outcomes in this challenging malignancy.

6 REFERENCES

- Aggarwal, B. B. Apoptosis and nuclear factor-kappa B: a tale of association and dissociation. *Biochemical pharmacology* **2000**, *60* (8), 1033–1039. DOI: 10.1016/s0006-2952(00)00393-2.
- Alexandrov, L. B., Nik-Zainal, S., Wedge, D. C., Aparicio, S. A.; Behjati, S., et al. Signatures of mutational processes in human cancer. *Nature* **2013**, *500* (7463), 415–421. DOI: 10.1038/nature12477.
- Amin, M. B., Paner, G. P., Alvarado-Cabrero, I., Young, A. N.; Stricker, H. J., et al. Chromophobe renal cell carcinoma: histomorphologic characteristics and evaluation of conventional pathologic prognostic parameters in 145 cases. *The American journal of surgical pathology* **2008**, *32* (12), 1822–1834. DOI: 10.1097/PAS.0b013e3181831e68.
- An, J. and Rettig, M. B. Mechanism of von Hippel-Lindau protein-mediated suppression of nuclear factor kappa B activity. *Molecular and cellular biology* **2005**, *25* (17), 7546–7556. DOI: 10.1128/MCB.25.17.7546-7556.2005.
- An, J. and Rettig, M. B. Epidermal growth factor receptor inhibition sensitizes renal cell carcinoma cells to the cytotoxic effects of bortezomib. *Molecular cancer therapeutics* **2007**, *6* (1), 61–69. DOI: 10.1158/1535-7163.MCT-06-0255.
- Anant, S. and Davidson, N. O. An AU-rich sequence element (UUUNA/UU) downstream of the edited C in apolipoprotein B mRNA is a high-affinity binding site for Apobec-1: binding of Apobec-1 to this motif in the 3' untranslated region of c-myc increases mRNA stability. *Molecular and cellular biology* **2000**, *20* (6), 1982–1992. DOI: 10.1128/MCB.20.6.1982-1992.2000.
- Anant, S., MacGinnitie, A. J.; Davidson, N. O. apobec-1, the catalytic subunit of the mammalian apolipoprotein B mRNA editing enzyme, is a novel RNA-binding protein. *The Journal of biological chemistry* **1995**, *270* (24), 14762–14767.
- Anant, S., Murmu, N., Houchen, C. W., Mukhopadhyay, D.; Riehl, T. E., et al. Apobec-1 protects intestine from radiation injury through posttranscriptional regulation of cyclooxygenase-2 expression. *Gastroenterology* **2004**, *127* (4), 1139–1149. DOI: 10.1053/j.gastro.2004.06.022.
- Annunziata, C. M., Davis, R. E., Demchenko, Y., Bellamy, W.; Gabrea, A., et al. Frequent engagement of the classical and alternative NF-kappaB pathways by diverse genetic abnormalities in multiple myeloma. *Cancer cell* **2007**, *12* (2), 115–130. DOI: 10.1016/j.ccr.2007.07.004.
- Antonelli, A., Tardanico, R., Balzarini, P., Arrighi, N.; Perucchini, L., et al. Cytogenetic features, clinical significance and prognostic impact of type 1 and type 2 papillary renal cell carcinoma. *Cancer genetics and cytogenetics* **2010**, *199* (2), 128–133. DOI: 10.1016/j.cancergencyto.2010.02.013.
- Apolonia, L., Schulz, R., Curk, T., Rocha, P.; Swanson, C. M., et al. Promiscuous RNA binding ensures effective encapsidation of APOBEC3 proteins by HIV-1. *PLoS pathogens* **2015**, *11* (1), e1004609. DOI: 10.1371/journal.ppat.1004609.
- Arabi, A., Ullah, K., Branca, R. M., Johansson, J.; Bandarra, D., et al. Proteomic screen reveals Fbw7 as a modulator of the NF-kB pathway. *Nat Commun* **2012**, *3*, 976. DOI: 10.1038/ncomms1975.
- Arias, J. F., Koyama, T., Kinomoto, M.; Tokunaga, K. Retroelements versus APOBEC3 family members: No great escape from the magnificent seven. *Front. Microbiol.* **2012**, *3*, 275. DOI: 10.3389/fmicb.2012.00275.

- Athanasiadis, A., Rich, A.; Maas, S. Widespread A-to-I RNA editing of Alu-containing mRNAs in the human transcriptome. *PLOS Biology* **2004**, *2* (12), e391. DOI: 10.1371/journal.pbio.0020391.
- Atkins, M., Jones, C. A.; Kirkpatrick, P. Sunitinib maleate. *Nature reviews. Drug discovery* **2006**, *5* (4), 279–280. DOI: 10.1038/nrd2012.
- Bach, D., Peddi, S., Mangeat, B., Lakkaraju, A.; Strub, K., et al. Characterization of APOBEC3G binding to 7SL RNA. *Retrovirology* [Online] **2008**, *5* (1), 54.
- Baldwin, A. S. Control of oncogenesis and cancer therapy resistance by the transcription factor NF-kappaB. *J Clin Invest* **2001**, *107* (3), 241–246. DOI: 10.1172/JCI11991.
- Barzak, F. M., Harjes, S., Kvach, M. V., Kurup, H. M.; Jameson, G. B., et al. Selective inhibition of APOBEC3 enzymes by single-stranded DNAs containing 2'-deoxyzebularine. *Organic & biomolecular chemistry* **2019**, *17* (43), 9435–9441. DOI: 10.1039/C9OB01781J.
- Basak, S., Kim, H., Kearns, J. D., Tergaonkar, V.; O'Dea, E., et al. A fourth IkappaB protein within the NF-kappaB signaling module. *Cell* **2007**, *128* (2), 369–381. DOI: 10.1016/j.cell.2006.12.033.
- Bassères, D. S. and Baldwin, A. S. Nuclear factor-kappaB and inhibitor of kappaB kinase pathways in oncogenic initiation and progression. *Oncogene* **2006**, *25* (51), 6817–6830. DOI: 10.1038/sj.onc.1209942.
- Baud, V. and Karin, M. Is NF-kappaB a good target for cancer therapy? Hopes and pitfalls. *Nature reviews. Drug discovery* **2009**, *8* (1), 33–40. DOI: 10.1038/nrd2781.
- Becht, E., Giraldo, N. A., Germain, C., Reyniès, A. de; Laurent-Puig, P., et al. Immune Contexture, Immunoscore, and Malignant Cell Molecular Subgroups for Prognostic and Theranostic Classifications of Cancers. *Advances in immunology* **2016**, *130*, 95–190. DOI: 10.1016/bs.ai.2015.12.002.
- Bedke, J., Albiges, L., Capitanio, U., Giles, R. H.; Hora, M., et al. The 2021 Updated European Association of Urology Guidelines on Renal Cell Carcinoma: Immune Checkpoint Inhibitor-based Combination Therapies for Treatment-naive Metastatic Clear-cell Renal Cell Carcinoma Are Standard of Care. *European Urology* **2021**, *80* (4), 393–397. DOI: 10.1016/j.eururo.2021.04.042.
- Beksac, A. T., Paulucci, D. J., Blum, K. A., Yadav, S. S.; Sfakianos, J. P., et al. Heterogeneity in renal cell carcinoma. *Urologic oncology* **2017**, *35* (8), 507–515. DOI: 10.1016/j.urolonc.2017.05.006.
- Bell, J. L., Wächter, K., Mühleck, B., Pazaitis, N.; Köhn, M., et al. Insulin-like growth factor 2 mRNA-binding proteins (IGF2BPs): post-transcriptional drivers of cancer progression? *Cellular and molecular life sciences : CMLS* **2013**, *70* (15), 2657–2675. DOI: 10.1007/s00018-012-1186-z.
- Ben-Neriah, Y. and Karin, M. Inflammation meets cancer, with NF-κB as the matchmaker. *Nature immunology* **2011**, *12* (8), 715–723. DOI: 10.1038/ni.2060.
- Bernard, J., Treton, D., Vermot-Desroches, C., Boden, C.; Horellou, P., et al. Expression of interleukin 13 receptor in glioma and renal cell carcinoma: IL13Ralpha2 as a decoy receptor for IL13. *Laboratory investigation; a journal of technical methods and pathology* **2001**, *81* (9), 1223–1231. DOI: 10.1038/labinvest.3780336.
- Beroukhim, R., Mermel, C. H., Porter, D., Wei, G.; Raychaudhuri, S., et al. The landscape of somatic copy-number alteration across human cancers. *Nature* **2010**, *463* (7283), 899–905. DOI: 10.1038/nature08822.
- Bersanelli, M., Casartelli, C., Buti, S.; Porta, C. Renal cell carcinoma and viral infections: A dangerous relationship? *World journal of nephrology* **2022**, *11* (1), 1–12. DOI: 10.5527/wjn.v11.i1.1.

- Bishop, K. N., Holmes, R. K.; Malim, M. H. Antiviral potency of APOBEC proteins does not correlate with cytidine deamination. *Journal of virology* **2006**, *80* (17), 8450–8458. DOI: 10.1128/jvi.00839-06.
- Blanc, V. and Davidson, N. O. APOBEC-1-mediated RNA editing. *Wiley interdisciplinary reviews. Systems biology and medicine* **2010**, *2* (5), 594–602. DOI: 10.1002/wsbm.82.
- Blankenship, C., Naglich, J. G., Whaley, J. M., Seizinger, B.; Kley, N. Alternate choice of initiation codon produces a biologically active product of the von Hippel Lindau gene with tumor suppressor activity. *Oncogene* **1999**, *18* (8), 1529–1535. DOI: 10.1038/sj.onc.1202473.
- Bocitto, M. and Wolin, S. L. Ro60 and Y RNAs: structure, functions, and roles in autoimmunity. *Critical Reviews in Biochemistry and Molecular Biology* **2019**, *54* (2), 133–152. DOI: 10.1080/10409238.2019.1608902.
- Bogerd, H. P., Wiegand, H. L., Hulme, A. E., Garcia-Perez, J. L.; O'Shea, K. S., et al. Cellular inhibitors of long interspersed element 1 and Alu retrotransposition. *Proceedings of the National Academy of Sciences of the United States of America* **2006**, *103* (23), 8780–8785. DOI: 10.1073/pnas.0603313103.
- Bohuslav, J., Chen, L.-F., Kwon, H., Mu, Y.; Greene, W. C. p53 induces NF-kappaB activation by an IkappaB kinase-independent mechanism involving phosphorylation of p65 by ribosomal S6 kinase 1. *The Journal of biological chemistry* **2004**, *279* (25), 26115–26125. DOI: 10.1074/jbc.M313509200.
- Bonizzi, G. and Karin, M. The two NF-kappaB activation pathways and their role in innate and adaptive immunity. *Trends in immunology* **2004**, *25* (6), 280–288. DOI: 10.1016/j.it.2004.03.008.
- Bonvin, M., Achermann, F., Greeve, I., Stroka, D.; Keogh, A., et al. Interferon-inducible expression of APOBEC3 editing enzymes in human hepatocytes and inhibition of hepatitis B virus replication. *Hepatology (Baltimore, Md.)* **2006**, *43* (6), 1364–1374. DOI: 10.1002/hep.21187.
- Bourara, K., Liegler, T. J.; Grant, R. M. Target cell APOBEC3C can induce limited G-to-A mutation in HIV-1. *PLoS pathogens* **2007**, *3* (10), 1477–1485. DOI: 10.1371/journal.ppat.0030153.
- Braga, E. A., Fridman, M. V., Loginov, V. I., Dmitriev, A. A.; Morozov, S. G. Molecular Mechanisms in Clear Cell Renal Cell Carcinoma: Role of miRNAs and Hypermethylated miRNA Genes in Crucial Oncogenic Pathways and Processes. *Frontiers in genetics* **2019**, *10*, 320. DOI: 10.3389/fgene.2019.00320.
- Brasier, A. R. The nuclear factor-kappaB-interleukin-6 signalling pathway mediating vascular inflammation. *Cardiovascular research* **2010**, *86* (2), 211–218. DOI: 10.1093/cvr/cvq076.
- Braun, D. A., Street, K., Burke, K. P., Cookmeyer, D. L.; Denize, T., et al. Progressive immune dysfunction with advancing disease stage in renal cell carcinoma. *Cancer cell* **2021**, *39* (5), 632–648.e8. DOI: 10.1016/j.ccell.2021.02.013.
- Brooks, A. D., Jacobsen, K. M., Li, W., Shanker, A.; Sayers, T. J. Bortezomib sensitizes human renal cell carcinomas to TRAIL apoptosis through increased activation of caspase-8 in the death-inducing signaling complex. *Molecular cancer research : MCR* **2010**, *8* (5), 729–738. DOI: 10.1158/1541-7786.MCR-10-0022.
- Bruin, E. C. de, McGranahan, N., Mitter, R., Salm, M.; Wedge, D. C., et al. Spatial and temporal diversity in genomic instability processes defines lung cancer evolution. *Science* **2014**, *346* (6206), 251–256. DOI: 10.1126/science.1253462.
- Burns, M. B., Lackey, L., Carpenter, M. A., Rathore, A.; Land, A. M., et al. APOBEC3B is an enzymatic source of mutation in breast cancer. *Nature* **2013a**, *494* (7437), 366–370. DOI: 10.1038/nature11881.

- Burns, M. B., Temiz, N. A.; Harris, R. S. Evidence for APOBEC3B mutagenesis in multiple human cancers. *Nature genetics* **2013b**, 45 (9), 977–983. DOI: 10.1038/ng.2701.
- Buss, H., Dörrie, A., Schmitz, M. L., Frank, R.; Livingstone, M., et al. Phosphorylation of serine 468 by GSK-3 β negatively regulates basal p65 NF- κ B activity. *The Journal of biological chemistry* **2004a**, 279 (48), 49571–49574. DOI: 10.1074/jbc.C400442200.
- Buss, H., Dörrie, A., Schmitz, M. L., Hoffmann, E.; Resch, K., et al. Constitutive and interleukin-1-inducible phosphorylation of p65 NF- κ B at serine 536 is mediated by multiple protein kinases including I κ B kinase (IKK)- α , IKK β , IKK ϵ , TRAF family member-associated (TANK)-binding kinase 1 (TBK1), and an unknown kinase and couples p65 to TATA-binding protein-associated factor II31-mediated interleukin-8 transcription. *The Journal of biological chemistry* **2004b**, 279 (53), 55633–55643. DOI: 10.1074/jbc.M409825200.
- Buss, H., Handschick, K., Jurrmann, N., Pekkonen, P.; Beuerlein, K., et al. Cyclin-dependent kinase 6 phosphorylates NF- κ B P65 at serine 536 and contributes to the regulation of inflammatory gene expression. *PloS one* **2012**, 7 (12), e51847. DOI: 10.1371/journal.pone.0051847.
- Cameron, M. J. and Kelvin, D. J. Cytokines and chemokines--their receptors and their genes: an overview. *Advances in experimental medicine and biology* **2003**, 520, 8–32. DOI: 10.1007/978-1-4615-0171-8_2.
- Campbell, J., Ciesielski, C. J., Hunt, A. E., Horwood, N. J.; Beech, J. T., et al. A novel mechanism for TNF- α regulation by p38 MAPK: involvement of NF- κ B with implications for therapy in rheumatoid arthritis. *Journal of immunology (Baltimore, Md. : 1950)* **2004**, 173 (11), 6928–6937. DOI: 10.4049/jimmunol.173.11.6928.
- Campbell, S., Uzzo, R. G., Allaf, M. E., Bass, E. B.; Cadeddu, J. A., et al. Renal Mass and Localized Renal Cancer: AUA Guideline. *The Journal of urology* **2017**, 198 (3), 520–529. DOI: 10.1016/j.juro.2017.04.100.
- Carter, A. B., Knudtson, K. L., Monick, M. M.; Hunninghake, G. W. The p38 mitogen-activated protein kinase is required for NF- κ B-dependent gene expression. The role of TATA-binding protein (TBP). *The Journal of biological chemistry* **1999**, 274 (43), 30858–30863. DOI: 10.1074/jbc.274.43.30858.
- Castro Barbosa, M. L. de, Da Conceicao, R. A., Fraga, A. G., Camarinha, B. D.; Carvalho Silva, G. C. de, et al. NF- κ B Signaling Pathway Inhibitors as Anticancer Drug Candidates. *Anti-cancer agents in medicinal chemistry* **2017**, 17 (4), 483–490. DOI: 10.2174/1871520616666160729112854.
- Chaipan, C., Smith, J. L., Hu, W.-S.; Pathak, V. K. APOBEC3G restricts HIV-1 to a greater extent than APOBEC3F and APOBEC3DE in human primary CD4+ T cells and macrophages. *J. Virol.* **2013**, 87 (1), 444–453. DOI: 10.1128/JVI.00676-12.
- Chan, K., Roberts, S. A., Klimczak, L. J., Sterling, J. F.; Saini, N., et al. An APOBEC3A hypermutation signature is distinguishable from the signature of background mutagenesis by APOBEC3B in human cancers. *Nature genetics* **2015**, 47 (9), 1067–1072. DOI: 10.1038/ng.3378.
- Chen, C. Y. and Shyu, A. B. AU-rich elements: characterization and importance in mRNA degradation. *Trends in Biochemical Sciences* **1995**, 20 (11), 465–470. DOI: 10.1016/s0968-0004(00)89102-1.
- Chen, F. E. and Ghosh, G. Regulation of DNA binding by Rel/NF- κ B transcription factors: structural views. *Oncogene* **1999**, 18 (49), 6845–6852. DOI: 10.1038/sj.onc.1203224.
- Chen, H., Wang, L.-W., Huang, Y.-Q.; Gong, Z.-J. Interferon- α induces high expression of APOBEC3G and STAT-1 in vitro and in vivo. *International Journal of Molecular Sciences* **2010**, 11 (9), 3501–3512. DOI: 10.3390/ijms11093501.

- Chen, L.-L., DeCerbo, J. N.; Carmichael, G. G. Alu element-mediated gene silencing. *The EMBO Journal* **2008**, *27* (12), 1694–1705. DOI: 10.1038/emboj.2008.94.
- Chen, L.-L. and Yang, L. ALU alternative Regulation for Gene Expression. *Trends in cell biology* **2017**, *27* (7), 480–490. DOI: 10.1016/j.tcb.2017.01.002.
- Chen, S. H., Li, X. X., Liao, W. S., Wu, J. H.; Chan, L. RNA editing of apolipoprotein B mRNA. Sequence specificity determined by in vitro coupled transcription editing. *The Journal of biological chemistry* **1990**, *265* (12), 6811–6816.
- Chen, Z., Wen, W., Bao, J., Kuhs, K. L.; Cai, Q., et al. Integrative genomic analyses of APOBEC-mutational signature, expression and germline deletion of APOBEC3 genes, and immunogenicity in multiple cancer types. *BMC medical genomics* **2019**, *12* (1), 131. DOI: 10.1186/s12920-019-0579-3.
- Chevrier, S., Levine, J. H., Zanotelli, V. R., Silina, K.; Schulz, D., et al. An Immune Atlas of Clear Cell Renal Cell Carcinoma. *Cell* **2017**, *169* (4), 736-749.e18. DOI: 10.1016/j.cell.2017.04.016.
- Chiu, Y.-L. and Greene, W. C. The APOBEC3 cytidine deaminases: an innate defensive network opposing exogenous retroviruses and endogenous retroelements. *Annual review of immunology* **2008**, *26*, 317–353. DOI: 10.1146/annurev.immunol.26.021607.090350.
- Chiu, Y.-L., Soros, V. B., Kreisberg, J. F., Stopak, K.; Yonemoto, W., et al. Cellular APOBEC3G restricts HIV-1 infection in resting CD4⁺ T cells. *Nature* **2005**, *435* (7038), 108–114. DOI: 10.1038/nature03493.
- Chiu, Y.-L., Witkowska, H. E., Hall, S. C., Santiago, M.; Soros, V. B., et al. High-molecular-mass APOBEC3G complexes restrict Alu retrotransposition. *Proceedings of the National Academy of Sciences of the United States of America* **2006**, *103* (42), 15588–15593. DOI: 10.1073/pnas.0604524103.
- Choueiri, T. K., Halabi, S., Sanford, B. L., Hahn, O.; Michaelson, M. D., et al. Cabozantinib Versus Sunitinib As Initial Targeted Therapy for Patients With Metastatic Renal Cell Carcinoma of Poor or Intermediate Risk: The Alliance A031203 CABOSUN Trial. *Journal of clinical oncology : official journal of the American Society of Clinical Oncology* **2017**, *35* (6), 591–597. DOI: 10.1200/JCO.2016.70.7398.
- Chow, W. H., Gridley, G., Fraumeni, J. F.; Järnholm, B. Obesity, hypertension, and the risk of kidney cancer in men. *New England Journal of Medicine* **2000**, *343* (18), 1305–1311. DOI: 10.1056/NEJM200011023431804.
- Chow, W.-H., Dong, L. M.; Devesa, S. S. Epidemiology and risk factors for kidney cancer. *Nature reviews. Urology* **2010**, *7* (5), 245–257. DOI: 10.1038/nrrol.2010.46.
- Chowdhury, N. and Drake, C. G. Kidney Cancer: An Overview of Current Therapeutic Approaches. *The Urologic clinics of North America* **2020**, *47* (4), 419–431. DOI: 10.1016/j.ucl.2020.07.009.
- Christian, F., Smith, E. L.; Carmody, R. J. The Regulation of NF- κ B Subunits by Phosphorylation. *Cells* **2016**, *5* (1). DOI: 10.3390/cells5010012.
- Clark, P. E. The role of VHL in clear-cell renal cell carcinoma and its relation to targeted therapy. *Kidney International* **2009**, *76* (9), 939–945. DOI: 10.1038/ki.2009.296.
- Constantin, D., Dubuis, G., Del Conde-Rubio, M. C.; Widmann, C. APOBEC3C, a nucleolar protein induced by genotoxins, is excluded from DNA damage sites. *The FEBS journal* **2022**, *289* (3), 808–831. DOI: 10.1111/febs.16202.
- Conticello, S. G. The AID/APOBEC family of nucleic acid mutators. *Genome biology* [Online] **2008**, *9* (6), 229.
- Conticello, S. G., Thomas, C. J., Petersen-Mahrt, S. K.; Neuberger, M. S. Evolution of the AID/APOBEC Family of Polynucleotide (Deoxy)cytidine Deaminases. *Mol Biol Evol* [Online] **2005**, *22* (2), 367–377.

- Coppin, C., Porzsolt, F., Awa, A., Kumpf, J.; Coldman, A., et al. Immunotherapy for advanced renal cell cancer. *The Cochrane database of systematic reviews* [Online] **2005**, No. 1, CD001425.
- Cortez, L. M., Brown, A. L., Dennis, M. A., Collins, C. D.; Brown, A. J., et al. APOBEC3A is a prominent cytidine deaminase in breast cancer. *PLoS genetics* **2019**, *15* (12), e1008545. DOI: 10.1371/journal.pgen.1008545.
- Criollo, A., Chereau, F., Malik, S. A., Niso-Santano, M.; Mariño, G., et al. Autophagy is required for the activation of NFκB. *Cell cycle (Georgetown, Tex.)* **2012**, *11* (1), 194–199. DOI: 10.4161/cc.11.1.18669.
- Dejardin, E. The alternative NF-kappaB pathway from biochemistry to biology: pitfalls and promises for future drug development. *Biochemical pharmacology* **2006**, *72* (9), 1161–1179. DOI: 10.1016/j.bcp.2006.08.007.
- Delviks-Frankenberry, K. A., Desimmie, B. A.; Pathak, V. K. Structural Insights into APOBEC3-Mediated Lentiviral Restriction. *Viruses* **2020**, *12* (6). DOI: 10.3390/v12060587.
- DiDonato, J. A., Mercurio, F.; Karin, M. NF-κB and the link between inflammation and cancer. *Immunological reviews* **2012**, *246* (1), 379–400. DOI: 10.1111/j.1600-065X.2012.01099.x.
- Ding, Q., Chang, C.-J., Xie, X., Xia, W.; Yang, J.-Y., et al. APOBEC3G promotes liver metastasis in an orthotopic mouse model of colorectal cancer and predicts human hepatic metastasis. *The Journal of Clinical Investigation* **2011**, *121* (11), 4526–4536. DOI: 10.1172/JCI45008.
- Djordjević, G., Matusan-Ilijas, K., Sinozić, E., Damante, G.; Fabbro, D., et al. Relationship between vascular endothelial growth factor and nuclear factor-kappaB in renal cell tumors. *Croatian medical journal* **2008**, *49* (5), 608–617. DOI: 10.3325/cmj.2008.5.608.
- Dobashi, S., Katagiri, T., Hirota, E., Ashida, S.; Daigo, Y., et al. Involvement of TMEM22 overexpression in the growth of renal cell carcinoma cells. *Oncology Reports* **2009**, *21* (2), 305–312.
- Dobrzanski, P., Ryseck, R. P.; Bravo, R. Specific inhibition of RelB/p52 transcriptional activity by the C-terminal domain of p100. *Oncogene* **1995**, *10* (5), 1003–1007.
- Dolcet, X., Llobet, D., Pallares, J.; Matias-Guiu, X. NF-κB in development and progression of human cancer. *Virchows Archiv : an international journal of pathology* **2005**, *446* (5), 475–482. DOI: 10.1007/s00428-005-1264-9.
- Du, H.-F., Ou, L.-P., Song, X.-D., Fan, Y.-R.; Yang, X., et al. Nuclear factor-κB signaling pathway is involved in phospholipase Cε-regulated proliferation in human renal cell carcinoma cells. *Molecular and cellular biochemistry* **2014**, *389* (1-2), 265–275. DOI: 10.1007/s11010-013-1948-4.
- Du Shi, Zhang, Z.; Kong, C. CARMA3 Transcriptional Regulation of STMN1 by NF-κB Promotes Renal Cell Carcinoma Proliferation and Invasion. *Technology in cancer research & treatment* **2021**, *20*, 15330338211027915. DOI: 10.1177/15330338211027915.
- DuBridge, R. B., Tang, P., Hsia, H. C., Leong, P. M.; Miller, J. H., et al. Analysis of mutation in human cells by using an Epstein-Barr virus shuttle system. *Molecular and cellular biology* **1987**, *7* (1), 379–387. DOI: 10.1128/mcb.7.1.379-387.1987.
- Ebrahimi, D., Alinejad-Rokny, H.; Davenport, M. P. Insights into the motif preference of APOBEC3 enzymes. *PLoS one* **2014**, *9* (1), e87679. DOI: 10.1371/journal.pone.0087679.
- Erstad, D. J. and Cusack, J. C. Targeting the NF-κB pathway in cancer therapy. *Surgical oncology clinics of North America* **2013**, *22* (4), 705–746. DOI: 10.1016/j.soc.2013.06.011.

- Escudier, B., Bellmunt, J., Négrier, S., Bajetta, E.; Melichar, B., et al. Phase III trial of bevacizumab plus interferon alfa-2a in patients with metastatic renal cell carcinoma (AVOREN): final analysis of overall survival. *Journal of clinical oncology : official journal of the American Society of Clinical Oncology* **2010**, *28* (13), 2144–2150. DOI: 10.1200/JCO.2009.26.7849.
- Escudier, B., Eisen, T., Stadler, W. M., Szczylik, C.; Oudard, S., et al. Sorafenib for treatment of renal cell carcinoma: Final efficacy and safety results of the phase III treatment approaches in renal cancer global evaluation trial. *Journal of clinical oncology : official journal of the American Society of Clinical Oncology* **2009**, *27* (20), 3312–3318. DOI: 10.1200/JCO.2008.19.5511.
- Eulalio, A., Behm-Ansmant, I.; Izaurralde, E. P bodies: at the crossroads of post-transcriptional pathways. *Nature Reviews Molecular Cell Biology* **2007**, *8* (1), 9–22. DOI: 10.1038/nrm2080.
- Fanourakis, G., Kyrodimos, E., Papanikolaou, V., Chrysovergis, A.; Kafiri, G., et al. APOBEC3B Is Co-Expressed with PKC α /NF- κ B in Oral and Oropharyngeal Squamous Cell Carcinomas. *Diagnostics (Basel, Switzerland)* **2023**, *13* (3). DOI: 10.3390/diagnostics13030569.
- Feng, Y., Goubran, M. H., Follack, T. B.; Chelico, L. Deamination-independent restriction of LINE-1 retrotransposition by APOBEC3H. *Scientific Reports* **2017**, *7* (1), 10881. DOI: 10.1038/s41598-017-11344-4.
- Fouad, Y. A. and Aanei, C. Revisiting the hallmarks of cancer. *American journal of cancer research* **2017**, *7* (5), 1016–1036.
- Fraser, I. D. and Germain, R. N. Navigating the network: signaling cross-talk in hematopoietic cells. *Nature immunology* **2009**, *10* (4), 327–331. DOI: 10.1038/ni.1711.
- Fridman, W. H., Zitvogel, L., Sautès-Fridman, C.; Kroemer, G. The immune contexture in cancer prognosis and treatment. *Nature reviews. Clinical oncology* **2017**, *14* (12), 717–734. DOI: 10.1038/nrclinonc.2017.101.
- Friew, Y. N., Boyko, V., Hu, W.-S.; Pathak, V. K. Intracellular interactions between APOBEC3G, RNA, and HIV-1 Gag: APOBEC3G multimerization is dependent on its association with RNA. *Retrovirology* **2009**, *6*, 56. DOI: 10.1186/1742-4690-6-56.
- Gaestel, M., Kotlyarov, A.; Kracht, M. Targeting innate immunity protein kinase signalling in inflammation. *Nature reviews. Drug discovery* **2009**, *8* (6), 480–499. DOI: 10.1038/nrd2829.
- Gallois-Montbrun, S., Holmes, R. K., Swanson, C. M., Fernández-Ocaña, M.; Byers, H. L., et al. Comparison of Cellular Ribonucleoprotein Complexes Associated with the APOBEC3F and APOBEC3G Antiviral Proteins. *J. Virol.* [Online] **2008**, *82* (11), 5636–5642.
- Gallois-Montbrun, S., Kramer, B., Swanson, C. M., Byers, H.; Lynham, S., et al. Antiviral Protein APOBEC3G Localizes to Ribonucleoprotein Complexes Found in P Bodies and Stress Granules. *J. Virol.* [Online] **2007**, *81* (5), 2165–2178.
- Georgakopoulos-Soares, I., Parada, G. E.; Hemberg, M. Secondary structures in RNA synthesis, splicing and translation. *Computational and structural biotechnology journal* **2022**, *20*, 2871–2884. DOI: 10.1016/j.csbj.2022.05.041.
- Gerlinger, M., Rowan, A. J., Horswell, S., Larkin, J.; Endesfelder, D., et al. Intratumor Heterogeneity and Branched Evolution Revealed by Multiregion Sequencing. *New England Journal of Medicine* **2012**, *366* (10), 883–892. DOI: 10.1056/NEJMoa1113205.
- Gerstberger, S., Hafner, M.; Tuschl, T. A census of human RNA-binding proteins. *Nature reviews. Genetics* **2014**, *15* (12), 829–845. DOI: 10.1038/nrg3813.
- Ghatalia, P., Yang, E. S., Lasseigne, B. N., Ramaker, R. C.; Cooper, S. J., et al. Kinase Gene Expression Profiling of Metastatic Clear Cell Renal Cell Carcinoma Tissue

- Identifies Potential New Therapeutic Targets. *PloS one* **2016**, *11* (8), e0160924. DOI: 10.1371/journal.pone.0160924.
- Ghosh, S. and Dass, J. F. Study of pathway cross-talk interactions with NF- κ B leading to its activation via ubiquitination or phosphorylation: A brief review. *Gene* **2016**, *584* (1), 97–109. DOI: 10.1016/j.gene.2016.03.008.
- Gilmore, T. D. NF- κ B, KBF1, dorsal, and related matters. *Cell* **1990**, *62* (5), 841–843. DOI: 10.1016/0092-8674(90)90257-f.
- Gilmore, T. D. The Rel1/NF- κ B/I κ B signal transduction pathway and cancer. *Cancer treatment and research* **2003**, *115*, 241–265.
- Gilmore, T. D. Introduction to NF- κ B: players, pathways, perspectives. *Oncogene* **2006**, *25* (51), 6680–6684. DOI: 10.1038/sj.onc.1209954.
- Giraldo, N. A., Becht, E., Vano, Y., Petitprez, F.; Lacroix, L., et al. Tumor-Infiltrating and Peripheral Blood T-cell Immunophenotypes Predict Early Relapse in Localized Clear Cell Renal Cell Carcinoma. *Clin Cancer Res* **2017**, *23* (15), 4416–4428. DOI: 10.1158/1078-0432.CCR-16-2848.
- Görlich, D. and Kutay, U. Transport between the cell nucleus and the cytoplasm. *Annual review of cell and developmental biology* [Online] **1999**, *15*, 607–660.
- Gowrishankar, B., Ibragimova, I., Zhou, Y., Slifker, M. J.; Devarajan, K., et al. MicroRNA expression signatures of stage, grade, and progression in clear cell RCC. *Cancer biology & therapy* **2014**, *15* (3), 329–341. DOI: 10.4161/cbt.27314.
- Graham, F. L., Smiley, J., Russell, W. C.; Nairn, R. Characteristics of a human cell line transformed by DNA from human adenovirus type 5. *The Journal of general virology* **1977**, *36* (1), 59–74. DOI: 10.1099/0022-1317-36-1-59.
- Granadillo Rodríguez, M., Flath, B.; Chelico, L. The interesting relationship between APOBEC3 deoxycytidine deaminases and cancer: a long road ahead. *Open biology* **2020**, *10* (12), 200188. DOI: 10.1098/rsob.200188.
- Gu, W., Katz, Z., Wu, B., Park, H. Y.; Li, D., et al. Regulation of local expression of cell adhesion and motility-related mRNAs in breast cancer cells by IMP1/ZBP1. *Journal of cell science* **2012**, *125* (Pt 1), 81–91. DOI: 10.1242/jcs.086132.
- Gu, W., Pan, F.; Singer, R. H. Blocking beta-catenin binding to the ZBP1 promoter represses ZBP1 expression, leading to increased proliferation and migration of metastatic breast-cancer cells. *Journal of cell science* **2009**, *122* (Pt 11), 1895–1905. DOI: 10.1242/jcs.045278.
- Gu, W., Wells, A. L., Pan, F.; Singer, R. H. Feedback regulation between zipcode binding protein 1 and beta-catenin mRNAs in breast cancer cells. *Molecular and cellular biology* **2008**, *28* (16), 4963–4974. DOI: 10.1128/MCB.00266-08.
- Guan, C., Zhou, X., Li, H., Ma, X.; Zhuang, J. NF- κ B inhibitors gifted by nature: The anticancer promise of polyphenol compounds. *Biomedicine & pharmacotherapy = Biomedecine & pharmacotherapie* **2022**, *156*, 113951. DOI: 10.1016/j.biopha.2022.113951.
- Guan, X., Chen, S., Liu, Y., Wang, L.-L.; Zhao, Y., et al. PUM1 promotes ovarian cancer proliferation, migration and invasion. *Biochemical and Biophysical Research Communications* **2018**, *497* (1), 313–318. DOI: 10.1016/j.bbrc.2018.02.078.
- Guo, H., Zhu, L., Huang, L., Sun, Z.; Zhang, H., et al. APOBEC Alteration Contributes to Tumor Growth and Immune Escape in Pan-Cancer. *Cancers* **2022**, *14* (12). DOI: 10.3390/cancers14122827.
- Gutschner, T., Hämmerle, M., Pazaitis, N., Bley, N.; Fiskin, E., et al. Insulin-like growth factor 2 mRNA-binding protein 1 (IGF2BP1) is an important protumorigenic factor in hepatocellular carcinoma. *Hepatology (Baltimore, Md.)* **2014**, *59* (5), 1900–1911. DOI: 10.1002/hep.26997.

- Haché, G., Mansky, L. M.; Harris, R. S. Human APOBEC3 proteins, retrovirus restriction, and HIV drug resistance. *AIDS reviews* **2006**, *8* (3), 148–157.
- Hakata, Y. and Miyazawa, M. Deaminase-Independent Mode of Antiretroviral Action in Human and Mouse APOBEC3 Proteins. *Microorganisms* **2020**, *8* (12). DOI: 10.3390/microorganisms8121976.
- Hamilton, K. E., Chatterji, P., Lundsmith, E. T., Andres, S. F.; Giroux, V., et al. Loss of Stromal IMP1 Promotes a Tumorigenic Microenvironment in the Colon. *Molecular cancer research : MCR* **2015**, *13* (11), 1478–1486. DOI: 10.1158/1541-7786.MCR-15-0224.
- Hammers, H., Plimack, E. R., Infante, J. R., Rini, B. I.; McDermott, D., et al. Updated results from a phase I study of nivolumab (Nivo) in combination with ipilimumab (Ipi) in metastatic renal cell carcinoma (mRCC): The CheckMate 016 study. *Annals of Oncology* **2016**, *27*, vi364. DOI: 10.1093/annonc/mdw378.16.
- Hancock, S. B. and Georgiades, C. S. Kidney Cancer. *Cancer journal (Sudbury, Mass.)* **2016**, *22* (6), 387–392. DOI: 10.1097/PPO.0000000000000225.
- Handschick, K., Beuerlein, K., Jurida, L., Bartkuhn, M.; Müller, H., et al. Cyclin-dependent kinase 6 is a chromatin-bound cofactor for NF- κ B-dependent gene expression. *Molecular cell* **2014**, *53* (2), 193–208. DOI: 10.1016/j.molcel.2013.12.002.
- Harris, R. S., Bishop, K. N., Sheehy, A. M., Craig, H. M.; Petersen-Mahrt, S. K., et al. DNA deamination mediates innate immunity to retroviral infection. *Cell* **2003**, *113* (6), 803–809. DOI: 10.1016/s0092-8674(03)00423-9.
- Harris, R. S. and Dudley, J. P. APOBECs and virus restriction. *Virology* **2015**, *479-480*, 131–145. DOI: 10.1016/j.virol.2015.03.012.
- Harris, R. S., Petersen-Mahrt, S. K.; Neuberger, M. S. RNA Editing Enzyme APOBEC1 and Some of Its Homologs Can Act as DNA Mutators. *Molecular cell* **2002**, *10* (5), 1247–1253.
- Häsler, J. and Strub, K. Alu elements as regulators of gene expression. *Nucleic Acids Res* **2006**, *34* (19), 5491–5497. DOI: 10.1093/nar/gkl706.
- Hayden, M. S. and Ghosh, S. Shared principles in NF-kappaB signaling. *Cell* **2008**, *132* (3), 344–362. DOI: 10.1016/j.cell.2008.01.020.
- Heinzelmann, J., Henning, B., Sanjmyatav, J., Posorski, N.; Steiner, T., et al. Specific miRNA signatures are associated with metastasis and poor prognosis in clear cell renal cell carcinoma. *World journal of urology* **2011**, *29* (3), 367–373. DOI: 10.1007/s00345-010-0633-4.
- Henderson, S. and Fenton, T. APOBEC3 genes: retroviral restriction factors to cancer drivers. *Trends in molecular medicine* **2015**, *21* (5), 274–284. DOI: 10.1016/j.molmed.2015.02.007.
- Henry, K. L., Kellner, D., Bajrami, B., Anderson, J. E.; Beyna, M., et al. CDK12-mediated transcriptional regulation of noncanonical NF- κ B components is essential for signaling. *Science signaling* **2018**, *11* (541). DOI: 10.1126/scisignal.aam8216.
- Hockel, M. Biological consequences of tumor hypoxia. *Seminars in Oncology* **2001**, *28*, 36–41. DOI: 10.1016/S0093-7754(01)90211-8.
- Hoesel, B. and Schmid, J. A. The complexity of NF- κ B signaling in inflammation and cancer. *Molecular Cancer* **2013**, *12*, 86. DOI: 10.1186/1476-4598-12-86.
- Hoffmann, A., Natoli, G.; Ghosh, G. Transcriptional regulation via the NF-kappaB signaling module. *Oncogene* **2006**, *25* (51), 6706–6716. DOI: 10.1038/sj.onc.1209933.
- Holden, L. G., Prochnow, C., Chang, Y. P., Bransteitter, R.; Chelico, L., et al. Crystal structure of the anti-viral APOBEC3G catalytic domain and functional implications. *Nature* **2008**, *456* (7218), 121–124. DOI: 10.1038/nature07357.

- Holmes, R. K., Koning, F. A., Bishop, K. N.; Malim, M. H. APOBEC3F can inhibit the accumulation of HIV-1 reverse transcription products in the absence of hypermutation. Comparisons with APOBEC3G. *The Journal of biological chemistry* **2007a**, *282* (4), 2587–2595. DOI: 10.1074/jbc.M607298200.
- Holmes, R. K., Malim, M. H.; Bishop, K. N. APOBEC-mediated viral restriction: not simply editing? *Trends in Biochemical Sciences* **2007b**, *32* (3), 118–128. DOI: 10.1016/j.tibs.2007.01.004.
- Hong, S. Y., Yoon, W. H., Park, J. H., Kang, S. G.; Ahn, J. H., et al. Involvement of two NF-kappa B binding elements in tumor necrosis factor alpha -, CD40-, and epstein-barr virus latent membrane protein 1-mediated induction of the cellular inhibitor of apoptosis protein 2 gene. *The Journal of biological chemistry* **2000**, *275* (24), 18022–18028. DOI: 10.1074/jbc.M001202200.
- Hoopes, J. I., Cortez, L. M., Mertz, T. M., Malc, E. P.; Mieczkowski, P. A., et al. APOBEC3A and APOBEC3B Preferentially Deaminate the Lagging Strand Template during DNA Replication. *Cell Reports* **2016**, *14* (6), 1273–1282. DOI: 10.1016/j.celrep.2016.01.021.
- Horn, A. V., Klawitter, S., Held, U., Berger, A.; Jaguva Vasudevan, A. A., et al. Human LINE-1 restriction by APOBEC3C is deaminase independent and mediated by an ORF1p interaction that affects LINE reverse transcriptase activity. *Nucleic Acids Res [Online]* **2014**, *42* (1), 396–416.
- Hsieh, A. C. and Ruggero, D. Targeting eukaryotic translation initiation factor 4E (eIF4E) in cancer. *Clin Cancer Res* **2010**, *16* (20), 4914–4920. DOI: 10.1158/1078-0432.CCR-10-0433.
- Hsieh, J. J., Le, V. H., Oyama, T., Ricketts, C. J.; Ho, T. H., et al. Chromosome 3p Loss-Orchestrated VHL, HIF, and Epigenetic Deregulation in Clear Cell Renal Cell Carcinoma. *Journal of clinical oncology : official journal of the American Society of Clinical Oncology* **2018**, *36* (36), JCO2018792549. DOI: 10.1200/JCO.2018.79.2549.
- Hsieh, J. J., Purdue, M. P., Signoretti, S., Swanton, C.; Albiges, L., et al. Renal cell carcinoma. *Nature Reviews Disease Primers [Online]* **2017**, *3*, nrdp20179.
- Hua, X., Chen, J., Ge, S., Xiao, H.; Zhang, L., et al. Integrated analysis of the functions of RNA binding proteins in clear cell renal cell carcinoma. *Genomics* **2021**, *113* (1 Pt 2), 850–860. DOI: 10.1016/j.ygeno.2020.10.016.
- Huang, A., Fone, P. D., Gandour-Edwards, R., White, R. W.; Low, R. K. Immunohistochemical analysis of BCL-2 protein expression in renal cell carcinoma. *The Journal of urology* **1999**, *162* (2), 610–613.
- Huang, D.-B., Vu, D.; Ghosh, G. NF-kappaB RelB forms an intertwined homodimer. *Structure (London, England : 1993)* **2005**, *13* (9), 1365–1373. DOI: 10.1016/j.str.2005.06.018.
- Huang, J., Liang, Z., Yang, B., Tian, H.; Ma, J., et al. Derepression of microRNA-mediated protein translation inhibition by apolipoprotein B mRNA-editing enzyme catalytic polypeptide-like 3G (APOBEC3G) and its family members. *The Journal of biological chemistry* **2007**, *282* (46), 33632–33640. DOI: 10.1074/jbc.M705116200.
- Hultquist, J. F., Lengyel, J. A., Refsland, E. W., LaRue, R. S.; Lackey, L., et al. Human and rhesus APOBEC3D, APOBEC3F, APOBEC3G, and APOBEC3H demonstrate a conserved capacity to restrict Vif-deficient HIV-1. *J. Virol.* **2011**, *85* (21), 11220–11234. DOI: 10.1128/jvi.05238-11.
- Hwang, J. K., Alt, F. W.; Yeap, L.-S. Related Mechanisms of Antibody Somatic Hypermutation and Class Switch Recombination. In *Mobile DNA III*; Craig, N. L., Chandler, M., Gellert, M., Lambowitz, A. M., Rice, P. A., Sandmeyer, S. B., Eds.; ASM Press: Washington, DC, USA, 2015; pp 325–348. DOI: 10.1128/9781555819217.ch15.

- Ioannidis, P., Mahaira, L., Papadopoulou, A., Teixeira, M. R.; Heim, S., et al. 8q24 Copy number gains and expression of the c-myc mRNA stabilizing protein CRD-BP in primary breast carcinomas. *International Journal of Cancer* **2003**, *104* (1), 54–59. DOI: 10.1002/ijc.10794;
- Ito, F., Fu, Y., Kao, S.-C. A., Yang, H.; Chen, X. S. Family-Wide Comparative Analysis of Cytidine and Methylcytosine Deamination by Eleven Human APOBEC Proteins. *Journal of molecular biology* **2017**, *429* (12), 1787–1799. DOI: 10.1016/j.jmb.2017.04.021.
- Izuishi, K., Kato, K., Ogura, T., Kinoshita, T.; Esumi, H. Remarkable tolerance of tumor cells to nutrient deprivation: possible new biochemical target for cancer therapy. *Cancer Res* **2000**, *60* (21), 6201–6207.
- Jacobs, E., Mills, J. D.; Janitz, M. The role of RNA structure in posttranscriptional regulation of gene expression. *Journal of genetics and genomics = Yi chuan xue bao* **2012**, *39* (10), 535–543. DOI: 10.1016/j.jgg.2012.08.002.
- Jaguva Vasudevan, A. A., Balakrishnan, K., Gertzen, C. G., Borvetó, F.; Zhang, Z., et al. Loop 1 of APOBEC3C Regulates its Antiviral Activity against HIV-1. *Journal of molecular biology* **2020**, *432* (23), 6200–6227. DOI: 10.1016/j.jmb.2020.10.014.
- Jalili, P., Bowen, D., Langenbucher, A., Park, S.; Aguirre, K., et al. Quantification of ongoing APOBEC3A activity in tumor cells by monitoring RNA editing at hotspots. *Nat Commun* **2020**, *11* (1), 2971. DOI: 10.1038/s41467-020-16802-8.
- Jamal-Hanjani, M., Wilson, G. A., McGranahan, N., Birkbak, N. J.; Watkins, T. B., et al. Tracking the Evolution of Non-Small-Cell Lung Cancer. *The New England journal of medicine* **2017**, *376* (22), 2109–2121. DOI: 10.1056/NEJMoa1616288.
- Jarmuz, A., Chester, A., Bayliss, J., Gisbourne, J.; Dunham, I., et al. An anthropoid-specific locus of orphan C to U RNA-editing enzymes on chromosome 22. *Genomics* **2002**, *79* (3), 285–296. DOI: 10.1006/geno.2002.6718.
- Jarvis, M. C., Ebrahimi, D., Temiz, N. A.; Harris, R. S. Mutation Signatures Including APOBEC in Cancer Cell Lines. *JNCI cancer spectrum* **2018**, *2* (1). DOI: 10.1093/jncics/pky002.
- Jennings, P., Weiland, C., Limonciel, A., Bloch, K. M.; Radford, R., et al. Transcriptomic alterations induced by Ochratoxin A in rat and human renal proximal tubular in vitro models and comparison to a rat in vivo model. *Archives of toxicology* **2012**, *86* (4), 571–589. DOI: 10.1007/s00204-011-0780-4.
- Jeon, K. I., Jeong, J. Y.; Jue, D. M. Thiol-reactive metal compounds inhibit NF-kappa B activation by blocking I kappa B kinase. *Journal of immunology (Baltimore, Md. : 1950)* **2000**, *164* (11), 5981–5989. DOI: 10.4049/jimmunol.164.11.5981.
- Ji, F., Liu, X., Zhang, Y., Liu, E.; Wen, J. *Construction of an Immune-related Gene Model for Predicting Prognosis and Immune Infiltration in Clear Cell Renal Cell Carcinoma*, 2022.
- Jia, X., Wei, S.; Xiong, W. CXCL5/NF-κB Pathway as a Therapeutic Target in Hepatocellular Carcinoma Treatment. *Journal of oncology* **2021**, *2021*, 9919494. DOI: 10.1155/2021/9919494.
- Jønson, L., Vikesaa, J., Krogh, A., Nielsen, L. K.; Hansen, T. v., et al. Molecular composition of IMP1 ribonucleoprotein granules. *Molecular & cellular proteomics : MCP* **2007**, *6* (5), 798–811. DOI: 10.1074/mcp.M600346-MCP200;
- Kalantzakos, T. J., Sebel, L. E., Trussler, J., Sullivan, T. B.; Burks, E. J., et al. MicroRNA Associated with the Invasive Phenotype in Clear Cell Renal Cell Carcinoma: Let-7c-5p Inhibits Proliferation, Migration, and Invasion by Targeting Insulin-like Growth Factor 1 Receptor. *Biomedicines* **2022**, *10* (10). DOI: 10.3390/biomedicines10102425.
- Kaltschmidt, B., Greiner, J. F., Kadhim, H. M.; Kaltschmidt, C. Subunit-Specific Role of NF-κB in Cancer. *Biomedicines* **2018**, *6* (2). DOI: 10.3390/biomedicines6020044.

- Kammerer-Jacquet, S.-F., Brunot, A., Pladys, A., Bouzille, G.; Dagher, J., et al. Synchronous Metastatic Clear-Cell Renal Cell Carcinoma: A Distinct Morphologic, Immunohistochemical, and Molecular Phenotype. *Clinical genitourinary cancer* **2017**, *15* (1), e1-e7. DOI: 10.1016/j.clgc.2016.06.007.
- Kane, R. C., Farrell, A. T., Saber, H., Tang, S.; Williams, G., et al. Sorafenib for the treatment of advanced renal cell carcinoma. *Clinical cancer research : an official journal of the American Association for Cancer Research* **2006**, *12* (24), 7271–7278. DOI: 10.1158/1078-0432.CCR-06-1249;
- Kang, D., Lee, Y.; Lee, J.-S. RNA-Binding Proteins in Cancer: Functional and Therapeutic Perspectives. *Cancers* **2020**, *12* (9). DOI: 10.3390/cancers12092699.
- Kaplanski, G. Interleukin-18: Biological properties and role in disease pathogenesis. *Immunological reviews* **2018**, *281* (1), 138–153. DOI: 10.1111/imr.12616.
- Karabulut, S. and Leszczynski, J. Molecular structure of aurothioglucose: a comprehensive computational study. *Tetrahedron* **2015**, *71* (12), 1815–1821. DOI: 10.1016/j.tet.2015.02.007.
- Karin, M. The beginning of the end: I κ B kinase (IKK) and NF- κ B activation. *The Journal of biological chemistry* **1999**, *274* (39), 27339–27342. DOI: 10.1074/jbc.274.39.27339.
- Karin, M. and Ben-Neriah, Y. Phosphorylation meets ubiquitination: the control of NF- κ B activity. *Annual review of immunology* **2000**, *18*, 621–663. DOI: 10.1146/annurev.immunol.18.1.621.
- Karin, M., Cao, Y., Greten, F. R.; Li, Z.-W. NF- κ B in cancer: from innocent bystander to major culprit. *Nature reviews. Cancer* **2002**, *2* (4), 301–310. DOI: 10.1038/nrc780.
- Kazazian, H. H., Wong, C., Youssoufian, H., Scott, A. F.; Phillips, D. G., et al. Haemophilia A resulting from de novo insertion of L1 sequences represents a novel mechanism for mutation in man. *Nature* **1988**, *332* (6160), 164–166. DOI: 10.1038/332164a0.
- Kechavarzi, B. and Janga, S. C. Dissecting the expression landscape of RNA-binding proteins in human cancers. *Genome Biol* **2014**, *15* (1), R14. DOI: 10.1186/gb-2014-15-1-r14.
- Kedde, M., van Kouwenhove, M., Zwart, W., Oude Vrielink, J. A.; Elkon, R., et al. A Pumilio-induced RNA structure switch in p27-3' UTR controls miR-221 and miR-222 accessibility. *Nature cell biology* **2010**, *12* (10), 1014–1020. DOI: 10.1038/ncb2105.
- Kedersha, N. L., Gupta, M., Li, W., Miller, I.; Anderson, P. RNA-binding proteins TIA-1 and TIAR link the phosphorylation of eIF-2 alpha to the assembly of mammalian stress granules. *The Journal of cell biology* **1999**, *147* (7), 1431–1442. DOI: 10.1083/jcb.147.7.1431.
- Keene, J. D. RNA regulons: coordination of post-transcriptional events. *Nature reviews. Genetics* **2007**, *8* (7), 533–543. DOI: 10.1038/nrg2111.
- Keisner, S. V. and Shah, S. R. Pazopanib: the newest tyrosine kinase inhibitor for the treatment of advanced or metastatic renal cell carcinoma. *Drugs* **2011**, *71* (4), 443–454. DOI: 10.2165/11588960-000000000-00000.
- Keith, B. and Simon, M. C. Hypoxia-inducible factors, stem cells, and cancer. *Cell* **2007**, *129* (3), 465–472. DOI: 10.1016/j.cell.2007.04.019.
- Kim, D., Langmead, B.; Salzberg, S. L. HISAT: a fast spliced aligner with low memory requirements. *Nature methods* **2015**, *12* (4), 357–360. DOI: 10.1038/nmeth.3317.
- Kim, D. D., Kim, T. T., Walsh, T., Kobayashi, Y.; Matisse, T. C., et al. Widespread RNA editing of embedded alu elements in the human transcriptome. *Genome Res.* **2004**, *14* (9), 1719–1725. DOI: 10.1101/gr.2855504.

- Kim, H. H., Abdelmohsen, K., Lal, A., Pullmann, R.; Yang, X., et al. Nuclear HuR accumulation through phosphorylation by Cdk1. *Genes & development* **2008**, *22* (13), 1804–1815. DOI: 10.1101/gad.1645808.
- Kim, M. Y., Hur, J.; Jeong, S. Emerging roles of RNA and RNA-binding protein network in cancer cells. *BMB reports* **2009**, *42* (3), 125–130. DOI: 10.5483/bmbrep.2009.42.3.125.
- Kim, M.-C., Jin, Z., Kolb, R., Borchering, N.; Chatzkel, J. A., et al. Updates on Immunotherapy and Immune Landscape in Renal Clear Cell Carcinoma. *Cancers* **2021**, *13* (22). DOI: 10.3390/cancers13225856.
- Kimmelman, A. C. and White, E. Autophagy and Tumor Metabolism. *Cell metabolism* **2017**, *25* (5), 1037–1043. DOI: 10.1016/j.cmet.2017.04.004.
- Kinomoto, M., Kanno, T., Shimura, M., Ishizaka, Y.; Kojima, A., et al. All APOBEC3 family proteins differentially inhibit LINE-1 retrotransposition. *Nucleic Acids Res* **2007**, *35* (9), 2955–2964. DOI: 10.1093/nar/gkm181.
- Kitamura, S., Ode, H.; Iwatani, Y. Structural Features of Antiviral APOBEC3 Proteins are Linked to Their Functional Activities. *Front. Microbiol.* [Online] **2011**, *2*, 258.
- Knisbacher, B. A., Gerber, D.; Levanon, E. Y. DNA Editing by APOBECs: A Genomic Preserver and Transformer. *Trends in Genetics* [Online] **2016**, *32* (1), 16–28.
- Köbel, M., Weidensdorfer, D., Reinke, C., Lederer, M.; Schmitt, W. D., et al. Expression of the RNA-binding protein IMP1 correlates with poor prognosis in ovarian carcinoma. *Oncogene* **2007**, *26* (54), 7584–7589. DOI: 10.1038/sj.onc.1210563;
- Kohn, M., Pazaitis, N.; Huttelmaier, S. Why YRNAs? About Versatile RNAs and Their Functions. *Biomolecules* **2013**, *3* (1), 143–156. DOI: 10.3390/biom3010143.
- Koito, A. and Ikeda, T. Apolipoprotein B mRNA-editing, catalytic polypeptide cytidine deaminases and retroviral restriction. *Wiley Interdisciplinary Reviews: RNA* **2012**, *3* (4), 529–541. DOI: 10.1002/wrna.1117.
- Koning, F. A., Newman, E. N., Kim, E.-Y., Kunstman, K. J.; Wolinsky, S. M., et al. Defining APOBEC3 expression patterns in human tissues and hematopoietic cell subsets. *J. Virol.* **2009**, *83* (18), 9474–9485. DOI: 10.1128/jvi.01089-09.
- Korus, M., Mahon, G. M., Cheng, L.; Whitehead, I. P. p38 MAPK-mediated activation of NF-kappaB by the RhoGEF domain of Bcr. *Oncogene* **2002**, *21* (30), 4601–4612. DOI: 10.1038/sj.onc.1205678.
- Koul, H. K., Pal, M.; Koul, S. Role of p38 MAP Kinase Signal Transduction in Solid Tumors. *Genes & cancer* **2013**, *4* (9-10), 342–359. DOI: 10.1177/1947601913507951.
- Kovacs, G. and Frisch, S. Clonal chromosome abnormalities in tumor cells from patients with sporadic renal cell carcinomas. *Cancer Res* **1989**, *49* (3), 651–659.
- Kozak, S. L., Marin, M., Rose, K. M., Bystrom, C.; Kabat, D. The Anti-HIV-1 Editing Enzyme APOBEC3G Binds HIV-1 RNA and Messenger RNAs That Shuttle between Polysomes and Stress Granules. *J. Biol. Chem.* [Online] **2006**, *281* (39), 29105–29119.
- Krützfeldt, J., Rajewsky, N., Braich, R., Rajeev, K. G.; Tuschl, T., et al. Silencing of microRNAs in vivo with 'antagomirs'. *Nature* **2005**, *438* (7068), 685–689. DOI: 10.1038/nature04303.
- Kvach, M. V., Barzak, F. M., Harjes, S., Schares, H. A.; Kurup, H. M., et al. Differential Inhibition of APOBEC3 DNA - Mutator Isozymes by Fluoro - and Non - Fluoro - Substituted 2' - Deoxyzebularine Embedded in Single - Stranded DNA. *Chembiochem* **2019**, *21* (7), 1028–1035. DOI: 10.1002/cbic.201900505.
- Lackey, L., Law, E. K., Brown, W. L.; Harris, R. S. Subcellular localization of the APOBEC3 proteins during mitosis and implications for genomic DNA deamination. *Cell cycle (Georgetown, Tex.)* **2013**, *12* (5), 762–772. DOI: 10.4161/cc.23713.

- Lai, Y., Zhao, Z., Zeng, T., Liang, X.; Chen, D., et al. Crosstalk between VEGFR and other receptor tyrosine kinases for TKI therapy of metastatic renal cell carcinoma. *Cancer cell international* **2018**, *18*, 31. DOI: 10.1186/s12935-018-0530-2.
- Lander, E. S., Linton, L. M., Birren, B., Nusbaum, C.; Zody, M. C., et al. Initial sequencing and analysis of the human genome. *Nature* **2001**, *409* (6822), 860–921. DOI: 10.1038/35057062.
- Langlois, M.-A., Beale, R. C., Conticello, S. G.; Neuberger, M. S. Mutational comparison of the single-domained APOBEC3C and double-domained APOBEC3F/G anti-retroviral cytidine deaminases provides insight into their DNA target site specificities. *Nucleic Acids Res* **2005**, *33* (6), 1913–1923. DOI: 10.1093/nar/gki343.
- Lee, J., Rhee, M. H., Kim, E.; Cho, J. Y. BAY 11-7082 is a broad-spectrum inhibitor with anti-inflammatory activity against multiple targets. *Mediators of inflammation* **2012**, *2012*, 416036. DOI: 10.1155/2012/416036.
- Lee-Felker, S. A., Felker, E. R., Tan, N., Margolis, D. J.; Young, J. R., et al. Qualitative and quantitative MDCT features for differentiating clear cell renal cell carcinoma from other solid renal cortical masses. *AJR. American journal of roentgenology* **2014**, *203* (5), W516-24. DOI: 10.2214/AJR.14.12460.
- Lellek, H., Kirsten, R., Diehl, I., Apostel, F.; Buck, F., et al. Purification and molecular cloning of a novel essential component of the apolipoprotein B mRNA editing enzyme-complex. *The Journal of biological chemistry* **2000**, *275* (26), 19848–19856. DOI: 10.1074/jbc.M001786200.
- Lenardo, M. J. and Baltimore, D. NF-kappa B: a pleiotropic mediator of inducible and tissue-specific gene control. *Cell* **1989**, *58* (2), 227–229. DOI: 10.1016/0092-8674(89)90833-7.
- Leonard, B., McCann, J. L., Starrett, G. J., Kosyakovsky, L.; Luengas, E. M., et al. The PKC/NF- κ B signaling pathway induces APOBEC3B expression in multiple human cancers. *Cancer Res* **2015**, *75* (21), 4538–4547. DOI: 10.1158/0008-5472.CAN-15-2171-T.
- Levanon, E. Y., Eisenberg, E., Yelin, R., Nemzer, S.; Hallegger, M., et al. Systematic identification of abundant A-to-I editing sites in the human transcriptome. *Nature Biotechnology* **2004**, *22* (8), 1001–1005. DOI: 10.1038/nbt996.
- Li, F., Aljahdali, I. A., Zhang, R., Nastiuk, K. L.; Krolewski, J. J., et al. Kidney cancer biomarkers and targets for therapeutics: survivin (BIRC5), XIAP, MCL-1, HIF1 α , HIF2 α , NRF2, MDM2, MDM4, p53, KRAS and AKT in renal cell carcinoma. *Journal of experimental & clinical cancer research : CR* **2021**, *40* (1), 254. DOI: 10.1186/s13046-021-02026-1.
- Li, J., Chen, Y., Li, M., Carpenter, M. A.; McDougale, R. M., et al. APOBEC3 multimerization correlates with HIV-1 packaging and restriction activity in living cells. *Journal of molecular biology* **2014**, *426* (6), 1296–1307. DOI: 10.1016/j.jmb.2013.12.014.
- Li, M., Shandilya, S. M., Carpenter, M. A., Rathore, A.; Brown, W. L., et al. First-in-class small molecule inhibitors of the single-strand DNA cytosine deaminase APOBEC3G. *ACS chemical biology* **2012**, *7* (3), 506–517. DOI: 10.1021/cb200440y.
- Lian, H., Yang, L., Cole, A., Sun, L.; Chiang, A. C.-A., et al. NF κ B-activated astroglial release of complement C3 compromises neuronal morphology and function associated with Alzheimer's disease. *Neuron* **2015**, *85* (1), 101–115. DOI: 10.1016/j.neuron.2014.11.018.
- Liang, C., Zhang, M.; Sun, S.-C. beta-TrCP binding and processing of NF-kappaB2/p100 involve its phosphorylation at serines 866 and 870. *Cellular signalling* **2006**, *18* (8), 1309–1317. DOI: 10.1016/j.cellsig.2005.10.011.

- Liao, G., Zhang, M., Harhaj, E. W.; Sun, S.-C. Regulation of the NF-kappaB-inducing kinase by tumor necrosis factor receptor-associated factor 3-induced degradation. *The Journal of biological chemistry* **2004**, *279* (25), 26243–26250. DOI: 10.1074/jbc.M403286200.
- Liao, Y., Smyth, G. K.; Shi, W. featureCounts: an efficient general purpose program for assigning sequence reads to genomic features. *Bioinformatics (Oxford, England)* **2014**, *30* (7), 923–930. DOI: 10.1093/bioinformatics/btt656.
- Liberzon, A., Birger, C., Thorvaldsdóttir, H., Ghandi, M.; Mesirov, J. P., et al. The Molecular Signatures Database (MSigDB) hallmark gene set collection. *Cell systems* **2015**, *1* (6), 417–425. DOI: 10.1016/j.cels.2015.12.004.
- Liddament, M. T., Brown, W. L., Schumacher, A. J.; Harris, R. S. APOBEC3F properties and hypermutation preferences indicate activity against HIV-1 in vivo. *Current Biology* **2004**, *14* (15), 1385–1391. DOI: 10.1016/j.cub.2004.06.050.
- Linehan, W. M., Srinivasan, R.; Schmidt, L. S. The genetic basis of kidney cancer: a metabolic disease. *Nature reviews. Urology* **2010**, *7* (5), 277–285. DOI: 10.1038/nrurol.2010.47.
- Linehan, W. M. and Zbar, B. Focus on kidney cancer. *Cancer cell* **2004**, *6* (3), 223–228. DOI: 10.1016/j.ccr.2004.09.006.
- Liptay, S., Schmid, R. M., Nabel, E. G.; Nabel, G. J. Transcriptional regulation of NF-kappa B2: evidence for kappa B-mediated positive and negative autoregulation. *Molecular and cellular biology* **1994**, *14* (12), 7695–7703. DOI: 10.1128/mcb.14.12.7695-7703.1994.
- Liu, C., Zhang, X., Huang, F., Yang, B.; Li, J., et al. APOBEC3G inhibits microRNA-mediated repression of translation by interfering with the interaction between Argonaute-2 and MOV10. *J. Biol. Chem.* **2012a**, *287* (35), 29373–29383. DOI: 10.1074/jbc.M112.354001.
- Liu, J., Valencia-Sanchez, M. A., Hannon, G. J.; Parker, R. MicroRNA-dependent localization of targeted mRNAs to mammalian P-bodies. *Nature cell biology* **2005**, *7* (7), 719–723. DOI: 10.1038/ncb1274.
- Liu, M.-Q., Zhou, D.-J., Wang, X., Zhou, W.; Ye, L., et al. IFN-λ3 inhibits HIV infection of macrophages through the JAK-STAT pathway. *PloS one* **2012b**, *7* (4), e35902. DOI: 10.1371/journal.pone.0035902.
- Liu, Y., Yin, B., Zhang, C., Zhou, L.; Fan, J. Hsa-let-7a functions as a tumor suppressor in renal cell carcinoma cell lines by targeting c-myc. *Biochemical and Biophysical Research Communications* **2012c**, *417* (1), 371–375. DOI: 10.1016/j.bbrc.2011.11.119.
- Livak, K. J. and Schmittgen, T. D. Analysis of relative gene expression data using real-time quantitative PCR and the 2(-Delta Delta C(T)) Method. *Post-transcriptional RNA Modification Methods* **2001**, *25* (4), 402–408. DOI: 10.1006/meth.2001.1262.
- Ljungberg, B., Albiges, L., Abu-Ghanem, Y., Bedke, J.; Capitanio, U., et al. European Association of Urology Guidelines on Renal Cell Carcinoma: The 2022 Update. *European Urology* **2022**, *82* (4), 399–410. DOI: 10.1016/j.eururo.2022.03.006.
- Ljungberg, B., Campbell, S. C., Cho, H. Y., Jacqmin, D.; Lee, J. E., et al. The Epidemiology of Renal Cell Carcinoma. *European Urology [Online]* **2011**, *60* (4), 615–621.
- Low, G., Huang, G., Fu, W., Moloo, Z.; Girgis, S. Review of renal cell carcinoma and its common subtypes in radiology. *World Journal of Radiology* **2016**, *8* (5), 484–500. DOI: 10.4329/wjr.v8.i5.484.
- Lu, C., Contreras, X.; Peterlin, B. M. P bodies inhibit retrotransposition of endogenous intracisternal a particles. *J. Virol.* **2011**, *85* (13), 6244–6251. DOI: 10.1128/JVI.02517-10.

- Luke, J. J., Bao, R., Sweis, R. F., Spranger, S.; Gajewski, T. F. WNT/ β -catenin Pathway Activation Correlates with Immune Exclusion across Human Cancers. *Clin Cancer Res* **2019**, *25* (10), 3074–3083. DOI: 10.1158/1078-0432.CCR-18-1942.
- Luo, C., Wang, S., Liao, W., Zhang, S.; Xu, N., et al. Upregulation of the APOBEC3 Family Is Associated with a Poor Prognosis and Influences Treatment Response to Raf Inhibitors in Low Grade Glioma. *International Journal of Molecular Sciences* **2021**, *22* (19). DOI: 10.3390/ijms221910390.
- Luo, Q., Zhu, H., Li, Y., Wu, Q.; Sun, J., et al. Expression Analysis of BIRC3 as One Target Gene of Transcription Factor NF- κ B for Esophageal Cancer. *Processes* **2022**, *10* (9), 1673. DOI: 10.3390/pr10091673.
- Ma, M., Shi, F., Zhai, R., Wang, H.; Li, K., et al. TGF- β promote epithelial-mesenchymal transition via NF- κ B/NOX4/ROS signal pathway in lung cancer cells. *Molecular biology reports* **2021**, *48* (3), 2365–2375. DOI: 10.1007/s11033-021-06268-2.
- Makhov, P., Joshi, S., Ghatalia, P., Kutikov, A.; Uzzo, R. G., et al. Resistance to Systemic Therapies in Clear Cell Renal Cell Carcinoma: Mechanisms and Management Strategies. *Molecular cancer therapeutics* **2018**, *17* (7), 1355–1364. DOI: 10.1158/1535-7163.MCT-17-1299.
- Mangeat, B., Turelli, P., Caron, G., Friedli, M.; Perrin, L., et al. Broad antiretroviral defence by human APOBEC3G through lethal editing of nascent reverse transcripts. *Nature* **2003**, *424* (6944), 99–103. DOI: 10.1038/nature01709.
- Marin, M., Golem, S., Rose, K. M., Kozak, S. L.; Kabat, D. Human immunodeficiency virus type 1 Vif functionally interacts with diverse APOBEC3 cytidine deaminases and moves with them between cytoplasmic sites of mRNA metabolism. *J. Virol.* **2008**, *82* (2), 987–998. DOI: 10.1128/JVI.01078-07.
- Mattioli, I., Sebald, A., Bucher, C., Charles, R.-P.; Nakano, H., et al. Transient and selective NF- κ B p65 serine 536 phosphorylation induced by T cell costimulation is mediated by I κ B kinase beta and controls the kinetics of p65 nuclear import. *Journal of immunology (Baltimore, Md. : 1950)* **2004**, *172* (10), 6336–6344. DOI: 10.4049/jimmunol.172.10.6336.
- Matušan-Ilijaš, K., Damante, G., Fabbro, D., Dorđević, G.; Hadžisejdić, I., et al. Osteopontin expression correlates with nuclear factor- κ B activation and apoptosis downregulation in clear cell renal cell carcinoma. *Pathology, research and practice* **2011**, *207* (2), 104–110. DOI: 10.1016/j.prp.2010.11.004.
- Mauger, D. M., Cabral, B. J., Presnyak, V., Su, S. V.; Reid, D. W., et al. mRNA structure regulates protein expression through changes in functional half-life. *Proceedings of the National Academy of Sciences of the United States of America* **2019**, *116* (48), 24075–24083. DOI: 10.1073/pnas.1908052116.
- Mazumder, B., Seshadri, V.; Fox, P. L. Translational control by the 3'-UTR: the ends specify the means. *Trends in Biochemical Sciences* **2003**, *28* (2), 91–98. DOI: 10.1016/S0968-0004(03)00002-1.
- McConkey, E. H. [83] The fractionation of RNA's by sucrose gradient centrifugation. *Nucleic Acids, Part A; Methods in Enzymology*; Elsevier, 1967; pp 620–634. DOI: 10.1016/S0076-6879(67)12095-8.
- McDaniel, Y. Z., Wang, D., Love, R. P., Adolph, M. B.; Mohammadzadeh, N., et al. Deamination hotspots among APOBEC3 family members are defined by both target site sequence context and ssDNA secondary structure. *Nucleic Acids Res* **2020**, *48* (3), 1353–1371. DOI: 10.1093/nar/gkz1164.
- McDougall, W. M., Okany, C.; Smith, H. C. Deaminase activity on single-stranded DNA (ssDNA) occurs in vitro when APOBEC3G cytidine deaminase forms homotetramers and higher-order complexes. *J. Biol. Chem.* **2011**, *286* (35), 30655–30661. DOI: 10.1074/jbc.M111.269506.

- Mei, Y., Yang, J.-P.; Qian, C.-N. For robust big data analyses: a collection of 150 important pro-metastatic genes. *Chinese journal of cancer* **2017**, *36* (1), 16. DOI: 10.1186/s40880-016-0178-z.
- Meier-Soelch, J., Mayr-Buro, C., Juli, J., Leib, L.; Linne, U., et al. Monitoring the Levels of Cellular NF- κ B Activation States. *Cancers* **2021**, *13* (21). DOI: 10.3390/cancers13215351.
- Meteoglu, I., Erdogdu, I. H., Meydan, N., Erkus, M.; Barutca, S. NF-KappaB expression correlates with apoptosis and angiogenesis in clear cell renal cell carcinoma tissues. *Journal of experimental & clinical cancer research : CR* **2008**, *27* (1), 53. DOI: 10.1186/1756-9966-27-53.
- Mickisch, G. H. Multimodality treatment of metastatic renal cell carcinoma. *Expert review of anticancer therapy* **2002**, *2* (6), 681–685. DOI: 10.1586/14737140.2.6.681.
- Middlebrooks, C. D., Banday, A. R., Matsuda, K., Udquim, K.-I.; Onabajo, O. O., et al. Association of germline variants in the APOBEC3 region with cancer risk and enrichment with APOBEC-signature mutations in tumors. *Nature genetics* **2016**, *48* (11), 1330–1338. DOI: 10.1038/ng.3670.
- Mignone, F., Gissi, C., Liuni, S.; Pesole, G. Untranslated regions of mRNAs. *Genome Biol* [Online] **2002**, *3* (3), reviews0004.1.
- Mikl, M. C., Watt, I. N., Lu, M., Reik, W.; Davies, S. L., et al. Mice deficient in APOBEC2 and APOBEC3. *Molecular and cellular biology* **2005**, *25* (16), 7270–7277. DOI: 10.1128/MCB.25.16.7270-7277.2005.
- MiRNA Regulation of the Translational Machinery*; Rhoads, R. E., Ed., 1st ed. 2010; Progress in molecular and subcellular biology 50; Springer Berlin Heidelberg; Imprint Springer: Berlin, Heidelberg, 2010.
- Mitchell, S., Vargas, J.; Hoffmann, A. Signaling via the NF κ B system. *Wiley interdisciplinary reviews. Systems biology and medicine* **2016**, *8* (3), 227–241. DOI: 10.1002/wsbm.1331.
- Modenini, G., Abondio, P.; Boattini, A. The coevolution between APOBEC3 and retrotransposons in primates. *Mobile DNA* **2022**, *13* (1), 27. DOI: 10.1186/s13100-022-00283-1.
- Mohibi, S., Chen, X.; Zhang, J. Cancer the'RBP'eutics-RNA-binding proteins as therapeutic targets for cancer. *Pharmacology & therapeutics* **2019**, *203*, 107390. DOI: 10.1016/j.pharmthera.2019.07.001.
- Morais, C., Gobe, G., Johnson, D. W.; Healy, H. The emerging role of nuclear factor kappa B in renal cell carcinoma. *The international journal of biochemistry & cell biology* **2011**, *43* (11), 1537–1549. DOI: 10.1016/j.biocel.2011.08.003.
- Morais, C., Pat, B., Gobe, G., Johnson, D. W.; Healy, H. Pyrrolidine dithiocarbamate exerts anti-proliferative and pro-apoptotic effects in renal cell carcinoma cell lines. *Nephrology, dialysis, transplantation : official publication of the European Dialysis and Transplant Association - European Renal Association* **2006**, *21* (12), 3377–3388. DOI: 10.1093/ndt/gfl543.
- Morgan, D., Garg, M., Tergaonkar, V., Tan, S. Y.; Sethi, G. Pharmacological significance of the non-canonical NF- κ B pathway in tumorigenesis. *Biochimica et biophysica acta. Reviews on cancer* **2020**, *1874* (2), 188449. DOI: 10.1016/j.bbcan.2020.188449.
- Mori, S., Takeuchi, T., Ishii, Y.; Kukimoto, I. Identification of APOBEC3B promoter elements responsible for activation by human papillomavirus type 16 E6. *Biochemical and Biophysical Research Communications* **2015**, *460* (3), 555–560. DOI: 10.1016/j.bbrc.2015.03.068.
- Moris, A., Murray, S.; Cardinaud, S. AID and APOBECs span the gap between innate and adaptive immunity. *Front. Microbiol.* **2014**, *5*, 534. DOI: 10.3389/fmicb.2014.00534.

- Motzer, R. J., Hutson, T. E., Tomczak, P., Michaelson, M. D.; Bukowski, R. M., et al. Overall survival and updated results for sunitinib compared with interferon alfa in patients with metastatic renal cell carcinoma. *Journal of clinical oncology : official journal of the American Society of Clinical Oncology* **2009**, *27* (22), 3584–3590. DOI: 10.1200/JCO.2008.20.1293.
- Motzer, R. J., Jonasch, E., Agarwal, N., Beard, C.; Bhayani, S., et al. Kidney Cancer, Version 3.2015. *J Natl Compr Canc Netw* [Online] **2015**, *13* (2), 151–159.
- Motzer, R. J., Penkov, K., Haanen, J., Rini, B.; Albiges, L., et al. Avelumab plus Axitinib versus Sunitinib for Advanced Renal-Cell Carcinoma. *The New England journal of medicine* **2019**, *380* (12), 1103–1115. DOI: 10.1056/NEJMoa1816047.
- Motzer, R. J., Rini, B. I., Bukowski, R. M., Curti, B. D.; George, D. J., et al. Sunitinib in patients with metastatic renal cell carcinoma. *JAMA* **2006**, *295* (21), 2516–2524. DOI: 10.1001/jama.295.21.2516;
- Motzer, R. J. and Russo, P. Systemic therapy for renal cell carcinoma. *The Journal of urology* **2000**, *163* (2), 408–417.
- Mucke, H. am. Patent highlights October–November 2015. *Pharmaceutical Patent Analyst* **2016**, *5* (2), 107–113. DOI: 10.4155/ppa.15.47.
- Mulero, M. C., Wang, V. Y.-F., Huxford, T.; Ghosh, G. Genome reading by the NF- κ B transcription factors. *Nucleic Acids Res* **2019**, *47* (19), 9967–9989. DOI: 10.1093/nar/gkz739.
- Müller, S., Bley, N., Glaß, M., Busch, B.; Rousseau, V., et al. IGF2BP1 enhances an aggressive tumor cell phenotype by impairing miRNA-directed downregulation of oncogenic factors. *Nucleic Acids Res* **2018**, *46* (12), 6285–6303. DOI: 10.1093/nar/gky229.
- Murakami, T., Tanaka, N., Takamatsu, K., Hakozaiki, K.; Fukumoto, K., et al. Multiplexed single-cell pathology reveals the association of CD8 T-cell heterogeneity with prognostic outcomes in renal cell carcinoma. *Cancer immunology, immunotherapy : CII* **2021**, *70* (10), 3001–3013. DOI: 10.1007/s00262-021-03006-2.
- Muramatsu, M., Kinoshita, K., Fagarasan, S., Yamada, S.; Shinkai, Y., et al. Class switch recombination and hypermutation require activation-induced cytidine deaminase (AID), a potential RNA editing enzyme. *Cell* **2000**, *102* (5), 553–563. DOI: 10.1016/S0092-8674(00)00078-7.
- Nagashima, Y. Chromophobe renal cell carcinoma: clinical, pathological and molecular biological aspects. *Pathology international* **2000**, *50* (11), 872–878. DOI: 10.1046/j.1440-1827.2000.01131.x.
- Nakajima, S., Kato, H., Takahashi, S., Johno, H.; Kitamura, M. Inhibition of NF- κ B by MG132 through ER stress-mediated induction of LAP and LIP. *FEBS Letters* **2011**, *585* (14), 2249–2254. DOI: 10.1016/j.febslet.2011.05.047.
- Narvaiza, I., Linfesty, D. C., Greener, B. N., Hakata, Y.; Pintel, D. J., et al. Deaminase-independent inhibition of parvoviruses by the APOBEC3A cytidine deaminase. *PLoS pathogens* **2009**, *5* (5), e1000439. DOI: 10.1371/journal.ppat.1000439.
- Natoli, G., Sacconi, S., Bosisio, D.; Marazzi, I. Interactions of NF- κ B with chromatin: the art of being at the right place at the right time. *Nature immunology* **2005**, *6* (5), 439–445. DOI: 10.1038/ni1196.
- Naumann, M., Nieters, A., Hatada, E. N.; Scheidereit, C. NF- κ B precursor p100 inhibits nuclear translocation and DNA binding of NF- κ B/rel-factors. *Oncogene* **1993**, *8* (8), 2275–2281.
- Navaratnam, N., Morrison, J. R., Bhattacharya, S., Patel, D.; Funahashi, T., et al. The p27 catalytic subunit of the apolipoprotein B mRNA editing enzyme is a cytidine deaminase. *The Journal of biological chemistry* **1993**, *268* (28), 20709–20712.

- Navaratnam, N. and Sarwar, R. An overview of cytidine deaminases. *International journal of hematology* **2006**, *83* (3), 195–200. DOI: 10.1532/IJH97.06032.
- Navarro, F., Bollman, B., Chen, H., König, R.; Yu, Q., et al. Complementary function of the two catalytic domains of APOBEC3G. *Virology* **2005**, *333* (2), 374–386. DOI: 10.1016/j.virol.2005.01.011.
- Newman, E. N., Holmes, R. K., Craig, H. M., Klein, K. C.; Lingappa, J. R., et al. Antiviral function of APOBEC3G can be dissociated from cytidine deaminase activity. *Current Biology* **2005**, *15* (2), 166–170. DOI: 10.1016/j.cub.2004.12.068.
- Ng, J. C., Quist, J., Grigoriadis, A., Malim, M. H.; Fraternali, F. Pan-cancer transcriptomic analysis dissects immune and proliferative functions of APOBEC3 cytidine deaminases. *Nucleic Acids Res* **2019**, *47* (3), 1178–1194. DOI: 10.1093/nar/gky1316.
- Ng, K. L., Yap, N. Y., Rajandram, R., Small, D.; Pailoor, J., et al. Nuclear factor-kappa B subunits and their prognostic cancer-specific survival value in renal cell carcinoma patients. *Pathology* **2018**, *50* (5), 511–518. DOI: 10.1016/j.pathol.2018.03.003.
- Niewiadomska, A. M., Tian, C., Tan, L., Wang, T.; Sarkis, P. T., et al. Differential inhibition of long interspersed element 1 by APOBEC3 does not correlate with high-molecular-mass-complex formation or P-body association. *Journal of virology* **2007**, *81* (17), 9577–9583. DOI: 10.1128/jvi.02800-06.
- Nik-Zainal, S., Alexandrov, L. B., Wedge, D. C., van Loo, P.; Greenman, C. D., et al. Mutational Processes Molding the Genomes of 21 Breast Cancers. *Cell* **2012**, *149* (5), 979–993. DOI: 10.1016/j.cell.2012.04.024.
- Nowak, D. E., Tian, B., Jamaluddin, M., Boldogh, I.; Vergara, L. A., et al. RelA Ser276 phosphorylation is required for activation of a subset of NF-kappaB-dependent genes by recruiting cyclin-dependent kinase 9/cyclin T1 complexes. *Molecular and cellular biology* **2008**, *28* (11), 3623–3638. DOI: 10.1128/MCB.01152-07.
- Nowarski, R. and Kotler, M. APOBEC3 Cytidine Deaminases in Double-Strand DNA Break Repair and Cancer Promotion. *Cancer Res* [Online] **2013**, *73* (12), 3494–3498. <http://cancerres.aacrjournals.org/content/canres/73/12/3494.full.pdf>.
- Nowarski, R., Wilner, O. I., Cheshin, O., Shahar, O. D.; Kenig, E., et al. APOBEC3G enhances lymphoma cell radioresistance by promoting cytidine deaminase-dependent DNA repair. *Blood* **2012**, *120* (2), 366–375. DOI: 10.1182/blood-2012-01-402123.
- O'Dea, E. L., Barken, D., Peralta, R. Q., Tran, K. T.; Werner, S. L., et al. A homeostatic model of I kappa B metabolism to control constitutive NF-kappa B activity. *Molecular systems biology* **2007**, *3*, 111. DOI: 10.1038/msb4100148.
- Oeckinghaus, A. and Ghosh, S. The NF-kappa B family of transcription factors and its regulation. *Cold Spring Harbor perspectives in biology* **2009**, *1* (4), a000034. DOI: 10.1101/cshperspect.a000034.
- Oeckinghaus, A., Hayden, M. S.; Ghosh, S. Crosstalk in NF-kB signaling pathways. *Nature immunology* **2011**, *12* (8), 695–708. DOI: 10.1038/ni.2065.
- Oliver, R. T., Nethersell, A. B.; Bottomley, J. M. Unexplained spontaneous regression and alpha-interferon as treatment for metastatic renal carcinoma. *British journal of urology* **1989**, *63* (2), 128–131. DOI: 10.1111/j.1464-410x.1989.tb05147.x.
- Olson, M. E., Abate-Pella, D., Perkins, A. L., Li, M.; Carpenter, M. A., et al. Oxidative Reactivities of 2-Furylquinolines: Ubiquitous Scaffolds in Common High-Throughput Screening Libraries. *Journal of medicinal chemistry* **2015**, *58* (18), 7419–7430. DOI: 10.1021/acs.jmedchem.5b00930.
- Olson, M. E., Harris, R. S.; Harki, D. A. APOBEC Enzymes as Targets for Virus and Cancer Therapy. *Cell chemical biology* **2018**, *25* (1), 36–49. DOI: 10.1016/j.chembiol.2017.10.007.

- Osawa, T., Takeuchi, A., Kojima, T., Shinohara, N.; Eto, M., et al. Overview of current and future systemic therapy for metastatic renal cell carcinoma. *Japanese journal of clinical oncology* **2019**, *49* (5), 395–403. DOI: 10.1093/jjco/hyz013.
- Oya, M., Horiguchi, A., Mizuno, R., Marumo, K.; Murai, M. Increased activation of CCAAT/enhancer binding protein-beta correlates with the invasiveness of renal cell carcinoma. *Clinical cancer research : an official journal of the American Association for Cancer Research* **2003a**, *9* (3), 1021–1027.
- Oya, M., Ohtsubo, M., Takayanagi, A., Tachibana, M.; Shimizu, N., et al. Constitutive activation of nuclear factor-kappaB prevents TRAIL-induced apoptosis in renal cancer cells. *Oncogene* **2001**, *20* (29), 3888–3896. DOI: 10.1038/sj.onc.1204525.
- Oya, M., Takayanagi, A., Horiguchi, A., Mizuno, R.; Ohtsubo, M., et al. Increased nuclear factor-kappa B activation is related to the tumor development of renal cell carcinoma. *Carcinogenesis* **2003b**, *24* (3), 377–384. DOI: 10.1093/carcin/24.3.377.
- Padala, S. A., Barsouk, A., Thandra, K. C., Saginala, K.; Mohammed, A., et al. Epidemiology of Renal Cell Carcinoma. *World journal of oncology* **2020**, *11* (3), 79–87. DOI: 10.14740/wjon1279.
- Pak, C. and Miyamoto, S. A new alpha in line between KRAS and NF-κB activation? *Cancer Discov* **2013**, *3* (6), 613–615. DOI: 10.1158/2159-8290.CD-13-0193.
- Paoli, P., Giannoni, E.; Chiarugi, P. Anoikis molecular pathways and its role in cancer progression. *Biochimica et biophysica acta* **2013**, *1833* (12), 3481–3498. DOI: 10.1016/j.bbamcr.2013.06.026.
- Patel, V. L., Mitra, S., Harris, R., Buxbaum, A. R.; Lionnet, T., et al. Spatial arrangement of an RNA zipcode identifies mRNAs under post-transcriptional control. *Genes & development* **2012**, *26* (1), 43–53. DOI: 10.1101/gad.177428.111.
- Pei, X., Li, M., Zhan, J., Yu, Y.; Wei, X., et al. Enhanced IMP3 Expression Activates NF-κB Pathway and Promotes Renal Cell Carcinoma Progression. *PLoS one* **2015**, *10* (4), e0124338. DOI: 10.1371/journal.pone.0124338.
- Peired, A. J., Lazzeri, E., Guzzi, F., Anders, H.-J.; Romagnani, P. From kidney injury to kidney cancer. *Kidney International* **2021**, *100* (1), 55–66. DOI: 10.1016/j.kint.2021.03.011.
- Peng, G., Lei, K. J., Jin, W., Greenwell-Wild, T.; Wahl, S. M. Induction of APOBEC3 family proteins, a defensive maneuver underlying interferon-induced anti-HIV-1 activity. *The Journal of experimental medicine* **2006**, *203* (1), 41–46. DOI: 10.1084/jem.20051512.
- Peng, J., Mo, R., Ma, J.; Fan, J. let-7b and let-7c are determinants of intrinsic chemoresistance in renal cell carcinoma. *World journal of surgical oncology* **2015**, *13*, 175. DOI: 10.1186/s12957-015-0596-4.
- Peng, T., Liu, B., Lin, S., Cao, C.; Wu, P., et al. APOBEC3G expression correlates with unfavorable prognosis and immune infiltration in kidney renal clear cell carcinoma. *Heliyon* **2022**, *8* (12), e12191. DOI: 10.1016/j.heliyon.2022.e12191.
- Peng, Z.-G., Zhao, Z.-Y., Li, Y.-P., Wang, Y.-P.; Hao, L.-H., et al. Host apolipoprotein B messenger RNA-editing enzyme catalytic polypeptide-like 3G is an innate defensive factor and drug target against hepatitis C virus. *Hepatology (Baltimore, Md.)* **2011**, *53* (4), 1080–1089. DOI: 10.1002/hep.24160.
- Peri, S., Devarajan, K., Yang, D.-H., Knudson, A. G.; Balachandran, S. Meta-analysis identifies NF-κB as a therapeutic target in renal cancer. *PLoS one* **2013**, *8* (10), e76746. DOI: 10.1371/journal.pone.0076746.
- Periyasamy, M., Singh, A. K., Gemma, C., Farzan, R.; Allsopp, R. C., et al. Induction of APOBEC3B expression by chemotherapy drugs is mediated by DNA-PK-directed activation of NF-κB. *Oncogene* **2021**, *40* (6), 1077–1090. DOI: 10.1038/s41388-020-01583-7.

- Perkins, N. D. The diverse and complex roles of NF- κ B subunits in cancer. *Nature reviews. Cancer* **2012**, *12* (2), 121–132. DOI: 10.1038/nrc3204.
- Perkins, N. D., Felzien, L. K., Betts, J. C., Leung, K.; Beach, D. H., et al. Regulation of NF-kappaB by cyclin-dependent kinases associated with the p300 coactivator. *Science (New York, N.Y.)* **1997**, *275* (5299), 523–527. DOI: 10.1126/science.275.5299.523.
- Piao, X.-M., Byun, Y. J., Zheng, C.-M., Song, S. J.; Kang, H. W., et al. A New Treatment Landscape for RCC: Association of the Human Microbiome with Improved Outcomes in RCC. *Cancers* **2023**, *15* (3). DOI: 10.3390/cancers15030935.
- Pick, A. M. and Nystrom, K. K. Pazopanib for the treatment of metastatic renal cell carcinoma. *Clinical therapeutics* **2012**, *34* (3), 511–520. DOI: 10.1016/j.clinthera.2012.01.014;
- Pires, B. R., Silva, R. C., Ferreira, G. M.; Abdelhay, E. NF-kappaB: Two Sides of the Same Coin. *Genes* **2018**, *9* (1). DOI: 10.3390/genes9010024.
- Popp, M. W. and Maquat, L. E. Leveraging Rules of Nonsense-Mediated mRNA Decay for Genome Engineering and Personalized Medicine. *Cell* **2016**, *165* (6), 1319–1322. DOI: 10.1016/j.cell.2016.05.053.
- Porter, D. F., Miao, W., Yang, X., Goda, G. A.; Ji, A. L., et al. easyCLIP analysis of RNA-protein interactions incorporating absolute quantification. *Nat Commun* **2021**, *12* (1), 1569. DOI: 10.1038/s41467-021-21623-4.
- Powell, L. M., Wallis, S. C., Pease, R. J., Edwards, Y. H.; Knott, T. J., et al. A novel form of tissue-specific RNA processing produces apolipoprotein-B48 in intestine. *Cell* **1987**, *50* (6), 831–840. DOI: 10.1016/0092-8674(87)90510-1.
- Prohaska, K. M., Bennett, R. P., Salter, J. D.; Smith, H. C. The multifaceted roles of RNA binding in APOBEC cytidine deaminase functions. *Wiley Interdisciplinary Reviews: RNA* **2014**, *5*. DOI: 10.1002/wrna.1226.
- Qi, H. and Ohh, M. The von Hippel-Lindau tumor suppressor protein sensitizes renal cell carcinoma cells to tumor necrosis factor-induced cytotoxicity by suppressing the nuclear factor-kappaB-dependent antiapoptotic pathway. *Cancer Res* **2003**, *63* (21), 7076–7080.
- Qin, H., Ni, H., Liu, Y., Yuan, Y.; Xi, T., et al. RNA-binding proteins in tumor progression. *Journal of hematology & oncology* **2020**, *13* (1), 90. DOI: 10.1186/s13045-020-00927-w.
- Raman, R. and Vaena, D. Immunotherapy in Metastatic Renal Cell Carcinoma: A Comprehensive Review. *BioMed research international* **2015**, *2015*, 367354. DOI: 10.1155/2015/367354.
- Ramana, C. V., Chatterjee-Kishore, M., Nguyen, H.; Stark, G. R. Complex roles of Stat1 in regulating gene expression. *Oncogene* **2000**, *19* (21), 2619–2627. DOI: 10.1038/sj.onc.1203525.
- Ran, X., Xiao, J., Zhang, Y., Teng, H.; Cheng, F., et al. Low intratumor heterogeneity correlates with increased response to PD-1 blockade in renal cell carcinoma. *Therapeutic advances in medical oncology* **2020**, *12*, 1758835920977117. DOI: 10.1177/1758835920977117.
- Rebhandl, S., Huemer, M., Greil, R.; Geisberger, R. AID/APOBEC deaminases and cancer. *Oncoscience* **2015**, *2* (4), 320–333. DOI: 10.18632/oncoscience.155.
- Reed, J. C. Bcl-2 and the regulation of programmed cell death. *The Journal of cell biology* **1994**, *124* (1-2), 1–6. DOI: 10.1083/jcb.124.1.1.
- Refsland, E. W., Stenglein, M. D., Shindo, K., Albin, J. S.; Brown, W. L., et al. Quantitative profiling of the full APOBEC3 mRNA repertoire in lymphocytes and tissues: implications for HIV-1 restriction. *Nucleic Acids Res* **2010**, *38* (13), 4274–4284. DOI: 10.1093/nar/gkq174.

- Reid, M. A. and Kong, M. Dealing with hunger: Metabolic stress responses in tumors. *Journal of carcinogenesis* **2013**, *12*, 17. DOI: 10.4103/1477-3163.119111.
- Reuter, S., Gupta, S. C., Chaturvedi, M. M.; Aggarwal, B. B. Oxidative stress, inflammation, and cancer: how are they linked? *Free radical biology & medicine* **2010**, *49* (11), 1603–1616. DOI: 10.1016/j.freeradbiomed.2010.09.006.
- Richardson, S. R., Narvaiza, I., Planegger, R. A., Weitzman, M. D.; Moran, J. V. APOBEC3A deaminates transiently exposed single-strand DNA during LINE-1 retrotransposition. *eLife* **2014**, *3*, e02008. DOI: 10.7554/eLife.02008.
- Rini, B. I., Campbell, S. C.; Escudier, B. Renal cell carcinoma. *The Lancet* **2009**, *373* (9669), 1119–1132. DOI: 10.1016/S0140-6736(09)60229-4.
- Rini, B. I., McDermott, D. F., Hammers, H., Bro, W.; Bukowski, R. M., et al. Society for Immunotherapy of Cancer consensus statement on immunotherapy for the treatment of renal cell carcinoma. *Journal for immunotherapy of cancer* **2016**, *4*, 81. DOI: 10.1186/s40425-016-0180-7.
- Roberts, S. A., Lawrence, M. S., Klimczak, L. J., Grimm, S. A.; Fargo, D., et al. An APOBEC cytidine deaminase mutagenesis pattern is widespread in human cancers. *Nature genetics* **2013**, *45* (9), 970–976. DOI: 10.1038/ng.2702.
- Robinson, M. D., McCarthy, D. J.; Smyth, G. K. edgeR: a Bioconductor package for differential expression analysis of digital gene expression data. *Bioinformatics (Oxford, England)* **2010**, *26* (1), 139–140. DOI: 10.1093/bioinformatics/btp616.
- Rohde, D., Hayn, H. K., Blatter, J.; Jakse, G. The efficacy of 2',2'-difluorodeoxycytidine (gemcitabine) combined with interferon in human renal cell carcinoma cell lines. *International Journal of Oncology* **1998**, *12* (6), 1361–1366. DOI: 10.3892/ijo.12.6.1361.
- Rosenthal, R., McGranahan, N., Herrero, J., Taylor, B. S.; Swanton, C. DeconstructSigs: delineating mutational processes in single tumors distinguishes DNA repair deficiencies and patterns of carcinoma evolution. *Genome Biol* **2016**, *17*, 31. DOI: 10.1186/s13059-016-0893-4.
- Saad, O. A., Li, W. T., Krishnan, A. R., Nguyen, G. C.; Lopez, J. P., et al. The renal clear cell carcinoma immune landscape. *Neoplasia (New York, N.Y.)* **2022**, *24* (2), 145–154. DOI: 10.1016/j.neo.2021.12.007.
- Sakai, N., Wada, T., Furuichi, K., Iwata, Y.; Yoshimoto, K., et al. p38 MAPK phosphorylation and NF-kappa B activation in human crescentic glomerulonephritis. *Nephrology, dialysis, transplantation : official publication of the European Dialysis and Transplant Association - European Renal Association* **2002**, *17* (6), 998–1004. DOI: 10.1093/ndt/17.6.998.
- Sakurai, H., Chiba, H., Miyoshi, H., Sugita, T.; Toriumi, W. IkappaB kinases phosphorylate NF-kappaB p65 subunit on serine 536 in the transactivation domain. *The Journal of biological chemistry* **1999**, *274* (43), 30353–30356. DOI: 10.1074/jbc.274.43.30353;
- Salamango, D. J., McCann, J. L., Demir, Ö., Brown, W. L.; Amaro, R. E., et al. APOBEC3B Nuclear Localization Requires Two Distinct N-Terminal Domain Surfaces. *Journal of molecular biology* **2018**, *430* (17), 2695–2708. DOI: 10.1016/j.jmb.2018.04.044.
- Salter, J. D., Bennett, R. P.; Smith, H. C. The APOBEC Protein Family: United by Structure, Divergent in Function. *Trends in Biochemical Sciences* **2016**, *41* (7), 578–594. DOI: 10.1016/j.tibs.2016.05.001.
- Salter, J. D. and Smith, H. C. Modeling the Embrace of a Mutator: APOBEC Selection of Nucleic Acid Ligands. *Trends in Biochemical Sciences* **2018**, *43* (8), 606–622. DOI: 10.1016/j.tibs.2018.04.013.

- Sánchez-Gastaldo, A., Kempf, E., González del Albac, A.; Duran, I. Systemic treatment of renal cell cancer: A comprehensive review. *Cancer Treatment Reviews* **2017**, *60*, 77–89. DOI: 10.1016/j.ctrv.2017.08.010.
- Saraconi, G., Severi, F., Sala, C., Mattiuz, G.; Conticello, S. G. The RNA editing enzyme APOBEC1 induces somatic mutations and a compatible mutational signature is present in esophageal adenocarcinomas. *Genome biology* [Online] **2014**, *15* (7), 417.
- Sari Khaleel, Christopher Ricketts, W. Marston Linehan, Mark Ball; Brandon Manley, et al. Genetics and Tumor Microenvironment of Renal Cell Carcinoma. *1* [Online] **2022**, *3* (6), 386–396.
- Sasaki, C. Y., Barberi, T. J., Ghosh, P.; Longo, D. L. Phosphorylation of RelA/p65 on serine 536 defines an I{kappa}B{alpha}-independent NF- κ B pathway. *The Journal of biological chemistry* **2005**, *280* (41), 34538–34547. DOI: 10.1074/jbc.M504943200.
- Sawyer, S. L., Emerman, M.; Malik, H. S. Ancient Adaptive Evolution of the Primate Antiviral DNA-Editing Enzyme APOBEC3G. *PLOS Biology* [Online] **2004**, *2* (9), e275.
- Scholtes, G. K., Sawyer, A. M., Vaca, C. C., Clerc, I.; Roh, M., et al. The von Hippel-Lindau Cullin-RING E3 ubiquitin ligase regulates APOBEC3 cytidine deaminases. *Translational research : the journal of laboratory and clinical medicine* **2021**, *237*, 1–15. DOI: 10.1016/j.trsl.2021.05.002.
- Schreck, R., Albermann, K.; Baeuerle, P. A. Nuclear factor kappa B: an oxidative stress-responsive transcription factor of eukaryotic cells (a review). *Free radical research communications* **1992**, *17* (4), 221–237. DOI: 10.3109/10715769209079515.
- Schreuder, M. I., van den Brand, M., Hebeda, K. M., Groenen, P. J.; van Krieken, J. H., et al. Novel developments in the pathogenesis and diagnosis of extranodal marginal zone lymphoma. *Journal of hematopathology* **2017**, *10* (3-4), 91–107. DOI: 10.1007/s12308-017-0302-2.
- Schulze-Osthoff, K., Ferrari, D., Riehemann, K.; Wesselborg, S. Regulation of NF-kappa B activation by MAP kinase cascades. *Immunobiology* **1997**, *198* (1-3), 35–49. DOI: 10.1016/S0171-2985(97)80025-3;
- Schumann, G. G. APOBEC3 proteins: major players in intracellular defence against LINE-1-mediated retrotransposition. *Biochemical Society transactions* **2007**, *35* (Pt 3), 637–642. DOI: 10.1042/BST0350637.
- SEER Cancer Statistics Review, 1975–2012, National Cancer Institute. Bethesda, MD, 2015.*
- Sen, G. L. and Blau, H. M. Argonaute 2/RISC resides in sites of mammalian mRNA decay known as cytoplasmic bodies. *Nature cell biology* **2005**, *7* (6), 633–636. DOI: 10.1038/ncb1265.
- Sen, R. and Baltimore, D. Multiple nuclear factors interact with the immunoglobulin enhancer sequences. *Cell* **1986**, *46* (5), 705–716. DOI: 10.1016/0092-8674(86)90346-6.
- Şenbabaoğlu, Y., Gejman, R. S., Winer, A. G., Liu, M.; van Allen, E. M., et al. Tumor immune microenvironment characterization in clear cell renal cell carcinoma identifies prognostic and immunotherapeutically relevant messenger RNA signatures. *Genome biology* [Online] **2016**, *17* (1), 231.
- Senftleben, U., Cao, Y., Xiao, G., Greten, F. R.; Krähn, G., et al. Activation by IKK α of a second, evolutionary conserved, NF-kappa B signaling pathway. *Science (New York, N. Y.)* **2001**, *293* (5534), 1495–1499. DOI: 10.1126/science.1062677.
- Serasanambati, M. and Chilakapati, S. R. Function of Nuclear Factor Kappa B (NF- κ B) in Human Diseases-A Review. *sijbs* **2016**, *2* (4), 368. DOI: 10.22205/sijbs/2016/v2/i4/103443.

- Serrano, J. C., Trentini, D. von, Berríos, K. N., Barka, A.; Dmochowski, I. J., et al. Structure-Guided Design of a Potent and Specific Inhibitor against the Genomic Mutator APOBEC3A. *ACS chemical biology* **2022**, *17* (12), 3379–3388. DOI: 10.1021/acscchembio.2c00796.
- Shandilya, S. M., Bohn, M.-F.; Schiffer, C. A. A computational analysis of the structural determinants of APOBEC3's catalytic activity and vulnerability to HIV-1 Vif. *Virology* **2014**, *471-473*, 105–116. DOI: 10.1016/j.virol.2014.09.023.
- Sharma, S., Patnaik, S. K., Taggart, R. T.; Baysal, B. E. The double-domain cytidine deaminase APOBEC3G is a cellular site-specific RNA editing enzyme. *Scientific Reports* **2016**, *6*. DOI: 10.1038/srep39100.
- Sharma, S., Patnaik, S. K., Taggart, R. T., Kannisto, E. D.; Enriquez, S. M., et al. APOBEC3A cytidine deaminase induces RNA editing in monocytes and macrophages. *Nature Communications* [Online] **2015**, *6*, 6881.
- Sheehy, A. M. and Erthal, J. APOBEC3 versus Retroviruses, Immunity versus Invasion: Clash of the Titans. *Molecular biology international* **2012**, *2012*, 974924. DOI: 10.1155/2012/974924.
- Sheehy, A. M., Gaddis, N. C., Choi, J. D.; Malim, M. H. Isolation of a human gene that inhibits HIV-1 infection and is suppressed by the viral Vif protein. *Nature* **2002**, *418* (6898), 646–650. DOI: 10.1038/nature00939.
- Shen, C. and Kaelin, W. G. The VHL/HIF axis in clear cell renal carcinoma. *Seminars in Cancer Biology* **2013**, *23* (1), 18–25. DOI: 10.1016/j.semcancer.2012.06.001.
- Sheth, U. and Parker, R. Decapping and decay of messenger RNA occur in cytoplasmic processing bodies. *Science* **2003**, *300* (5620), 805–808. DOI: 10.1126/science.1082320.
- Shih, V. F.-S., Tsui, R., Caldwell, A.; Hoffmann, A. A single NFκB system for both canonical and non-canonical signaling. *Cell research* **2011**, *21* (1), 86–102. DOI: 10.1038/cr.2010.161.
- Shilova, O. N., Tsyba, D. L.; Shilov, E. S. Mutagenic Activity of AID/APOBEC Deaminases in Antiviral Defense and Carcinogenesis. *Molecular biology* **2022**, *56* (1), 46–58. DOI: 10.1134/S002689332201006X.
- Shuch, B., Riggs, S. B., LaRochelle, J. C., Kabbinavar, F. F.; Avakian, R., et al. Neoadjuvant targeted therapy and advanced kidney cancer: observations and implications for a new treatment paradigm. *BJU international* **2008**, *102* (6), 692–696. DOI: 10.1111/j.1464-410X.2008.07660.x.
- Silke, J. and Vucic, D. IAP family of cell death and signaling regulators. *Methods in enzymology* **2014**, *545*, 35–65. DOI: 10.1016/B978-0-12-801430-1.00002-0.
- Silvas, T. V. and Schiffer, C. A. APOBEC3s: DNA-editing human cytidine deaminases. *Protein science : a publication of the Protein Society* **2019**, *28* (9), 1552–1566. DOI: 10.1002/pro.3670.
- Simon, P., Sargent, R.; Rabson, A. Inhibitor of apoptosis protein BIRC3 (API2, cIAP2, AIP1) is upregulated by the non-canonical NFκB pathway. *Cancer Res* [Online] **2007**, *67* (9_Supplement), 5327.
- Sinha, R., Winer, A. G., Chevinsky, M., Jakubowski, C.; Chen, Y.-B., et al. Analysis of renal cancer cell lines from two major resources enables genomics-guided cell line selection. *Nat Commun* [Online] **2017**, *8* (1), 15165.
- Slaton, J. W., Inoue, K., Perrotte, P., El-Naggar, A. K.; Swanson, D. A., et al. Expression levels of genes that regulate metastasis and angiogenesis correlate with advanced pathological stage of renal cell carcinoma. *The American Journal of Pathology* **2001**, *158* (2), 735–743. DOI: 10.1016/S0002-9440(10)64016-3.

- Slobbe, R. L., Pluk, W., van Venrooij, W. J.; Pruijn, G. J. Ro ribonucleoprotein assembly in vitro. Identification of RNA-protein and protein-protein interactions. *Journal of molecular biology* **1992**, *227* (2), 361–366. DOI: 10.1016/0022-2836(92)90890-v.
- Smialek, M. J., Ilaslan, E., Sajek, M. P.; Jaruzelska, J. Role of PUM RNA-Binding Proteins in Cancer. *Cancers* **2021**, *13* (1). DOI: 10.3390/cancers13010129.
- Smith, H. C. APOBEC3G: a double agent in defense. *Trends in Biochemical Sciences* **2011**, *36* (5), 239–244. DOI: 10.1016/j.tibs.2010.12.003.
- Smith, H. C. RNA binding to APOBEC deaminases; Not simply a substrate for C to U editing. *RNA biology* [Online] **2016**, 1–13.
- Smith, H. C., Bennett, R. P., Kizilyer, A., McDougall, W. M.; Prohaska, K. M. Functions and regulation of the APOBEC family of proteins. *RNA Editing & Developmental Cell Behavior* **2012**, *23* (3), 258–268. DOI: 10.1016/j.semcdb.2011.10.004.
- Soubrier, C., Danilin, S., Lindner, V., Steger, J.; Rothhut, S., et al. Targeting the nuclear factor-kappaB rescue pathway has promising future in human renal cell carcinoma therapy. *Cancer Res* **2007**, *67* (24), 11668–11676. DOI: 10.1158/0008-5472.CAN-07-0632.
- Staudt, L. M. Oncogenic activation of NF-kappaB. *Cold Spring Harbor perspectives in biology* **2010**, *2* (6), a000109. DOI: 10.1101/cshperspect.a000109.
- Stenglein, M. D., Burns, M. B., Li, M., Lengyel, J.; Harris, R. S. APOBEC3 proteins mediate the clearance of foreign DNA from human cells. *Nature structural & molecular biology* **2010**, *17* (2), 222–229. DOI: 10.1038/nsmb.1744.
- Sternberg, C. N., Davis, I. D., Mardiak, J., Szczylik, C.; Lee, E., et al. Pazopanib in locally advanced or metastatic renal cell carcinoma: results of a randomized phase III trial. *Journal of clinical oncology : official journal of the American Society of Clinical Oncology* **2010**, *28* (6), 1061–1068. DOI: 10.1200/JCO.2009.23.9764.
- Stöhr, N., Köhn, M., Lederer, M., Glass, M.; Reinke, C., et al. IGF2BP1 promotes cell migration by regulating MK5 and PTEN signaling. *Genes & development* **2012**, *26* (2), 176–189. DOI: 10.1101/gad.177642.111.
- Stuart, J. J., Egly, L. A., Wong, G. H.; Kaspar, R. L. The 3' UTR of human MnSOD mRNA hybridizes to a small cytoplasmic RNA and inhibits gene expression. *Biochemical and Biophysical Research Communications* **2000**, *274* (3), 641–648. DOI: 10.1006/bbrc.2000.3189.
- Su, B., Zhao, W., Shi, B., Zhang, Z.; Yu, X., et al. Let-7d suppresses growth, metastasis, and tumor macrophage infiltration in renal cell carcinoma by targeting COL3A1 and CCL7. *Molecular Cancer* **2014**, *13*, 206. DOI: 10.1186/1476-4598-13-206.
- Subramanian, A., Tamayo, P., Mootha, V. K., Mukherjee, S.; Ebert, B. L., et al. Gene set enrichment analysis: a knowledge-based approach for interpreting genome-wide expression profiles. *Proceedings of the National Academy of Sciences of the United States of America* **2005**, *102* (43), 15545–15550. DOI: 10.1073/pnas.0506580102.
- Sugihara, T., Kobori, A., Imaeda, H., Tsujikawa, T.; Amagase, K., et al. The increased mucosal mRNA expressions of complement C3 and interleukin-17 in inflammatory bowel disease. *Clinical and experimental immunology* **2010**, *160* (3), 386–393. DOI: 10.1111/j.1365-2249.2010.04093.x.
- Sun, S.-C. and Ley, S. C. New insights into NF-kappaB regulation and function. *Trends in immunology* **2008**, *29* (10), 469–478. DOI: 10.1016/j.it.2008.07.003.
- Suspène, R., Aynaud, M.-M., Koch, S., Padeloup, D.; Labetoulle, M., et al. Genetic editing of herpes simplex virus 1 and Epstein-Barr herpesvirus genomes by human APOBEC3 cytidine deaminases in culture and in vivo. *J. Virol.* **2011**, *85* (15), 7594–7602. DOI: 10.1128/JVI.00290-11.

- Swanton, C., McGranahan, N., Starrett, G. J.; Harris, R. S. APOBEC Enzymes: Mutagenic Fuel for Cancer Evolution and Heterogeneity. *Cancer Discov* [Online] **2015**, *5* (7), 704–712.
- Szostak, E. and Gebauer, F. Translational control by 3'-UTR-binding proteins. *Briefings in functional genomics* **2013**, *12* (1), 58–65. DOI: 10.1093/bfpg/els056.
- Tabata, M., Sato, Y., Kogure, Y., McClure, M. B.; Oshikawa-Kumade, Y., et al. Inter- and intra-tumor heterogeneity of genetic and immune profiles in inherited renal cell carcinoma. *Cell Reports* **2023**, *42* (7), 112736. DOI: 10.1016/j.celrep.2023.112736.
- Tafari, M., Pucci, B., Russo, A., Schito, L.; Pellegrini, L., et al. Modulators of HIF1 α and NF κ B in Cancer Treatment: Is it a Rational Approach for Controlling Malignant Progression? *Frontiers in pharmacology* **2013**, *4*, 13. DOI: 10.3389/fphar.2013.00013.
- Tam, A. B., Mercado, E. L., Hoffmann, A.; Niwa, M. ER stress activates NF- κ B by integrating functions of basal IKK activity, IRE1 and PERK. *PloS one* **2012**, *7* (10), e45078. DOI: 10.1371/journal.pone.0045078.
- Tang, C.-H. and Tsai, C.-C. CCL2 increases MMP-9 expression and cell motility in human chondrosarcoma cells via the Ras/Raf/MEK/ERK/NF- κ B signaling pathway. *Biochemical pharmacology* **2012**, *83* (3), 335–344. DOI: 10.1016/j.bcp.2011.11.013.
- Tang, P. A. and Heng, D. Y. Programmed death 1 pathway inhibition in metastatic renal cell cancer and prostate cancer. *Current oncology reports* **2013**, *15* (2), 98–104. DOI: 10.1007/s11912-012-0284-2.
- Tang, W., Fei, Y.; Page, M. Biological significance of RNA editing in cells. *Molecular biotechnology* **2012**, *52* (1), 91–100. DOI: 10.1007/s12033-012-9498-7.
- Thapa, R. J., Chen, P., Cheung, M., Nogusa, S.; Pei, J., et al. NF- κ B inhibition by bortezomib permits IFN- γ -activated RIP1 kinase-dependent necrosis in renal cell carcinoma. *Molecular cancer therapeutics* **2013**, *12* (8), 1568–1578. DOI: 10.1158/1535-7163.MCT-12-1010.
- Thielen, B. K., McNevin, J. P., McElrath, M. J., Hunt, B. V.; Klein, K. C., et al. Innate immune signaling induces high levels of TC-specific deaminase activity in primary monocyte-derived cells through expression of APOBEC3A isoforms. *J. Biol. Chem.* **2010**, *285* (36), 27753–27766. DOI: 10.1074/jbc.M110.102822.
- Thompson, R. H., Dong, H.; Kwon, E. D. Implications of B7-H1 expression in clear cell carcinoma of the kidney for prognostication and therapy. *Clinical cancer research : an official journal of the American Association for Cancer Research* **2007**, *13* (2 Pt 2), 709s-715s. DOI: 10.1158/1078-0432.CCR-06-1868.
- Thompson, R. H., Kuntz, S. M., Leibovich, B. C., Dong, H.; Lohse, C. M., et al. Tumor B7-H1 is associated with poor prognosis in renal cell carcinoma patients with long-term follow-up. *Cancer Res* **2006**, *66* (7), 3381–3385. DOI: 10.1158/0008-5472.CAN-05-4303.
- Tieri, P., Termanini, A., Bellavista, E., Salvioli, S.; Capri, M., et al. Charting the NF- κ B pathway interactome map. *PloS one* **2012**, *7* (3), e32678. DOI: 10.1371/journal.pone.0032678.
- Traber, K. E., Okamoto, H., Kurono, C., Baba, M.; Saliou, C., et al. Anti-rheumatic compound aurothioglucose inhibits tumor necrosis factor-alpha-induced HIV-1 replication in latently infected OM10.1 and Ach2 cells. *International immunology* **1999**, *11* (2), 143–150. DOI: 10.1093/intimm/11.2.143.
- Tritschler, F., Braun, J. E., Motz, C., Igraja, C.; Haas, G., et al. DCP1 forms asymmetric trimers to assemble into active mRNA decapping complexes in metazoa. *Proceedings of the National Academy of Sciences of the United States of America* **2009**, *106* (51), 21591–21596. DOI: 10.1073/pnas.0909871106.

- Tsujimoto, Y. Bcl-2 family of proteins: life-or-death switch in mitochondria. *Bioscience reports* **2002**, *22* (1), 47–58. DOI: 10.1023/A:1016061006256.
- Turajlic, S., Larkin, J.; Swanton, C. SnapShot: Renal Cell Carcinoma. *Cell* **2015**, *163* (6), 1556-1556.e1. DOI: 10.1016/j.cell.2015.11.026.
- Turelli, P., Mangeat, B., Jost, S., Vianin, S.; Trono, D. Inhibition of hepatitis B virus replication by APOBEC3G. *Science* **2004**, *303* (5665), 1829. DOI: 10.1126/science.1092066.
- Turner, M. D., Nedjai, B., Hurst, T.; Pennington, D. J. Cytokines and chemokines: At the crossroads of cell signalling and inflammatory disease. *Biochimica et biophysica acta* **2014**, *1843* (11), 2563–2582. DOI: 10.1016/j.bbamcr.2014.05.014.
- Ulivi, V., Giannoni, P., Gentili, C., Cancedda, R.; Descalzi, F. p38/NF-kB-dependent expression of COX-2 during differentiation and inflammatory response of chondrocytes. *Journal of cellular biochemistry* **2008**, *104* (4), 1393–1406. DOI: 10.1002/jcb.21717;
- Uriu, K., Kosugi, Y., Suzuki, N., Ito, J.; Sato, K. Elucidation of the Complicated Scenario of Primate APOBEC3 Gene Evolution. *J. Virol.* **2021**, *95* (12). DOI: 10.1128/jvi.00144-21.
- Vainer, G., Vainer-Mosse, E., Pikarsky, A., Shenoy, S. M.; Oberman, F., et al. A role for VICKZ proteins in the progression of colorectal carcinomas: regulating lamellipodia formation. *The Journal of Pathology* **2008**, *215* (4), 445–456. DOI: 10.1002/path.2376.
- Vallabhapurapu, S. and Karin, M. Regulation and function of NF-kappaB transcription factors in the immune system. *Annual review of immunology* **2009**, *27*, 693–733. DOI: 10.1146/annurev.immunol.021908.132641.
- van Dijk, B. A., Schouten, L. J., Oosterwijk, E., Hulsbergen-van de Kaa, C. A.; Kiemeneij, L. A., et al. Cigarette smoking, von Hippel-Lindau gene mutations and sporadic renal cell carcinoma. *British Journal of Cancer* **2006**, *95* (3), 374–377. DOI: 10.1038/sj.bjc.6603281.
- van Nostrand, E. L., Freese, P., Pratt, G. A., Wang, X.; Wei, X., et al. A large-scale binding and functional map of human RNA-binding proteins. *Nature* **2020a**, *583* (7818), 711–719. DOI: 10.1038/s41586-020-2077-3.
- van Nostrand, E. L., Pratt, G. A., Shishkin, A. A., Gelboin-Burkhart, C.; Fang, M. Y., et al. Robust transcriptome-wide discovery of RNA-binding protein binding sites with enhanced CLIP (eCLIP). *Nature methods* **2016**, *13* (6), 508–514. DOI: 10.1038/nmeth.3810.
- van Nostrand, E. L., Pratt, G. A., Yee, B. A., Wheeler, E. C.; Blue, S. M., et al. Principles of RNA processing from analysis of enhanced CLIP maps for 150 RNA binding proteins. *Genome biology* [Online] **2020b**, *21* (1), 90.
- van Riel, P. L., van de Putte, L. B., Gribnau, F. W.; Macrae, K. D. Comparison of auranofin and aurothioglucose in the treatment of rheumatoid arthritis: a single blind study. *Clinical rheumatology* **1984**, *3 Suppl 1*, 51–56. DOI: 10.1007/BF03342622.
- Vanden Berghe, W., Plaisance, S., Boone, E., Bosscher, K. de; Schmitz, M. L., et al. p38 and extracellular signal-regulated kinase mitogen-activated protein kinase pathways are required for nuclear factor-kappaB p65 transactivation mediated by tumor necrosis factor. *The Journal of biological chemistry* **1998**, *273* (6), 3285–3290. DOI: 10.1074/jbc.273.6.3285.
- Vartanian, J.-P., Guétard, D., Henry, M.; Wain-Hobson, S. Evidence for editing of human papillomavirus DNA by APOBEC3 in benign and precancerous lesions. *Science* **2008**, *320* (5873), 230–233. DOI: 10.1126/science.1153201.
- Venkatesan, S., Angelova, M., Bartkova, J., Bakhroum, S. F.; Bartek, J., et al. APOBEC3 as a driver of genetic intratumor heterogeneity. *Molecular & Cellular Oncology* [Online] **2022**.

- Versteeg, R., van Schaik, B. D., van Batenburg, M. F., Roos, M.; Monajemi, R., et al. The human transcriptome map reveals extremes in gene density, intron length, GC content, and repeat pattern for domains of highly and weakly expressed genes. *Genome Res.* **2003**, *13* (9), 1998–2004. DOI: 10.1101/gr.1649303.
- Vikesaa, J., Hansen, T. V., Jønson, L., Borup, R.; Wewer, U. M., et al. RNA-binding IMPs promote cell adhesion and invadopodia formation. *The EMBO Journal* **2006**, *25* (7), 1456–1468. DOI: 10.1038/sj.emboj.7601039.
- Vivar Chevez, A. R. de, Finke, J.; Bukowski, R. The role of inflammation in kidney cancer. *Advances in experimental medicine and biology* **2014**, *816*, 197–234. DOI: 10.1007/978-3-0348-0837-8_9.
- Wach, S., Taubert, H., Weigelt, K., Hase, N.; Köhn, M., et al. RNA Sequencing of Collecting Duct Renal Cell Carcinoma Suggests an Interaction between miRNA and Target Genes and a Predominance of Deregulated Solute Carrier Genes. *Cancers* **2019**, *12* (1). DOI: 10.3390/cancers12010064.
- Wahren, M., Mellqvist, E., Vene, S., Ringertz, N. R.; Pettersson, I. Nuclear colocalization of the Ro 60 kDa autoantigen and a subset of U snRNP domains. *European journal of cell biology* **1996**, *70* (3), 189–197.
- Walther, M. M., Choyke, P. L., Glenn, G., Lyne, J. C.; Rayford, W., et al. Renal cancer in families with hereditary renal cancer: prospective analysis of a tumor size threshold for renal parenchymal sparing surgery. *The Journal of urology* **1999**, *161* (5), 1475–1479. DOI: 10.1016/s0022-5347(05)68930-6.
- Wan, F. and Lenardo, M. J. Specification of DNA binding activity of NF-kappaB proteins. *Cold Spring Harbor perspectives in biology* **2009**, *1* (4), a000067. DOI: 10.1101/cshperspect.a000067.
- Wang, C. Y., Cusack, J. C., Liu, R.; Baldwin, A. S. Control of inducible chemoresistance: enhanced anti-tumor therapy through increased apoptosis by inhibition of NF-kappaB. *Nature medicine* **1999**, *5* (4), 412–417. DOI: 10.1038/7410.
- Wang, J., Xi, Z., Xi, J., Zhang, H.; Li, J., et al. Somatic mutations in renal cell carcinomas from Chinese patients revealed by whole exome sequencing. *Cancer cell international* **2018a**, *18*, 159. DOI: 10.1186/s12935-018-0661-5.
- Wang, Y., Tang, X., Yu, B., Gu, Y.; Yuan, Y., et al. Gene network revealed involvements of Birc2, Birc3 and Tnfrsf1a in anti-apoptosis of injured peripheral nerves. *PloS one* **2012**, *7* (9), e43436. DOI: 10.1371/journal.pone.0043436.
- Wang, Z., Zhong, M., Song, Q., Pascal, L. E.; Yang, Z., et al. Anti-apoptotic factor Birc3 is up-regulated by ELL2 knockdown and stimulates proliferation in LNCaP cells. *American journal of clinical and experimental urology* **2019**, *7* (4), 223–231.
- Wang, Z.-L., Li, B., Luo, Y.-X., Lin, Q.; Liu, S.-R., et al. Comprehensive Genomic Characterization of RNA-Binding Proteins across Human Cancers. *Cell Reports* **2018b**, *22* (1), 286–298. DOI: 10.1016/j.celrep.2017.12.035.
- Wedekind, J. E., Dance, G. S., Sowden, M.; Smith, H. C. Messenger RNA editing in mammals: New members of the APOBEC family seeking roles in the family business. *Trends in Genetics* [Online] **2003**, *19* (4), 207–216.
- Weidensdorfer, D., Stöhr, N., Baude, A., Lederer, M.; Köhn, M., et al. Control of c-myc mRNA stability by IGF2BP1-associated cytoplasmic RNPs. *RNA (New York, N. Y.)* **2009**, *15* (1), 104–115. DOI: 10.1261/rna.1175909.
- Weinstein, J. N., Collisson, E. A., Mills, G. B., Shaw, K. R.; Ozenberger, B. A., et al. The Cancer Genome Atlas Pan-Cancer analysis project. *Nature genetics* **2013**, *45* (10), 1113–1120. DOI: 10.1038/ng.2764.
- Weiss, L. and Ward, P. M. Cell detachment and metastasis. *Cancer metastasis reviews* **1983**, *2* (2), 111–127. DOI: 10.1007/BF00048965.

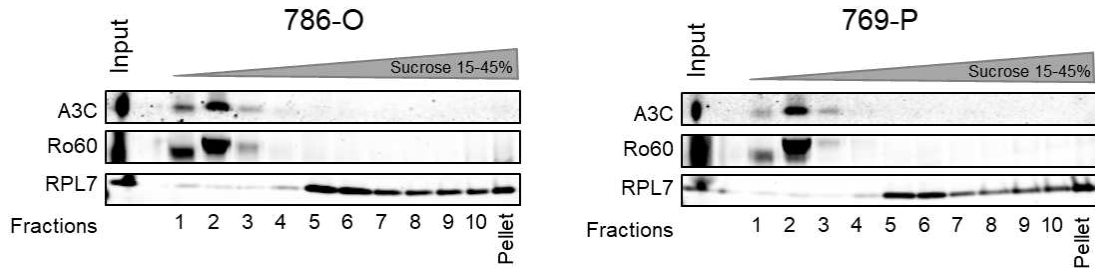
- Wek, R. C. and Staschke, K. A. How do tumours adapt to nutrient stress? *The EMBO Journal* **2010**, *29* (12), 1946–1947. DOI: 10.1038/emboj.2010.110.
- Welsh, S. J. and Fife, K. Pazopanib for the treatment of renal cell carcinoma. *Future oncology (London, England)* **2015**, *11* (8), 1169–1179. DOI: 10.2217/fon.14.274.
- White, P. T. and Cohen, M. S. The discovery and development of sorafenib for the treatment of thyroid cancer. *Expert opinion on drug discovery* **2015**, *10* (4), 427–439. DOI: 10.1517/17460441.2015.1006194.
- Wichroski, M. J., Robb, G. B.; Rana, T. M. Human retroviral host restriction factors APOBEC3G and APOBEC3F localize to mRNA processing bodies. *PLoS pathogens* **2006**, *2* (5), e41. DOI: 10.1371/journal.ppat.0020041.
- Wittkopp, C. J., Adolph, M. B., Wu, L. I., Chelico, L.; Emerman, M. A Single Nucleotide Polymorphism in Human APOBEC3C Enhances Restriction of Lentiviruses. *PLoS pathogens* **2016**, *12* (10), e1005865. DOI: 10.1371/journal.ppat.1005865.
- Wörmann, S. M., Zhang, A., Thege, F. I., Cowan, R. W.; Rupani, D. N., et al. APOBEC3A drives deaminase domain-independent chromosomal instability to promote pancreatic cancer metastasis. *Nature cancer* **2021**, *2* (12), 1338–1356. DOI: 10.1038/s43018-021-00268-8.
- Wu, Y., Wei, X., Feng, H., Hu, B.; Liu, B., et al. Transcriptome Analyses Identify an RNA Binding Protein Related Prognostic Model for Clear Cell Renal Cell Carcinoma. *Frontiers in genetics* **2020**, *11*, 617872. DOI: 10.3389/fgene.2020.617872.
- Wurth, L. Versatility of RNA-Binding Proteins in Cancer. *Comparative and functional genomics* **2012**, *2012*, 178525. DOI: 10.1155/2012/178525.
- Xiao, X., Yang, H., Arutiunian, V., Fang, Y.; Besse, G., et al. Structural determinants of APOBEC3B non-catalytic domain for molecular assembly and catalytic regulation. *Nucleic Acids Res* **2017**, *45* (12), 7494–7506. DOI: 10.1093/nar/gkx362.
- Xie, M., Lv, Y., Liu, Z., Zhang, J.; Liang, C., et al. Identification and validation of a four-miRNA (miRNA-21-5p, miRNA-9-5p, miR-149-5p, and miRNA-30b-5p) prognosis signature in clear cell renal cell carcinoma. *Cancer management and research* **2018**, *10*, 5759–5766. DOI: 10.2147/CMAR.S187109.
- Xiong, C., Liu, H., Chen, Z., Yu, Y.; Liang, C. Prognostic role of survivin in renal cell carcinoma: A system review and meta-analysis. *European journal of internal medicine* **2016**, *33*, 102–107. DOI: 10.1016/j.ejim.2016.06.009.
- Xu, F., Liu, T., Zhou, Z., Zou, C.; Xu, S. Comprehensive Analyses Identify APOBEC3A as a Genomic Instability-Associated Immune Prognostic Biomarker in Ovarian Cancer. *Frontiers in immunology* **2021**, *12*, 749369. DOI: 10.3389/fimmu.2021.749369.
- Xu, Y., Wu, W., Han, Q., Wang, Y.; Li, C., et al. Post-translational modification control of RNA-binding protein hnRNPK function. *Open biology* **2019**, *9* (3), 180239. DOI: 10.1098/rsob.180239.
- Yagoda, A., Abi-Rached, B.; Petrylak, D. Chemotherapy for advanced renal-cell carcinoma: 1983-1993. *Seminars in Oncology* **1995**, *22* (1), 42–60.
- Yamanaka, S., Balestra, M. E., Ferrell, L. D., Fan, J.; Arnold, K. S., et al. Apolipoprotein B mRNA-editing protein induces hepatocellular carcinoma and dysplasia in transgenic animals. *Proceedings of the National Academy of Sciences of the United States of America* **1995**, *92* (18), 8483–8487. DOI: 10.1073/pnas.92.18.8483.
- Yamazaki, H., Shirakawa, K., Matsumoto, T., Matsui, H.; Maruyama, W., et al. Aberrantly Expressed APOBEC3B Induces Mutations in Multiple Myeloma. *Blood* **2016**, *128* (22), 4453. DOI: 10.1182/blood.V128.22.4453.4453.
- Yang, J. P., Merin, J. P., Nakano, T., Kato, T.; Kitade, Y., et al. Inhibition of the DNA-binding activity of NF-kappa B by gold compounds in vitro. *FEBS Letters* **1995**, *361* (1), 89–96. DOI: 10.1016/0014-5793(95)00157-5.

- Yates, A. D., Achuthan, P., Akanni, W., Allen, J.; Allen, J., et al. Ensembl 2020. *Nucleic Acids Res* **2020**, *48* (D1), D682–D688. DOI: 10.1093/nar/gkz966.
- Yoshida, S., Kato, T., Sakurada, S., Kurono, C.; Yang, J. P., et al. Inhibition of IL-6 and IL-8 induction from cultured rheumatoid synovial fibroblasts by treatment with aurothioglucose. *International immunology* **1999**, *11* (2), 151–158. DOI: 10.1093/intimm/11.2.151.
- Yu, Q., Chen, D., König, R., Mariani, R.; Unutmaz, D., et al. APOBEC3B and APOBEC3C are potent inhibitors of simian immunodeficiency virus replication. *The Journal of biological chemistry* **2004**, *279* (51), 53379–53386. DOI: 10.1074/jbc.M408802200.
- Zack, T. I., Schumacher, S. E., Carter, S. L., Cherniack, A. D.; Saksena, G., et al. Pan-cancer patterns of somatic copy number alteration. *Nature genetics* **2013**, *45* (10), 1134–1140. DOI: 10.1038/ng.2760.
- Zandi, E., Rothwarf, D. M., Delhase, M., Hayakawa, M.; Karin, M. The I κ B kinase complex (IKK) contains two kinase subunits, IKK α and IKK β , necessary for I κ B phosphorylation and NF- κ B activation. *Cell* **1997**, *91* (2), 243–252. DOI: 10.1016/s0092-8674(00)80406-7.
- Zarnegar, B., Yamazaki, S., He, J. Q.; Cheng, G. Control of canonical NF- κ B activation through the NIK-IKK complex pathway. *Proceedings of the National Academy of Sciences of the United States of America* **2008**, *105* (9), 3503–3508. DOI: 10.1073/pnas.0707959105.
- Zeng, W., Chang, H., Ma, M.; Li, Y. CCL20/CCR6 promotes the invasion and migration of thyroid cancer cells via NF- κ B signaling-induced MMP-3 production. *Experimental and molecular pathology* **2014**, *97* (1), 184–190. DOI: 10.1016/j.yexmp.2014.06.012.
- Zhang, B., Babu, K. R., Lim, C. Y., Kwok, Z. H.; Li, J., et al. A comprehensive expression landscape of RNA-binding proteins (RBPs) across 16 human cancer types. *RNA biology* **2020**, *17* (2), 211–226. DOI: 10.1080/15476286.2019.1673657.
- Zhang, H. The inhibitory effect of apolipoprotein B mRNA-editing enzyme catalytic polypeptide-like 3G (APOBEC3G) and its family members on the activity of cellular microRNAs. *Progress in molecular and subcellular biology* **2010**, *50*, 71–83. DOI: 10.1007/978-3-642-03103-8_5.
- Zhang, H. and Sun, S.-C. NF- κ B in inflammation and renal diseases. *Cell & Bioscience* **2015**, *5*, 63. DOI: 10.1186/s13578-015-0056-4.
- Zhang, H., Yang, B., Pomerantz, R. J., Zhang, C.; Arunachalam, S. C., et al. The cytidine deaminase CEM15 induces hypermutation in newly synthesized HIV-1 DNA. *Nature* **2003**, *424* (6944), 94–98. DOI: 10.1038/nature01707.
- Zhang, J. and Chen, X. Posttranscriptional regulation of p53 and its targets by RNA-binding proteins. *Current molecular medicine* **2008**, *8* (8), 845–849. DOI: 10.2174/156652408786733748.
- Zhang, J. and Zhang, Q. VHL and Hypoxia Signaling: Beyond HIF in Cancer. *Biomedicines* **2018**, *6* (1). DOI: 10.3390/biomedicines6010035.
- Zhang, S., Guo, Y., Hu, Y., Gao, X.; Bai, F., et al. The role of APOBEC3C in modulating the tumor microenvironment and stemness properties of glioma: evidence from pancancer analysis. *Frontiers in immunology* **2023**, *14*, 1242972. DOI: 10.3389/fimmu.2023.1242972.
- Zhang, W., Du, J., Yu, K., Wang, T.; Yong, X., et al. Association of potent human antiviral cytidine deaminases with 7SL RNA and viral RNP in HIV-1 virions. *J. Virol.* **2010**, *84* (24), 12903–12913. DOI: 10.1128/JVI.01632-10.
- Zhang, X., Yamashita, M., Uetsuki, H.; Kakehi, Y. Angiogenesis in renal cell carcinoma: Evaluation of microvessel density, vascular endothelial growth factor and matrix

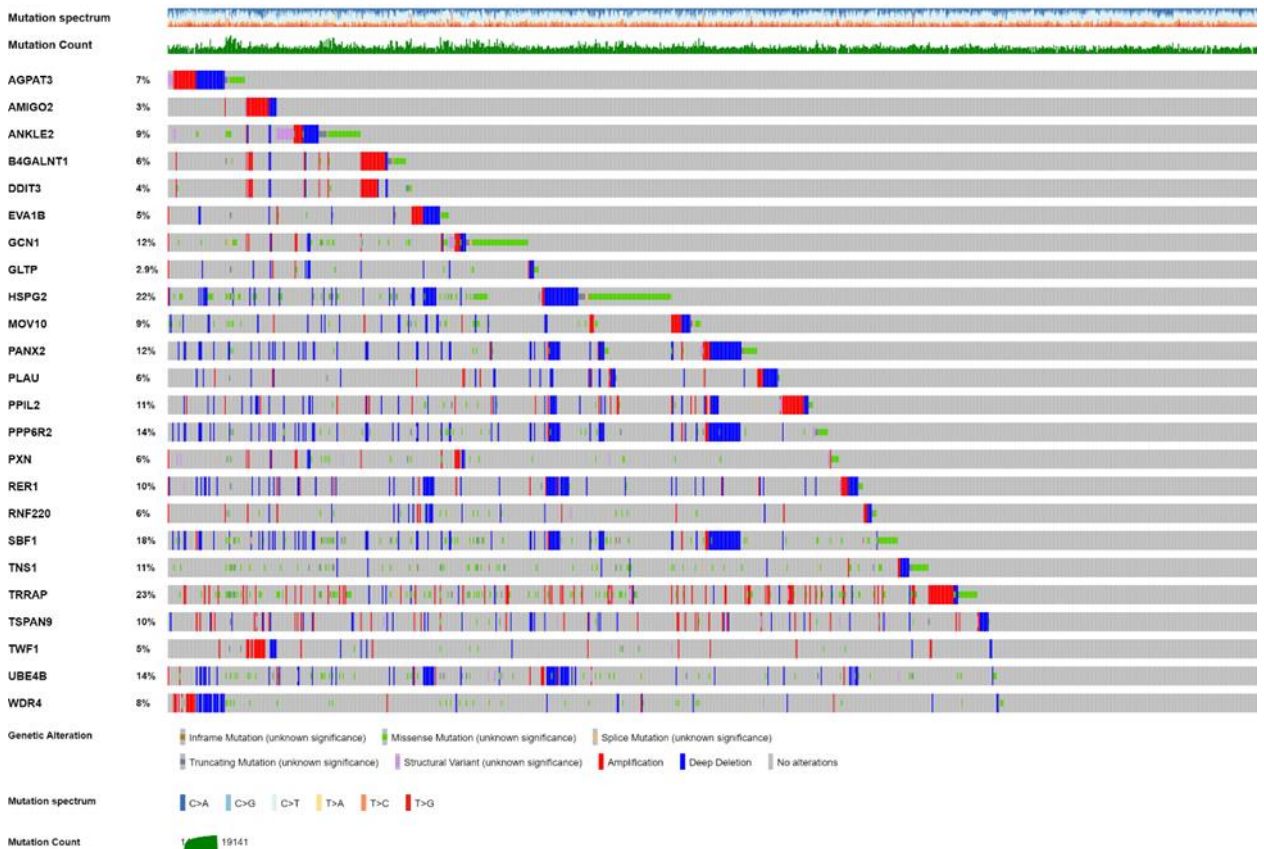
- metalloproteinases. *International journal of urology : official journal of the Japanese Urological Association* **2002**, 9 (9), 509–514. DOI: 10.1046/j.1442-2042.2002.00511.x.
- Zhong, H., Voll, R. E.; Ghosh, S. Phosphorylation of NF-kappa B p65 by PKA stimulates transcriptional activity by promoting a novel bivalent interaction with the coactivator CBP/p300. *Molecular cell* **1998**, 1 (5), 661–671. DOI: 10.1016/s1097-2765(00)80066-0.
- Zhu, Z., He, A., Lin, L., Xu, C.; Cai, T., et al. Biological functions and prognostic value of RNA Binding Proteins in clear cell Renal Cell Carcinoma. *Journal of Cancer* **2020**, 11 (22), 6591–6600. DOI: 10.7150/jca.49175.
- Zhu, Z., Ji, X., Zhu, W., Cai, T.; Xu, C., et al. Comprehensive bioinformatics analyses of APOBECs family and identification of APOBEC3D as the unfavorable prognostic biomarker in clear cell renal cell carcinoma. *Journal of Cancer* **2021**, 12 (23), 7101–7110. DOI: 10.7150/jca.61972.

7 APPENDIX

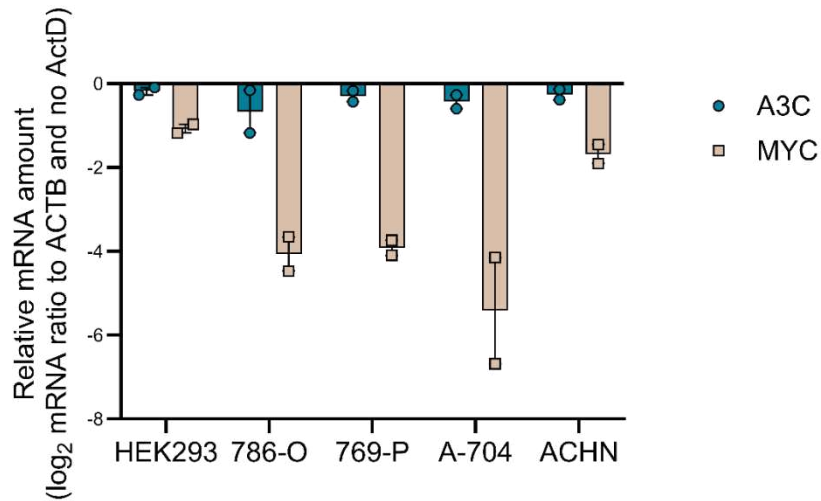
7.1 Supplemental Figures



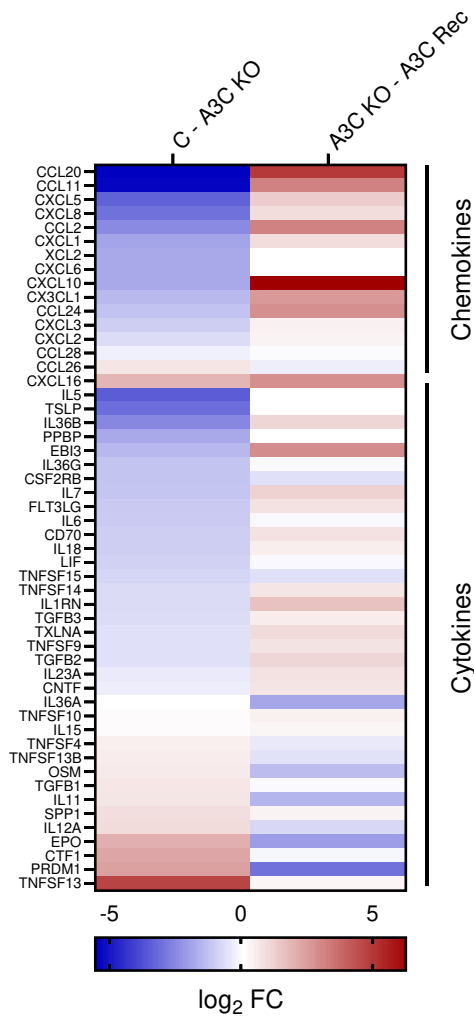
Supplemental Figure 1. A3C localizes to fractions containing low molecular weight complexes. Total cell lysates from the ccRCC-derived cell lines 786-O (left) and 769-P (right) were separated by ultracentrifugation on a sucrose gradient (15-45%). WB analyses show the distribution of A3C, Ro60 and RPL7 in fractions of the sucrose gradient.



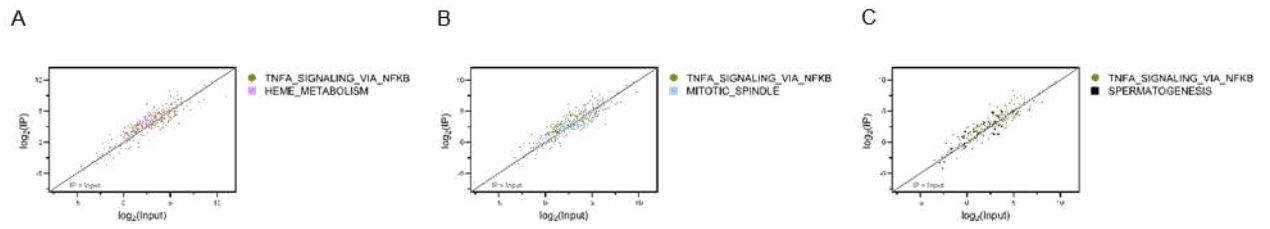
Supplemental Figure 2. Putative editing targets of A3C exhibit genomic C-to-T mutations. Genomic mutation frequencies of putative A3C editing targets (list from Figure 9D) were analyzed using the CCLE dataset (Broad, 2019) and cBioPortal (identifier: <https://bit.ly/3NmyQlZ>).



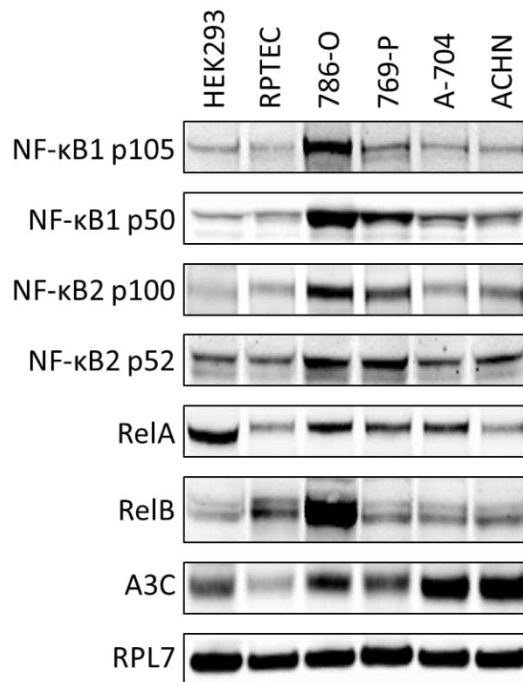
Supplemental Figure 3. A3C mRNA decay in diverse cell lines. A3C and MYC mRNA amount was analyzed in HEK2993, ACHN, A-704, 786-O and 769-P cells upon ActD treatment for 120 min. Transcript abundance was normalized to ACTB and DMSO-treated cells. Data represent two independent experiments.



Supplemental Figure 4. Expression of chemokines and cytokines is affected by A3C levels. Heat map indicates the log₂ FC of chemokines and cytokines according to www.bu.edu/nf-kb/gene-resources/target-genes/ and (Cameron, Kelvin, 2003; Turner et al., 2014) upon KO of A3C and rescue of A3C in 786-O cells (FPKM in C > 0.005).



Supplemental Figure 5. Binding partners of A3C belong to diverse HALLMARK gene sets. Scatter plots show putative binding partners of A3C identified in the RIP-seq of 786-O A3C Rec cells (mean FPKM in input > 0.1). Depicted are transcripts belonging to the HALLMARK gene set 'TNFA_SIGNALING_VIA_NFKB' (yellow) in comparison to other HALLMARK gene sets that are not negatively enriched in 786-O C vs. A3C KO GSEA: 'HEME_METABOLISM' (purple; **A**), 'MITOTIC_SPINDLE' (blue; **B**) and 'SPERMATOGENESIS' (black; **C**).



Supplemental Figure 6. Protein levels of NF-κB subunits in diverse cell lines. WBs show protein levels of the NF-κB subunits NF-κB1 (unprocessed, p105; processed, p50), NF-κB2 (unprocessed, p100; processed, p52), RelA and RelB in normal kidney cell lines (HEK293 and RPTEC/TERT1), ccRCC-derived cell lines (786-O, 769-P and A-704) and a papRCC-derived cell line (ACHN). RPL7 was used for quantification.

7.2 Supplemental Tables

Supplemental Table 1: Putative editing targets of A3C

Gene	Strand	Altered position	Reference	Alteration	Editing recovered in 786-O A3C Rec	Impact of editing site	Editing confirmed with Sanger sequencing	log2FC_C vs A3C KO	FDR_C vs A3C KO	log2FC_A3C KO vs A3C Rec	FDR_A3C KO vs A3C Rec
AC073111.3	1	150371531	C	T	no	Leu>Leu		0	1	-0.499438341	0
ACO2	1	41515521	C	T	yes	3' UTR		-0.4586807	3.75E-11	0.598670825	1.22E-14
AGPAT3	1	43983452	C	T	yes	Pro>Pro	yes	0.363998941	2.15E-16	-0.034509606	4.29E-28
AMIGO2	-1	47077656	G	A	yes	His>Tyr		0.32680145	1.26E-08	0.030964078	1
ANKLE2	-1	132754951	G	A	yes	5' UTR		-0.44270973	6.73E-16	-0.357036198	1.98E-10
ATF4	1	39521042	C	T	yes	Leu>Leu	yes	-0.20105954	0.0197864	-0.239721538	0.002964503
B4GALNT1	-1	57628241	G	A	yes	Asn>Asn		-0.77136747	3.18E-25	0.675921257	1.08E-19
B4GALT3	-1	161174011	G	A	yes	3' UTR		-0.34579764	7.42E-08	-0.273686926	4.04E-05
CBX6	-1	38862790	G	A	yes	Ser>Ser	yes	0	1	0	1
CD99	1	2714441	C	T	yes	Asp>Asp		0.847054945	1.04E-27	-0.899778233	7.14E-32
CDC16	1	114239439	C	T	yes	3' UTR		0.271218416	0.0112141	-0.339404916	0.00055223
COL4A2	1	110512732	C	T	yes	3' UTR		-0.74777203	2.67E-27	0.409848315	1.27E-08
COL7A1	-1	48584149	G	A	no	Asp>Asp		-0.57025275	3.87E-14	0.859251833	7.38E-32
CPSF1	-1	144398573	G	A	yes	belongs to 3' UTR UBAS2 (-1)		-1.18629317	0.6204509	0.641835912	1
CRLF1	-1	18575811	G	A	yes	Phe>Phe		-0.04709218	1	0.350549323	0.005998013
DDIT3	-1	57517377	G	A	yes	3' UTR		-0.53404325	9.17E-21	0.24141777	0.000116168
DNAJC11	-1	6634514	G	A	yes	3' UTR	yes	-0.22826393	0.063851	0.845986208	3.92E-22
EVA1B	-1	36322287	G	A	yes	3' UTR		-0.57046837	3.82E-12	0.702180612	2.29E-18
FAM129A	-1	184792665	G	A	yes	reads belong to SART3		-0.15944323	0.6872793	-0.134615865	0.87154633
FCD	1	108524369	C	T	yes	Thr>Thr		1.27899407	1.02E-80	-1.666005091	9.23E-135
GAS6	-1	113822106	G	A	yes	3' UTR	yes	-0.46620052	1.19E-08	0.532194971	3.23E-11
GCN1	-1	120127384	G	A	yes	3' UTR	yes	-0.09312842	0.7121474	-0.047713775	1
GLTP	-1	109852268	G	A	yes	3' UTR	yes	0.0269946125	1	0.338498523	5.31E-06
GMEB2	-1	63588387	G	A	yes	Ala>Val		0	1	0	1
GSTM5	1	109737079	C	T	no	Thr>Thr		-1.32434456	8.64E-25	1.9679334248	8.67E-53
HSPG2	-1	21864961	G	A	yes	Thr>Thr	yes	0.312036762	0.0004901	0.265937886	0.003884333
INTS1	-1	1503061	G	A	no	Tyr>Tyr		-1.23549335	4.69E-92	0.550833175	1.10E-18
LAMB3	-1	209650009	G	A	yes	Ser>Ser		0.382490824	3.75E-06	0.012924709	1
MAD1L1	-1	2217977	G	A	no	Gly>Gly		-0.10650494	0.5229647	-0.079407161	0.921934624
MAD1L2	-1	3544903	G	A	yes	Pro>Ser		-0.6794425	1.76E-17	0.931515009	4.52E-33
MFDSD12	1	112700426	C	T	yes	3' UTR		-0.6794425	1.76E-17	0.931515009	4.52E-33
MOV10	1	112694059	C	T	yes	3' UTR		-0.66386778	2.52E-28	0.609961353	2.82E-24
NOL9	-1	6521817	G	A	yes	3' UTR		-0.12278415	0.5805561	-0.683681092	6.92E-16
PANX2	1	50179297	C	T	yes	Pro>Ser		-0.54984048	2.48E-19	0.312257692	1.28E-06
PARP1	-1	226383066	G	A	yes	3' UTR		-0.33839875	1.94E-05	0.66301695	6.13E-20
PLAU	1	73916706	C	T	yes	Asp>Asp		-0.46066693	3.66E-06	0.727975926	1.13E-14
PLEC	-1	143921781	G	A	yes	Phe>Phe		-0.63407733	3.40E-20	0.33676175	4.02E-06
PLOD1	1	11949898	C	T	yes	Asn>Asn		0.068812052	1	0.40813953	8.01E-05
POLR2A	1	7514346	C	T	no	Arg>Cys		0.023090091	1	-0.2968992452	0.000241811
POM121C	-1	75475137	G	A	no	site belongs to B4GALT3 (-1)		-0.59691713	4.25E-15	-0.041810835	1
PP1L2	1	21684910	C	T	yes	3' UTR		0.180875814	0.0429103	-0.961455694	1.81E-45
PPM1F	-1	21934188	G	A	yes	3' UTR		-0.25316695	0.1588557	0.232909401	0.197897227
PPOX	1	161175215	C	T	yes	Ser>Ser		-0.2692983	0.000152	-0.572596698	4.21E-18
PPP6R2	1	50435068	C	T	yes	Thr>Thr	yes	-0.1557707	0.0238358	0.37948383	9.57E-12
PITG1P	-1	44849611	G	A	yes	3' UTR		0.225559034	0.0035744	-0.042328008	1
PXN	-1	120212461	G	A	yes	3' UTR		-0.07588871	1	0.320096886	1.35E-05
REP1	1	150371531	C	T	no	3' UTR	yes	-0.72462272	4.62E-32	0.422434626	2.76E-11
RER1	1	2404771	C	T	yes	3' UTR		-1.75667971	5.54E-112	2.200677857	2.96E-176
RHOF	-1	121778315	G	A	yes	3' UTR		-0.620055597	8.94E-23	0.707328721	3.89E-30
RNF220	1	44651263	C	T	yes	3' UTR					

Gene	Strand	Altered position	Reference	Alteration	Editing recovered in 786-O A3C Rec	Impact of editing site	Editing confirmed with Sanger sequencing	log ₂ FC_C vs A3C KO	FDR_C vs A3C KO	log ₂ FC_A3C KO vs A3C Rec	FDR_A3C KO vs A3C Rec
RNF220	1	44651313	C	T	yes	3' UTR		-0.62005597	8.94E-23	0.707328721	3.89E-30
RPS5	1	58387307	C	T	yes	3' UTR		-0.45135854	5.96E-06	0.555680048	7.96E-09
RTEL1	1	63659310	C	T	yes	5' UTR		-0.1539783	1	0.415195056	0.094338804
RTEL1-TNFRSF6B	1	63659310	C	T	yes	same site as previous		0.099269177	1	0.348679325	0.100329842
SAFB2	-1	5610034	G	A	no			-0.19383982	0.0284688	-0.136086279	0.237297222
SBF1	-1	50445532	G	A	yes	3' UTR	yes	-0.34098622	0.0001312	-0.057433393	1
SCARF2	-1	20431352	G	A	no			-0.51596888	1.68E-11	0.181339198	0.074076119
SNAP47	1	227732656	C	T	yes	encoded on -1		-0.33726202	3.20E-05	0.449522067	3.13E-09
STK24	-1	98453048	G	A	yes	3' UTR		0.294315151	6.85E-06	-0.605463408	2.02E-23
STK35	1	2147284	C	T	yes	3' UTR		-0.1554596	0.1283252	0.20966924	0.01186061
TAF13	-1	109062756	G	A	yes	(longer) 3' UTR		-0.35781044	0.0003972	-0.08822408	1
THRAP3	1	36286651	C	T	yes	Tyr>Tyr		-0.19395526	0.0153745	-0.004561648	3.91E-157
TNS1	-1	217880962	G	A	yes	Ser-Ser		-2.16438802	3.43E-107	2.633213586	3.84E-06
TRRAP	1	99013061	C	T	yes	3' UTR		0.176017079	0.2734229	-0.45421831	5.60E-13
TSPAN9	1	3283392	C	T	yes	3' UTR		-0.14133635	0.1601615	0.475117088	0.94282273
TULP3	1	2939734	C	T	yes	3' UTR		-0.66573232	3.79E-22	0.081359933	0.94282273
TWIF1	-1	43797822	G	A	yes	Asp>Asp		0.397177665	5.15E-06	-0.083962698	1
UBE4B	1	10180036	C	T	yes	3' UTR		-0.4218064	2.32E-08	0.523171473	8.35E-13
UCK2	1	165909261	C	T	yes	3' UTR		-0.17576162	0.0119826	0.335636564	1.34E-08
URB1	-1	32345569	G	A	yes	Ser>Ser		-0.40715083	1.54E-06	0.344557443	7.06E-05
WDR4	-1	42847250	G	A	yes	Intron im 3' UTR	yes	-0.62974496	6.30E-19	0.724196126	2.55E-25
YDJC	-1	21629564	G	A	yes	intron		-0.41463513	3.11E-06	-0.114624956	0.686722221
ZBTB7B	1	155015050	C	T	yes	lle>lle		-0.4299169	1.44E-07	0.662779443	7.22E-18

Supplemental Table 2: Regulators of the NF- κ B pathway. Gene sets were used from the Molecular Signature Database (<https://www.gsea-msigdb.org/gsea/msigdb/index.jsp>) to compile a list of putative NF- κ B regulators.

Hallmark gene set	Gene ontology biological process gene sets
HALLMARK_TNFA_SIGNALING_VIA_NFKB	NFKBIA_TARGET_GENES
	NFRKB_TARGET_GENES
	GOBP_REGULATION_OF_NIK_NF_KAPPAB_SIGNALING
	GOBP_I_KAPPAB_KINASE_NF_KAPPAB_SIGNALING
	GOBP_NEGATIVE_REGULATION_OF_I_KAPPAB_KINASE_NF_KAPPAB_SIGNALING
	GOBP_NEGATIVE_REGULATION_OF_NF_KAPPAB_TRANSCRIPTION_FACTOR_ACTIVITY
	GOBP_NEGATIVE_REGULATION_OF_NIK_NF_KAPPAB_SIGNALING
	GOBP_NIK_NF_KAPPAB_SIGNALING
	GOBP_I_KAPPAB_KINASE_NF_KAPPAB_SIGNALING
	GOBP_POSITIVE_REGULATION_OF_I_KAPPAB_KINASE_NF_KAPPAB_SIGNALING
	GOBP_POSITIVE_REGULATION_OF_NF_KAPPAB_TRANSCRIPTION_FACTOR_ACTIVITY
	GOBP_POSITIVE_REGULATION_OF_NIK_NF_KAPPAB_SIGNALING

Supplemental Table 3: Putative mRNA-binding partners of A3C involved in regulating the NF- κ B pathway. Significantly enriched protein-coding genes from the A3C-IP (FC \geq 2; p < 0.05; mean FPKM in input > 0.1) were compared with reported NF- κ B signaling pathway regulators (see Supplemental Table 2).

Putative mRNA-binding partners of A3C involved in regulating the NF- κ B pathway					
ACKR3	CLOCK	GCNT2	MBP	PPP1R3B	TFDP2
ADAM12	CLPTM1	GEM	MBTPS1	PPP2R5C	TFG
ADAMTS12	COPS8	GID4	MFHAS1	PRDX3	TGFA
ADCY7	CPNE2	GLCCI1	MID2	PRKCE	TICAM2
ADGRG1	CRMP1	GLI2	MKRN2	PSMF1	TIFA
ADIPOR1	CSAD	GLIS3	MN1	PTGER4	TIPARP
AGAP1	CTH	GNAS	MSRB3	PTGFR	TIRAP
AGO3	CYLD	GPR89A	MTDH	PTPRD	TLR3
ALG9	CYP1B1	GTF3C2	MTPN	PTPRE	TLR6
ALMS1	CYP4F11	HACD3	MXD1	RAPH1	TMEM106A
AMPD3	DAP	HNRNPH3	MYC	RASSF2	TMEM178B
ANKH	DCK	ID2	MYD88	RC3H2	TNFAIP8
ARHGAP42	DICER1	IL15RA	NDFIP1	RELA	TNFRSF11A
ARHGEF12	DSCC1	IL18R1	NDFIP2	RIOK3	TNFRSF19
ATP2C1	DSE	IL1RAP	NEK6	RIPK2	TRAF3
AZI2	DUSP22	IL6ST	NFAT5	ROR1	TRAF3IP2
B4GALT1	EDA2R	IRAK4	NFE2L2	RWDD3	TRAF5
B4GALT5	EFR3A	IRS2	NFIB	SERPINB8	TRAF6
BACE1	EGFR	KALRN	NIPAL3	SH3BGRL3	TRAM1
BCL3	EGR1	KCTD10	NKIRAS1	SIDT2	TRAM2
BCL6	EIF2AK2	KCTD6	NKIRAS2	SIRPA	TRIB1
BHLHE40	EIF4G2	KLF10	NPAT	SLC16A6	TRIM14
BIRC2	ENAH	KLF4	NR1D1	SLC20A1	TRIM59
BIRC3	ENY2	KLF6	NRAS	SLC30A7	TRIM6
BIVM	F2R	KLF9	NRXN3	SLC35G1	TRIM62
BLCAP	FAM104A	LHFPL2	NSD1	SLC38A1	UBE2V1
BMP2	FAM217B	LIMD1	OTULIN	SLC44A2	USP10
BRPF3	FANCD2OS	LIMS1	PANX1	SLC51A	USP38
BTBD11	FARP1	LITAF	PCNX1	SLC7A6	VAPA
BTRC	FER	LPAR1	PDLIM5	SLC9A1	VEPH1
CAV1	FOS	LRCH3	PDPK1	SMAD9	WDSUB1
CCL2	FOSL1	LURAP1L	PELI1	ST7	WIPF1
CD164	FOXN3	MAN1A2	PFKFB2	STPG1	WNT5A
CD44	FOXP2	MAN2A2	PHLDA2	TAB2	ZDHHC17
CDK6	FRS2	MAP3K7	PIK3R1	TAB3	ZDHHC3
CHP1	G0S2	MAPK10	PKP4	TAF4	ZEB2
CHUK	G3BP2	MAPK8	PNRC1	TBC1D8	ZNF675
CIZ1	GADD45A	MATR3	PPM1A	TCAIM	
CLCF1	GALNT10	MAVS	PPM1H	TCF4	

7.3 List of Figures

Figure 1: Origin, stages and histotypes of renal cell carcinoma (RCC).....	1
Figure 2: The role of pVHL and HIF-1 α in ccRCC progression.	4
Figure 3: Phosphorylation and dimerization of NF- κ B subunits.	8
Figure 4: Overview of the canonical and non-canonical NF- κ B pathway.	11
Figure 5: Structure and catalytic activity of APOBEC3 (A3) cytidine deaminase family	17
Figure 6: Functions of cytidine deamination by the APOBEC family	20
Figure 7: Differences in sucrose density gradient profiles and binding partners between A3C and A3G indicate distinct functions within the A3 protein family	52
Figure 8: Subcellular localization of A3C.....	53
Figure 9: C-to-T editing is probably not the main function of A3C.....	55
Figure 10: The 3' untranslated region (UTR) of A3C contains regulatory elements.....	57
Figure 11: Clinical association of A3C levels in ccRCC.....	59
Figure 12: Confirmation of elevated A3C levels in a separate RCC cohort and RCC-derived cell lines	60
Figure 13: Putative regulation of A3C expression by miRNA or RNA-binding proteins (RBPs).....	62
Figure 14: The effect on expression of A3C upon deletion of its 3' UTR	64
Figure 15: IFN- α does not induce expression of A3C.....	65
Figure 16: A3C expression is elevated upon exposure to diverse stress factors.	67
Figure 17: The NF- κ B signaling pathway is impaired upon A3C KO	68
Figure 18: Altered A3C expression levels correlate with altered NF- κ B activity	70
Figure 19: Expression of clinically relevant NF- κ B target genes is reduced upon A3C depletion....	72
Figure 20: Reduced expression of NF- κ B target genes upon A3C depletion is a global effect in RCC cell lines.....	74
Figure 21: The network of NF- κ B interactors.....	75
Figure 22: A3C associates with transcripts of NF- κ B signaling pathway regulators	76
Figure 23: A3C depletion results in reduced expression of NF- κ B signaling pathway regulators ...	78
Figure 24: A3C could potentially stabilize transcripts of NF- κ B signaling pathway regulators.....	79
Figure 25: Upon A3C depletion, the nuclear translocation of NF- κ B subunits is impaired	82

Figure 26: The phosphorylation cascade resulting in NF- κ B activation is affected at different stages in 786-O and 769-P upon A3C depletion.	83
Figure 27: Cell viability under stress conditions depends on A3C expression levels.....	85
Figure 28: Elevated A3C expression is associated with cell survival <i>in cellulo</i> and <i>in vivo</i>	86
Figure 29: Upon A3C depletion, ccRCC-derived cells are more susceptible to drug treatment.....	87
Figure 30: The regulation of A3C gene expression is multifaceted.	95
Figure 31: Putative function of A3C in ccRCC.	104
Figure 32: Impaired cell viability upon Aurothioglucose treatment may not be mediated by A3C	106
Supplemental Figure 1: A3C localizes to fractions containing low molecular weight complexes	I
Supplemental Figure 2: Putative editing targets of A3C exhibit genomic C-to-T mutations	I
Supplemental Figure 3: A3C mRNA decay in diverse cell lines	II
Supplemental Figure 4: Expression of chemokines and cytokines is affected by A3C levels.....	II
Supplemental Figure 5: Binding partners of A3C belong to diverse HALLMARK gene sets	III
Supplemental Figure 6: Protein levels of NF- κ B subunits in diverse cell lines	III

7.4 List of Tables

Table 1: Commercial kits.....	25
Table 2: Composition of standard buffers	26
Table 3: Primary antibodies	27
Table 4: Secondary antibodies.....	28
Table 5: Commercial and generated plasmids.....	29
Table 6: Parental cell lines	30
Table 7: Cell clones generated by the CRISPR/Cas9 system	30
Table 8: Patient tissue samples.....	31
Table 9: Oligonucleotides for molecular cloning	32
Table 10: Oligonucleotides for qRT-PCR	33
Table 11: Oligonucleotides for editing targets	34
Table 12: Oligonucleotides for PCR/Sanger sequencing/semiquantitative RT-PCR	35
Table 13: sgRNAs for establishing CRISPR/Cas9-mediated cell clones	35
Table 14: shRNAs for shRNA-mediated inhibition of gene expression.....	35
Table 15: siRNAs for siRNA-mediated gene knockdown	35
Table 16: Hybridization probes for Northern blot	36
Table 17: Devices used in this study	37
Table 18: Procedure of a PCR.....	38
Table 19: Procedure of a qRT-PCR	41
Table 20: Licenses for graphics created with BioRender	50
Supplemental Table 1: Putative editing targets of A3C.....	IV
Supplemental Table 2: Regulators of the NF- κ B pathway	VI
Supplemental Table 3: Putative mRNA-binding partners of A3C involved in regulating the NF- κ B pathway.....	VII

List of Abbreviations

3'	3-prime
5'	5-prime
A	Adenine
A3	APOBEC3
ActD	Actinomycin D
ADAR	Adenosine deaminase acting on RNA
AGO2	Argonaute RISC catalytic component 2
AID	Activation-induced deaminase
ANOVA	Analysis of variance
APOBEC	Apolipoprotein B mRNA-editing catalytic polypeptide-like
ATCC	American type culture collection
AuTG	Aurothioglucose
BC	Bead control
bp	Base pair
BS	Binding site
C	Cytidine
CCLE	Cancer cell line encyclopedia
ccRCC	Clear cell RCC
CD	Cytidine deaminase
CDS	Coding sequence
CLIP	Cross-linking-immunoprecipitation
cDNA	Complementary DNA
ChIP	Chromatin immunoprecipitation
chrRCC	Chromophobe RCC
CRISPR	Clustered regularly interspaced short palindromic repeats
d	Days
DAVID	Database for annotation, visualization and integrated discovery
DCP1A	mRNA-decapping enzyme 1A
DEG	Differentially expressed genes
DMEM	Dulbecco's modified eagle's medium
DMSO	Dimethylsulfoxid
DNA	Desoxyribonucleic acid
dNTP	Desoxynucleoside triphosphate
EC	Effective concentration
<i>E. coli</i>	<i>Escherichia coli</i>
EDTA	Ethylenediaminetetraacetate
EEF2	Eukaryotic elongation factor 2
EGFR	Epidermal growth factor receptor
EIF4E	Eukaryotic translation initiation factor 4E
ER	Endoplasmic reticulum
ERK1/2	Extracellular signal-regulated kinase 1/2
EV	Empty vector
FACS	Fluorescence-activated cell sorting
FBS	Fetal bovine serum
FC	Fold change
FDA	Food and drug administration
FDR	False discovery rate
FFL	Firefly luciferase

FPKM	Fragments per kilobase million mapped reads
G	Guanine
gDNA	Genomic DNA
GFP	Green fluorescent protein
GLB	Gradient lysis buffer
GRC	Genome reference consortium
GSEA	Gene set enrichment analysis
GSK	Glycogen synthase kinase
h	Hours
HEK293T	Human embryonic kidney 293 T antigen
HIF	Hypoxia-inducible factor
HPV	Human papillomavirus
HR	Hazard ratio
HRE	Hypoxia response element
I	Inosine
IAP	inhibitor of apoptosis
Ig	Immunoglobulin
IGF2BP1	Insulin-like growth factor 2 mRNA-binding proteins
IGV	Integrative genomics viewer
I κ B	Inhibitor of NF- κ B
IKK/IKKB	I κ B kinases
kb	Kilobase
KD	Knockdown
kDa	Kilodalton
KO	Knockout
LB	Lysogeny broth
LINE	Long interspersed nuclear elements
LTR	Long terminal repeats
MAPK	Mitogen-activated protein kinase
min	Minutes
miRNA	Micro RNA
mRCC	Metastatic RCC
mRNA	Messenger RNA
mRNP	Messenger RNP
n	Number
NB	Northern blot
NCBI	National Center for Biotechnology Information
NF- κ B	Nuclear factor 'kappa-light-chain-enhancer' of activated B-cells
NFRKB	Nuclear factor related to kappaB binding protein
NGS	Next generation sequencing
NIK	NF- κ B-inducing kinase
NLS	Nuclear localization sequence
nM	Nanomolar
nm	Nanometer
NT	Non-malignant kidney tissue
OE	Overexpression
PABP	PolyA-binding protein
PAGE	Polyacrylamide gel electrophoresis
papRCC	Papillary RCC
PBS	Phosphate-buffered saline
PCR	Polymerase chain reaction

PD	Pulldown
PDGF	Platelet-derived growth factor
pH	Potential of hydrogen
PTB	Polypyrimidine tract binding proteins
pVHL	Protein VHL
qRT-PCR	Quantitative real-time PCR
RBP	RNA-binding protein
RCC	Renal cell carcinoma
Rel	Reticuloendotheliosis
RFP	Red fluorescent protein
RIP	RNA co-immunoprecipitation
RISC	RNA-induced silencing complex
RL	Renilla luciferase
RNA	Ribonucleic acid
RNase	Ribonuclease
RNP	Ribonucleoprotein
RPL	Ribosomal protein L
rpm	Revolutions per minute
RPTEC	Renal proximal tubule epithelial cells
RT	Room temperature
RT	Reverse transcription
s	Sense
SBP	Streptavidin-binding peptide
SD	Standard deviation
SDS	Sodium dodecylsulfate
SDS-PAGE	SDS-polyacrylamide gel electrophoresis
SEM	Standard error of the mean
seq	Sequencing
Ser	Serine
SFR	SBP-FLAG-RFP
sgRNA	Small guide RNA
shRNA	Small hairpin RNA
SINE	Short interspersed nuclear element
siRNA	Small interfering RNA
snRNA	Small nuclear RNA
snoRNA	Small nucleolar RNA
SNP	Single-nucleotide polymorphism
ssDNA	Single-stranded DNA
STAT1	Signal transducer and activator of transcription 1
T	Thymine
TAE	Tris acetate EDTA
TBE	Tris borate EDTA
TCGA	The cancer genome atlas
TEAD	Transcriptional enhanced associate domain
TF	Transcription factors
TGFA	Transforming growth factor alpha
TMM	Trimmed mean of the M-values
TPM	Transcripts per million mapped reads
TRAIL	Tumor necrosis factor-related apoptosis-inducing ligand
tRNA	Transfer RNA
U	Uridine

Ub	Ubiquitin
UTR	Untranslated region
UV	Ultraviolet
V	Volt
VCL	Vinculin
VEGF	Vascular endothelial growth factor
VHL	von Hippel–Lindau
Vif	Viral infectivity factor
WB	Western blot
WT	Wildtype
YB1	Y-box binding protein 1
%	Percent
% (v/v)	Percent by volume
% (w/v)	Percent weight per volume
°C	Centigrade
µg	Microgram
µl	Microliter
µM	Micromolar
µm	Micrometer

DANKSAGUNG

An dieser Stelle möchte ich zunächst allen danken, die an der praktischen Bearbeitung und der Fertigstellung dieser Arbeit beteiligt waren.

Ich danke dir, Stefan, für die Betreuung meiner Arbeit, für den Input und die materielle Unterstützung. Mein Dank geht auch an die Mitglieder der AG Hüttelmaier, die mir mit Rat und Tat zur Seite standen.

Ein spezieller Dank geht an die AG Köhn. Ich möchte euch für die vielen gemeinsamen Stunden im Labor danken. Danke für eure Unterstützung, unser gemeinsames Durchhalten, wenn Experimente mal nicht geklappten, die gegenseitige Ermutigung und die Freude über unsere Fortschritte. Die Zusammenarbeit mit euch hat meine Zeit in Halle auf jeden Fall bereichert und für viele schöne Erinnerungen gesorgt.

Marcel, dir danke ich für die stetige Unterstützung und Anleitung während meiner Doktorarbeit. Deine Ratschläge und ermutigenden Worte haben dazu beigetragen, dass ich dieses Projekt abschließen konnte.

Zum Schluss möchte ich noch ganz besonders meiner kleinen Familie danken, die bald um ein Mitglied größer wird. Ich danke dir, Robert, für die Momente der Ruhe, die du mir geschaffen hast, wenn ich mich konzentrieren musste. Dir, Jaron, danke ich für die Momente der Ablenkung, die du mir beschert hast, wenn ich mal abschalten musste. Ihr seid mir eine große Stütze.

CURRICULUM VITAE

Personal Details:

Name: Nora Hase
Nationality: German

Education:

PhD Student | Martin Luther University Halle/Wittenberg | 01/2017 – 04/2024

- Biochemistry, Cell Biology

Master of Science | Humboldt University Berlin | 10/2013 – 03/2016

- Molecular Life Science

Bachelor of Science | University Rostock | 10/2009 – 03/2013

- Biology

Attending Student | Metropolitan State College of Denver | 01/2009 – 05/2009

- Introduction to Environmental Science
- Human Biology

High School | Käthe Kollwitz Gymnasium Rostock | 07/1999 – 07/2008

Work Experience:

Research Assistant | 07/2016 – 01/2017

- Cancer Research UK Cambridge Institute, Cambridge, UK

Student Research Assistant | 04/2014 – 03/2016

- Department of Molecular Genetics, Humboldt University Berlin

Internship in Rainforest Conservation | 04/2013 – 09/2013

- Lisanyacu, Ecuador

Student Research Assistant | 12/2012 – 03/2013

- Institute of Biology, University Rostock

DAAD RISE Internship | 09/2012 – 11/2012

- Fisheries and Marine Science, Institute Pertanian Bogor, Bogor, Indonesia

DAAD RISE Internship | 08/2011 – 10/2011

- School of Human Kinetics, University of British Columbia, Vancouver, Canada

LIST OF PUBLICATIONS

APOBEC3C-mediated NF- κ B Activation enhances Clear Cell Renal Cell Carcinoma Progression

Molecular Oncology [2025]

Hase, N., Misiak, D., Taubert, H., Hüttelmaier, S., Gekle, M., Köhn, M.

doi: 10.1002/1878-0261.13721

Short Talks

FEBS Open Bio [2023]

doi: 10.1002/2211-5463.13608

RNA Sequencing of Collecting Duct Renal Cell Carcinoma suggests an Interaction between miRNA and Target Genes and a Predominance of deregulated Solute Carrier Genes

Cancers [2019]

Wach, S., Taubert, H., Weigelt, K., **Hase, N.**, Köhn, M., Misiak, D., Hüttelmaier, S., Stöhr, C.G.

doi: 10.3390/cancers12010064

Unexpected functional Versatility of the Pentatricopeptide Repeat Proteins PGR3, PPR5 and PPR10

Nucleic Acids Research [2018]

Rojas, M., Ruwe, H., Miranda, R.G., Zoschke, R., **Hase, N.**, Schmitz-Linneweber, C. and Barkan, A.

doi: 10.1093/nar/gky737

EIDESSTATTLICHE ERKLÄRUNG

Hiermit versichere ich, dass ich die vorliegende Dissertation selbstständig und ohne fremde Hilfe verfasst habe. Ich habe keine anderen als die von mir angegebenen Quellen und Hilfsmittel benutzt. Die eingereichte schriftliche Fassung der Arbeit entspricht der auf dem elektronischen Speichermedium. Mit der vorliegenden Arbeit bewerbe ich mich erstmals um die Erlangung des Doktorgrades *doctor rerum naturalium*.

Rostock, 22.04.2024

Ort, Datum

Unterschrift